

Université du Québec  
Institut National de la Recherche Scientifique  
Centre Énergie Matériaux Télécommunications

## **DESIGN AND DEVELOPMENT OF A NEW STIMULI-RESPONSIVE LINKER FOR BIOMEDICAL APPLICATIONS**

Par  
Fatemeh Zare

Thèse présentée pour l'obtention du grade de Philosophiae Doctor (Ph.D.)  
en sciences de Énergie et Matériaux

### **Jury d'évaluation**

Président du jury et examineur interne	Prof. Fiorenzo Vetrone INRS-Centre Énergie Matériaux Télécommunications Varenes, Québec, Canada
Examineur externe	Prof. Nicolas Bertrand Faculty of Pharmacy, Université Laval Québec, Québec, Canada
Examineur externe	Prof. Jeanne Leblond Chain Faculty of Pharmacy, Université de Montréal Montréal, Québec, Canada
Directeur de recherche	Prof. Marc A. Gauthier INRS-Centre Énergie Matériaux Télécommunications Varenes, Québec, Canada

## ACKNOWLEDGEMENTS

The research effort behind this thesis is not a single-man work. Therefore, I would like to acknowledge those people who had, in different ways, contributed to its construction.

I want to express my deep gratitude to my research advisor Prof. Marc A. Gauthier, for accepting me into his group and giving me the opportunity to pursue my Ph.D. study in my field of interest. I am so thankful for all his support, supervision, advice, and help, especially for being very patient and kind during the entire period. I have learned a lot from his dedication and scientific insight, which help me to become more critical in decision-making steps. I have grown a lot under his supervision, scientifically and in personality. For all this, I thank you!

I would also like to acknowledge Prof. Jean-Christophe Leroux and Alessandro Potenza for their help in this study and their scientific advice. I appreciate all their help and support.

I would like to thank Prof. Jean-François Cailhier, who let me be trained in his group for cell experiments and for giving me the opportunity to work with Dr. Patrick Laplante. I appreciate all their help in training and fruitful discussions on the scientific aspects of the work.

It was a great pleasure to work with friendly colleagues who accompanied me at INRS, namely, Dr. Andrea Greschner, Dr. Esen Sokullu, Dr. Sharifun Nahar, Ahlem Meziadi, Dr. Ahlem Zaghmi, Dr. Anees Palapuravan, Dr. Tom Congdon, Dr. Xu Geng, Dr. Hu Lei, Sabine Messoudi, Julie Gaudet, Dr. Amir Hassanpour, Kevin Coutu, and Tazib Rahaman. I had wonderful times with them and am very thankful for their presence, support, and help. I would also like to extend my thanks to Dr. Andrea A Greschner for training me in many lab techniques, for discussions on scientific aspects, and for her lovey support whenever I needed her.

I want to thank all the people at INRS with whom I had the opportunity to interact and who made my time at INRS-EMT worthwhile and memorable. Cybelle, Reza, Alborz, Denis, Naser, Daniele, Gaëtan, Arash, Marija, Andrea, Cheng, Elena, Artiom, Hamid, Atie, Amir, and many others.

I would also like to thank the jury members who kindly agreed to evaluate this thesis and take part in the realization of one of my biggest dreams, the doctorate project.

Most importantly, I want to thank my family, especially my mother, sisters, and grandmother, for their support, love, and encouragement during this study.

Last but not least, I would like to thank my fiance, Anthony, for the time, patience, and precious support he always give me.

## FOREWORD

This thesis is written based on the INRS Guide-2022, an article-based version in order to fulfill the last requirement of the Ph.D. program.

It consists of an abstract (English and French versions), synopsis (required when a thesis or dissertation is written in English), general introduction, scientific papers (Article 1 and Article 2) in which I am the first author, general discussion and conclusion, bibliography, and appendix which will be further discussed in below.

Synopsis includes the main points discussed in the document and explains the working hypotheses, research objectives, methodology, and results in much more detail than the abstract does.

**Chapter 1**, presents a brief overview of redox-responsive chemical bonds and materials for therapeutic, diagnostic, and theranostic applications. It also provides information about various endogenous reactive species, their equilibria, and their roles in physiological and pathological processes within the human body. Furthermore, it summarized the information about endogenous reactive species-responsive chemical bonds and materials, including their structures, mechanism of action, selectivity, reactivity (sensitivity and rate of reaction), applications, opportunities, limitations, and a corresponding review of the literature. This chapter ends with research objectives and the structure of the thesis.

**Chapter 2**, published as “Consecutive alkylation, “Click”, and “Clip” reactions for the traceless methionine-based conjugation and release of methionine-containing peptides”; Fatemeh Zare, Alessandro Potenza, Andrea A Greschner, Marc A Gauthier. *Biomacromolecules* (2022). I carried out most experiments, and was responsible for data collection, analysis as well as manuscript composition and revision. Alessandro Potenza was a Master’s student at ETH Zurich university, who contributed by carrying out the data collection and analysis of some experiments, including the preparation of fluorescent peptide (Rho)FPAMAG, bioconjugation of (Rho)FPAMAG and human serum albumin, modification of FPAMAG by 1-bromo-2-butyne, and measuring the stability of 1b-gsh bioconjugates in the presence of 10 mM cysteine. Dr. Andrea A Greschner contributed to manuscript writing and revision. Prof. Marc A Gauthier was the supervisory author and was involved with concept formation, manuscript composition, and revision.

**Chapter 3**, will be submitted for publication as “Biological fate of sulfonium vinyl sulfides – A competition between reactive nitrogen species, radical thiols, and thiol nucleophiles”; Fatemeh

Zare, Patrick Laplante, Jean-Francois Cailhier, and Marc A Gauthier. I carried out most experiments, was responsible for designing the experiments, data collection, analysis, as well as manuscript composition and revision. Dr. Patrick Laplante trained me for *in vitro* experiments, provided some guidance, and prepared the cell cultures (RAW 264.7 and THP-1). Prof. Jean-Francois Cailhier provided support and some guidance for cells experiments. Prof. Marc A Gauthier was the supervisory author and was involved with concept formation, manuscript composition, and revision.

**Chapter 4**, presents a general discussion, conclusions, and perspectives on possible future works based on the results obtained in this thesis.

**Chapter 5**, includes the bibliography used in this thesis. It should be noted that the references used for each scientific paper are included in this chapter.

**Chapter 6**, presents Appendix contained additional information in order to complement the main text and provide elements that are essential for understanding and supporting its content. It includes:

- Appendix I, presents Supplementary information for Article 1.
- Appendix II presents Supplementary information for Article 2.
- Appendix III, includes the copyright permission of the presented Figures in Chapter 1.



## RÉSUMÉ

Espèces réactives endogènes, y compris les espèces réactives de l'oxygène (ROS), les espèces réactives de l'azote (RNS) et les espèces réactives du soufre (RSS) sont en équilibre complexe les unes avec les autres et jouent un rôle vital dans les processus physiologiques. Cependant, la surexpression et la dérégulation de leurs équilibres dans le cadre de processus physiopathologiques conduisent à l'apparition et au développement de nombreuses maladies. Par conséquent, les liaisons chimiques qui répondent à ces stimuli biologiques sont importantes pour de nombreuses applications pharmaceutiques et biotechnologiques. Jusqu'à présent, diverses liaisons chimiques sensibles aux ROS, RNS et RSS ont été développées et appliquées pour des applications thérapeutiques, diagnostiques et théranostiques. Compte tenu de la diversité des applications envisagées pour de telles liaisons chimiques, il est pertinent d'explorer de nouvelles variantes avec des profils de réactivité différents de ceux actuellement trouvés dans la littérature.

Ce travail présente une nouvelle liaison chimique, la liaison sulfure de vinyle sulfonium qui pourrait être installée sur des molécules de thioéther telles que des peptides contenant de la méthionine. La première partie de cette thèse a présenté les réactions et les facteurs impliqués dans la préparation de la liaison sulfure de vinyle sulfonium. Pour illustrer le potentiel de ces réactions, un alcyne déficiente en électrons a été installé de manière sélective sur le résidu méthionine de quatre peptides modèles et utilisée pour préparer une variété de bioconjugués par une réaction Click bien connue (addition nucléophile thiol-allène). Pour illustrer la polyvalence, une variété de bioconjugués ont été préparées (peptide-peptide; peptide-fluorophore; peptide-polymère; peptide-protéine). Notre résultat a démontré que la liaison sulfure de vinyle sulfonium peut être préparée avec des réactifs/réactifs facilement accessibles et sans aucun intermédiaire destructeur. De plus, la liaison sulfure de vinyle sulfonium présentait le potentiel de la réaction Clip (addition radicale thiol-ène) en présence de radicaux thiols, ce qui induisait la libération complète des peptides d'origine via un processus de fragmentation simultané à la régénération de leur résidu méthionine non modifié (en minutes). Le résultat obtenu a démontré le potentiel de cette stratégie Click/Clip et du sulfure de vinyle sulfonium dans le secteur biotechnologique.

La deuxième partie de cette thèse explore la réactivité d'une liaison de sulfure de vinyle sulfonium vis-à-vis des niveaux physiologiquement pertinents de différentes catégories d'espèces réactives et élucide la nature compétitive de ce processus dans les cellules. Les résultats indiquent que ces liaisons répondent aux thiols nucléophiles (heures/jours), aux radicaux thiols (minutes) et aux

espèces azotées réactives (RNS; minutes) dans des conditions modèles conduisant à la libération d'un peptide contenant de la méthionine dans les deux premiers cas et à l'hydroxynitration dans le troisième cas. En présence de cellules et donc de concentrations biologiquement pertinentes de diverses espèces réactives, le RNS a surpassé les radicaux thiols pour la réaction avec le sulfure de vinyle sulfonium, tandis que la réaction avec les thiols nucléophiles restait attendue à des temps plus longs (heures/jours). Ce travail prépare donc le terrain pour l'utilisation prévisible de ces liens dans les secteurs biotechnologique et pharmaceutique.

Mots-clés: Chimie du clic; lieu; bioconjugué; Clip chimie; thiol radicalaire; thioéther; sulfonium; Méthionine; espèces réactives.

## ABSTRACT

Endogenous reactive species, including reactive oxygen species (ROS), reactive nitrogen species (RNS), and reactive sulfur species (RSS), are in complex equilibria with one another and play vital roles in physiological processes. However, their overexpression and the dysregulation of their equilibria under pathophysiological processes can lead to the onset and development of numerous diseases. Therefore, chemical linkages that respond to these biological stimuli are important for many pharmaceutical and biotechnological applications. Up to now, various ROS-, RNS-, and RSS-responsive chemical linkages have been developed and applied for therapeutic, diagnostic, and theranostic applications. Considering the diversity of applications foreseen for such chemical linkages, it is relevant to explore new variants with responsivity profiles that are different from those presently found in the literature.

This work presents a new chemical linkage, the sulfonium vinyl sulfide group that can be installed on thioether molecules such as methionine-containing peptides. The first part of this thesis presents the reactions and factors involved in the preparation of sulfonium vinyl sulfide bond. To illustrate the potential of these reactions, an electron-deficient alkyne was conveniently and selectively installed on the methionine residue of four model peptides and used to prepare a variety of bioconjugates by a well-known Click reaction (nucleophilic thiol–allene addition). To illustrate versatility, a variety of bioconjugates were prepared (peptide–peptide; peptide–fluorophore; peptide–polymer; peptide–protein). Our results demonstrated that the sulfonium vinyl sulfide group can be prepared with readily accessible reactants/reagents and without significant side-reactions. Furthermore, the sulfonium vinyl sulfide groups exhibited the potential of Clip reaction (radical thiol–ene addition) in the presence of radical thiols, which induced the full release of the original peptides *via* a fragmentation process concurrent with the regeneration of their unmodified methionine residue (in minutes). The obtained results demonstrate the potential of this Click/Clip strategy and sulfonium vinyl sulfide in the biotechnological sector.

The second part of this thesis explores the responsiveness of a sulfonium vinyl sulfide linker towards physiologically-relevant levels of different categories of reactive species and elucidates the competitive nature of this process in cells. Results indicate that these linkers respond to nucleophilic thiols (hours/days), radical thiols (minutes), and reactive nitrogen species (minutes) under model conditions leading to the release of a methionine-containing peptide in the first two cases and to hydroxynitration in the third case. In the presence of cells and hence biologically-relevant concentrations of various reactive species, RNS outcompeted radical thiols for reaction

with the sulfonium vinyl sulfide, while reaction with nucleophilic thiols remained expected at longer times (hours/days). This work, therefore, sets the stage for predictably using such linkages in the biotechnological and pharmaceutical sectors.

Keywords: Click chemistry; Linker; Bioconjugate; Clip chemistry; Radical thiol; Thioether; Sulfonium; Methionine; Reactive species.

## SYNOPSIS IN FRENCH

### Conception et développement d'un nouveau lieur sensible aux stimuli pour des applications biomédicales

#### 1. Introduction

Les espèces réactives endogènes, y compris les espèces réactives de l'oxygène, de l'azote et du soufre (RONSS), jouent un rôle vital dans la régulation des événements biologiques tels que la réponse immunitaire, la signalisation et la réponse au stress oxydatif,<sup>1-3</sup> et existent en équilibre complexe les uns avec les autres.<sup>4</sup> La dérégulation de ces équilibres est la cause sous-jacente de multiples processus physiopathologiques qui peuvent être liés à l'apparition et au développement de plusieurs maladies, telles que l'inflammation, le diabète, le cancer et les maladies neurodégénératives.<sup>5,6</sup> Les espèces réactives de l'oxygène (ROS), y compris le radical anion superoxyde ( $O_2^{\cdot-}$ ), le peroxyde d'hydrogène ( $H_2O_2$ ), le radical hydroxyle ( $\cdot OH$ ), l'oxygène singulet ( $^1O_2$ ) et l'acide hypochloreux (HOCl) sont des biomolécules oxydantes avec un potentiel d'oxydation important.<sup>7</sup> Des concentrations élevées de ROS génèrent un stress oxydatif, ce qui entraîne des dommages potentiels aux diverses biomolécules telles que les lipides membranaires, les protéines, les lipoprotéines et l'acide désoxyribonucléique (DNA).<sup>8-10</sup> Par ailleurs, les espèces réactives azotées (RNS) désignent l'oxyde nitrique ( $\cdot NO$ ) et ses produits réactifs secondaires, tels que le nitroxyde (HNO) et le peroxydinitrite ( $ONOO^-$ ).<sup>11</sup> Les RNS peuvent affecter de manière significative les mécanismes cellulaires de régulation redox en raison de leur potentiel d'oxydation et de nitration. En général, le potentiel d'oxydation des RNS est le plus souvent inférieur à celui des ROS.<sup>12</sup> Cependant,  $ONOO^-$ , un oxydant biologique instable et un agent nitrant, a montré une capacité oxydante élevée.<sup>12,13</sup> Le radical thiyle ( $RS^{\cdot}$ ), une espèce soufrée réactive (RSS), est également reconnu comme agent oxydant,<sup>14</sup> produit lors du piégeage radical du GSH dans le processus métabolique cellulaire.<sup>15</sup>  $RS^{\cdot}$  est un médiateur important dans le processus redox intracellulaire, entraînant des dommages cellulaires en réagissant avec les chaînes acyles insaturées des phospholipides et des thiols protéiques.<sup>16,17</sup> D'autre part, les biomolécules d'espèces soufrées réactives (RSS), en particulier les thiols (RSH), agissent comme des agents réducteurs biologiques et jouent un rôle important dans le maintien d'un environnement cellulaire réduit et la régulation de l'état redox cellulaire.<sup>6,18</sup> Le GSH est le thiol réducteur intracellulaire le plus abondant (1–10 mM intracellulaire et 2–20  $\mu M$  extracellulaire) et en équilibre avec sa forme oxydée (GSSG).<sup>19,20</sup> Le GSH est également un réactif antioxydant

essentiel dans des conditions physiologiques normales et prévient les dommages cellulaires causés par RONS.<sup>21,22</sup> Sous stress oxydatif et niveau élevé de RONS, la concentration de GSH est augmentée et entraîne une altération de l'équilibre redox cellulaire (rapports GSH: GSSG), ce qui peut provoquer des réactions d'oxydation et d'échange de disulfure au niveau de résidus cystéine spécifiques des protéines.<sup>23</sup> En conséquence, le GSH a été la cible principale de divers systèmes sensibles à la réduction pour plusieurs raisons, notamment son niveau intracellulaire élevé par rapport à la concentration extracellulaire,<sup>24</sup> augmentation de quatre fois du niveau de GSH intracellulaire dans les tissus tumoraux par rapport aux cellules normales, et importance du niveau altéré de GSH dans les états pathologiques et les maladies humaines<sup>23,25,26,27</sup>

En conséquence, le développement de liaisons chimiques qui répondent aux espèces réactives biologiques est un domaine de recherche important dans les secteurs pharmaceutique et biotechnologique. Jusqu'à présent, plusieurs liaisons chimiques et matériaux ont été développés par diverses approches pour cibler ces biomolécules réactives pour des applications thérapeutiques, diagnostiques et théranostiques.<sup>28-32</sup> L'application de ces liaisons chimiques et matériaux est corrélée avec leurs mécanismes d'action, leur sélectivité et leur réactivité (sensibilité et vitesse de réaction) vis-à-vis du RONSS. Ils peuvent être utilisés pour libérer des molécules de médicament à partir de supports, en tant qu'éléments sensibles pour des capteurs chimiques, en tant que groupes de changement de polarité pour modifier les propriétés physiques/chimiques des systèmes d'administration de médicaments, parmi de nombreuses autres applications.<sup>33</sup>

De plus, les réactions dites "Click" ont révolutionné la recherche dans de nombreux domaines de la chimie, de la science des matériaux et de l'étude des systèmes biologiques.<sup>34-37</sup> Le principe directeur de la chimie Click est que les réactions doivent être à haut rendement avec des sous-produits facilement purifiés et sûrs, être régio- et stéréo-spécifiques, et les réactifs doivent présenter une cinétique de couplage rapide dans des conditions douces avec une tolérance élevée aux groupes fonctionnels et aux solvants.<sup>38</sup> De plus, le procédé devrait idéalement être insensible à l'eau ou à l'air avec des matières premières et des réactifs facilement disponibles, simples, de portée étendue, et générer un produit chimiquement inerte et stable. Plusieurs réactions chimiques présentent (la plupart) de ces caractéristiques, et de nouvelles variantes importantes continuent d'être découvertes.<sup>39,40</sup> De plus, un certain nombre de réactions Click réversibles ont été décrites dans la littérature et comprennent les cycloadditions de Diels-Alder, l'addition de Michael (par exemple, thiol-maléimide), les réactions carbonyle non aldol (par exemple, formation d'hydrazone et d'oxime) et les réactions d'échange de disulfure, entre

autres.<sup>41-43</sup> Ces réactions réversibles sont cependant des processus d'équilibre qui impliquent que si une étape Click rapide peut être possible, l'étape Clip correspondante est proportionnellement plus lente et peut nécessiter des interventions qui peuvent être gênantes ou destructrices pour les biomolécules (dilution, chauffage prolongé, acidification, etc.). En tant que tel, dans la mesure de nos connaissances, la réalisation d'une conjugaison via une réaction Click et d'une libération avec une seconde réaction Clip distincte, via des processus ne reposant pas sur des équilibres chimiques et se produisant dans des conditions physiologiques exploitant les groupes fonctionnels naturels sur les peptides/protéines, sont rares.

De plus, malgré une faible abondance de méthionine dans les protéines (~2%), la fonctionnalisation des protéines à travers ces résidus a attiré une certaine attention. En fait, le rôle fonctionnel limité des résidus de méthionine dans les protéines par rapport à d'autres résidus en fait une excellente option pour le marquage des protéines.<sup>44,45</sup> Par conséquent, plusieurs stratégies ont été développées pour que la bioconjugaison sélective de la méthionine s'applique à une large gamme d'applications pharmaceutiques.

Compte tenu de la diversité des applications envisagées des liaisons chimiques endogènes réactives-espèces réactives, il est pertinent d'explorer de nouvelles variantes avec des profils de réactivité différents de ceux actuellement trouvés dans la littérature. Dans ce cadre, nous avons visé à:

(1) Combinez deux réactions bien connues, y compris la réaction Click (addition nucléophile thiol-allène) et la réaction Clip (addition radicale thiol-ène) afin de fournir une nouvelle liaison chimique, une liaison sulfure de vinyle sulfonium, installée sur un résidu méthionine de différents peptides pour préparer et désassembler les bioconjugués d'une manière Click/Clip (**Figure 1**). Pour explorer le potentiel et la polyvalence de ces réactions, quatre peptides modèles contenant des résidus de méthionine ont été utilisés afin de préparer une variété de bioconjugués (peptide-peptide; peptide-fluorophore; peptide-polymère; peptide-protéine). En outre, la stabilité et la réactivité des bioconjugués contenant du sulfure de vinyle sulfonium ont été étudiées lors de l'exposition à différentes espèces réactives, y compris  $H_2O_2$ ,  $\cdot OH$ , radicaux thiyle et thiols, et dans des cultures de cellules bactériennes.

(2) Évaluer le potentiel du groupement sulfure de vinyle sulfonium dans la détection du peroxy-nitrite ( $ONOO^-$ ) en concevant et en synthétisant une sonde sensible à base de FRET (contenant un lieu de sulfure de vinyle sulfonium) et une sonde de contrôle à base de FRET (en l'absence de sulfure de vinyle sulfonium lieu). En outre, la réaction compétitive de concentrations biologiquement pertinentes de diverses espèces réactives, RNS et RSS, avec le lieu de sulfure

de vinyle sulfonium a été évaluée et caractérisée dans différentes lignées cellulaires afin de démontrer la réactivité du lieu de sulfure de vinyle sulfonium dans des environnements complexes.

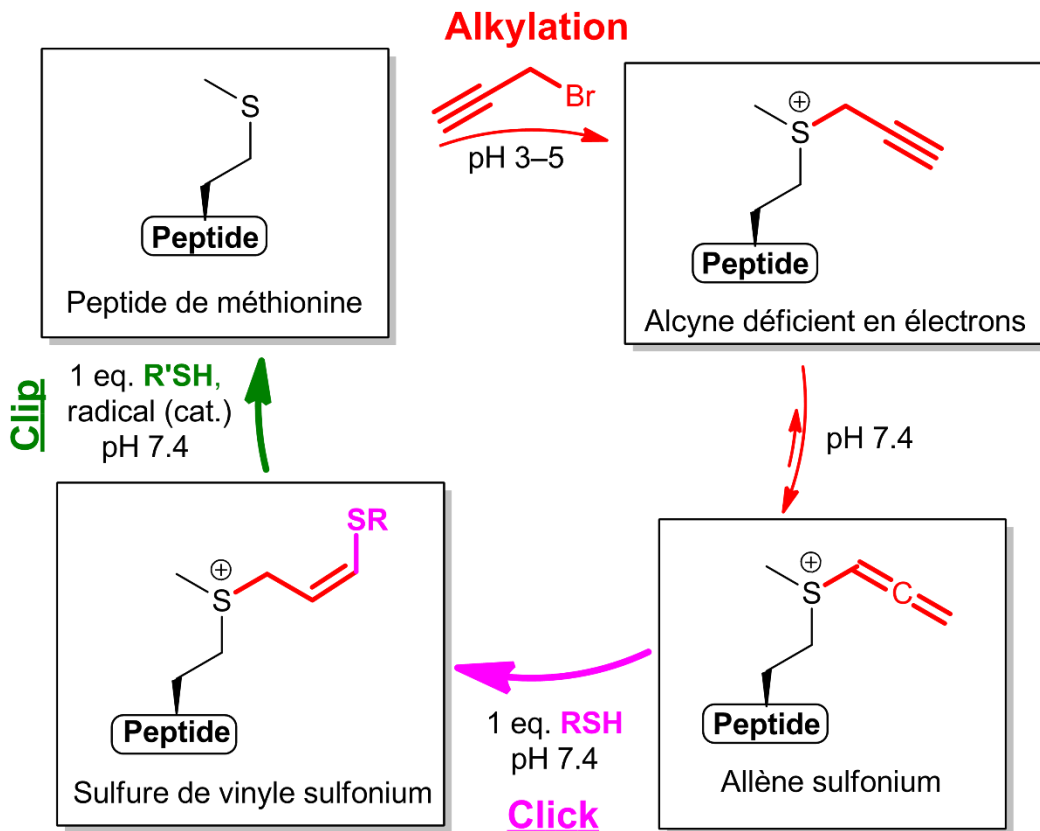


**Figure 1** Les peptides contenant de la méthionine (thioéther) peuvent être sélectivement et commodément alkylés pour produire un allène de sulfonium. Cette entité peut être modifiée par une réaction Click (addition nucléophile thiol-allène), donnant un sulfure de vinyle sulfonium. Ce dernier peut subir une réaction Click ultérieure (ajout radical de thiol-ène) pour régénérer le peptide original contenant de la méthionine (thioéther).

## 2. Méthodes expérimentales

### 2.1 Préparation de bioconjugués contenant du sulfure de vinyle sulfonium

#### 2.1.1 Alkylation de peptides contenant de la méthionine, y compris FPAMAG, sulfoxyde FPAM(O)AG, peptide fluorescent (Rho)FPAMAG, HDMNKVLDL et HDMNK(Cy5)VLDL

Solutions de peptides, dont FPAMAG (**1a**), sulfoxyde FPAM(O)AG (**2a**), peptide fluorescent (Rho)FPAMAG (**3a**), HDMNKVLDL (**4a**; antinflammine-2) et HDMNK(Cy5)VLDL (**5a**) (200  $\mu\text{L}$ ,  $\sim 1.1 \text{ mg}\cdot\text{mL}^{-1}$ ) ont été préparés dans de l'acide formique 100 mM pH 3 à température ambiante dans

un flacon HPLC. Ensuite, environ 22.1, 21.5, 11.64 et 12.1  $\mu\text{L}$  (10  $\text{eq. molaires}$ ) de bromure de propargyle ont été ajoutés à partir d'une solution mère (80% en volume de bromure de propargyle dans du toluène dilué dans de l'éthanol à la concentration finale de 0.17 M) à la solution de **1a**, **2a**, **3a**, et **4a**, respectivement (concentration finale de peptide de 1  $\text{mg}\cdot\text{mL}^{-1}$ ). La réaction a été mélangée doucement et la progression de la réaction a été contrôlée par LC-MS. Des synthèses à plus grande échelle ont également été réalisées en multipliant par dix la concentration et le volume de ces réactions. Les composés produits, y compris FPAM(allène)AG (**1b**), (Rho)FPAM(allène)AG (**3b**) et HDM(allène)NKVLDL (**4b**) ont été isolés par HPLC préparative, récupérés par lyophilisation et stockés à  $-80\text{ }^{\circ}\text{C}$  jusqu'à utilisation. Une concentration plus faible ( $0.3\text{ mg}\cdot\text{mL}^{-1}$ ), un tampon contenant 10% en volume de DMF et 50  $\text{eq.}$  du bromure de propargyle ont été utilisés dans le cas de **5a**, pour réduire la perte due à l'adhésion au flacon et pour favoriser la conversion en HDM(allène)NK(Cy5)VLDL (**5b**).

### 2.1.2 Réaction Click par addition de thiol-allène nucléophile

- **Cliquez par addition de thiol-allène nucléophile avec de la cystéine, des thiols peptidiques, de la fluorescéine SAMSA et du mPEG-SH**

Différentes conditions ont été explorées pour cette réaction. À titre d'exemple représentatif, le peptide allénique, y compris **1b**, **4b** et **5b** (0,5 mg, 1  $\text{eq. molaire}$ ) et le thiol (1 à 10  $\text{eq. molaires}$ ) ont été transférés dans le même flacon HPLC étanche aux gaz. Le mélange a ensuite été purgé par  $\text{N}_2$  pendant 10 min. Ensuite, 0.5 mL de tampon phosphate 100 mM purgé au  $\text{N}_2$  a été ajouté au mélange pour donner une concentration finale de peptide de 1  $\text{mg}\cdot\text{mL}^{-1}$ . La progression de la réaction a été suivie pendant 24 h par LC-MS et le conjugué résultant a été isolé par HPLC préparative, récupéré par lyophilisation et stocké à  $-80\text{ }^{\circ}\text{C}$  jusqu'à son utilisation. Pour étudier la dépendance au pH de la réaction, le pH du tampon phosphate 100 mM purgé au  $\text{N}_2$  a été ajusté à 6.5 ou 8.5 avec des solutions concentrées de HCl ou de NaOH. Une concentration plus faible ( $0.5\text{ mg}\cdot\text{mL}^{-1}$ ) et un tampon contenant 10% en volume de DMF ont été utilisés pour préparer le **5b**-CPP(Cy3), afin de réduire les pertes.

- **Réaction Click par addition de thiol-allène nucléophile avec de l'albumine sérique humaine**

Des solutions d'albumine sérique humaine (0.1 mL, 1  $\text{mg}\cdot\text{mL}^{-1}$  dans un tampon phosphate 100 mM pH 8.5) et **3b** (63.1  $\mu\text{L}$ , 0.24 mM dans  $\text{H}_2\text{O}$  + 0.1% TFA) ont été mélangées dans un flacon HPLC étanche aux gaz, puis 36.9  $\mu\text{L}$  de tampon phosphate 100 mM pH 8.5 ont été ajoutés (Remarque : Cys-34 sur HSA était d'environ  $61 \pm 5\%$  sous sa forme réduite libre dans le matériau

de départ, tel que déterminé par titrage à l'aide de 2,2'-dipyridyldisulfure). La composition de la solution a été contrôlée par LC-MS. Le temps de rétention du conjugué étant identique à celui de la sérumalbumine humaine native, l'augmentation de l'absorbance à 574 nm de ce pic, associée à Rho ( $\epsilon_{574} = 78\,000\text{ cm}^{-1}\cdot\text{M}^{-1}$ ), a été utilisée pour estimer la conversion à **3b**-HSA.

### 2.1.3 Préparation de la sonde contenant du sulfure de vinyle sulfonium (**6d**)

Une solution de peptide Ac-K(N<sub>3</sub>)-GSGMGGRKKRRQRRR-NH<sub>2</sub> (**6a**) (880.7  $\mu\text{L}$ ,  $\sim 5.7\text{ mg}\cdot\text{mL}^{-1}$ ) a été préparée dans de l'acide formique 100 mM pH 3 à température ambiante dans un flacon HPLC. Ensuite, 119.3  $\mu\text{L}$  (10 éq. molaires) de bromure de propargyle ont été ajoutés à partir d'une solution mère (80% en volume de bromure de propargyle dans du toluène dilué dans de l'éthanol à la concentration finale de 0.2 M). Cela a donné une concentration finale de peptide de  $5\text{ mg}\cdot\text{mL}^{-1}$ . La réaction a été mélangée doucement et la progression de la réaction a été suivie par LC-MS. Ensuite, **6b** a été isolé par chromatographie préparative, récupéré par lyophilisation et stocké à  $-80\text{ }^\circ\text{C}$  jusqu'à son utilisation. Dans la deuxième étape, le **6b** purifié (1 mg, 1 éq. molaire) dans du tampon phosphate 100 mM pH 7,4 (712.4  $\mu\text{L}$ ) a été purgé par N<sub>2</sub> pendant 10 min puis mis à réagir avec 2 éq. molaires d'une solution de fluorescéine SAMSA déprotégée purgée au N<sub>2</sub> (284.6  $\mu\text{L}$ , 3.36 mM) dans l'obscurité. Ensuite, l'échantillon a été scellé et purgé par N<sub>2</sub> pendant 5 minutes supplémentaires. L'avancement de la réaction a été suivi et caractérisé par LC-MS. Après environ 4 h, le **6c** produit a été isolé par chromatographie préparative, récupéré par lyophilisation et stocké à  $-80\text{ }^\circ\text{C}$  jusqu'à son utilisation. Dans la troisième étape, le **6c** purifié (1 mg, 1 éq. molaire) a été mélangé avec 2 éq. molaires AFDye<sub>647</sub> DBCO ( $\sim 0.90\text{ mg}$ ) et ajouté à 2 mL de tampon phosphate (100 mM, pH 7,4) contenant 5% en volume de DMF. Le mélange a été laissé réagir dans l'obscurité pendant environ 3 h. Finalement, le **6d** produit a été isolé par chromatographie préparative, confirmé par spectrométrie de masse, récupéré par lyophilisation et stocké à  $-80\text{ }^\circ\text{C}$  jusqu'à son utilisation.

### 2.2 Préparation de la sonde de contrôle (**7c**)

1.05 mg de peptide **7a** (Ac-K(N<sub>3</sub>)-GSGCGGRKKRRQRRR-NH<sub>2</sub>, 1952.11 g/mol) et 4,27 mg de fluorescéine-5-maléimide ont été dissous séparément dans 1 mL de tampon phosphate purgé au N<sub>2</sub> (100 mM, pH 7) et 1 mL de DMF purgé au N<sub>2</sub> à température ambiante, respectivement. Par la suite, 2 éq. de fluorescéine-5-maléimide (51.7  $\mu\text{L}$ , 10 mM dans DMF) a été ajouté à la solution de **7a** et laissé à l'obscurité pour réagir pendant une nuit. Le **7b** produit a ensuite été isolé par chromatographie préparative, récupéré par lyophilisation et stocké à  $-80\text{ }^\circ\text{C}$  jusqu'à son utilisation. Dans l'étape suivante, le **7b** purifié (1 mg, 1 éq. molaire) a été mélangé avec 2 éq. molaires AFDye 647 DBCO ( $\sim 0.95\text{ mg}$ ) et ajouté à 2 mL de tampon phosphate (100 mM, pH 7,4) contenant

5% en volume de DMF. Le mélange a été laissé réagir dans l'obscurité pendant environ 3 h. Finalement, le **7c** produit a été isolé par chromatographie préparative, récupéré par lyophilisation et stocké à -80 °C jusqu'à son utilisation.

### 2.3 Stabilité vis-à-vis de la substitution nucléophile

Différentes conditions ont été explorées pour cette réaction. À titre d'exemple illustratif, des solutions de conjugués, y compris **1b**-GSH, **4b**-GSH, **5b**-CPP(Cy3) et **6d** (50  $\mu$ L, 2 mg·mL<sup>-1</sup>) ont été préparées dans un tampon phosphate dégazé 100 mM (pH 7.4) dans des flacons HPLC étanches aux gaz. Ensuite, un volume approprié de solution de thiol (50  $\mu$ L, 20 mM de GSH ou de Cys dans un tampon phosphate dégazé de 100 mM) a été ajouté pour atteindre une concentration finale de peptide de 1 mg·mL<sup>-1</sup> et une concentration finale de thiol de 10 mM. La composition de la solution a été contrôlée par LC-MS sur une période de 24 h. Un tampon contenant 10% en volume de DMF et 2% en volume de DMF a été utilisé dans le cas de **5b**-CPP(Cy3) et **6d**, respectivement, pour favoriser la solubilité. Ensuite, la composition de la solution a été contrôlée par LC-MS sur une période de 24 h.

### 2.4 Réaction Clip par addition de radical thiol-ène

Solutions de bioconjugué, y compris **1b**-GSH, **5b**-CPP(Cy3), **6d** et **7c** (~90.6  $\mu$ L, ~1.1 mg·mL<sup>-1</sup>) contenant 1.1–10 éq. de GSH ou 10 éq. molaire de cystéine ont été préparés dans du tampon phosphate 100 mM pH 7,4, 6,5 ou 8,5 dans une cuvette rectangulaire en quartz. Ensuite, du DMPA (~9.4  $\mu$ L, 1.5 éq. molaire, à partir d'une solution mère de 15 mM dans du méthanol) a été ajouté à température ambiante. Un tampon contenant 10, 2 et 2 vol% DMF a été utilisé dans le cas de **5b**-CPP(Cy3), **6d** et **7c**, respectivement, pour réduire les pertes. La concentration finale de **5b**-CPP(Cy3) dans du DMF/tampon phosphate 100 mM pH 7.4 (10% v/v) était de 0.1, 0.3, 0.8 ou 1 mg·mL<sup>-1</sup>. Les échantillons ont été irradiés jusqu'à 15 min à 365 nm à l'aide d'une lampe UV UVGL-15 4 W (UVP, LLC) placée en contact avec la cuvette. La composition de la solution a été contrôlée par LC-MS. L'intensité de fluorescence de **5b**-CPP(Cy3) a été contrôlée avant et après irradiation avec un lecteur de microplaques Cytation 5 (Biotek Instrument, VT) en utilisant les paramètres suivants:  $\lambda_{\text{ex}}/\lambda_{\text{em}}$  549/595 nm (Cy3);  $\lambda_{\text{ex}}/\lambda_{\text{em}}$  646/672 nm (Cy5);  $\lambda_{\text{ex}}/\lambda_{\text{em}}$  549/672 nm (FRET). Les spectres ont également été enregistrés  $\lambda_{\text{ex}}/\lambda_{\text{em}}$  549/585–700 nm. L'intensité de fluorescence des échantillons contenant **6d** ou **7c** a été contrôlée à chaque 2 min d'irradiation à la lumière UV avec un lecteur de microplaques Cytation 5 (Biotek Instrument, VT) en utilisant les paramètres suivants:  $\lambda_{\text{ex}}/\lambda_{\text{em}}$  480/673 nm (FRET);  $\lambda_{\text{ex}}/\lambda_{\text{em}}$  480/519 nm (fluorescéine);  $\lambda_{\text{ex}}/\lambda_{\text{em}}$  643/672 nm (AFDye<sub>647</sub>).

## 2.5 Stabilité des bioconjugués au H<sub>2</sub>O<sub>2</sub> et à la lumière UV

Différentes conditions ont été explorées pour cette réaction. Comme protocole illustratif, des solutions de bioconjugué (90 µL, 1.1 mg·mL<sup>-1</sup> dans du tampon phosphate 100 mM) ont été incubées en présence de 1–10 éq. de H<sub>2</sub>O<sub>2</sub> et 0–10 éq. molaire. de GSH dans une cuvette en quartz. Le volume de la solution a ensuite été ajusté avec le même tampon pour donner une concentration finale de peptide de 0.1 mg·mL<sup>-1</sup>. Les échantillons ont été incubés sans ou avec irradiation externe jusqu'à 15 min à 365 nm à l'aide d'une lampe UV UVGL-15 4 W (UVP, LLC) placée en contact avec la cuvette.

## 2.6 Stabilité en présence de peroxyinitrite

0.13 mg de **2b**-GSH a été dissous dans 0.9 mL de tampon phosphate (100 mM, pH 7.4). Éq molaire différente de peroxyinitrite (0, 1, et 5 éq.) ont ensuite été ajoutés à la solution de chaque échantillon. Un volume approprié de tampon phosphate (100 mM, pH 7.4) a été ajouté à chaque échantillon pour atteindre une concentration finale en FPAM(sulfure de vinyle–GSH)AG de 0.1 mg·mL<sup>-1</sup>. La composition de la solution a été contrôlée par LC-MS sur une période de 3 heures. De plus, 0.5 mg de **6d** ou **7c** ont été dissous séparément dans 1 mL de tampon phosphate contenant 0.5% en volume de DMF (100 mM, pH 7.4). Le volume pertinent d'éq. molaire différent. d'ONOO<sup>-</sup> (0, 1, 2, 5 et 10 éq.) et un volume approprié de tampon phosphate (100 mM, pH 7.4) ont ensuite été rapidement ajoutés aux solutions de sonde pour atteindre une concentration finale de sonde de 10 µM dans du phosphate tampon contenant 0.5% en volume de DMF (100 mM, pH 7.4). La composition de la solution a été contrôlée par LC-MS. L'intensité de fluorescence de chaque échantillon a été immédiatement lue avec un lecteur de microplaques Cytation 5 (Biotek Instrument, VT) en utilisant les paramètres suivants:  $\lambda_{ex}/\lambda_{em}$  480/673 nm (FRET);  $\lambda_{ex}/\lambda_{em}$  480/519 nm (Fluorescéine);  $\lambda_{ex}/\lambda_{em}$  643/672 nm (AFDye<sub>647</sub>). Les spectres ont également été enregistrés  $\lambda_{ex}/\lambda_{em}$  480/499–800 nm;  $\lambda_{ex}/\lambda_{em}$  640/660–800 nm.

## 2.7 Réactivité de **5b**–CPP(Cy3) en présence de bactéries

*Escherichia coli* B (HER1024; obtenu du Centre de référence Félix d'Hérelle pour les virus bactériens, Université Laval, Québec) ont été cultivés dans du milieu Luria-Bertani (LB) à 37 °C (1 seule colonie dans 10 mL de LB). Le lendemain matin, la culture bactérienne a été diluée 1000 fois dans du milieu LB frais (c'est-à-dire 20 µL de culture dans 20 mL de LB). Les bactéries ont ensuite été cultivées jusqu'à la phase logarithmique (~4 h) à 37 °C sur un incubateur à agitation. La croissance a été contrôlée par densité optique à 600 nm jusqu'à ce qu'environ 0.5 soit atteint (environ ~5 × 10<sup>8</sup> cellules·mL<sup>-1</sup>). Les cellules ont ensuite été récoltées par centrifugation pendant

15 minutes à 5 000 tr/min, puis lavées avec 20 mL de solution saline tamponnée au phosphate de Dulbecco (DPBS) pH 7.4. Les cellules ont ensuite été exposées à 20 mL d'une solution 10  $\mu\text{M}$  de **5b**-CPP(Cy3) dans un tampon phosphate 100 mM pH 7.4 à 37 °C dans l'obscurité pendant 30 minutes. Les cellules ont été récupérées par centrifugation (15 min à 5000 rpm) et lavées avec du DPBS pour éliminer le bioconjugué extracellulaire. Les cellules bactériennes ont été mises en suspension dans 20 mL d'un tampon phosphate 100 mM et des aliquotes de 900  $\mu\text{L}$  ont été transférées dans quatre flacons Eppendorf, auxquels ont été ajoutés 100  $\mu\text{L}$  de 0, 5, 10 ou 50 mM de  $\text{H}_2\text{O}_2$  (la concentration finale de  $\text{H}_2\text{O}_2$  était 0  $\mu\text{M}$ , 500  $\mu\text{M}$ , 1 mM et 5 mM, respectivement). Ensuite, l'intensité de fluorescence de chaque échantillon a été contrôlée pendant 2 h à 37 °C avec un lecteur de microplaques ( $\lambda_{\text{ex}}/\lambda_{\text{em}}$  550/672 nm; 550/595 nm; 646/672 nm). Le niveau d'espèces réactives de l'oxygène induites par  $\text{H}_2\text{O}_2$  a été estimé en utilisant du  $\text{H}_2\text{DCFDA}$  10  $\mu\text{M}$  (1 mg dans 200  $\mu\text{L}$  de DMSO dilué 1000 fois dans du tampon phosphate 100 mM) au lieu de **5b**-CPP(Cy3) et l'intensité de fluorescence des échantillons a été contrôlée pendant 2 h à 37 °C avec un lecteur de microplaques ( $\lambda_{\text{ex}}/\lambda_{\text{em}}$  485/528 nm).

## 2.8 Exposition de **6d/7c** aux cellules

Des cellules RAW 264.7 et THP1 ont étéensemencées dans des plaques à 96 puits pour atteindre la population souhaitée de  $2 \times 10^5$  et  $5 \times 10^5$  cellules $\cdot\text{mL}^{-1}$ , respectivement. Après cela, ils ont été lavés avec une solution saline tamponnée au phosphate (1x, pH 7.2-7.4) et incubés avec une solution de 100  $\mu\text{L}$  contenant 10  $\mu\text{M}$  **6d** ou **7c**, tBHP (50  $\mu\text{M}$  et 250  $\mu\text{M}$ ) ou LPS (0, 10  $\mu\text{g} \cdot \text{mL}^{-1}$ ) dans une solution saline tamponnée au phosphate (1x, pH 7.2-7.4) contenant 2% v/v de FBS à 37 °C. L'intensité de fluorescence a été mesurée sur 2 h d'incubation par un lecteur de microplaques en utilisant les paramètres suivants :  $\lambda_{\text{ex}}/\lambda_{\text{em}}$  480/673 nm (FRET);  $\lambda_{\text{ex}}/\lambda_{\text{em}}$  480/519 nm (Fluorescéine);  $\lambda_{\text{ex}}/\lambda_{\text{em}}$  643/672 nm (AFDye<sub>647</sub>).

## 2.9 Traitements cellulaires bloquant les thiols par DTNB ou NEM

Le composé imperméable à la membrane 5,5'-dithio-bis-(acide 2-nitrobenzoïque) (DTNB) et le composé perméable à la membrane N-éthylmaléimide (NEM) ont été utilisés pour inactiver les groupes fonctionnels thiol cellulaires et évaluer l'impact du glutathion et des radicaux thiols sur la rupture de la liaison sulfure de vinyle sulfonium dans les cellules subissant un stress oxydatif. En conséquence, les cellules vivantesensemencées (cellules RAW 264.7 et THP-1) dans des plaques à 96 puits ont été lavées avec une solution saline tamponnée au phosphate (1 x, pH 7.2-7.4) pour éliminer le milieu. Chaque cellule contenant un puits a ensuite été incubée avec une solution **6d** ou **7c** (10  $\mu\text{L}$ , 0.1 mM) dans une solution saline tamponnée au phosphate (1 x, pH

7.2-7.4) contenant 5% en volume de DMF et 2% de FBS, une solution de NEM (10  $\mu\text{L}$ , 10 mM) ou solution DTNB (10  $\mu\text{L}$ , 25 mM) dans une solution saline tamponnée au phosphate (1 $\times$ , pH 7.2-7.4) contenant 2% de FBS, solution tBHP (10  $\mu\text{L}$  de 0, 0.5 et 2.5 mM) ou solution LPS (10  $\mu\text{L}$ , 0.1  $\text{mg}\cdot\text{mL}^{-1}$ ) de solution saline tamponnée au phosphate (1 $\times$ , pH 7.2-7.4) contenant 2% de FBS, et un volume approprié de solution saline tamponnée au phosphate (1 $\times$ , pH 7.2-7.4) contenant 2% FBS pour atteindre 100  $\mu\text{L}$  de solution par puits avec une concentration finale souhaitée de composés (10  $\mu\text{M}$  **6d** , 10  $\mu\text{M}$  **7c**, 1 mM NEM, 2.5 mM DTNB, 0, 50 ou 250  $\mu\text{M}$  tBHP et 0 ou 10  $\mu\text{g}\cdot\text{mL}^{-1}$  LPS). Il convient de mentionner que le pourcentage volumique final de DMF et de FBS était de 0.5% et 2% à chaque puits. Ensuite, l'intensité de fluorescence de chaque puits a été immédiatement mesurée pendant 2.5 h à 37 °C par un lecteur de microplaques ( $\lambda_{\text{ex}}/\lambda_{\text{em}}$  480/673 nm (FRET);  $\lambda_{\text{ex}}/\lambda_{\text{em}}$  480/519 nm (fluorescéine);  $\lambda_{\text{ex}}/\lambda_{\text{em}}$  643/672 nm (AFDye<sub>647</sub>)).

### 3. Résultats et discussion

#### 3.1 Alcyne déficient en électrons à base de peptides

L'alkylation sélective des résidus de méthionine dans les peptides/protéines est un outil courant en biologie chimique et enzymologie pour évaluer le rôle potentiel de ces résidus dans les événements de liaison et catalytiques.<sup>46</sup> Il est donc généralement considéré comme non destructeur de la structure des protéines et de l'intégrité des résidus autres que la méthionine exposée au solvant. En dessous de pH  $\sim$ 5, le thioéther de la méthionine est le seul groupe fonctionnel nucléophile sur les protéines et peut être sélectivement modifié avec des agents alkylants. Pour illustrer le potentiel de cette deuxième réaction à des fins de bioconjugaison, quatre modèles de peptides contenant de la méthionine ont été modifiés avec du bromure de propargyle pour produire des alcynes déficients en électrons (**Figure 2**). Pour tester des peptides avec différents groupes fonctionnels hydrophiles et pendants, le peptide modèle **1a** (592.71 Da) ainsi que **4a** (1084.25 Da) ont été choisis pour l'analyse. Des analogues de ces deux peptides portant différents fluorophores (Rhodamine, Rho; Cyanine 5, Cy5) à différents endroits ont également été testés pour évaluer la compatibilité avec les sondes optiques (**3a** et **5a** sur la **Figure 2a**).<sup>47,48</sup> La réaction entre le bromure de propargyle et ces peptides était quantitative et sélective vis-à-vis de la méthionine, et les peptides résultants ont été facilement isolés à partir de réactifs avec les poids moléculaires attendus (**Figure 2b**). L'oxydation préalable de la méthionine sur **1a** en **2a** a empêché l'alkylation, ce qui confirme en outre que la modification était sélective vis-à-vis de la méthionine (**Figure 2b**). Les adduits résultants **1b** et **4b** étaient stables au pH acide utilisé pour l'alkylation, bien que l'hydratation<sup>49</sup> and [2,3]-sigmatropic rearrangement<sup>50,51</sup> ont été observés lors d'une incubation prolongée à un pH proche de la neutralité (**1b** et **4b** sont restés

intacts à 40 et 70%, respectivement, après 15 h d'incubation; **Figure 2a,c**. Cette stabilité était tout à fait suffisante compte tenu de la vitesse de la réaction ultérieure (*vide infra*), et des différences de stabilité ont été attribuées à la séquence peptidique près de la méthionine qui peut influencer l'isomérisation alcyne/allène et l'accessibilité de l'alcyne déficient en électrons. Il est important de mentionner, cependant, que la stratégie proposée est la plus appropriée pour les peptides et les composés qui peuvent être manipulés/purifiés à un pH acide, ce qui empêche l'hydratation. En effet, alors qu'une tentative réussie a été faite pour alkyler le résidu méthionine du site actif de la protéine  $\alpha$ -chymotrypsine, la manipulation de la protéine alkylée à un pH proche de la neutralité pour la purification a conduit à l'hydratation de l'allène de sulfonium, comme en témoigne la spectrométrie de masse (données non présentées). Par conséquent, il est important de reconnaître cette limitation du présent concept, ou de prendre des précautions pour manipuler l'allène de sulfonium dans des conditions acides pour préserver son intégrité pour une réaction ultérieure avec des thiols (*vide infra*). En ce qui concerne les autres réactions secondaires, des travaux antérieurs ont montré que les modifications de l'allène avaient peu d'effet sur la vitesse ou l'efficacité du réarrangement [2,3]-sigmatropique.<sup>50</sup> Le remplacement du bromure de propargyle par du bromure de 2-butyrique a empêché l'isomérisation en un allène ainsi que les réactions ultérieures décrites ci-dessous et, par conséquent, les modifications au-delà de celles naturellement produites par la réaction du bromure de propargyle avec la méthionine n'ont pas été prises en compte dans cette étude.

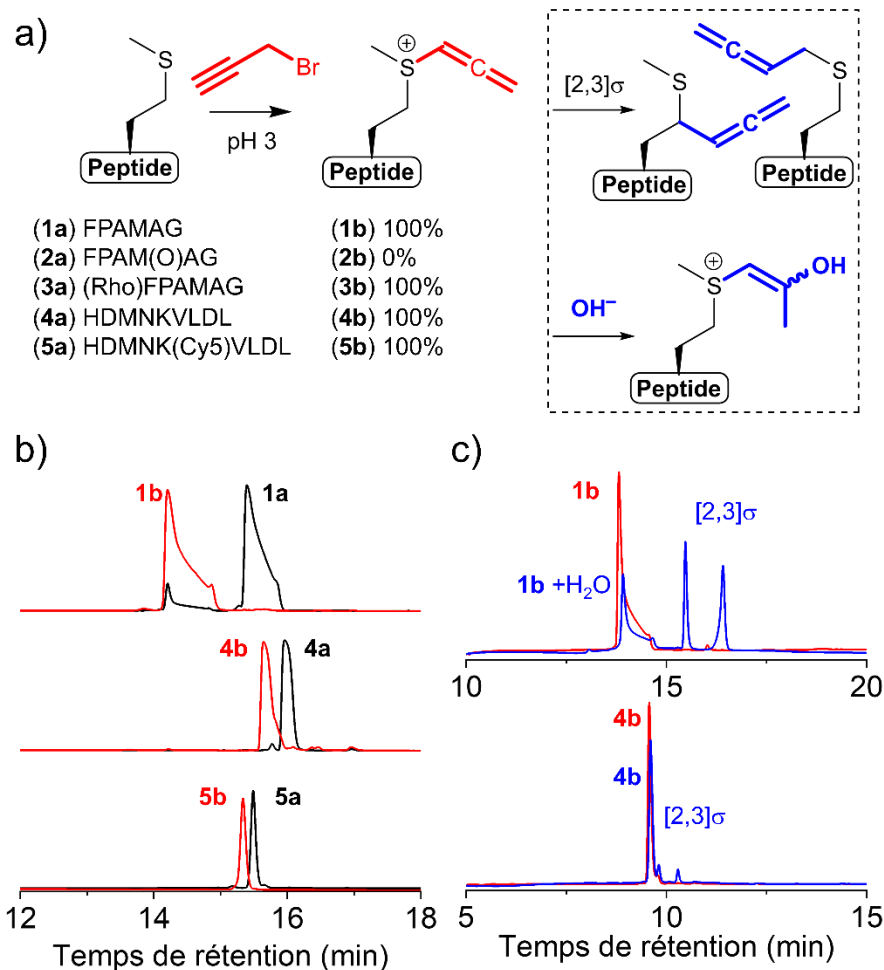


**Figure 2** Alkylation de peptides contenant de la méthionine. (a,b) La réaction du bromure de propargyle est sélective vis-à-vis du thioéther de méthionine en dessous de pH ~5 et se produit sans réactions secondaires. (a,c) L'incubation de l'adduit à pH neutre induit une isomérisation de l'alcyne en un allène, qui peut subir un réarrangement ou une hydratation [2,3]-sigmatropique lors d'une incubation prolongée. 1b est plus sensible à ces réactions que 4b.

### 3.2 Click – Ajout de thiol–allène nucléophile

Les quatre peptides alléniques ci-dessus ont été mis à réagir avec des thiols pour illustrer la portée de cette réaction dans le secteur biotechnologique. Ceux-ci comprenaient le  $\beta$ ME, le GSH, le mPEG–SH, la fluorescéine SAMSA déprotégée, l'albumine sérique humaine et le CPP(Cy3) pour couvrir des molécules avec une large gamme de poids moléculaires, de groupes fonctionnels et de propriétés physiques. Toutes les réactions se sont déroulées sans heurts à pH 7.4 et une conversion > 80% a généralement été obtenue en 1 à 2 h, en utilisant des quantités stoechiométriques de réactifs. La progression de la réaction a été surveillée par chromatographie

liquide-spectrométrie de masse et n'a révélé aucune réaction secondaire significative (**Figure 3a,b**).

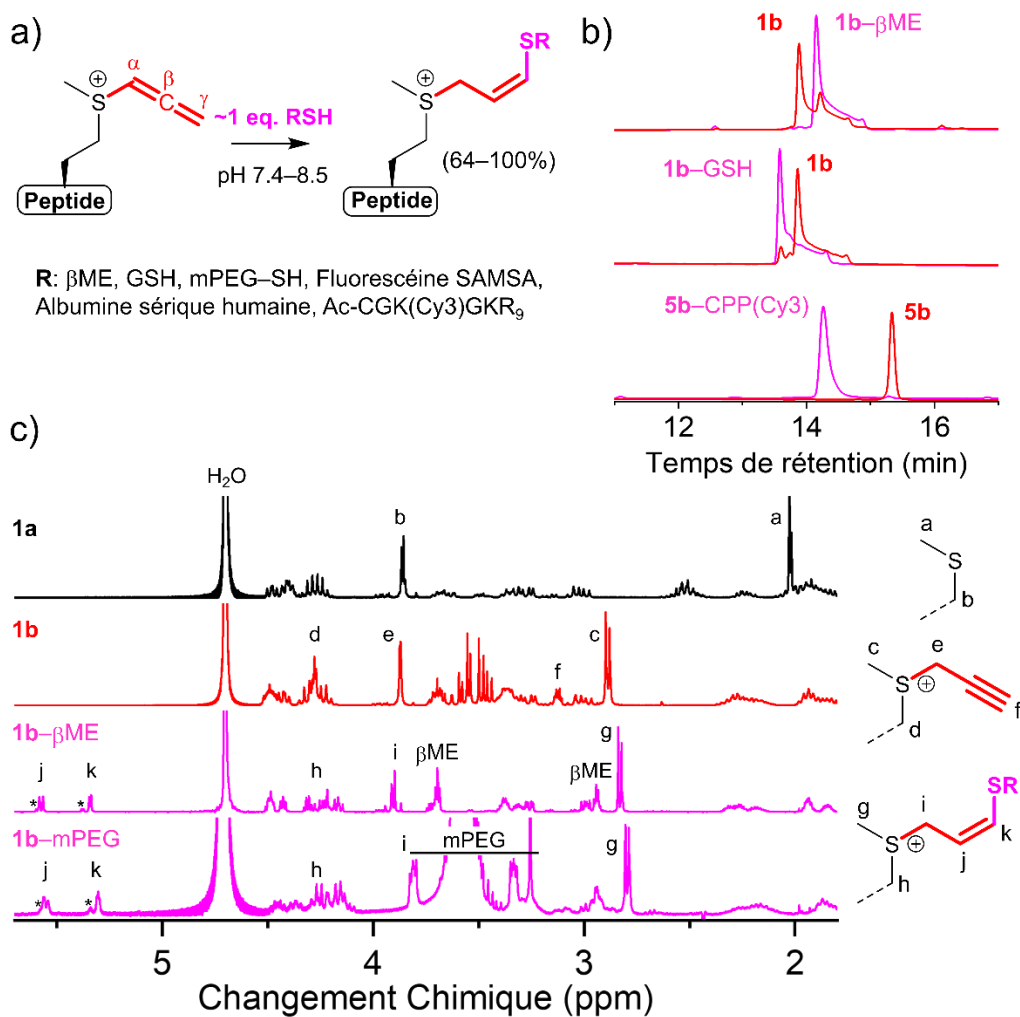


**Figure 3** Préparation de bioconjugué par addition de thiol-allène nucléophile Click. (a,b) Chromatogrammes représentatifs montrant que la réaction des peptides alléniques avec des thiols se déroule avec une conversion élevée et sans réaction secondaire. (c) Spectres RMN  $^1\text{H}$  attribués sélectionnés démontrant une conjugaison réussie à la chaîne latérale thioéther de la méthionine. Les pics mineurs annotés par "\*" représentent l'isomère trans du sulfure de vinyle sulfonium (structure non représentée).

Pour examiner la régiosélectivité de la réaction, la spectroscopie  $^1\text{H}$  NMR a été utilisée. Comme illustré à la **Figure 3c**, un ensemble de pics majeurs a été observé à  $\sim 5.5$  et  $\sim 5.3$  ppm pour le sulfure de vinyle sulfonium de **1b- $\beta$ ME** (sélectionné car il s'agit du conjugué le moins complexe sur le plan structural), aux côtés d'un autre ensemble de pics mineurs à  $\sim 5.6$  et  $\sim 5.4$  ppm représentant  $\sim 15\%$  du total. Pour évaluer la stabilité des conjugués formés, **1b-GSH**, **4b-GSH**

et **5b**–CPP(Cy3) ont été incubés dans 10 mM de GSH pH 7.4, ce qui imite la concentration en thiol de l'espace intracellulaire. En accord avec Kramer *et al.*,<sup>52</sup> l'incubation prolongée avec le nucléophile thiol (sous une atmosphère inerte) a conduit à une récupération très lente des peptides natifs, atteignant une conversion d'environ 20 à 30% après 1 jour (**Figure 4a,b**). Le mécanisme attendu de cette réaction implique l'addition nucléophile d'un thiol au carbone adjacent au sulfonium, et aucune réaction secondaire n'a été observée (**Figure 4b**). Fait intéressant, en raison de la nature fortement électrophile de l'ion sulfonium, cette réaction entraîne la libération des peptides entièrement non modifiés **1a**, **4a** et **5a** avec récupération du thioéther d'origine de la méthionine et aucune autre altération du peptide. Ainsi, cette stratégie de bioconjugaison est particulièrement intéressante pour libérer lentement les peptides natifs des bioconjugués en présence de thiols. Dans la cystéine 10 mM, la vitesse de libération de **1a** à partir de **1b**–GSH est restée lente, mais était plus rapide en raison du pKa de thiol inférieur de la cystéine par rapport au glutathion. Ces résultats sont intéressants car les concentrations physiologiquement pertinentes de thiols dans le sang sont inférieures d'environ trois ordres de grandeur (dans la gamme micromolaire), ce qui indique la stabilité à long terme de ces liaisons dans le sang. La modification de l'allène en position  $\gamma$  par réaction dans un tampon phosphate neutre semble donc bénéfique et nécessaire pour obtenir une libération lente de peptides par addition nucléophile de thiols (et d'autres processus Clip discutés dans la section suivante). Dans l'ensemble, la réaction intermoléculaire thiol-allène étudiée ici est régiosélective dans les conditions employées et une conversion quantitative peut être rapidement obtenue avec des quantités stoechiométriques de réactifs thiol facilement accessibles (y compris de petites molécules, des fluorophores, des peptides, des polymères et des protéines). De plus, l'adduit résultant est très stable, même vers des concentrations de thiols largement supérieures à celles trouvées dans le sang.

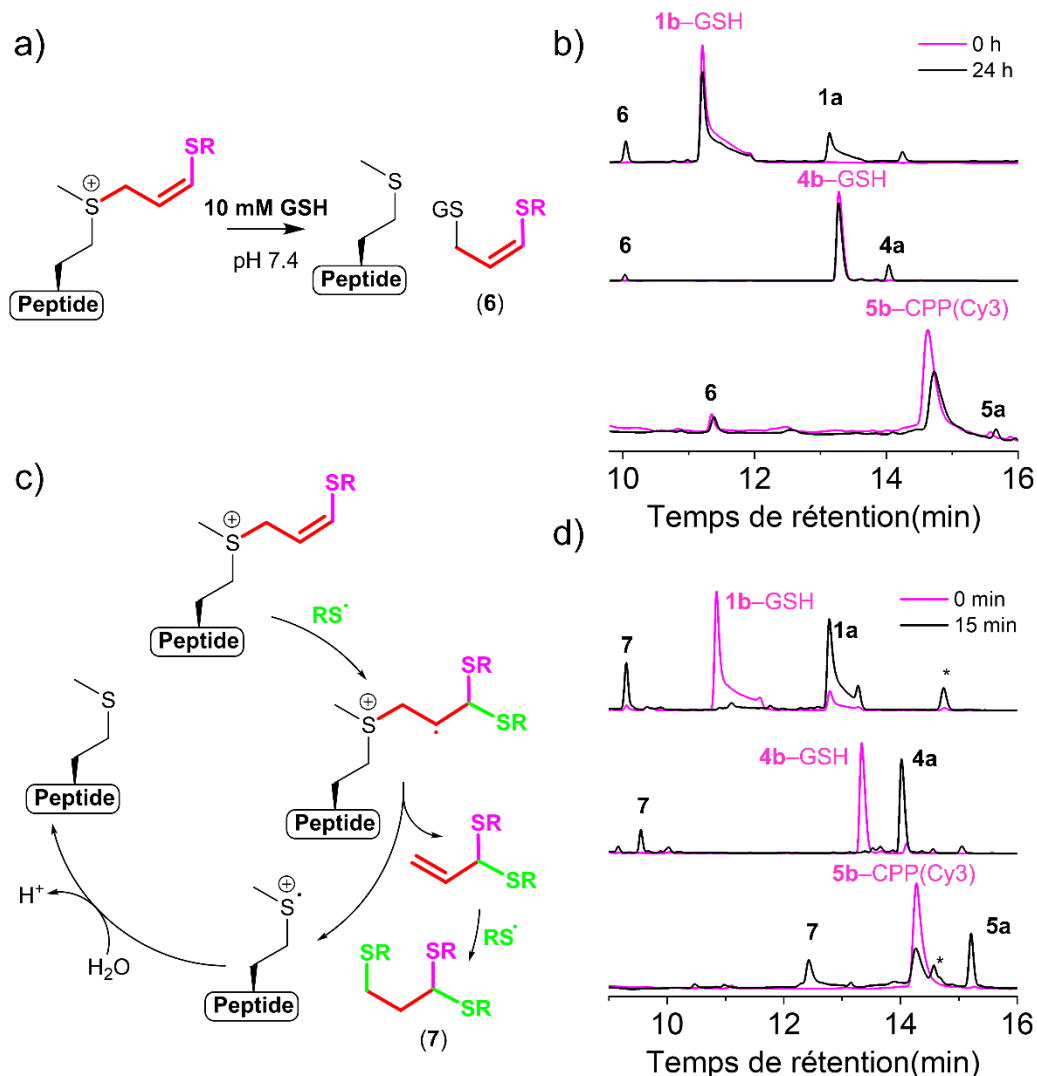


**Figure 4** Stabilité des bioconjugués vis-à-vis des nucléophiles et Clip des bioconjugués par addition radicalaire thiol-ène. (a) Les nucléophiles thiols peuvent réagir au niveau du carbone adjacent au sulfonium, libérant ainsi le thioéther d'origine de la méthionine. (b) Ce processus s'est produit lentement sans réactions secondaires, comme en témoignent les chromatogrammes représentatifs de trois bioconjugués. (c) Les radicaux thiyle induisent une réaction de fragmentation qui libère le thioéther d'origine de la méthionine en quelques minutes. (d) Ce processus s'est produit rapidement (<15 min) sans réactions secondaires, comme en témoignent les chromatogrammes représentatifs de trois bioconjugués. «\*» désigne les pics du générateur de photo-radicaux.

### 3.3 Clip – Addition radicalaire de thiol-ène

Compte tenu de la stabilité relative des adduits Click ci-dessus en présence de grandes quantités de thiols et pendant des périodes prolongées, une tentative exploratoire a été faite pour ajouter une deuxième molécule de thiol à trois bioconjugués de sulfure de vinyle sulfonium **1b-GSH**, **4b-GSH** et **5b-CPP(Cy3)** par addition radicalaire de thiol-ène, une autre réaction de Click bien connue.<sup>53</sup> Étonnamment, plutôt que d'observer l'ajout attendu d'un deuxième thiol, la dégradation

très rapide des conjugués **1b**-GSH, **4b**-GSH et **5b**-CPP(Cy3) a été observée parallèlement à la régénération du peptide original contenant de la méthionine, **1a**, **4a**, et **5a**, respectivement (**Figure 4c,d**). Cette réaction était très efficace (généralement 70 à 100% de conversion en 15 min), s'est déroulée dans un milieu aqueux neutre et s'est produite en présence de quantités presque stoechiométriques de thiol et d'une source de radicaux libres. Il est prévu que l'addition radicalaire de thiol-ène initie un processus de fragmentation semblable à celui rapporté pour les sels de sulfonium allylique, conformément au mécanisme connu pour la polymérisation cationique utilisant des sels de sulfonium allyl (**Figure 4c**).<sup>54</sup> En bref, le radical thiol s'ajoute au groupe vinyle et produit un cation radical instable qui se décompose en un thioéther (le peptide original contenant de la méthionine), un dithioacétal et un proton, dont les deux premiers sont observés par chromatographie (**Figure 4d**). Comme ce procédé est a priori compatible avec le maintien de la structure/fonction des biomolécules et de la fluorescence de Cy3/Cy5, il pourrait être utilisé pour diverses applications biotechnologiques. Bien que la stabilité aqueuse du dithioacétal n'ait pas été examinée plus avant dans ce travail, la libération à la fois des molécules de thiol et de l'acroléine devrait se produire lentement dans des conditions acides. La toxicité des sous-produits de la réaction Clip justifierait une enquête dans de futurs travaux *in vivo*.

Les radicaux thiyle sont hautement autoréactifs et donc de courte durée. Par conséquent, il va de soi que la formation de liaisons disulfure obtenue par auto-réactivité entrerait en compétition avec la réaction thiol-ène souhaitée et que cette compétition influencera fortement l'efficacité de la réaction Clip. En effet, il a été observé que la réaction Clip était plus efficace lors de l'augmentation de la concentration absolue du bioconjugué, du thiol et de la source radicalaire, pour favoriser la réaction radicalaire thiol-ène. De plus, la conversion de la réaction Clip n'a été influencée ni par le pH de l'environnement ni par la structure du radical thiyle, atteignant plus de > 90% de conversion en présence de différentes sources de thiol (GSH ou cystéine) à différents pH (6.5, 7.4, et 8.5) dans les 15 min. En revanche, lorsque les radicaux thiyle ont été produits beaucoup plus lentement, comme par exposition aux UV de H<sub>2</sub>O<sub>2</sub> (plutôt que le générateur de photo-radicaux DMPA) en présence de thiols, très peu de réaction a été observée (<6%). L'exposition des bioconjugués à H<sub>2</sub>O<sub>2</sub> seul dans l'obscurité ou sous exposition à la lumière UV pour générer des radicaux hydroxyles n'a pas affecté la stabilité du bioconjugué. À la lumière de ces résultats, il a été considéré que les radicaux thiyle générés naturellement dans l'espace intracellulaire des cellules lorsque les thiols récupèrent des espèces réactives à l'oxygène pourraient potentiellement initier la réaction thiol-ène Clip. Cependant, leur faible abondance attendue et leur courte durée de vie (ce qui rend leur concentration très difficile à évaluer) ainsi

que la forte concentration d'espèces thiol dans l'espace intracellulaire défavoriserait la réaction Clip par rapport à la formation de liaisons disulfure.

Pour obtenir des informations préliminaires sur la stabilité des liaisons de sulfure de vinyle sulfonium vis-à-vis des thiols et des radicaux thiyl d'origine biologique (à leurs concentrations naturelles), **5b**-CPP(Cy3) a été incubé avec *E. coli* subissant différents degrés de stress oxydatif (induit par l'incubation avec 0–5 mM H<sub>2</sub>O<sub>2</sub>). En effet, cette expérience a été réalisée pour compléter les données de stabilité obtenues dans les solutions modèles ci-dessus (par exemple, 10 mM de glutathion) en vue d'une utilisation future dans des applications biotechnologiques, et non spécifiquement conçues pour élucider l'implication des thiols ou des radicaux thiyl dans une réaction. En effet, la très faible abondance attendue des radicaux thiyl (même si leurs niveaux sont altérés par H<sub>2</sub>O<sub>2</sub>) ainsi que la forte concentration attendue en thiols intracellulaires (~20 mM dans le cas d'*E. coli*) défavorisent fortement par nature le radical thiyl- induit une réaction Clip sur la base d'arguments cinétiques, comme discuté ci-dessus. Comme illustré à la **Figure 5a,b**, la réaction Clip de cette sonde dans des conditions modèles a produit un clivage de 70% du bioconjugué parallèlement à une diminution correspondante d'environ 70% de l'intensité du signal de transfert d'énergie de fluorescence-résonance (FRET) entre Cy3/Cy5. Il a donc été considéré que l'intensité du FRET pouvait être utilisée pour surveiller l'intégrité du bioconjugué par spectroscopie dans des environnements complexes. En présence d'*E. coli*, le FRET est resté relativement constant au cours de la période de 2 h étudiée (diminution d'environ 25% du signal; **Figure 5c**) et ne dépendait pas beaucoup de l'exposition au H<sub>2</sub>O<sub>2</sub>. Ces résultats suggèrent que cette libération de 5a se produit très probablement par réaction avec des thiols nucléophiles, et non avec des radicaux thiyl. Cependant, compte tenu de la très faible abondance et de la courte durée de vie des espèces thiyl, ce qui les rend très difficiles à caractériser, ainsi que de la réactivité croisée des agents bloquants pour les radicaux thiols/thiyl, il n'a pas été possible d'ignorer complètement les implications des radicaux thiyl à cette étape. En fin de compte, la stabilité du sulfure de vinyle sulfonium reste très pertinente pour les expériences de marquage (temps d'exposition court) ainsi que pour les applications de délivrance intracellulaire de médicaments (libération sur des temps plus longs). Cependant, les travaux futurs devraient examiner la question non triviale de la caractérisation de l'emplacement et des espèces

impliquées dans la libération de peptides de méthionine à partir de bioconjugués de sulfure de vinyle sulfonium, qui dépend probablement de la structure du conjugué lui-même.

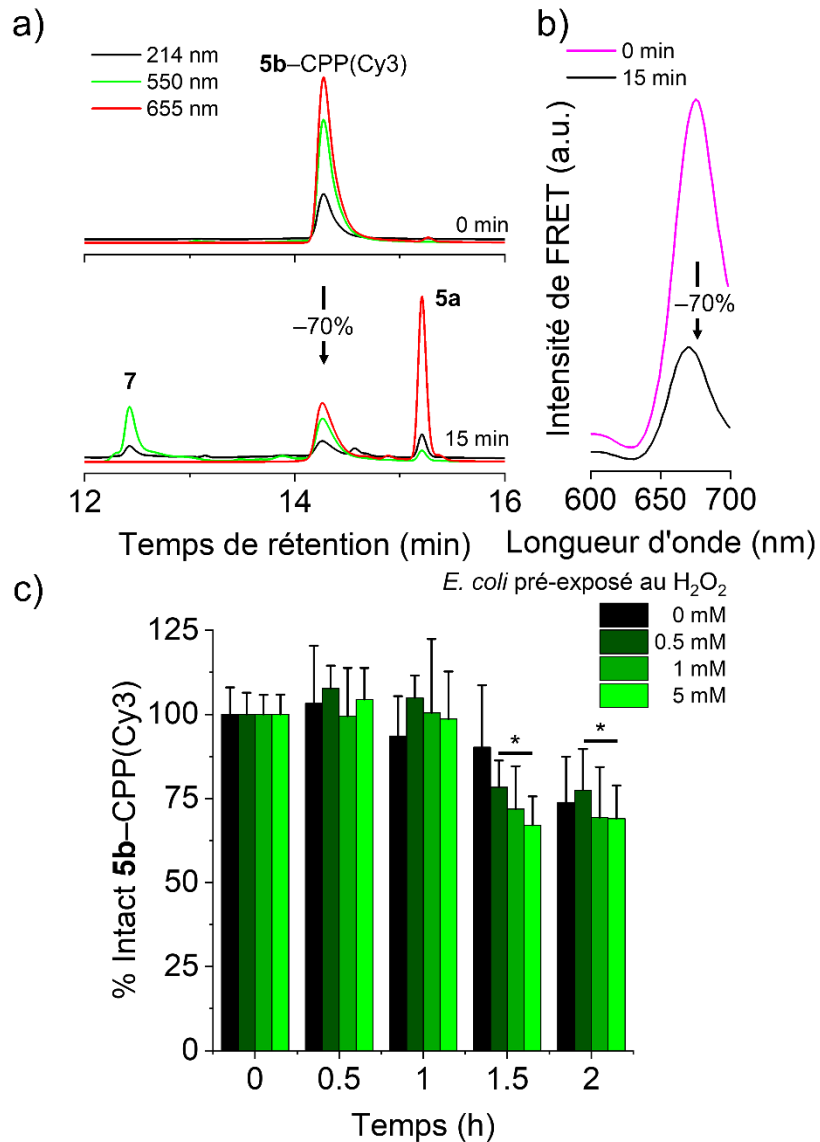
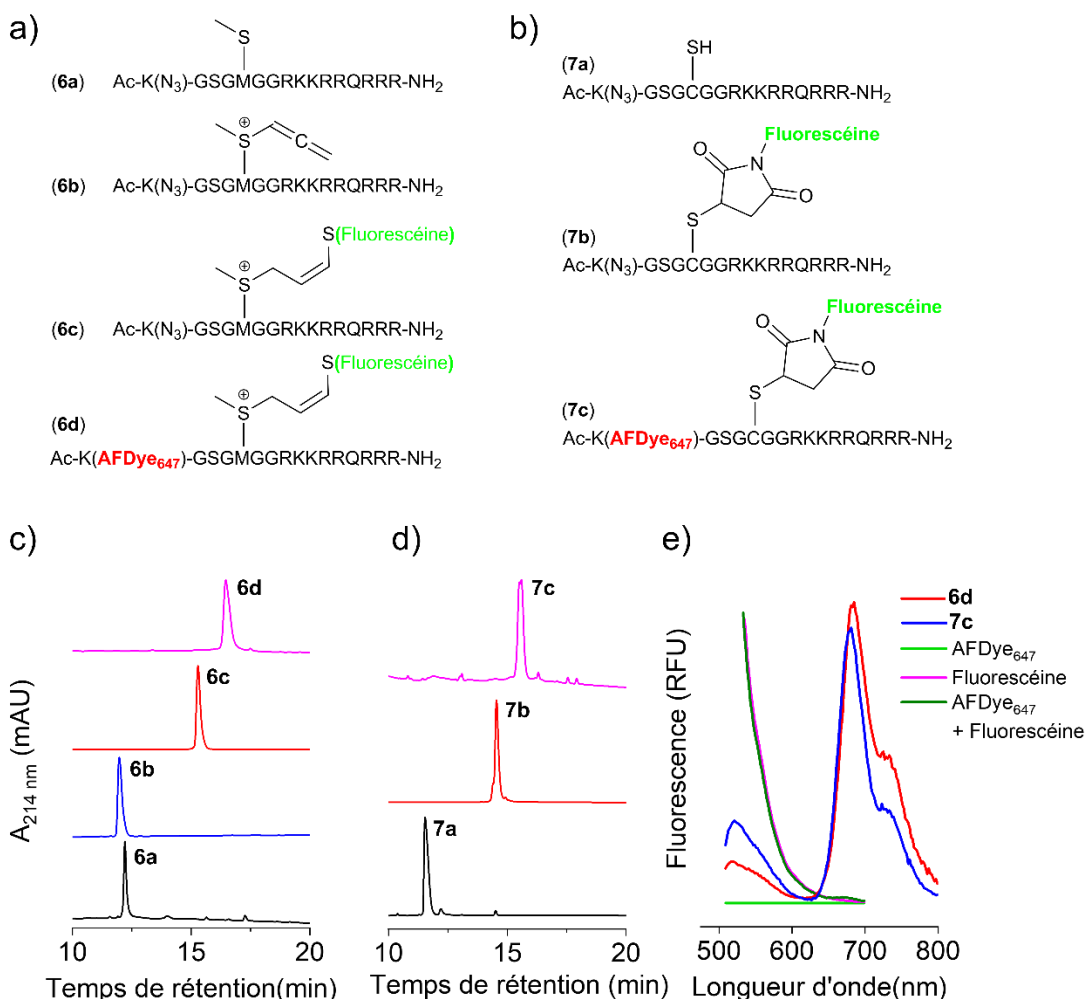


Figure 5

Stabilité d'un bioconjugué de sulfure de vinyle sulfonium en présence d'espèces réactives de cellules bactériennes. (a) L'exposition de 5b-CPP(Cy3) à des thiols radicaux produit une libération d'environ 70% du peptide 5a contenant de la méthionine. Chromatogrammes présentés à trois longueurs d'onde d'absorbance avant et après une réaction Clip de 15 minutes. (b) Clip s'est produit en même temps qu'une réduction d'environ 70% de l'intensité de FRET, illustrant que ce paramètre peut être utilisé pour suivre la stabilité du bioconjugué dans des environnements plus complexes. (c) L'incubation de 5b-CPP(Cy3) avec des cellules bactériennes subissant différents niveaux de stress oxydatif de H<sub>2</sub>O<sub>2</sub> produit très peu ou pas de changement de FRET sur une période d'une heure, avec quelques petites différences apparaissant à 1.5 h (Moyenne + SD, n = 3). "\*" indique une différence statistiquement significative par rapport à la valeur au temps zéro (ANOVA à mesures répétées, Tukey, p < 0.05).

### 3.4 Conception et synthèse de sondes FRET de sulfure de vinyle sulfonium et de contrôle

Afin de surveiller la stabilité des liaisons de sulfure de vinyle sulfonium en présence de cellules, une sonde à base de FRET a été conçue sur la base d'un peptide pénétrant dans les cellules, Tat<sub>49–57</sub>, prolongé sur son côté N-terminal avec une courte séquence peptidique contenant de l'azidolysine (pour la conjugaison du fluorophore accepteur AFDye<sub>647</sub> via la chimie Click sans cuivre) et un résidu méthionine. Cette séquence peptidique pénétrant dans les cellules a été choisie en faveur de la nona-arginine utilisée dans nos travaux précédents, en raison de la propension rapportée de cette dernière à l'auto-agrégation,<sup>55</sup> ce qui a compliqué les analyses ultérieures d'un point de vue technique. Pour préparer la sonde sensible (**6d**), le résidu méthionine du peptide (**6a**) a d'abord été alkylé en un allène sulfonium (**6b**) avec du bromure de propargyle dans des conditions acides, puis modifié avec le fluorophore donneur (fluorescéine SAMSA; déprotégé en sa forme thiol) par addition de thiol-allène nucléophile pour donner le peptide de sulfure de vinyle sulfonium fluorescent (**6c**). Par la suite, le fluorophore accepteur (DBCO–AFDye<sub>647</sub>) a été introduit sur le groupe azido du peptide par chimie Click sans cuivre pour donner **6d** (**Figure 6a,c**). Une sonde témoin (**7c**) contenant un thioéther plutôt qu'une liaison sulfure de vinyle sulfonium a été préparée par une approche similaire mais en remplaçant le résidu méthionine sur **6a** par une cystéine (**7a** sur la **Figure 6b,d**). Le groupe thiol sur ce peptide a été alkylé avec de la fluorescéine-5-maléimide pour produire une liaison thioéther stable (**7b**). De plus, les deux sondes présentaient des intensités similaires de FRET lors de l'excitation du fluorophore donneur ( $\lambda_{\text{ex}}/\lambda_{\text{em}}$  485/625–800 nm), ce qui n'était pas le cas pour une solution témoin constituée d'un mélange des fluorophores libres (**Figure 6e**).



**Figure 6** Sondes de sulfure de vinyle sulfonium et de thioéther à base de FRET. (a,b) Schéma de synthèse pour préparer 6d et 7c à partir du peptide 6a contenant de la méthionine et du peptide 7a contenant de la cystéine, respectivement. (c,d) Chromatogrammes représentatifs de composés purifiés. (e) Les spectres de fluorescence ( $\lambda_{ex}$  485 nm) démontrent FRET pour 6d et 7c, mais pas pour les mélanges des fluorophores individuels.

### 3.5 Réaction avec les thiols radicaux et les nucléophiles thiols

En accord avec nos travaux antérieurs, la liaison sulfure de vinyle sulfonium de 6d était très stable en présence de thiols lors d'une incubation prolongée dans des conditions imitant le cytosol (c'est-à-dire 10 mM de glutathion, pH 7.4). Comme illustré sur la **Figure 7a**, 6d est resté >92% intact sur 24 h, sur la base de l'intégration du pic du conjugué d'origine. Au cours de cette période, l'addition nucléophile lente de glutathion au carbone adjacent au sulfonium en 6d a produit un fragment peptidique avec la récupération du résidu méthionine d'origine (6e) ainsi qu'un adduit fluorescent de glutathion (6f), sans réactions secondaires. Pour valider la réactivité du sulfure de vinyle sulfonium 6d vis-à-vis d'une réaction radical thiol-ène Clip (avec un effet simultané sur l'intensité du signal FRET), 6d ont été mis à réagir avec des thiols radicaux générés à partir de

10 éq. de glutathion et 1.5 éq. d'amorceur photoradicalaire dans un tampon phosphate neutre. Le schéma de la réaction est présenté sur la **Figure 7b**. Les résultats présentés à la **Figure 7c** illustrent qu'après une exposition de 15 minutes à la lumière ultraviolette à 366 nm, ~60% du sulfure de vinyle sulfonium fragmenté pour libérer le peptide modifié AFDye<sub>647</sub> (**6e**, avec le résidu de méthionine d'origine intact) aux côtés d'un autre adduit fluorescent de glutathion (**6g**). De plus, l'intensité du signal FRET a chuté d'environ 60% avec cette transformation (**Figure 7d**), indiquant que ce paramètre peut être utilisé pour surveiller quantitativement la stabilité de la liaison sulfure de vinyle sulfonium dans la culture cellulaire. En parallèle, une augmentation d'environ 350% de l'intensité de fluorescence du canal fluorescéine ( $\lambda_{ex}/\lambda_{em}$  480/519 nm) a été observée sur la même période en raison de l'arrêt du FRET. L'intensité de fluorescence du canal AFDye<sub>647</sub> ( $\lambda_{ex}/\lambda_{em}$  643/672 nm) n'a pas changé significativement par rapport à sa valeur initiale.

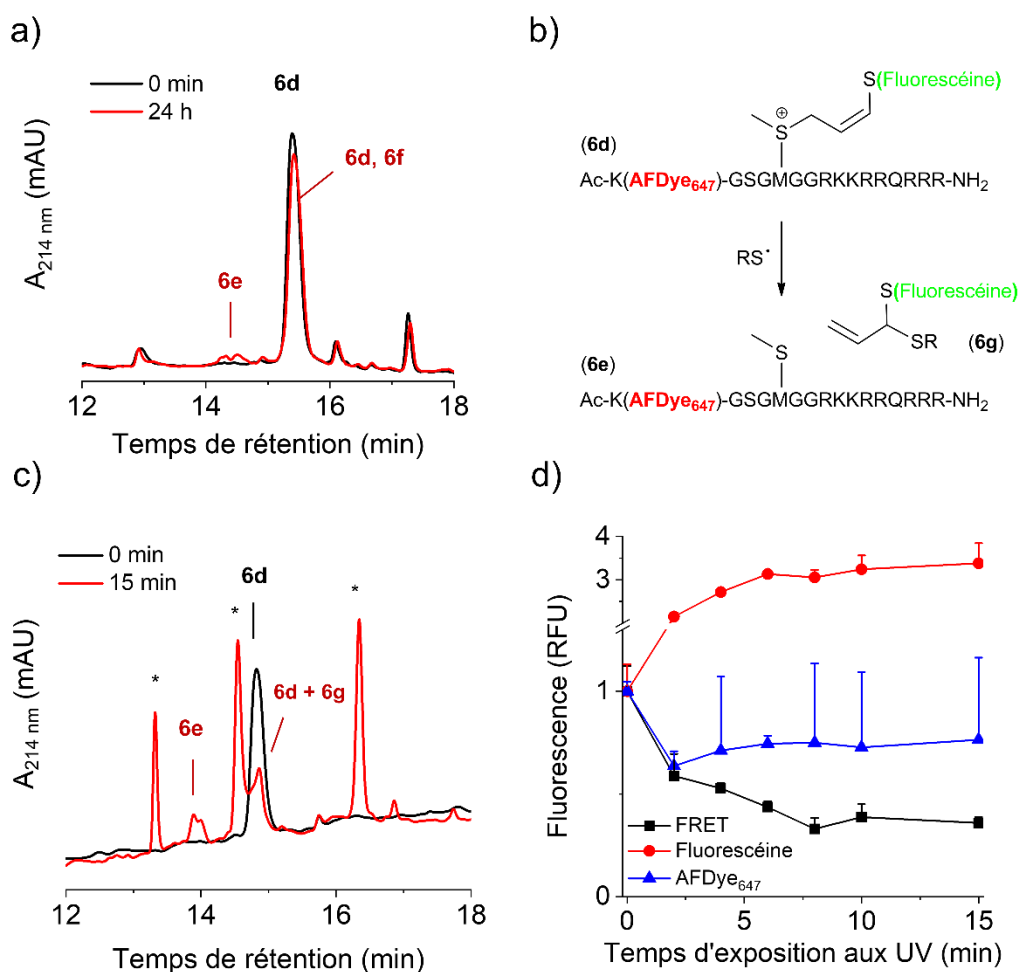


**Figure 7** Réaction avec les thiols radicaux et les nucléophiles thiols. (a) Chromatogramme illustrant la stabilité de 6d/7c dans du GSH 10 mM sur 24 h. (b) Schéma illustrant les produits formés par réaction de 6d avec un radical thiol. (c,d) Chromatogramme illustratif et évolution des propriétés optiques du 6d exposé aux thiols radicaux. Les données dans le volet d sont présentées sous la forme Moyenne + SD (n = 3). \*\*\* désigne les pics du générateur de photo-radicaux.

### 3.6 La nitration au peroxy-nitrite ( $\text{ONOO}^-$ ) comme modèle RNS

Pour évaluer la réactivité des sulfures de vinyle de sulfonium vis-à-vis du RNS, **6d** et **7c** ont été incubés avec 0 à 5 éq. de peroxy-nitrite. Comme illustré sur les **Figures 8a,c**, **7c** est resté relativement stable en présence de jusqu'à 2 éq. peroxy-nitrite, comme en témoigne seulement un petit changement dans le chromatogramme et les signaux fluorescents (canal FRET et canaux des deux fluorophores). Curieusement, lorsque **6d** a été exposé jusqu'à 2 éq. peroxy-nitrite, l'intensité du signal FRET a augmenté de 160% et s'est également accompagnée d'une augmentation de 350% de l'intensité du canal fluoresceine (**Figure 8b,d**). Lors de l'exposition à

une éq. molaire plus élevée de peroxy-nitrite (5 et 10 éq.), une dégradation substantielle de **6d** et **7c** a été observée par chromatographie ainsi que par une diminution de tous les signaux fluorescents (FRET et fluorophores individuels). De plus, le peroxy-nitrite peut conduire à l'hydroxynitrosylation du sulfure de vinyle sulfonium. En tant que tel, l'augmentation de la fluorescence observée pour **6d** (canaux fluorescéine et FRET) lors de l'hydroxynitrosylation du sulfure de vinyle sulfonium peut être attribuée à un changement de structure chimique et de polarité locale près de la fluorescéine. Comme ce processus se produit plus rapidement que la dégradation de l'un ou l'autre des fluorophores, la sonde **6d** présente d'abord une augmentation de la fluorescence due à ce phénomène et est suivie d'une diminution en présence de quantités plus élevées de peroxy-nitrite. Dans l'ensemble, en raison de la stabilité de **6d** en présence de niveaux biologiquement pertinents de ROS pour la durée de l'expérience, ce système de sonde est très intéressant pour caractériser la compétition entre les thiols radicaux et le RNS dans un milieu biologique complexe - quelque chose qui est difficile à accomplir - en raison des changements orthogonaux de ses propriétés de fluorescence résultant de la réaction avec l'une ou l'autre des espèces.

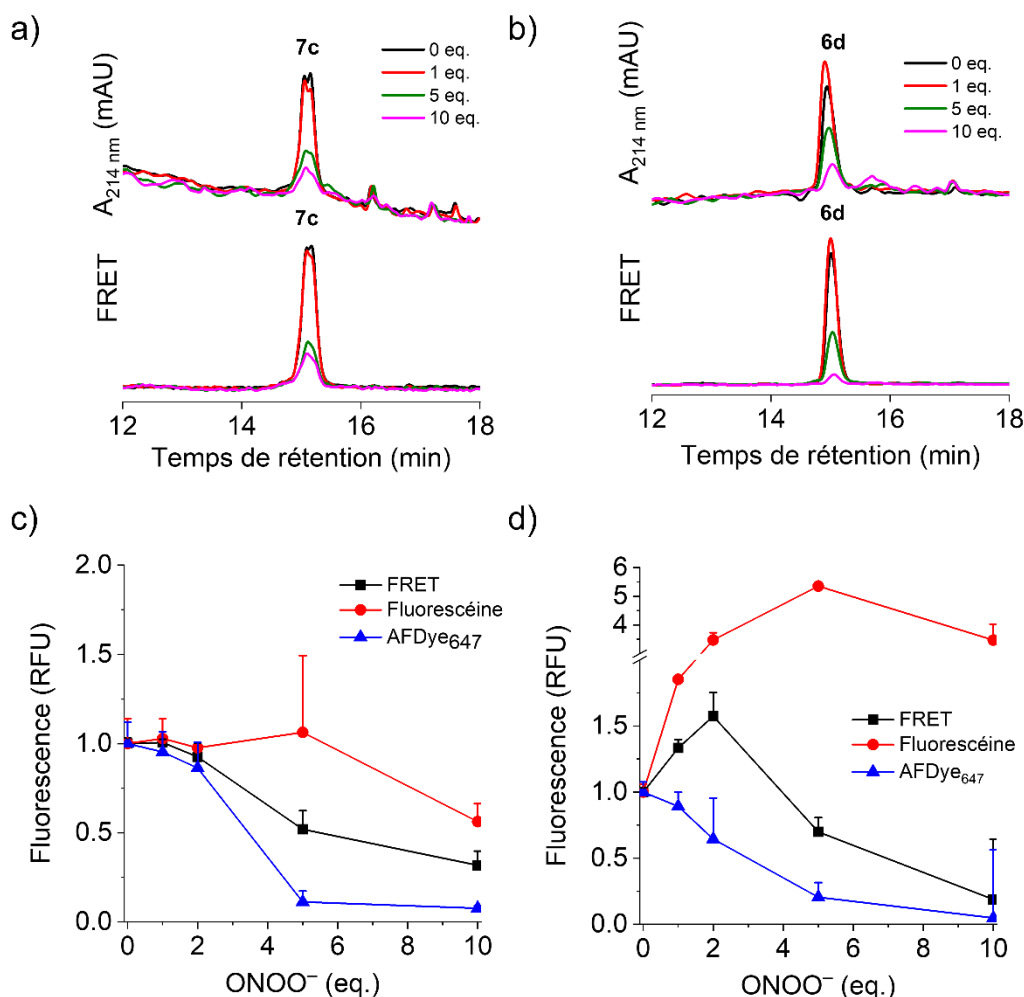


**Figure 8** Stabilité de 7c/6d en présence de peroxy-nitrite. (a,c) 7c est stable vers ~2 eq. de peroxy-nitrite, au-dessus duquel on observe une perte d'intensité de fluorescence. (b,d) L'exposition de 6d au peroxy-nitrite conduit d'abord à une augmentation de l'intensité de la fluorescéine et du FRET, puis à une diminution ultérieure. Pour les volets c et d, les valeurs sont données sous la forme Mean + SD (n = 3).

### 3.7 Réactivité des sulfures de vinyle sulfonium dans des modèles de culture cellulaire de stress oxydatif

Pour évaluer la compétition RNS et les thiols radicaux pour les liaisons de sulfure de vinyle sulfonium en culture cellulaire, des macrophages permanents de souris RAW 264.7 et des lignées cellulaires monocytes humaines adhérentes THP-1 ont été choisis comme modèles *in vitro*. Pour modifier la quantité d'espèces réactives naturellement générées par ces cellules, les cultures ont été exposées à l'hydroperoxyde de tert-butyle ROS (tBHP) et au lipopolysaccharide (LPS), un composant de la paroi cellulaire des bactéries gram-négatives. Pour caractériser le stress oxydatif, les niveaux de ROS ont été quantifiés à l'aide de H<sub>2</sub>DCFDA, et la concentration de thiols

intracellulaires a été mesurée à l'aide de thiol tracker violet, à la fois en fonction de la concentration de tBHP/LPS et du temps. En général, l'exposition des deux lignées cellulaires aux facteurs de stress a entraîné une augmentation de la concentration de ROS en fonction de la concentration et du temps, et un effet plus spectaculaire a été observé pour le tBHP, probablement car il s'agit lui-même d'un ROS. Parallèlement, une réduction de la concentration de thiols intracellulaires a été observée pour les deux lignées cellulaires après une exposition de deux heures aux facteurs de stress.

Le sulfure de vinyle sulfonium **6d** et le thioéther **7c** ont été ajoutés aux cellules à une concentration minimalement cytotoxique et les modifications de l'intensité de FRET et des canaux fluorophores individuels ont été surveillées avec le temps (**Figure 9**). Comme prévu, le signal FRET de la sonde thioéther **7c** est resté constant au cours de l'expérience de 150 minutes, indiquant la stabilité de la sonde peptidique et de ses constituants. En revanche, le signal FRET de **6d** a augmenté avec le temps pour atteindre un plateau à ~200% de sa valeur initiale sur une période de ~2 h, ce qui suggère une hydroxynitration du sulfure de vinyle sulfonium par RNS. Très peu ou pas d'effet du LPS ou du tBHP sur la cinétique d'augmentation de la fluorescence a été observé, ce qui, en combinaison avec les données des sections précédentes, suggère que les ROS ne sont pas impliqués dans les changements affectant **7c** (ou au plus contribuent dans une moindre mesure). De plus, l'ajout de DTNB et de NEM pour bloquer les thiols extracellulaires et totaux, respectivement, n'a pas non plus eu un grand effet sur la cinétique de l'évolution du signal FRET à partir de **6d**, indiquant l'absence (ou tout au plus minime) de participation des thiols ou RSS dans les changements affectant **6d**, sur la courte période de l'expérience (**Figure 9**). Néanmoins, le signal plateau FRET atteint en présence de NEM était plus faible que pour les autres expériences, suggérant le piégeage d'espèces radicalaires par ce dernier. Des résultats similaires ont été observés pour les deux lignées cellulaires et seules de modestes différences de cinétique ont été observées. Ainsi, l'analyse globale des résultats ci-dessus indique que l'hydroxynitration du sulfure de vinyle sulfonium surpasse les autres réactions, en particulier la réaction radicale thiol-ène Clip qui conduirait à la libération de **6a** à partir de **6d**.

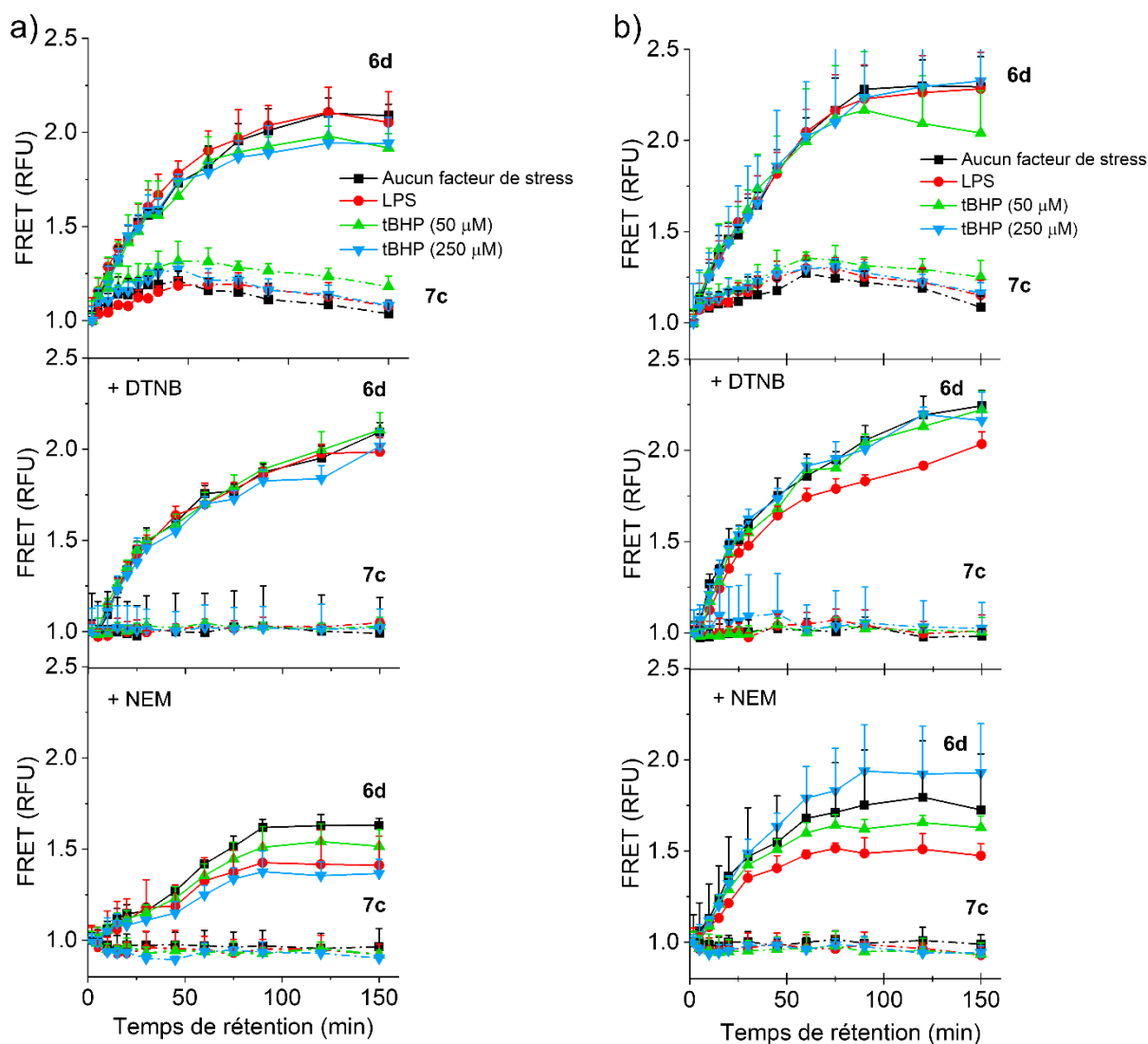


**Figure 9** Réactivité des sulfures de vinyle sulfonium en culture cellulaire. Évolution du signal FRET de 6d/7c en présence de cellules RAW 264.7 (a) et THP-1 (b) exposées à différents stresseurs et agents d'extinction thiol. Données présentées sous forme de moyenne + SD (n = 3).

#### 4. Conclusion et perspectives

Ce travail a présenté une combinaison de deux réactions bien connues qui obéissent à la plupart des critères de la chimie Click et qui pourraient de manière inattendue être utilisées pour préparer et désassembler des bioconjugués de manière Click/Clip. À la suite de la réaction Click, une liaison sulfure de vinyle sulfonium a été générée en tant que liaison dans une variété de bioconjugaisons à base de peptides contenant des résidus de méthionine sans réactions secondaires et processus nocifs pour les fluorophores de différentes familles. Fait intéressant, les liaisons sulfure de vinyle sulfonium ont subi une réaction radicale thiol-ène Clip en quelques

minutes en présence de radicaux thiyle, entraînant la dissociation du lieu qui a conduit à la libération du peptide original contenant de la méthionine avec récupération complète de sa chaîne latérale thioéther et sans réactions secondaires. Compte tenu de la commodité de cette stratégie Click/Clip, du caractère facilement accessible des réactifs/réactifs et de la pertinence biologique de ces derniers, ce concept trouve de nombreuses applications dans le secteur biotechnologique. Cette étude a également indiqué la réactivité des lieux de sulfure de vinyle sulfonium vis-à-vis des niveaux physiologiquement pertinents d'autres espèces réactives, notamment le peroxyne (un modèle de RNS),  $H_2O_2$  et  $\cdot OH$  (modèles de ROS) et les thiols nucléophiles (modèle de RSS). Nos lieux présentés présentaient une grande stabilité vis-à-vis des modèles de ROS. Cependant, ils répondent aux thiols nucléophiles (heures/jours), aux thiols radicalaires (minutes) et aux espèces azotées réactives (RNS; minutes) dans des conditions modèles conduisant à la libération d'un peptide contenant de la méthionine dans les deux premiers cas et à l'hydroxynitration dans les deux cas. Le troisième cas. La facilité de synthèse et la réactivité combinées aux thiols radicalaires, RNS, thiols nucléophiles, dans différentes conditions, font des sulfures de vinyle sulfonium de nouveaux groupes fonctionnels polyvalents pour créer des entités réactives et biodégradables.

# TABLE OF CONTENTS

---

<b>ACKNOWLEDGEMENTS</b> .....	<b>III</b>
<b>FOREWORD</b> .....	<b>IV</b>
<b>RÉSUMÉ</b> .....	<b>VII</b>
<b>ABSTRACT</b> .....	<b>IX</b>
<b>SYNOPSIS IN FRENCH</b> .....	<b>XI</b>
<b>TABLE OF CONTENTS</b> .....	<b>XXXVIII</b>
<b>LIST OF TABLES</b> .....	<b>XLI</b>
<b>LIST OF FIGURES</b> .....	<b>XLIII</b>
<b>LIST OF EQUATIONS</b> .....	<b>XLIX</b>
<b>LIST OF ACRONYMS AND ABBREVIATION</b> .....	<b>LI</b>
<b>1 INTRODUCTION</b> .....	<b>1</b>
1.1 OVERVIEW OF REDOX-RESPONSIVE SYSTEMS FOR THERAPEUTIC, DIAGNOSTIC, AND THERANOSTIC APPLICATIONS.....	1
1.1.1 <i>Reduction-responsive chemical bonds</i> .....	3
1.1.2 <i>Oxidation-responsive chemical bonds and materials</i> .....	4
1.2 PATHOPHYSIOLOGICAL EVENTS OF ENDOGENOUS REACTIVE SPECIES.....	5
1.2.1 <i>Reactive Oxygen Species (ROS)</i> .....	6
1.2.2 <i>Reactive Nitrogen Species (RNS)</i> .....	10
1.2.3 <i>Reactive Sulfur Species (RSS)</i> .....	13
1.3 ENDOGENOUS REACTIVE SPECIES-RESPONSIVE CHEMICAL BONDS AND MATERIALS FOR VARIOUS BIOMEDICAL APPLICATIONS.....	16
1.3.1 <i>RONS-responsive chemical bonds and materials</i> .....	16
1.3.2 <i>RS-responsive chemical bonds and materials</i> .....	44
1.4 CONCLUSION AND OUTLOOK.....	49
1.5 RESEARCH OBJECTIVES .....	51
1.6 STRUCTURE OF THE THESIS .....	52
<b>2 ARTICLE 1</b> .....	<b>55</b>
2.1 INTRODUCTION .....	57
2.2 MATERIALS AND METHODS.....	59
2.2.1 <i>Materials</i> .....	59
2.2.2 <i>Equipment</i> .....	60
2.2.3 <i>Preparation of sulfoxide FPAM(O)AG (2a)</i> .....	61

2.2.4	<i>Preparation of fluorescent peptide (Rho)FPAMAG (3a)</i> .....	61
2.2.5	<i>Alkylation of methionine-containing peptides</i> .....	61
2.2.6	<i>Click by nucleophilic thiol–allene addition with cysteine, peptide thiols, SAMSA fluorescein, and mPEG–SH</i> .....	62
2.2.7	<i>Click by nucleophilic thiol–allene addition with human serum albumin</i> .....	62
2.2.8	<i>Stability towards nucleophilic substitution</i> .....	62
2.2.9	<i>Clip by radical thiol–ene addition</i> .....	63
2.2.10	<i>Stability of bioconjugates to H<sub>2</sub>O<sub>2</sub> and UV light</i> .....	63
2.2.11	<i>Responsiveness of 5b–CPP(Cy3) in the presence of bacteria</i> .....	63
2.3	RESULTS AND DISCUSSION.....	64
2.3.1	<i>Peptide-based electron-deficient alkyne</i> .....	64
2.3.2	<i>Click – Nucleophilic thiol–allene addition</i> .....	66
2.3.3	<i>Clip – Radical thiol–ene addition</i> .....	71
2.4	CONCLUSIONS.....	74
<b>3</b>	<b>ARTICLE 2</b> .....	<b>75</b>
3.1	INTRODUCTION .....	76
3.2	MATERIALS AND METHODS.....	77
3.2.1	<i>Materials</i> .....	77
3.2.2	<i>Equipment</i> .....	78
3.2.3	<i>Preparation of the sulfonium vinyl sulfide probe (1d)</i> .....	78
3.2.4	<i>Preparation of the control probe (2c)</i> .....	79
3.2.5	<i>Stability towards nucleophilic substitution</i> .....	79
3.2.6	<i>Clip by radical thiol–ene addition</i> .....	80
3.2.7	<i>Peroxynitrite solution preparation</i> .....	80
3.2.8	<i>Stability in the presence of peroxynitrite</i> .....	80
3.2.9	<i>The effect of peroxynitrite on fluorophores</i> .....	81
3.2.10	<i>The effect of peroxynitrite on 1d and 2c</i> .....	81
3.2.11	<i>Cell culture preparation</i> .....	81
3.2.12	<i>Cellular ROS Assay</i> .....	82
3.2.13	<i>Cellular Thiol assay</i> .....	82
3.2.14	<i>Exposure of 1d/2c to cells</i> .....	83
3.2.15	<i>Cellular thiol blocking treatments by DTNB or NEM</i> .....	83
3.2.16	<i>Cell viability assay</i> .....	83
3.3	RESULTS AND DISCUSSION.....	84
3.3.1	<i>Design and synthesis of sulfonium vinyl sulfide and control FRET probes</i> .....	84
3.3.2	<i>Reaction with radical thiols and thiol nucleophiles</i> .....	85
3.3.3	<i>Nitration with peroxynitrite (ONOO<sup>-</sup>) as a model RNS</i> .....	87

3.3.4	<i>Reactivity of sulfonium vinyl sulfides in cell culture models of oxidative stress</i> .....	89
3.4	DISCUSSION.....	91
3.5	CONCLUSIONS.....	92
<b>4</b>	<b>GENERAL DISCUSSION, CONCLUSION, AND PERSPECTIVES</b> .....	<b>95</b>
4.1	THE MOST SIGNIFICANT ACHIEVEMENT OF THIS THESIS.....	95
4.2	THE MOST SIGNIFICANT LIMITATION OF THIS WORK.....	98
4.3	HOW THIS WORK IS DIFFERENT FROM THE WORK OF OTHERS.....	98
4.4	WHAT IS LEFT TO BE DONE (FUTURE PERSPECTIVES) .....	99
4.5	HOW WILL THIS WORK BENEFIT SOCIETY? .....	100
<b>5</b>	<b>BIBLIOGRAPHIE</b> .....	<b>101</b>
<b>6</b>	<b>APPENDIX</b> .....	<b>140</b>
6.1	APPENDIX I: SUPPLEMENTARY INFORMATION OF ARTICLE 1 .....	140
6.2	APPENDIX II: SUPPLEMENTARY INFORMATION OF ARTICLE 2 .....	163
6.3	APPENDIX III: LETTERS OF COPYRIGHT PERMISSION .....	181

## LIST OF TABLES

TABLE 1.1	ENDOGENOUS REACTIVE SPECIES (RONSSS) INVOLVED IN MULTIPLE PATHOPHYSIOLOGICAL PROCESSES .....	5
-----------	--	---



## LIST OF FIGURES

- FIGURE 1.1 EQUILIBRIA OF MAJOR BIOLOGICAL REACTIVE SPECIES DISCUSSED IN THIS CONTRIBUTION. ALL ENDOGENOUS REACTIVE SPECIES, INCLUDING ROS, RNS, AND RSS, EXIST IN COMPLEX EQUILIBRIA WITH ONE ANOTHER TO REGULATE VARIOUS BIOLOGICAL EVENTS. DYSREGULATION OF ANY OF THE EQUILIBRIA MAY AFFECT THE OTHER AND RESULT IN CAUSING MULTIPLE PATHOPHYSIOLOGICAL PROCESSES LINKED TO SEVERAL DISEASES. .... 6
- FIGURE 1.2 THE OXIDATION/REDUCTION REACTIONS OF GS<sup>•</sup>, AS A THIOL RADICAL, IN BIOLOGICAL SYSTEMS..... 15
- FIGURE 1.3 PTX NANOCRYSTALS WERE COATED WITH ROS-RESPONSIVE POLYMERIC STABILIZERS CONTAINING THIOETHER BONDS. IN THE PRESENCE OF ROS, THIOETHER BONDS OF STABILIZER UNDERWENT OXIDATION, LEADING TO DESORPTION OF STABILIZERS FROM THE SURFACE OF NANOCRYSTALS AND RESULTED IN DESTABILIZATION AND ALTERING SIZE DISTRIBUTION FOR PROMOTING CELLULAR UPTAKE OF THE NANOCRYSTALS..... 17
- FIGURE 1.4 (A) SCHEMATIC ILLUSTRATION OF A FLUORESCENT PROBE AND RESPONSIVENESS TOWARD <sup>-</sup>OCL. (B) FLUORESCENCE SPECTRA OF THE PROBE IN THE PRESENCE OF VARIOUS ROS AND BIOLOGICALLY RELEVANT ANALYTES: PBS, 100 MM <sup>-</sup>OCL AND 1 MM OF <sup>•</sup>OH, H<sub>2</sub>O<sub>2</sub>, HNO, T-BUOO<sup>•</sup>, O<sub>2</sub><sup>-</sup>, ONOO<sup>-</sup>, GSH, Cys, Hcy, AND DTT. .... 19
- FIGURE 1.5 SCHEMATIC ILLUSTRATION OF AN AMPHIPHILIC ALIPHATIC POLYCARBONATE CONTAINING SELENIUM FOR OXIDATION-RESPONSIVE DRUG DELIVERY VEHICLE. IN RESPONSE TO 100 MM H<sub>2</sub>O<sub>2</sub>, THE OXIDATION OF SELENIUM GROUPS IN THE BACKBONE OF POLYCARBONATE UNDERWENT OXIDATION, LEADING TO HYDROPHOBIC-HYDROPHILIC TRANSITION OF NANOPARTICLES AND RESULTED IN THE RELEASE OF LOADED DOX. .... 20
- FIGURE 1.6 THE PHOTSENSITIVE TELLURIUM-CONTAINING MULTILAYER FILM WAS STRUCTURED BY UTILIZING TELLURIUM-CONTAINING MICELLES, PHOTSENSITIZER, AND POLYSTYRENE SULFONATE AS BUILDING BLOCKS. UNDER VISIBLE LIGHT, TELLURIUM WAS OXIDIZED TO Te=O BY EXPOSURE TO GENERATED <sup>1</sup>O<sub>2</sub>. Te=O INCREASED THE HYDROPHILICITY OF THE MICELLES, FOLLOWED BY AN IMBALANCE BETWEEN THE LAYERS OF THE MULTILAYER FILM AND THE RELEASE OF ENCAPSULATED DRUG. .... 21
- FIGURE 1.7 OXIDATION STEPS OF DISULFIDE BONDS IN OXIDATIVE ENVIRONMENTS. DISULFIDES BONDS UNDERGO OXIDATION IN THE PRESENCE OF RONS AND RESULT IN THE GENERATION OF THIOSULFINATES, THIOSULFONATES, AND SULFONATES. THIOSULFINATES AND THIOSULFONATES LEAD TO THE POLARITY ENHANCEMENT OF NANOCARRIERS. .... 22
- FIGURE 1.8 A PRODRUG NANO-ASSEMBLY PTX-SS-CIT AND ITS RESPONSIVENESS TOWARD H<sub>2</sub>O<sub>2</sub> FOR DRUG RELEASE IN TUMOR CELLS. A) THREE DISULFIDE-BOND-BRIDGED PRODRUG NANOASSEMBLIES (PTX-SS-CIT) WERE FORMED BY CONJUGATION OF PTX AND CIT THROUGH 3 DIFFERENT LENGTHS OF THE CARBON CHAIN THAT CONTAINED DISULFIDE BOND. B) *IN VITRO*, PTX RELEASE FROM H<sub>2</sub>O<sub>2</sub>-TRIGGERED PTX-SS-CIT CONTAINED 1, 2, OR 3 CARBON BONDS (A-PTX-SS-CIT, B-PTX-SS-CIT, AND  $\gamma$ -PTX-SS-CIT,

	RESPECTIVELY) WAS INCREASED BY INCREASING THE CONCENTRATION OF H <sub>2</sub> O <sub>2</sub> (1, 5, AND 10 mM) AND DECREASING THE LENGTH OF CARBON CHAINS. ....	23
FIGURE 1.9	SCHEME OF A) REDUCTION AND B) OXIDATION REACTIONS OF DISELENIDE BONDS IN THE PRESENCE OF GSH AND ROS, RESPECTIVELY. ....	24
FIGURE 1.10	(A) SCHEME OF PRODRUG NANOPARTICLES PREPARATION BY UTILIZING DIFFERENT LINKERS BETWEEN PTX AND CIT FOR CANCER THERAPY. THE RELEASE OF PTX FROM PRODRUG NANOPARTICLES WAS ACHIEVED UPON EXPOSURE TO (B) 1 mM H <sub>2</sub> O <sub>2</sub> AND (C) 10 mM H <sub>2</sub> O <sub>2</sub> DUE TO THE LINKER OXIDATION, WHICH CAN FACILITATE THE HYDROLYSIS OF ADJACENT ESTER BONDS. THE PRODRUGS NANOPARTICLES CONTAINED SE EXHIBITED THE HIGHEST RELEASE RATE IN BOTH CONDITIONS. ....	25
FIGURE 1.11	SCHEME OF OXIDATION AND TRANSFORMATION OF VINYL IN THE PRESENCE OF <sup>1</sup> O <sub>2</sub> . <sup>1</sup> O <sub>2</sub> CAN REACT WITH THE DOUBLE BOND OF VINYL DISULFIDE AND FORM UNSTABLE DIOXETANE INTERMEDIATES, SPONTANEOUSLY FOLLOWED BY BOND CLEAVAGE AND GENERATION OF TWO CARBONYL PRODUCTS. S-VINYL SULFOXIDE ALSO CAN BE GENERATED FROM THE DIRECT REACTION OF A SULFUR ATOM OF VINYL DISULFIDE WITH <sup>1</sup> O <sub>2</sub> . ....	27
FIGURE 1.12	SCHEME OF OXIDATION AND DEGRADATION OF THIOKETAL BONDS BY RONS. RONS CAN OXIDIZE A SULFUR OF THIOKETAL BONDS AND LEAD TO THE GENERATION OF THE RESPECTIVE KETONES OR ALDEHYDES COMPONENTS BY FORMING A THONIUM INTERMEDIATE AND ITS CONSEQUENCE HYDROLYSIS. ....	28
FIGURE 1.13	SCHEME FOR THE OXIDATION OF OXALATE BONDS UPON EXPOSURE TO H <sub>2</sub> O <sub>2</sub> . THE OXIDATION OF OXALATE GROUPS LED TO THE GENERATION OF THEIR CORRESPONDING ALCOHOLS OR DIOLS AND INTERMEDIATE DIOXETANEDIONE, FOLLOWED BY THE GENERATION OF CO <sub>2</sub> . ....	30
FIGURE 1.14	REACTION MECHANISM OF BORONIC ACIDS/ESTERS OXIDATION IN THE PRESENCE OF H <sub>2</sub> O <sub>2</sub> AS A MODEL OF RONS. (A) THE NUCLEOPHILE OXYGEN OF H <sub>2</sub> O <sub>2</sub> CAN ATTACK THE BORON ATOM OF BORONIC ACIDS/ESTERS AND LEAD TO R MIGRATION TO OXYGEN, FOLLOWED BY HYDROLYSIS INTO CORRESPONDING ALCOHOL AND BORONIC ACID. (B) IN ARYLBORONIC ACIDS/ESTERS, PHENYL GROUP WILL BE CLEAVED FROM BORON AFTER OXIDATION OF C–B BOND BY H <sub>2</sub> O <sub>2</sub> . THE PROCESS LEADS TO THE RELEASE OF ROH, BORONIC ACID, AND QUINONE METHIDE. ....	32
FIGURE 1.15	H <sub>2</sub> O <sub>2</sub> -SENSING MECHANISM OF AB1. UNDER REACTION WITH H <sub>2</sub> O <sub>2</sub> , THE PHENYL BORONIC ESTER GROUP OF AB1 UNDERWENT CLEAVAGE, RESULTING IN THE RELEASE OF DDAO WITH RED-SHIFTED EMISSION WAVELENGTH ( $\lambda_{EX}/\lambda_{EM}$ 600/660 NM) DUE TO A STRONG INTRAMOLECULAR CHARGE TRANSFER (ICT) PROCESS. ....	34
FIGURE 1.16	OXIDATION AND REDUCTION REACTIONS OF FERROCENE. ....	35
FIGURE 1.17	SELF-ASSEMBLY OF PEG-B-PMAEFC AND RESPONSIVENESS TOWARD ~0.6 M (1.4% V/V) H <sub>2</sub> O <sub>2</sub> , FOLLOWED BY RELEASING RHODAMINE B FROM NANOPARTICLES, WHICH WAS CONFIRMED BY ENHANCEMENT IN FLUORESCENCE INTENSITY. ....	37
FIGURE 1.18	THE OXIDATION REACTION OF CY5.5 IN THE PRESENCE OF RONS, SUCH AS ONOO <sup>-</sup> LED TO THE BREAKAGE OF THE CARBON–CARBON DOUBLE BOND OF THE SPECIFIC SITE OF CY5.5. ....	38
FIGURE 1.19	SCHEME OF CYANINE REDUCTION AND HYDROCYANINE OXIDATION. CYANINE UNDERGOES A REDUCTION REACTION IN THE PRESENCE OF NABH <sub>4</sub> THAT LEADS TO THE GENERATION OF NON-FLUORESCENT AND MEMBRANE-PERMEABLE HYDROCYANINE.	

	WHILE HYDROCYANINE CAN BE OXIDIZED IN THE PRESENCE OF ROS, E.G., $O_2^{\cdot-}$ AND $\cdot OH$ , TO TURN ON THE FLUORESCENCE SIGNAL BY PRODUCING CYANIN. ....	40
FIGURE 1.20	(A) SCHEME OF A PHOTON-UPCONVERTING NANOPROBE (UCN) INCORPORATING HCY5 AND CY7 ONTO THE UCN SURFACE. (B) OXIDATION OF HCY5 AND CY7 IN THE PRESENCE OF $O_2^{\cdot-}$ AND $ONOO^-$ , RESPECTIVELY.....	41
FIGURE 1.21	STRUCTURE OF POLY(L-METHIONINE)-BASED GEL AND ROS TRIGGERED POLYMERIC HYDROPHOBICITY TRANSITION DUE TO THIOETHER OXIDATION. ....	43
FIGURE 1.22	OXIDANTS, SUCH AS $H_2O_2$ AND $ONOO^-$ , <sup>403</sup> CAN LEAD TO THE OXIDATION OF PROLINE RESIDUES AND RESULT IN THE CLEAVAGE OF THE PARENT POLYPEPTIDE CHAIN. ....	43
FIGURE 1.23	AN INTRODUCTION OF ARS UNITS INTO BORON-DIPYRROMETHENE (BODIPY) BY A PHOTOCATALYSIS APPROACH AND THROUGH $ARS^{\cdot}$ . (A) UNDER THE LIGHT, BODIPY 1 ACTS AS A PHOTOSENSITIZER, LEADING TO $ARS^{\cdot}$ GENERATION AND FOLLOWED BY THE PRODUCTION OF A-ARS- AND A,A'-(ARS) <sub>2</sub> -SUBSTITUTED BODIPY. (B) BY INCREASING THE REACTION TIME OF BODIPY 1 WITH ARSH (IN THF UNDER EXPOSURE TO LIGHT), THE DECREASE IN THE ABSORBANCE OF BODIPY 1 SIMULTANEOUSLY OCCURRED WITH THE INCREASE IN THE ABSORBANCE OF BODIPY 1A AND 1AA. (C) PHOTOGRAPHS OF BODIPY 1A AND BODIPY 1AA IN THF UPON EXPOSURE TO A UV LAMP AT 365 NM...	45
FIGURE 1.24	BODIPY-BCD FOR GSH RADICALS ( $GS^{\cdot}$ ) FLUORESCENCE SENSING. (A) BODIPY-BCD PROBE WAS PREPARED BY THE MODIFICATION OF BODIPY WITH BCD. BODIPY-BCD AND $GS^{\cdot}$ UNDERWENT THE RADICAL CROSS-COUPLED REACTION AT A-POSITIONS OF BODIPY. BY INCREASING THE CONCENTRATION OF $GS^{\cdot}$ ( $H_2O_2$ (10 $\mu M$ )/ $Fe^{2+}$ (10-160 $\mu M$ )) (B) THE ABSORBANCE (AT 501 NM) AND (C) THE FLUORESCENCE ( $\Lambda_{EX}/\Lambda_{EM}$ 491/520 NM) INTENSITY OF BODIPY DECREASED, ACCOMPANIED BY THE APPEARANCE OF TWO NEW RED-SHIFTED PEAKS RELATED TO BODIPY-BCD+ $GS^{\cdot}$ AND BODIPY-BCD+2 $GS^{\cdot}$ . ....	46
FIGURE 1.25	MECHANISM OF $RS^{\cdot}$ -INITIATED THIOL-ENE REACTIONS IMPLICATING AN ALLYL SULFIDE BOND. THE ADDITION OF $RS^{\cdot}$ TO THE DOUBLE BOND OF THE ALLYL SULFIDE FORMS AN UNSTABLE INTERMEDIATE, WHICH FURTHER UNDERGOES A B-SCISSION, FOLLOWED BY THE GENERATION OF A NEW DOUBLE BOND AND $RS^{\cdot}$ SPECIES. ....	47
FIGURE 1.26	PHOTOACTIVATION OF THIOL-CONTAINING DRUGS IN CANCER CELLS DUE TO $RS^{\cdot}$ -MEDIATED THIOL-ENE REACTIONS. A) THIOL-CONTAINING DRUGS HAVE BEEN CAGED AND DEACTIVATED BY UTILIZING ISOBUTYLENE STRUCTURES AS A BRIDGE BETWEEN THIOL GROUPS. UPON EXPOSURE TO UV LIGHT, THE GENERATED RADICAL THIOLS AND ALLYL SULFIDE BONDS UNDERWENT THIOL-ENE REACTION, THEN RELEASED THE ACTIVATED DRUGS. B) THE STAPLED LARGAZOLE INDUCED MORE CELL SURVIVAL IN CANCER CELLS THAN THE CORRESPONDING LARGAZOLE AND LARGAZOLE THIOLS DUE TO THE PROTECTION OF THIOLS GROUP BY ISOBUTYLENE STRUCTURE THAT LED TO THE DEACTIVATION OF LARGAZOLE. C) THE UV IRRADIATION OF PREMIXED STAPLED LARGAZOLE (SL) AND DPAP SHOWED CONSIDERABLY LOWER CELL SURVIVAL THAN THE CORRESPONDING NON-IRRADIATION GROUP, WHICH PROVED THE PHOTOACTIVATION OF LARGAZOLE IN CANCER CELLS. ....	48
FIGURE 2.1	METHIONINE (THIOETHER)-CONTAINING PEPTIDES CAN BE SELECTIVELY AND CONVENIENTLY ALKYLATED TO PRODUCE A SULFONIUM ALLENE. THIS ENTITY MAY BE MODIFIED BY A CLICK REACTION (NUCLEOPHILIC THIOL-ALLENE ADDITION), YIELDING A SULFONIUM VINYL SULFIDE. THE LATTER CAN UNDERGO A SUBSEQUENT CLIP REACTION	

	(RADICAL THIOL–ENE ADDITION) TO REGENERATE THE ORIGINAL METHIONINE (THIOETHER)-CONTAINING PEPTIDE. THE DETAILS OF EACH REACTION (E.G., RELEASED MATERIALS) IS PROVIDED IN FOLLOWING PAGES.....	59
FIGURE 2.2	ALKYLATION OF METHIONINE-CONTAINING PEPTIDES. (A,B) REACTION OF PROPARGYL BROMIDE IS SELECTIVE TO THE THIOETHER OF METHIONINE BELOW PH ~5 AND OCCURS WITHOUT SIDE REACTIONS. (A,C) INCUBATION OF THE ADDUCT AT NEUTRAL PH INDUCES AN ISOMERIZATION FROM THE ALKYNE TO AN ALLENE, WHICH CAN UNDERGO [2,3]-SIGMATROPIC REARRANGEMENT OR HYDRATION UPON PROLONGED INCUBATION. 1B IS MORE SUSCEPTIBLE TO THESE REACTIONS THAN 4B.....	66
FIGURE 2.3	BIOCONJUGATE PREPARATION BY CLICK NUCLEOPHILIC THIOL–ALLENE ADDITION. (A,B) REPRESENTATIVE CHROMATOGRAMS SHOWING THAT REACTION OF ALLENIC PEPTIDES WITH THIOLS PROCEEDS WITH HIGH CONVERSION AND WITHOUT SIDE-REACTION. QUANTITATIVE DATA IN TABLE S1. FULL CHROMATOGRAMS AND MASS SPECTRA ARE PROVIDED IN THE SUPPLEMENTARY INFORMATION (FIGURES S6,7). (C) SELECTED ASSIGNED <sup>1</sup> H NMR SPECTRA DEMONSTRATING SUCCESSFUL CONJUGATION TO THE THIOETHER SIDE-CHAIN OF METHIONINE. MINOR PEAKS ANNOTATED WITH “*” REPRESENT THE TRANS ISOMER OF THE SULFONIUM VINYL SULFIDE (STRUCTURE NOT SHOWN).....	68
FIGURE 2.4	STABILITY OF BIOCONJUGATES TOWARDS NUCLEOPHILES AND CLIP OF BIOCONJUGATES BY RADICAL THIOL–ENE ADDITION. (A) THIOL NUCLEOPHILES CAN REACT AT THE CARBON ADJACENT THE SULFONIUM, THEREBY RELEASING THE ORIGINAL THIOETHER OF METHIONINE. THE MECHANISM OF THE REACTION IS PROVIDED IN THE SUPPLEMENTARY INFORMATION (FIGURE S16A). (B) THIS PROCESS OCCURRED SLOWLY WITHOUT SIDE-REACTIONS, AS EVIDENCED IN THE REPRESENTATIVE CHROMATOGRAMS FOR THREE BIOCONJUGATES. (C) RADICAL THIOLS INDUCE A FRAGMENTATION REACTION THAT RELEASES THE ORIGINAL THIOETHER OF METHIONINE IN MINUTES. (D) THIS PROCESS OCCURRED RAPIDLY (<15 MIN) WITHOUT SIDE-REACTIONS, AS EVIDENCED IN THE REPRESENTATIVE CHROMATOGRAMS FOR THREE BIOCONJUGATES.....	70
FIGURE 2.5	STABILITY OF A SULFONIUM VINYL SULFIDE BIOCONJUGATE IN THE PRESENCE OF REACTIVE SPECIES FROM BACTERIAL CELLS. (A) THE EXPOSURE OF 5B–CPP(CY3) TO RADICAL THIOLS YIELDS A ~70% RELEASE OF THE METHIONINE-CONTAINING PEPTIDE 5A. CHROMATOGRAMS SHOWN AT THREE ABSORBANCE WAVELENGTHS BEFORE AND AFTER A 15-MIN CLIP REACTION. (B) CLIP OCCURRED CONCURRENTLY WITH A ~70% REDUCTION IN THE INTENSITY OF FRET, ILLUSTRATING THAT THIS PARAMETER CAN BE USED TO TRACK THE STABILITY OF THE BIOCONJUGATE IN MORE COMPLEX ENVIRONMENTS. (C) INCUBATION OF 5B–CPP(CY3) WITH BACTERIAL CELLS EXPERIENCING DIFFERENT LEVELS OF OXIDATIVE STRESS FROM H <sub>2</sub> O <sub>2</sub> PRODUCES VERY LITTLE OR NO CHANGE TO FRET OVER A 1-H PERIOD, WITH SOME SMALL DIFFERENCES APPEARING AT 1.5 H (MEAN + SD, N = 3).....	73
FIGURE 3.1	FRET-BASED SULFONIUM VINYL SULFIDE AND THIOETHER PROBES. (A,B) SYNTHETIC SCHEME TO PREPARE 1D AND 2C FROM METHIONINE-CONTAINING PEPTIDE 1A AND CYSTEINE-CONTAINING PEPTIDE 2A, RESPECTIVELY. (C,D) REPRESENTATIVE CHROMATOGRAMS OF PURIFIED COMPOUNDS. (E) FLUORESCENCE SPECTRA ( $\lambda_{\text{EX}}$ 485 NM) DEMONSTRATE FRET FOR 1D AND 2C, BUT NOT FOR MIXTURES OF THE INDIVIDUAL FLUOROPHORES. ....	85
FIGURE 3.2	REACTION WITH RADICAL THIOLS AND THIOL NUCLEOPHILES. (A) CHROMATOGRAM ILLUSTRATING THE STABILITY OF 1D/2C IN 10 MM GSH OVER 24 H. (B) SCHEME	

ILLUSTRATING THE PRODUCTS FORMED BY REACTION OF 1D WITH A RADICAL THIOL (15 MIN UV IRRADIATION OF 10 EQ. GSH AND 1.5 EQ. PHOTOINITIATOR). (C,D) ILLUSTRATIVE CHROMATOGRAM AND EVOLUTION OF OPTICAL PROPERTIES OF 1D EXPOSED TO RADICAL THIOLS.....87

FIGURE 3.3 STABILITY OF 2C/1D IN THE PRESENCE OF PEROXYNITRITE. (A,C) 2C IS STABLE TOWARDS ~2 EQ. OF PEROXYNITRITE, ABOVE WHICH LOSS OF FLUORESCENCE INTENSITY IS OBSERVED. (B,D) EXPOSURE OF 1D TO PEROXYNITRITE FIRST LEADS TO AN INCREASE OF FLUORESCENCE AND FRET INTENSITY, THEN TO A SUBSEQUENT DECREASE.....89

FIGURE 3.4 RESPONSIVENESS OF SULFONIUM VINYL SULFIDES IN CELL CULTURE. EVOLUTION OF THE FRET SIGNAL OF 1D/2C IN THE PRESENCE OF RAW 264.7 (A) AND THP-1 (B) CELLS EXPOSED TO DIFFERENT STRESSORS AND THIOL QUENCHING AGENTS.....91



## LIST OF EQUATIONS

- (1)  $O_2 + Fe^{+2} \rightarrow Fe^{+3} + O_2^{\cdot-}$
- (2)  $O_2 + e^- \rightarrow O_2^{\cdot-}$
- (3)  $2 O_2^{\cdot-} + 2 H_2O \rightarrow H_2O_2 + O_2 + 2 \cdot OH$
- (4)  $O_2^{\cdot-} + H_2O_2 \rightarrow O_2 + \cdot OH + \cdot OH$
- (5)  $Fe^{+2} + H_2O_2 \rightarrow Fe^{+3} + \cdot OH + \cdot OH$
- (6)  $HOCl + H_2O_2 \rightarrow \cdot O_2 + Cl^-$
- (7)  $H_2O_2 + Cl^- \rightarrow HOCl + \cdot OH$
- (8)  $L\text{-Arginine} + O_2 + NADPH \rightarrow L\text{-Citrulline} + \cdot NO + NADP^+$
- (9)  $O_2^{\cdot-} + \cdot NO \rightarrow ONOO^-$
- (10)  $HNO + O_2 \rightarrow ONOOH$
- (11)  $ONOO^- + CO_2 \rightarrow ONOOCO_2^-$
- (12)  $ONOOH \rightarrow \cdot OH + \cdot NO_2$
- (13)  $ONOOH \rightarrow NO_3^- + H^+$
- (14)  $ONOOCO_2^- \rightarrow \cdot NO_2 + CO_3^{\cdot-}$
- (15)  $ONOOCO_2^- \rightarrow NO_3^- + CO_2$
- (16)  $HNO + HNO \rightarrow [HONNOH] \rightarrow N_2O + H_2O$
- (17)  $RSH + DNA^{\cdot} \rightarrow DNA + RS^{\cdot}$
- (18)  $GSSG + \text{protein-SH} \leftrightarrow \text{protein-SSG} + GSH$
- (19)  $RSH + \cdot OH \rightarrow RS^{\cdot} + H_2O$
- (20)  $Fe^{3+} + RSH \rightarrow Fe^{2+} + RS^{\cdot} + H^+$
- (21)  $Cu^{2+} + RSH \rightarrow Cu^+ + RS^{\cdot} + H^+$
- (22)  $GSH + \cdot NO_2 \rightarrow GS^{\cdot} + NO_2^- + H^+$
- (23)  $GSH + ONOO^- \rightarrow GS^{\cdot} + H_2O + \cdot NO_2$
- (24)  $RS^{\cdot} + \cdot NO_2 \rightarrow RSONO$



## LIST OF ACRONYMS AND ABBREVIATION

**Ars:** Thiophenol

**BODIPY:** 4,4-Difluoro-4-bora-3a,4a-diaza-s-indacene

**Ce6:** Chlorin e6

**CIT:** Citronellol

**Dil:** 1,1'-dioctadecyl-3,3,3',3'-tetramethylindocarbocyanine perchlorate

**DiO:** 3,3'-dioctadecyloxacarbo-cyanine perchlorate

**DNA:** Deoxyribonucleic acid

**DOX:** Doxorubicin hydrochloride

**DTNB:** 5,5'-dithio-bis-(2-nitrobenzoic acid)

**DTT:** Dithiothreitol

***E. coli:*** *Escherichia coli*

**FRET:** Fluorescence resonance energy transfer

**GSH:** Glutathione

**H<sub>2</sub>O<sub>2</sub>:** Hydrogen peroxide

**HNO:** Nitroxyl

**HOCl:** Hypochlorous acid

**HPLC:** High Performance Liquid Chromatography

**HPOX:** p-Hydroxybenzyl alcohol-incorporated copolyoxalate

**LPS:** Lipopolysaccharide

**mPEG:** Methoxy polyethylene glycol

**mPEG-SH:** Poly(ethylene glycol) methyl ether thiol

**MW:** Molecular weight

**NIR:** Near-infrared

**nm:** nanometer (unit)

**NMR:** Nuclear magnetic resonance

**$\cdot$ NO:** Nitric oxide

**$\text{O}_2^{\cdot-}$ :** Superoxide anion radical

**$^1\text{O}_2$ :** Singlet oxygen

**$\cdot\text{OCl}$ :** Hypochlorite anion

**OD:** Optical density

**$\cdot\text{OH}$ :** Hydroxyl radical

**$\text{ONOO}^-$ :** Peroxynitrite

**PBS:** Phosphate Buffered Saline

**PCL:** Poly( $\epsilon$ -caprolactone)

**PDLLA:** Poly(D,L-lactic acid) (PDLLA)

**PDT:** Photodynamic therapy

**PEG:** Polyethylene glycol

**PMA:** Phorbol-12-myristate 13-acetate

**PPADT:** Poly(1,4-phenyleneacetone dimethylene thioketal)

**PPS:** Polypropylene sulfide

**PSS:** Poly(styrenesulfonate)

**PTX:** Paclitaxel

**RNS:** Reactive Nitrogen Species

**RONs:** Reactive oxygen and nitrogen species

**RONSS:** Reactive oxygen, nitrogen, and sulfur species

**ROS:** Reactive Oxygen Species

**RS<sup>•</sup>:** Radical thiol

**RSH:** Thiol

**RSS:** Reactive Sulfur Species

**SIN-1:** 3-morpholinopyridone

**UV:** Ultraviolet

**β-CD:** β-cyclodextrin





# 1 INTRODUCTION

---

## 1.1 Overview of redox-responsive systems for therapeutic, diagnostic, and theranostic applications

For decades, researchers have developed a variety of nanosystems for a multitude of therapeutic, diagnostic, and theranostic (the combination of therapeutic and diagnosis) applications to treat and monitor the pathological conditions within the human body.<sup>56</sup> To date, a series of smart nanoplateforms, such as polymeric and metallic nanoparticles, liposomes, micelles, nanogels, and peptidic nanoparticles<sup>57,58</sup> have been explored to obtain effective targeting nanostructures with the combination of a diverse selection of targeting, diagnostic, and therapeutic components. They provide the release of different payloads, such as drugs, biomolecules, and imaging agents at specific biological sites in response to exogenous stimuli (e.g., temperature, magnetic field, ultrasound (US), light, electric pulse/ high energy radiation) and/or endogenous stimuli (e.g., pH variations, hormone and enzyme levels, and redox reactive biological species).<sup>59,60</sup> Furthermore, numerous imaging technologies, including X-ray and computed tomography (CT) imaging, radionuclide imaging (e.g., positron emission tomography (PET) and single-photon emission computed tomography imaging (SPECT)), magnetic resonance imaging (MRI), and optical imaging (e.g., bioluminescent (BLI) and fluorescence imaging (FI)) have been developed for the diagnosis of diseases, monitoring of the treatment process, and evaluation of drug targeting to particular pathological sites.<sup>61,62</sup> These image technologies can be combined with therapeutic technologies to develop theranostic agents. Moreover, imaging techniques can be combined with diverse therapeutic methods, such as gene therapy (GT), photodynamic therapy (PDT), chemotherapy (CHT), and photothermal therapy (PTT). The combination of therapeutic and diagnostic technologies can also occur by the covalent conjugation between therapeutic molecules and imaging agents *via* chemical reactions or co-encapsulation in nanoplateforms to deliver them in the targeted sites.<sup>63</sup> Among all endogenous stimuli, the differences in the cellular redox state of normal and diseased cells become an increasing focus of research due to the higher efficiency of redox-responsive systems.<sup>64–66</sup> Various redox-responsive systems have been developed to target biorelevant redox molecules, including reactive oxygen species (ROS), reactive nitrogen species (RNS), and reactive sulfur species (RSS) for therapeutic, diagnostic, and theranostic applications.<sup>28–32</sup>

Reactive oxygen, nitrogen, and sulfur species (RONSS) are biomolecules that are involved in essential cellular redox activities in all living organisms.<sup>67</sup> These chemically reactive biological

molecules are in complex equilibria with one another<sup>4</sup> and play vital roles in physiological processes, such as immune response, cellular regulatory, cellular signalling, oxidative stress response.<sup>1-3</sup> However, overexpression and dysregulation of their equilibria under pathophysiological processes result in an abnormal generation and accumulation of RONS that can lead to the onset and development of numerous diseases, such as cardiovascular diseases, diabetes, neurodegenerative diseases (Alzheimer's disease and Parkinson's disease), and cancer.<sup>5,23,68,69</sup> ROS, including superoxide anion radical ( $O_2^{\cdot-}$ ), hydrogen peroxide ( $H_2O_2$ ), hydroxyl radical ( $HO^{\cdot}$ ), singlet oxygen ( $^1O_2$ ), and hypochlorous acid (HOCl) are biomolecules with significant oxidation potential.<sup>7</sup> High concentrations of ROS can generate oxidative stress, which leads to potential damage to various biomolecules such as membranes lipids, proteins, lipoproteins, and deoxyribonucleic acid (DNA).<sup>8-10</sup> Furthermore, RNS refer to nitric oxide ( $\cdot NO$ ) and its secondary reactive products, such as nitroxyl (HNO) and peroxynitrite ( $ONOO^-$ ).<sup>11</sup> RNS can significantly affect cellular mechanisms of redox regulations due to their oxidation and nitration potential. In general, the oxidation potential of RNS is most often lower than that of ROS.<sup>12</sup> However,  $ONOO^-$ , an unstable biological oxidant and nitrating agent, exhibits a high oxidizing capacity.<sup>12,13</sup> Radical thiols ( $RS^{\cdot}$ ), a model RSS, is also recognized as an oxidizing agent,<sup>14</sup> mainly produced during the radical scavenging of glutathione (GSH) in the cellular metabolic process.<sup>15</sup>  $RS^{\cdot}$  is an important mediator in the intracellular redox process, leading to cell damage by reacting with unsaturated acyl chains of phospholipids and protein thiols.<sup>16,17</sup> On the other hand, RSS biomolecules, particularly thiols (RSH), act as biological reducing agents and play important roles in maintaining a reduced cellular environment and regulating cellular redox state.<sup>6,18</sup> GSH is the most abundant intracellular reducing thiol (1–10 mM intracellular and 2–20  $\mu M$  extracellular) and in equilibrium with its oxidized form (GSSG).<sup>19,20</sup> GSH is also an essential antioxidant reagent under normal physiological conditions and prevents cell damages caused by reactive oxygen and nitrogen species (RONS).<sup>21,22</sup> Under oxidative stress and elevated level of RONS, the concentration of GSH is increased and results in the alteration of cellular redox balance (GSH: GSSG ratios), which can cause the oxidation and disulfide exchange reactions at specific cysteine residues of proteins.<sup>23</sup> Accordingly, GSH has been the main target of various reduction-responsive systems due to several reasons, including its high intracellular level compared to extracellular concentration,<sup>24</sup> four times increase in the level of intracellular GSH in tumor tissues compared to normal cells, and the importance of the altered level of the GSH in pathological conditions and human disease<sup>23,25,26,27</sup>

Since 2001, concurrent with enhanced knowledge about the role of RSS in oxidative stress and biological redox reactions, the development of reduction-responsive materials has attracted considerable interest.<sup>6,70</sup> However, oxidation-responsive systems have attracted attention more recently owing to the effects of biological oxidizing agents in physiological and pathological events. One of the first examples of such systems is polypropylene sulfide (PPS), reported in 2004.<sup>71,72</sup> Over the past several years, remarkable progress has been made in developing reduction- and oxidation-responsive chemical bonds and materials to advance the redox-responsive nanoplatforams for various applications.<sup>30–32,64,65</sup> Furthermore, the application of these chemical bonds and materials is correlated with their mechanisms of action, selectivity, and reactivity (sensitivity and rate of reaction) toward RONSS.

### 1.1.1 Reduction-responsive chemical bonds

Disulfide (S-S), diselenide (Se-Se), and ditelluride (Te-Te) bonds have been developed to target GSH as a model of biological reducing agents for drug delivery and cancer therapy,<sup>73,74</sup> thiol detection/imaging,<sup>21,31,75</sup> and theranostics<sup>32,76</sup>. Disulfide bonds are the most common reduction-responsive functional groups. These bonds exhibit stability in blood circulation and the extracellular environment containing low concentrations of reducing thiols.<sup>76,77</sup> Disulfide bonds undergo a reversible cleavage into free thiols in the presence of thiol-based reducing agents, such as GSH *via* the thiol–disulfide exchange reaction.<sup>21</sup> Disulfide-bearing nanocarriers have been utilized to physically encapsulate or chemically conjugate the cargos (therapeutic and diagnostic agents) in various reduction-responsive systems for drug delivery,<sup>43,78</sup> thiol detection,<sup>21</sup> and theranostic applications.<sup>79</sup> The reduction responsiveness of disulfide bonds toward thiols is thermodynamically favored but kinetically slow due to the large kinetic barrier thiol-disulfide reaction.<sup>80,81</sup> To overcome this issue, some researchers utilized reducing agents, such as tris(2-carboxyethyl)phosphine (TCEP) and tris(3-hydroxypropyl)phosphine (THPP), in their reduction-responsive systems containing disulfide bonds to achieve rapid and irreversible disulfide bond breakage.<sup>82, 83–85</sup> The Reduction of disulfide bonds was also evaluated in the presence of dithiothreitol (DTT). This reducing agent is frequently used as an analogue of GSH and exhibited faster disulfide bonds breakage compared GSH due to the higher reducing power of DTT.<sup>86,87</sup> Furthermore, the rate of thiol-disulfide bond reaction can also be increased and decreased by the electrostatic attraction and repulsion between thiol and disulfide bonds in the redox buffer, respectively.<sup>88,89</sup> Overall, the responsiveness of disulfide bonds toward intracellular thiols (e.g., 10 mM GSH) can be slow and require several hours. Compared to disulfide bonds, diselenide<sup>90</sup> and ditelluride<sup>91</sup> bonds generally undergo faster cleavage and reduction in response to reductive

conditions (e.g., GSH) due to their lower bond energy (S-S (266 kJ/mol), Se-Se (192 kJ/mol), and Te-Te (149 kJ/mol))<sup>92</sup>. However, ditelluride bonds rarely used as reduction-responsive bond compared to disulfides and diselenides.<sup>93,94</sup>

### 1.1.2 Oxidation-responsive chemical bonds and materials

Sulfur-containing functional groups, including methionine, thioether, disulfide, thioketal, and vinyl disulfide have been widely used as oxidation-responsive chemical bonds for biomedical applications<sup>95</sup> due to their responsiveness toward RONS and the nontoxicity of this biological element (S) that has been found in many amino acids (e.g., cysteine, methionine, homocysteine, and taurine) and enzymes.<sup>96</sup> Furthermore, boronic acids/esters-, oxalate-, ferrocene-, cyanine-, hydrocyanine-, polyproline-, BODIPY-, and allyl sulfide-containing materials, have also been developed and utilized as oxidation-responsive nanoplateforms to target biological oxidizing agents, such as ROS, RNS, and RS<sup>•</sup> for biomedical applications.<sup>67,97–100</sup> Among all endogenous oxidizing agents, H<sub>2</sub>O<sub>2</sub> has been most commonly used for exploring the responsiveness of oxidation-responsive systems<sup>30,101</sup> due to its longer half-time (10<sup>-3</sup> – 10<sup>-5</sup> s),<sup>102,103</sup> making it the most abundant oxidant agent in eukaryotes (1–10 nM)<sup>103</sup>. In contrast, RS<sup>•</sup> has rarely been investigated as a stimulus for oxidation-responsive systems.

Upon exposure to RONS, these chemical bonds undergo oxidation reactions that usually lead to polarity transition (hydrophobicity to hydrophilicity) of corresponding nanocarriers and/or the breakage of chemical bonds, favoring the release of payloads (e.g., therapeutic or diagnostic agents).<sup>28,72</sup> For instance, in the presence of oxidizing agents, chalcogen groups of methionine- and chalcogen ether-containing materials can experience one or two steps of oxidation, leading to enhancement in aqueous solubility,<sup>12</sup> which can make them the suitable options for drug delivery systems and ROS scavenging. However, the oxidation of the disulfide, diselenide, vinyl disulfide, thioketal, boronic acids and esters, oxalate, and proline groups lead to bond breakage,<sup>12</sup> making them great candidates for therapeutic, diagnostic, and theranostic applications. Furthermore, despite vinyl disulfide bond showing selectivity toward singlet oxygen, most of the introduced oxidation-responsive chemical bonds and materials have exhibited responsiveness toward a broad spectrum of oxidizing biomolecules.<sup>97</sup> Furthermore, chemical bonds and materials with lower response rates, such as polyproline-based materials, can be employed for sustained-release systems.<sup>104</sup> However, the ones (e.g., boronic acids/esters and cyanine) with high sensitivity and response rates can be great options to detect oxidizing agents and better understanding the biological and pathological processes.<sup>105</sup>

Overall, redox-responsive chemical bonds and materials have a profound impact on the field of biomedical and biomaterials due to their responsiveness toward RONSS. Despite several approaches that have been explored in this area, the reported RONSS-responsive chemical bonds and materials still face some limitations and challenges. Undeniably, to achieve efficient chemical bonds and materials for various biomedical applications, it is of substantial importance to understand the role of reactive biological species in the progress of different pathologies in order to achieve efficient chemical bonds and materials for different biomedical applications.

## 1.2 Pathophysiological events of endogenous reactive species

This section presents comprehensive information about endogenous reactive species that are relevant to the objectives of this thesis. The presented information includes their properties and routes of formation, their equilibria with one another, and their role in the progress of various diseases. Endogenous reactive species (**Table 1.1**) play vital roles in regulating biological events such as immune response, signalling, and oxidative stress response,<sup>1-3</sup> and exist in complex equilibria with one another (**Figure 1.1**).<sup>4</sup> Dysregulation of these equilibria is the underlying cause of multiple pathophysiological processes that may link with the onset and development of several diseases, such as inflammation, diabetes, cancer, and neurodegenerative diseases.<sup>5,6</sup> While understanding the role of reactive species in the development of different pathologies is of great importance, it is equally crucial to RONSS-responsive materials to facilitate the diagnosis or to stimulate the release of therapeutic agents from nanocarrier systems.

**Table 1.1** Endogenous reactive species (RONSSS) involved in multiple pathophysiological processes

ROS	RNS	RSS
$O_2^{\cdot-}$	$\cdot NO$	$RS^{\cdot}$
$H_2O_2$	$HNO$	$RS^{\cdot}$
$\cdot OH$	$ONOO^-$	
$^{\cdot} OCl$	$\cdot NO_2$	
$^1O_2$		

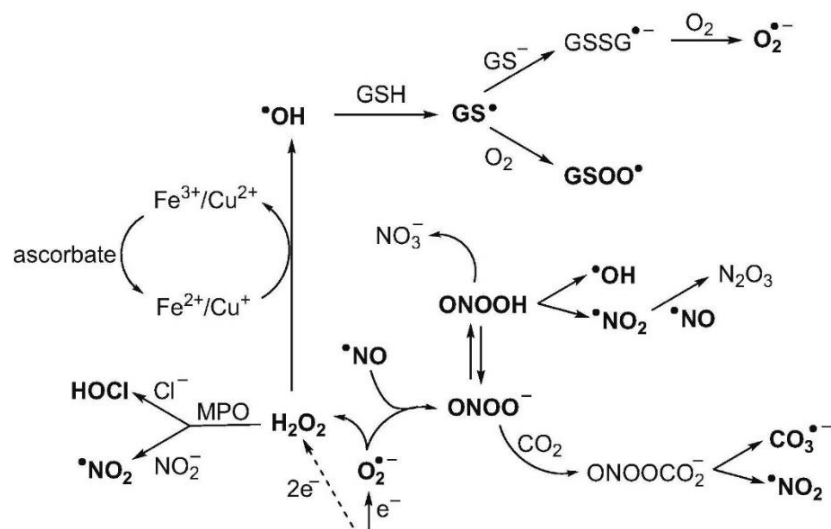


**Figure 1.1** Equilibria of major biological reactive species discussed in this contribution. All endogenous reactive species, including ROS, RNS, and RSS, exist in complex equilibria with one another to regulate various biological events. Dysregulation of any of the equilibria may affect the other and result in causing multiple pathophysiological processes linked to several diseases. Reproduced with permission from Ref.<sup>4</sup>

### 1.2.1 Reactive Oxygen Species (ROS)

ROS are generally referred to as a class of oxygen-containing chemical species generated from molecular oxygen ( $O_2$ ) during biological processes in humans and other living organisms.<sup>106</sup> They can be produced from either endogenous or exogenous sources. The majority of endogenous ROS are derived from mitochondrial respiration.<sup>107</sup> Furthermore, the peroxisomes and endoplasmic reticulum are also other endogenous sources of ROS, where oxygen consumption is high.<sup>10,108</sup> Furthermore, ROS can be generated in response to environmental stimulation such as ultraviolet (UV) light pollution, alcohol, tobacco smoke, heavy metals, and other deleterious factors.<sup>10</sup> ROS are generally classified into two groups based on their radical or non-radical nature. Radical ROS (e.g.,  $O_2^{\bullet-}$ , and  $\bullet OH$ ) are highly reactive due to the presence of one unpaired electron.<sup>109</sup> On the other hand, non-radical ROS (e.g.,  $H_2O_2$ ,  $\bullet OCl$ , and  $^1O_2$ ) are more stable compared to radical ROS and are either oxidizing agents or converted into radicals in living organisms.<sup>110,111</sup>

In addition, low to moderate concentrations of ROS, and in particular,  $H_2O_2$ , play critical roles in numerous physiological functions such as cellular signalling pathways, mitogenic response, redox regulation, and immune function.<sup>1,5,112</sup> For instance, ROS can be generated by phagocytes (neutrophils, macrophages, monocytes) as a part of the immune mechanism to extinguish pathogenic microbes.<sup>113</sup> Furthermore, ROS can be divided into other classifications, such as

primary and secondary. Primary ROS (e.g.,  $O_2^{\cdot-}$ , and  $H_2O_2$ ) are primarily produced and predominantly associated with cell signalling. Typically, primary ROS can be regulated by enzymes such as superoxide dismutase, catalase, and peroxidases, and undergo reversible reactions with biomolecules. However, secondary ROS (e.g.,  $\cdot OH$ ,  $\cdot OCl$ , and  $^1O_2$ ) are more reactive and can irreversibly damage the biomolecules. Indeed, these molecules are more toxic and less controllable than primary ROS due to the lack of specific enzymatic systems to eliminate or control their levels.<sup>1,114</sup>

### 1.2.1.1 Oxidative stress

Oxidative stress is defined as an imbalance between the generation and accumulation of ROS in cells and tissues and their elimination by endogenous biological and antioxidant systems.<sup>115,116</sup> High concentrations of ROS generate oxidative stress, which can lead to potential damage to the various biomolecules such as membrane lipids, proteins, lipoproteins, and deoxyribonucleic acid (DNA), and can even lead to cell death.<sup>8-10</sup> In other words, overproduction of ROS can cause and increase of oxidative stress and is associated with the onset and/or progression of numerous diseases, including neurodegenerative diseases, inflammation, diabetes, cardiovascular diseases, autoimmune diseases, and cancer, as well as ageing.<sup>10,117,118</sup> Hence, physiological ROS scavengers are essential to maintain redox balance and regulation of signalling pathways. Superoxide dismutase, glutathione peroxidase, catalase, and thioredoxin are potent antioxidative enzymes with relatively low concentrations that can scavenge endogenous ROS. Nonenzymatic antioxidant amino acids and proteins are also ROS scavengers. However, compared to enzymatic antioxidants, they exhibit low reactivity and must be present at the high intracellular concentration (>0.1 M).<sup>113</sup>

### 1.2.1.2 Properties of Some ROS

Different ROS have distinctive reactivity, half-life, lipid solubility, and biologic activity. The properties of selected examples discussed later in this contribution are given here.

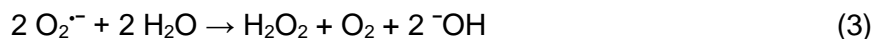
**Superoxide Anion Radical ( $O_2^{\cdot-}$ )**.  $O_2^{\cdot-}$  is generated by enzymatic (autoxidation reaction, Eq. 1) and non-enzymatic reactions (electron transfer to molecular oxygen, Eq. 2). Different enzymes can generate  $O_2^{\cdot-}$ , including xanthine oxidase, lipoxygenase, cyclooxygenase, and NADPH-dependent oxidase.<sup>119,120</sup> It exhibits low reactivity with biomolecules and is found mainly in the mitochondria.<sup>121</sup> At low pH, it exists as hydroperoxyl radical ( $HO_2$ ). However, it is mainly in the form of  $O_2^{\cdot-}$  at biological pH. As a reducing agent, it reduces iron complexes, such as ferric-

ethylene diaminetetraacetic acid (Fe<sup>+</sup>-EDTA) from Fe<sup>+3</sup> to Fe<sup>+2</sup>. It also can act as an oxidizing agent by e.g., oxidizing ascorbic acid and tocopherol.<sup>122</sup>



O<sub>2</sub><sup>·-</sup> is related to the regulation of inflammatory pathways, such as activation of pro-inflammatory cytokines and activation of inflammasomes.<sup>123</sup> Furthermore, mitochondrial superoxide dismutase converts O<sub>2</sub><sup>·-</sup> to H<sub>2</sub>O<sub>2</sub> by a dismutation reaction.<sup>122</sup> However, the mutation of superoxide dismutase 1 can cause familial amyotrophic lateral sclerosis, which is a progressive neurodegenerative disorder.<sup>124</sup>

**Hydrogen Peroxide (H<sub>2</sub>O<sub>2</sub>)**. H<sub>2</sub>O<sub>2</sub> is an ROS that has been vastly studied. *In vivo*, it can be generated through various biological processes. For instance, superoxide dismutase catalyzes the generation of H<sub>2</sub>O<sub>2</sub> by dismutation of O<sub>2</sub><sup>·-</sup> (Eq. 3). H<sub>2</sub>O<sub>2</sub> is a non-radical ROS and can readily penetrate biological membranes. It plays several roles in the regulation of cell growth, proliferation, modulation of apoptosis, and endothelial inflammatory responses.<sup>125,126</sup> H<sub>2</sub>O<sub>2</sub> can be catalytically eliminated by catalase, glutathione peroxidase, and peroxiredoxins.<sup>127</sup>



H<sub>2</sub>O<sub>2</sub> is a strong two-electron oxidant, but its reactions with most biological molecules are slow.<sup>128</sup> However, H<sub>2</sub>O<sub>2</sub> can indirectly damage cells at low concentrations by the production of OH<sup>·</sup>, which causes damage to cellular proteins, lipids, and nucleic acids.<sup>125</sup> At higher concentrations, it deactivates the cellular energy-producing enzymes such as glyceraldehyde-3-phosphate dehydrogenase.<sup>126</sup> Furthermore, in normal cells, the concentration of H<sub>2</sub>O<sub>2</sub> ranges between 1–8 μM and increases to 10–1000 μM in activated macrophages. The level of H<sub>2</sub>O<sub>2</sub> can elevate to 20 times higher in inflammatory lung disease.<sup>129</sup>

**Hydroxyl Radical (·OH)**. ·OH is a highly reactive radical ROS.<sup>130</sup> It is one of the most toxic ROS that can strongly damage different biomolecules, including DNA, proteins, lipids, and carbohydrates.<sup>131</sup> It is mainly produced by two major reactions, 1) the Haber–Weiss reaction (Eq. 4), the reaction of H<sub>2</sub>O<sub>2</sub> and O<sub>2</sub><sup>·-</sup><sup>132</sup>, and 2) the Fenton reaction (Eq. 5), the reaction of H<sub>2</sub>O<sub>2</sub> and metal ions (Fe<sup>+2</sup> or Cu<sup>+</sup>).<sup>133</sup> Under stress conditions, an excess O<sub>2</sub><sup>·-</sup> induces ferritin (an intracellular protein that stores iron) to release the free iron and stimulating the Fenton reaction to generate ·OH.<sup>134</sup>



Accordingly, metal ions including iron, zinc, and copper are strong  $\cdot\text{OH}$  mediators. Overproduction of  $\cdot\text{OH}$  affects the abnormal aggregation of  $\beta$ -amyloid peptide, which can lead to oxidative stress in the brain and can be followed by neurodegeneration (Alzheimer's disease).<sup>135</sup>

**Singlet Oxygen ( $^1\text{O}_2$ )**.  $^1\text{O}_2$  is an electronically-excited, meta-stable state of molecular oxygen.<sup>136</sup> The generation of  $^1\text{O}_2$  can be done by activating myeloid cells such as neutrophils (Eq. 6)<sup>137</sup> and eosinophils.<sup>138</sup> It can also be produced by enzymatic reactions catalyzed by some enzymes, including lactoperoxidase,<sup>139</sup> lipoxygenases,<sup>140</sup> and dioxygenases.<sup>138</sup>



$^1\text{O}_2$  is a highly reactive oxidizing agent and toxic ROS, which can cause damage to biological molecules (e.g., DNA)<sup>141</sup> and tissues.<sup>138</sup> Furthermore,  $^1\text{O}_2$  is generated photochemically in areas exposed to UV irradiation. Indeed, the side-effects of UV radiation are due to the high toxicity of  $^1\text{O}_2$ .<sup>142</sup> The effects of  $^1\text{O}_2$  in the modulation of pathological and physiological processes are being investigated.

**Hypochlorous Acid (HOCl)**. HOCl is a strong ROS and a major oxidant generated by activated neutrophils at the site of inflammation during a reaction catalyzed by myeloperoxidase from  $\text{H}_2\text{O}_2$  and chloride (Eq. 7).<sup>143</sup>



At physiological pH, both HOCl and the hypochlorite anion ( $^-\text{OCl}$ ) exist at closely equimolar concentrations due to its  $pK_a$  (7.5).<sup>144</sup> HOCl participates in oxidation reactions. For instance, it can oxidize thiols and other biomolecules, such as tryptophan, urate, pyridine nucleotides, and ascorbate.<sup>145</sup> It is also a chlorinating agent that affects some biomolecules, including amines, tyrosyl residues, DNA, cholesterol, and unsaturated lipids.<sup>146</sup> Notably, the plasma myeloperoxidase concentration is higher than usual for rheumatoid arthritis patients. Accordingly, this leads to elevated HOCl concentrations causes damage to collagen due to chlorination of the tyrosine residues.<sup>147</sup> In addition, the intracellular detection of HOCl might be limited due to the rapid reaction of HOCl with thiols and amines.

## 1.2.2 Reactive Nitrogen Species (RNS)

RNS are another important group of chemically reactive species in pathophysiological events. They are a set of compounds with different properties and reactivity that are derived from nitric oxides, including nitric oxide ( $\cdot\text{NO}$ ), peroxynitrite ( $\text{ONOO}^-$ ), and nitroxyl ( $\text{HNO}$ ). This category of reactive species has been acknowledged as playing a vital role in the physiological regulation of many cells, including smooth muscle cells, platelets, cardiomyocytes, and neurons. However, similar to ROS, they can be harmful to living cells by mediating cellular toxicity and metabolic damage.<sup>11</sup>

In biological systems,  $\cdot\text{NO}$  is the primary RNS and the source of all RNS. One of the main pathways of RNS generation is through the rapid reaction of  $\cdot\text{NO}$  with  $\text{O}_2^{\cdot-}$ , which is catalyzed by nitric oxide synthases to form  $\text{ONOO}^-$ . This reaction scavenges and neutralizes  $\text{O}_2^{\cdot-}$  and  $\cdot\text{NO}$ . In contrast,  $\text{ONOO}^-$ , the secondary RNS, is more toxic and can irreversibly damage biomolecules.<sup>148</sup> It is less controllable as no specific enzyme exists to inhibit it.  $\text{ONOO}^-$  can react with thiols of low molecular weight molecules and proteins to form radical thiols, eventually leading to their oxidation. The reaction of  $\text{ONOO}^-$  with GSH is considered the main route of  $\text{ONOO}^-$  inhibition and prevention of  $\text{ONOO}^-$ -dependent cell damage.<sup>149,150</sup> Thiols, however, can aggravate damage under some circumstances.<sup>151</sup>

### 1.2.2.1 Nitrosative stress

As mentioned above, a low concentration of RNS (especially  $\cdot\text{NO}$ ) is physiologically essential. However, the dysregulated synthesis or overproduction of  $\cdot\text{NO}$  leads to nitrosative stress and toxic physiological consequences, leading to cell injury and death. Nitrosative stress is closely linked to the elevated level of ROS (oxidative stress), including  $\text{O}_2^{\cdot-}$ .<sup>152,153</sup> For instance, the reaction of  $\cdot\text{NO}$  with  $\text{O}_2^{\cdot-}$  leads to the formation of  $\text{ONOO}^-$ , a potent biological oxidant that can damage many biological molecules.<sup>13,152,154</sup> Nitrosative stress can cause numerous pathological conditions and various pro-inflammatory diseases such as cardiovascular, atherosclerosis, and rheumatoid arthritis.<sup>155-157</sup> Nitrosative stress may lead to the oxidation, nitration (addition of  $\text{NO}_2$ ), nitrosation (addition of  $\text{NO}^+$ ), and nitrosylation ( $\text{NO}$ ) of various classes of biomolecules, including DNA and RNA bases, lipids, proteins, and metal cofactors.<sup>158-160</sup> For instance, the reaction between  $\text{ONOO}^-$  and guanosine forms 8-nitroguanosine (8- $\text{NO}_2$ -Guo),<sup>161</sup> leading to apoptosis by increasing the rates of mutations and by promoting genome instability, and inter- and intra-strand DNA crosslinks.<sup>11</sup> Furthermore, RNS can react with double-bonds of unsaturated cellular lipids, including fatty acid components of cell membranes, to generate nitro-fatty acid

derivatives.<sup>162,163</sup> RNS can also lead to the generation of nitro-hydroxy and nitrohydroperoxy lipids at double-bond sites of fatty acid.<sup>164</sup> Moreover, proteins are another target of RNS, leading to some post-translational modifications of proteins such as S-nitrosylation, glutathionylation, and tyrosine nitration. These modifications may alter the structure and function of proteins, resulting in numerous pathological conditions. For instance, elevated plasma levels of 3-nitrotyrosine can cause cardiovascular diseases.<sup>157</sup> Furthermore, iron-sulfur [Fe-S] clusters, heme-iron, non-heme iron, and copper-containing enzymes can be deactivated by the reaction with RNS,<sup>165</sup> followed by interruption of the ATP production may result in cell death.<sup>166–168</sup>

### 1.2.2.2 Properties of Some RNS

**Nitric oxide ( $\cdot\text{NO}$ ).**  $\cdot\text{NO}$  is a free radical species generated by different types of nitric oxide synthases in many organisms. For instance, the oxidation of one of the terminal guanidino nitrogen atoms converts L-arginine to L-citrulline concurrent with the production of  $\cdot\text{NO}$  (Eq. 8).



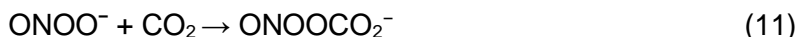
In addition,  $\cdot\text{NO}$  is highly diffusible through the cytoplasm and plasma membrane due to its lipid and aqueous solubility.<sup>169,170</sup> It is also an important second messenger for modulating numerous cellular activities in neurotransmission, smooth muscle relaxation, blood pressure, and immune regulation.<sup>171</sup> Notably, nitrosylation of the ferrous heme by reversible covalent binding is one of the most well-known  $\cdot\text{NO}$  interactions that lead to cell-signalling.<sup>158</sup> However, high  $\cdot\text{NO}$  levels are a key mediator of neurodegeneration associated with numerous diseases, such as Parkinson's disease (PD) and Alzheimer's disease (AD).<sup>172</sup> Moreover, elevated  $\cdot\text{NO}$  levels are observed in inflammatory arthritis, colorectal and bladder cancer, and stroke.<sup>173–176</sup>

**Peroxynitrite ( $\text{ONOO}^-$ ).**  $\text{ONOO}^-$  is a potent oxidant and an effective nitrating agent in many physiological and pathological processes. Endogenous  $\text{ONOO}^-$  is generated by the non-enzymatic reaction of  $\cdot\text{NO}$  and  $\text{O}_2^{\cdot-}$  (Eq. 9).<sup>13</sup> It can also be generated by the reaction of HNO and  $\text{O}_2$  at physiological pH (Eq. 10).<sup>177</sup> However, the biological relevance of the latter is still unknown due to the more rapid reaction of HNO with cellular thiols compared to molecular oxygen.

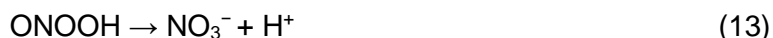


$\text{ONOO}^-$  is an unstable biological oxidant with an extremely short half-life (< 10–20 ms).<sup>12</sup> It is a source of highly oxidizing radicals by transformation to other highly reactive molecules such as

peroxynitrous acid (ONOOH;  $pK_a$  6.8) or unstable nitrosoperoxocarbonate anion (ONOOCO<sub>2</sub><sup>-</sup>) by the reaction with CO<sub>2</sub> (Eq. 11).<sup>178</sup>



ONOOH further undergoes O–O bond cleavage to form both <sup>•</sup>OH and <sup>•</sup>NO<sub>2</sub> (Eq. 12) or undergoes isomerization to form the nitrate anion (NO<sub>3</sub><sup>-</sup>) (Eq. 13).<sup>179</sup>



Nitrosoperoxocarbonate anion decomposes to the nitrogen dioxide radical (<sup>•</sup>NO<sub>2</sub>) and carbonate radical anion (Eq. 14), or to nitrate and CO<sub>2</sub> (Eq. 15).<sup>178</sup>



It is worth mentioning that the reactivity of ONOO<sup>-</sup> is shifted toward nitration at physiological concentrations of carbon dioxide.<sup>180</sup> Subsequently, the generation of <sup>•</sup>NO<sub>2</sub> makes ONOO<sup>-</sup> both an oxidizing and nitrating agent of biomolecules.<sup>181</sup> In general, ONOO<sup>-</sup> can oxidize thiols and decompose carbohydrates as well as modify lipids (*via* oxidation and nitration), proteins (*via* nitration, nitrosylation, and oxidation), and nucleic acids (*via* oxidation and nitration).<sup>182</sup> Noteworthy, nitrotyrosine, the nitration of tyrosine at the 3-position, is considered as a biomarker of ONOO<sup>-</sup> production *in vivo*.<sup>183</sup> Furthermore, the chemical properties of ONOO<sup>-</sup> make it a crucial pathogenic mediator in the onset and progression of many diseases, including inflammation, cancer, cardiovascular disease, circulatory shock, ischemic stroke, reinjury, atherosclerosis, and diabetes.<sup>184</sup> Furthermore, hypertension is related to ONOO<sup>-</sup> generation and <sup>•</sup>NO degradation that reduces endothelium-mediated vasodilation and the development of hypertension.<sup>185</sup>

In terms of beneficial effects, ONOO<sup>-</sup> can modulate various cell signal transduction pathways *in vitro*.<sup>186</sup> ONOO<sup>-</sup> has been also recognized as a key cytotoxic effector of immune system cells (macrophages) against invading pathogens such as *Escherichia coli*<sup>187</sup> and *Trypanosoma cruzi*.<sup>188</sup> The pathogenic role and beneficial effects of ONOO<sup>-</sup> *in vivo* have not been easily or fully characterized due to its short biological half-life, lack of a reliable method to measure and monitor its level *in vivo*, and the production of <sup>•</sup>NO<sub>2</sub> (a biomarker of ONOO<sup>-</sup>) through two biological pathways including ONOO<sup>-</sup>-dependent and myeloperoxidase-catalyzed oxidation of nitrite by H<sub>2</sub>O<sub>2</sub>.<sup>12</sup>

**Nitroxyl (HNO).** HNO is a one-electron reduced and protonated form of  $\cdot\text{NO}$ . Endogenous HNO can be generated through two possible mechanisms. One of these is NOS-dependent pathways (under certain cofactor conditions), and the other is a direct reduction of  $\cdot\text{NO}$  via mitochondrial cytochrome c, manganese superoxide dismutase, ubiquinol, hemoglobin, or xanthine oxidase.<sup>189</sup>

HNO is an exclusive species with potent oxidation activity that can participate in pathological and physiological mechanisms through direct interaction with biological compounds such as thiols and thiol-containing proteins.<sup>190</sup> Moreover, HNO can induce DNA strand breakage *in vitro* and *in vivo*, and nitration of tyrosine residues of proteins.<sup>191–193</sup> In addition, HNO undergoes a dimerization reaction by nitrous oxide reductase (NOR), leading to the formation of nitrous oxide (Eq. 16).<sup>194</sup> Notably, detection, identification of the endogenous sources and elucidating the role of HNO *in vivo* are challenging due to its rapid reaction with different biomolecules and dimerization reaction.<sup>195</sup>



### 1.2.3 Reactive Sulfur Species (RSS)

RSS are sulfur-containing reactive biomolecules that can act either as oxidizing or as reducing agents in order to maintain and regulate cellular redox state.<sup>6,18</sup> Thiols act as reducing agents and are essential for cellular physiological events. In fact, they play critical roles in repairing radical-induced damage to vital cellular components such as DNA and proteins, leading to the formation of radical thiols ( $\text{RS}\cdot$ ) (Eq. 17).<sup>196,197</sup> Similar to the rest of biological reactive species, the dysregulation of RSS equilibria can cause pathological conditions.



#### 1.2.3.1 Properties of some RSS

**Glutathione (GSH).** As explained previously, GSH is the most abundant soluble thiol antioxidant in normal cells, with high concentrations in the cytosol (1–11 mM), nucleus (3–15 mM), and mitochondria (5–11 mM).<sup>148,198</sup> GSH scavenges RONS, partially leading to the generation of radical thiols ( $\text{RS}\cdot$ ). In fact, the cellular ratio of GSH/GSSG can be used to define the level of oxidative stress of an organism.<sup>199</sup> Oxidative and nitrosative stress lead to more consumption of GSH to scavenge RONS, leading to increase the generation of  $\text{RS}\cdot$ .<sup>200</sup> These reactions eventually increase the concentration of GSSG, which may irreversibly oxidize and eventually damage

many thiol-containing proteins and enzymes. For instance, the reaction of GSSG with a protein thiol group produces protein–glutathione-mixed disulfides (protein-SSG) through the protein S-glutathionylation reaction (Eq. 18). Protein-SSG adducts exhibit a higher half-life than GSSG<sup>148</sup> and can be implicated in diabetes, cardiovascular and lung diseases, cancer, and neurodegenerative diseases. In addition, GSNO also can promote protein S-glutathionylation.<sup>201</sup>



**Radical Thiols (RS<sup>•</sup>).** RS<sup>•</sup> are sulfur-centered free radicals generated from one-electron oxidation of thiols (RSH). Furthermore, oxidative environments can modify protein thiols (protein–SH) and form RS<sup>•</sup> (protein–S<sup>•</sup>).<sup>198,202</sup> RS<sup>•</sup> are generated through various pathways, but only a few are considered the major ones.

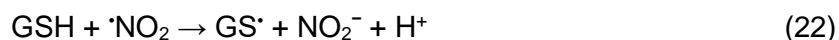
The direct reaction between RSH and one-electron ROS (e.g., O<sub>2</sub><sup>•-</sup> and <sup>•</sup>OH) produces RS<sup>•</sup> (Eq. 19) by hydrogen abstraction. Furthermore, peroxidases including lactoperoxidase, prostaglandin hydroperoxidase, and myoglobin can indirectly generate RS<sup>•</sup> from thiols and H<sub>2</sub>O<sub>2</sub> or ROOH.<sup>202–204</sup>



RS<sup>•</sup> can also be produced by transition metal-catalyzed thiol oxidation.<sup>203</sup> For instance, the reduction of Cu<sup>2+</sup> to Cu<sup>+</sup> or Fe<sup>3+</sup> to Fe<sup>2+</sup> by GSH is a reaction of importance for maintaining cellular redox homeostasis that leads to the generation of RS<sup>•</sup> (Eq. 20-21).<sup>205,206</sup>



RNS also can generate RS<sup>•</sup> through the oxidation of both low- and high-molecular-weight thiols.<sup>22,207</sup> In cells with high concentrations of ONOO<sup>-</sup>, the decomposition of ONOO<sup>-</sup> produces <sup>•</sup>NO<sub>2</sub>, and CO<sub>3</sub><sup>•-</sup>, which induces the oxidation of low-molecular-weight thiols, e.g., GSH and cysteine, by one-electron transfer. For instance, <sup>•</sup>NO<sub>2</sub> can oxidize GSH and generate GS<sup>•</sup> intermediates (Eq. 22), which initiate the further free radical chain reaction.<sup>22</sup>



Furthermore, in the presence of excess GSH, GS<sup>•</sup> is formed from a direct reaction of ONOO<sup>-</sup> (Eq. 23), which eventually leads to the formation of S-nitroglutathione (GSNO<sub>2</sub>).<sup>208</sup>



In addition,  $\text{ONOO}^-$  can mediate the oxidation of high-molecular-weight biomolecules (protein thiols) to free radical intermediates. For instance, it is able to oxidize the single cysteine residue of bovine serum albumin, resulting in the formation of a protein cysteinyl radical.<sup>207</sup>

In general,  $\text{RS}^\bullet$  are involved in various oxidation/reduction reactions, including electron transfer, hydrogen abstraction, and additional reactions with numerous biological compounds such as RNS, ROS, and RSS (**Figure 1.2**).<sup>209</sup> In normal biological systems, the rates of  $\text{RS}^\bullet$  production are low enough to prevent the high steady-state radical concentrations for dimerization reactions. Thus, the beneficial effect of  $\text{RS}^\bullet$  production might be more significant than its harmful effects.

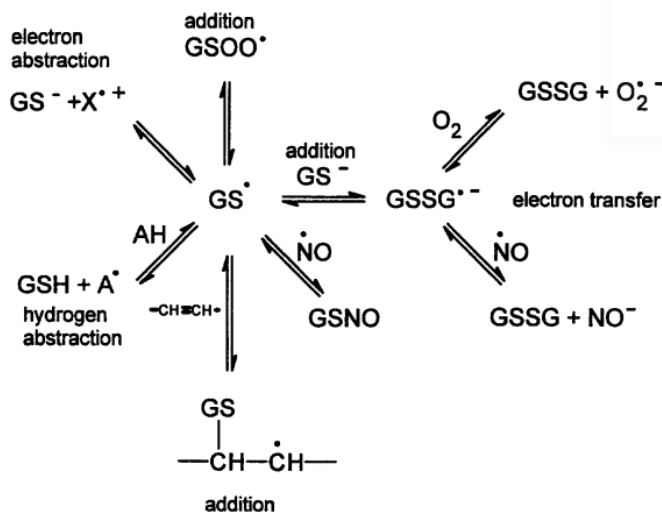


**Figure 1.2** The oxidation/reduction reactions of  $\text{GS}^\bullet$ , as a thiol radical, in biological systems. Reproduced with permission from Ref.<sup>209</sup>

For instance,  $\text{RSONO}$  generated from the reaction of  $\text{RS}^\bullet$  and  $\bullet\text{NO}_2$  (Eq. 24) decomposes to  $\text{RSNO}$  through a transnitrosylation reaction and transfers a  $\bullet\text{NO}$  from one protein's thiol to another one, leading to S-nitrosylation of the thiol-containing biomolecules (Eq. 25). S-nitrosylation plays important roles in cellular signal transduction. For instance, under physiological oxidative stress, S-nitrosylation of the thiols prevents their further cellular oxidative modification.<sup>210</sup> However, oxidative and nitrosative stress can affect enzymatic activity, subcellular localization, protein–protein interactions, and protein stability by increasing  $\text{RS}^\bullet$  and  $\bullet\text{NO}_2$  and subsequent S-nitrosylation of the thiols and protein S-nitrosylation.<sup>211–213</sup>





On the other hand, RSOH can undergo glutathionylation through the direct reaction with GSH to regenerate RSH. However, further oxidation leads to irreversible oxidation of RSOH to sulfinic (RSO<sub>2</sub>H) or sulfonic acids (RSO<sub>3</sub>H), which can cause partial or total loss of the biological activity of proteins.<sup>209,214</sup> Noteworthy, analyzing pathways involving RS<sup>•</sup> is challenging because their high chemical reactivity results in half-lives that are often on the microsecond timescale.<sup>215</sup>

### 1.3 Endogenous reactive species–responsive chemical bonds and materials for various biomedical applications

The specific chemical reactivity of various reactive species, described in the previous section, can inspire the development of RONS-responsive chemical bonds and materials used for therapeutic, diagnostic, and theranostic applications. As GSH-responsive chemical bonds and materials have been explained previously (as model of thiol-responsive system), this part aimed to present the additional information about RONS- and RS<sup>•</sup>-responsive chemical bonds and materials, including their structure, mechanism of action, selectivity, reactivity (sensitivity and rate of reaction), applications, opportunities, and limitations.

#### 1.3.1 RONS-responsive chemical bonds and materials

##### 1.3.1.1 Thioether, Selenide, and Telluride

- **Thioether**

Thioether bonds may be oxidized in the presence of a variety of RONS, including H<sub>2</sub>O<sub>2</sub>, <sup>-</sup>OCl, ONOO<sup>-</sup>, <sup>1</sup>O<sub>2</sub>, and <sup>•</sup>OH.<sup>216–219</sup> The oxidation of the thioether into a more polar sulfoxide or sulfone can be used to increase the aqueous solubility of nanocarriers.<sup>220,71</sup> To date, the polarity transformation of thioether groups has been developed for various biomedical applications.<sup>221</sup> The changes in the solubility of nanocarriers can promote the disassembly of nanocarriers loaded cargos (e.g., drugs, biomolecules, and imaging agents) at oxidative microenvironments.

Thioether bonds have been mainly applied for drug delivery applications. They can be utilized as a linker or in the structure of polymers.<sup>123–125</sup> For instance, polypropylene sulfide (PPS) is a well-known RONS-responsive hydrophobic polymer that has been exploited for drug delivery to sites undergoing oxidative stress.<sup>101</sup> Thioether-containing materials, including PPS show different sensitivity toward different RONS. For instance, they are not responsive towards O<sub>2</sub><sup>•-</sup>.<sup>224</sup>

However, they can be oxidized to sulfoxide or sulfone with relatively high concentrations of other RONS (e.g.,  $>500 \mu\text{M H}_2\text{O}_2$ ).<sup>104</sup> Yi *et al.* showed that *in vitro*, the reaction of hydrogel nanocarrier contained PPS with  $\text{H}_2\text{O}_2$  (500 mM) led to  $>90\%$  percent release of lipophilic indocarbocyanine dye Dil, as a model of a hydrophobic drug, in one day due to the oxidation of sulfide.<sup>225</sup> Furthermore, Fuhrman *et al.* evaluated the stabilizing potential of thioether-contained amphiphilic block copolymers for paclitaxel (PTX) nanocrystals as well as the effect of thioether oxidation by endogenous ROS on the size and dissolution of PTX nanocrystals.<sup>220</sup> Accordingly, the authors coated the PTX nanocrystals with thioether-containing polymeric stabilizers prepared from hydrophilic mPEG and hydrophobic polyester block bearing thioether branches (**Figure 1.3**). Upon exposure to ROS ( $1 \text{ mM H}_2\text{O}_2$ ,  $0.1 \text{ mM FeSO}_4$ ), the thioether branches underwent oxidation, followed by polarity changes in the hydrophobic block of the stabilizer resulting in nanocrystal growth that may promote the cellular uptake of the nanocrystals. However, the thioether groups didn't indicate any oxidation and increment size in the presence of 10 times diluted ROS ( $100 \mu\text{M H}_2\text{O}_2$ ,  $10 \mu\text{M FeSO}_4$ ). Moreover, the oxidation of thioether groups with  $\text{OCl}^-$  was much faster than  $\text{H}_2\text{O}_2$  and may lead to two oxidation steps, resulting in sulfone production. For instance, exposure of aqueous dispersions of PPS nanoparticles to  $\sim 2 \mu\text{M}$  of  $\text{OCl}^-$  increased transmittance from 50% to 90% just in  $\sim 1 \text{ min}$  incubation due to particle swelling caused by oxidation of the thioether to sulfoxides and sulfones.<sup>226</sup> Based on another observation, the oxidation of PPS chain with  $1.0 \text{ eq. OCl}^-$  also result in generation of significant amounts of sulfones in 20 h.<sup>227</sup>

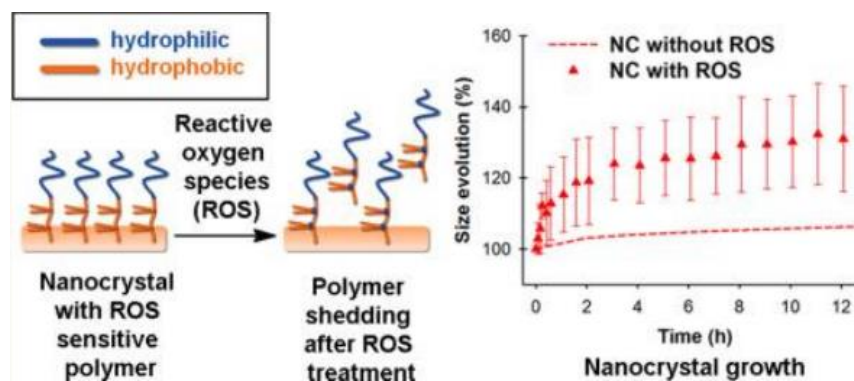


**Figure 1.3** PTX nanocrystals were coated with ROS-responsive polymeric stabilizers containing thioether bonds. In the presence of ROS, thioether bonds of stabilizer underwent oxidation, leading to desorption of stabilizers from the surface of nanocrystals and resulted in destabilization and altering size distribution for promoting cellular uptake of the nanocrystals. Reproduced with permission from Ref.<sup>220</sup>

Thioether groups have also been utilized for the detection of endogenous RONS. For instance, Gupta *et al.* prepared a diblock polymer of PPS and N,N-dimethylacrylamide, (poly( $\text{PS}_{74}\text{-b-DMA}_{310}$ )), which formed micelles that could be loaded with different fluorophores including Nile

red, 3,3'-dioctadecyloxacarbocyanine perchlorate (DiO), and 1,1'-dioctadecyl-3,3,3',3'-tetramethylindocarbocyanine perchlorate (Dil) as model drugs.<sup>217</sup> Nile red is a hydrophobic fluorophore that is strongly fluorescent in the hydrophobic core of intact micelles. However, its fluorescence intensity decreases in aqueous solutions. Exposure of the micelles to 100  $\mu\text{M}$   $\text{ONOO}^-$  for 15 min at physiological pH led to the release of 20% of loaded Nile red, due to oxidation of PPS. Furthermore, fluorescence resonance energy transfer (FRET) of a pair of fluorophores (Dil/DiO) was used and loaded into micelles to prove the release of model drugs *in vitro* due to endogenous oxidants generated by lipopolysaccharide (LPS)-treated RAW 264.7 macrophages. The release of Dil and DiO from micelles results in a decrease in FRET signals due to less possibility in the energy transfer between dyes. Accordingly, 40% reduction in the FRET signal from the Dil and DiO pair was confirmed in LPS-stimulated RAW 264.7 macrophages, confirming that drug release of the system could be achieved in response to ROS produced *in vitro*. Besides PPS, other thioether-containing materials have also been utilized for RONS detection. For instance, Wu *et al.* have combined an  $^-$ OCl-inert fluorophore, benzoxadiazole, as the energy donor and an  $^-$ OCl-sensitive fluorophore, 4,7-bis(2-thienyl)-2,1,3-benzoselenadiazole (SeTBT), as the energy acceptor in order to detect  $^-$ OCl by FRET (**Figure 1.4a**).<sup>216</sup> In the presence of  $^-$ OCl, the sulfide group of SeTBT can be oxidized to a sulfoxide and disturb the FRET process and its emission in far-red to near-infrared (NIR) channel. However, the emission of benzoxadiazole was enhanced in the green channel. Ultimately, the intensity of the FRET signal from the probe (10  $\mu\text{g/mL}$ ) decreased within 5 min in the presence of  $^-$ OCl (100  $\mu\text{M}$ ) by oxidation of the sulfide group of energy acceptors. However, this probe was not sensitive to up to 1 mM of other potentially interfering species, including ROS ( $^{\cdot}\text{OH}$ ,  $\text{H}_2\text{O}_2$ ,  $\text{HNO}$ ,  $t\text{-BuOO}^{\cdot}$ ,  $\text{O}_2^{\cdot-}$ ,  $\text{ONOO}^-$ ) or reducing agents (GSH, Cys, Hcy, DTT; **Figure 1.4b**).

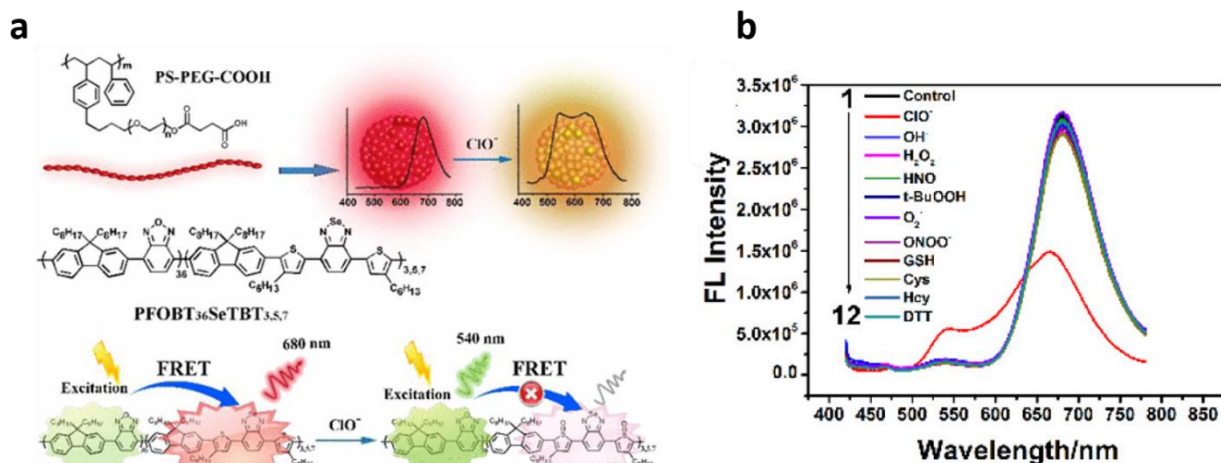


**Figure 1.4** (a) Schematic illustration of a fluorescent probe and responsiveness toward  ${}^{-}\text{OCl}$ . (b) Fluorescence spectra of the probe in the presence of various ROS and biologically relevant analytes: PBS,  $100\ \mu\text{M}$   ${}^{-}\text{OCl}$  and  $1\ \text{mM}$  of  ${}^{\bullet}\text{OH}$ ,  $\text{H}_2\text{O}_2$ ,  $\text{HNO}$ ,  $\text{t-BuOO}^{\bullet}$ ,  $\text{O}_2^{\bullet-}$ ,  $\text{ONOO}^-$ , GSH, Cys, Hcy, and DTT. Reproduced with permission from Ref.<sup>216</sup>

The responsiveness of thioether groups toward  ${}^1\text{O}_2$  has been exploited for light-triggered spatiotemporal drug release in photodynamic and anticancer therapy.<sup>228–230</sup> Deng *et al.* utilized the self-assembled diblock copolymer mPEG-b-PPS loaded DOX and IR780 to form nanoparticles for anticancer therapy *in vitro*.<sup>219</sup> IR780 is a heptamethine dye that can generate  ${}^1\text{O}_2$  upon irradiation at a wavelength of 808 nm.<sup>231</sup> The particles remained 84% intact under physiological conditions during 12 h and without irradiation.<sup>219</sup> However, after 20 s exposure to a 808-nm laser, around 75% drug was released in the following 4 h in 4T1 cells. This was explained by the oxidation of PPS that partially promoted the disassembly of the system. As a result, the light-triggered drug release is significantly improved under irradiation and by increasing irradiation time due to increased ROS generation.

#### • Selenoether and Telluroether

Selenoether- and telluroether-containing materials have also been used for biomedical applications due to their hydrophobic to hydrophilic transition caused by RONS, including  $\text{H}_2\text{O}_2$ ,  ${}^{-}\text{OCl}$ ,  $\text{ONOO}^-$ ,  ${}^1\text{O}_2$ , and  $\text{O}_2^{\bullet-}$ .<sup>232–235</sup> Compared to thioether groups, these chemical bonds exhibit more responsiveness, as the reactivity of chalcogens increases with decreasing electronegativity of the elements ( $\text{S} < \text{Se} < \text{Te}$ ).<sup>101,97</sup> For instance, Ma *et al.* compared the responsiveness of a selenium-containing amphiphilic block copolymer (PEG-PUSe-PEG) with its polysulfide analogue (PEG-PUS-PEG) toward  $\text{H}_2\text{O}_2$ . They showed that the replacement of thioether by selenoether groups increased the release of loaded DOX from 41% to 72% in 10 h reaction in the presence

42.6 mM H<sub>2</sub>O<sub>2</sub>.<sup>236</sup> Furthermore, Fang *et al.* investigated the responsiveness of telluroether-containing hyperbranched polymers toward biologically relevant concentration of H<sub>2</sub>O<sub>2</sub> (100 μM).<sup>234</sup> Accordingly, they synthesized an amphiphilic hyperbranched polymer by utilizing telluroether groups as branches and PEG as a shell. Their polymer showed more than a 3-fold increase in diameter upon exposure to 100 μM H<sub>2</sub>O<sub>2</sub> in around 20 h, due to telluroether oxidation that led to aggregation and swelling of the polymer.

The oxidation of selenoether- and telluroether-containing materials in the presence of H<sub>2</sub>O<sub>2</sub> have been utilized for drug delivery and cancer therapy.<sup>96</sup> For instance, Yang *et al.* prepared a selenium-containing amphiphilic aliphatic polycarbonate as an oxidation-responsive drug delivery vehicle.<sup>237</sup> For this purpose, DOX, a fluorescent anticancer drug, was encapsulated in the hydrophobic core of a self-assembled selenium-containing polymer (**Figure 1.5**). The authors showed that the selenium in the backbone of the hydrophobic polycarbonate underwent oxidation upon exposure to 100 μM H<sub>2</sub>O<sub>2</sub>, increasing the polymer's hydrophilicity and leading to 30% drug release after a 12 h incubation.

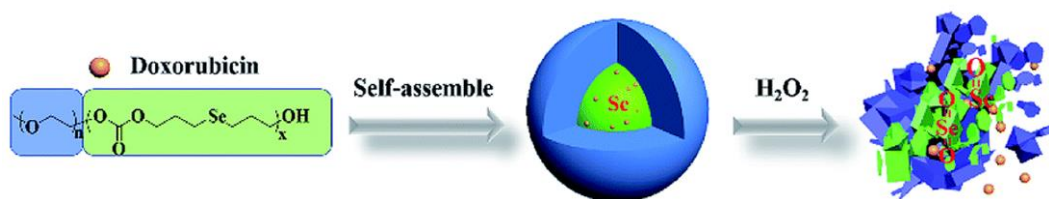


**Figure 1.5** Schematic illustration of an amphiphilic aliphatic polycarbonate containing selenium for oxidation-responsive drug delivery vehicle. In response to 100 μM H<sub>2</sub>O<sub>2</sub>, the oxidation of selenium groups in the backbone of polycarbonate underwent oxidation, leading to hydrophobic–hydrophilic transition of nanoparticles and resulted in the release of loaded DOX. Reproduced with permission from Ref.<sup>237</sup>

Furthermore, the selenoether- and telluroether-containing materials showed great potential in chemotherapy and phototherapy due to their responsiveness toward <sup>1</sup>O<sub>2</sub>.<sup>238,239</sup> For instance, Wang *et al.* employed the responsiveness of selenoethers toward <sup>1</sup>O<sub>2</sub> to develop NIR light-responsive nanoparticles.<sup>238</sup> The authors prepared amphiphilic selenium-containing polymeric nanoparticles by coupling PEG, bis(hydroxypropyl) selenide, and hexamethylene diisocyanate and encapsulation of different molecules e.g., DOX. Eventually, selenoether-containing nanoparticles indicated around 40% drug (i.e., DOX) release induced by <sup>1</sup>O<sub>2</sub>-mediated Se oxidation after 12 h incubation under 5 min post irradiation to NIR light (785 nm, 1.0 W cm<sup>-2</sup>). In another example, Fan *et al.* prepared a photosensitive tellurium-containing multilayer film to combine photo-controlled photodynamic with chemotherapy in response to <sup>1</sup>O<sub>2</sub>.<sup>239</sup> As shown in **Figure 1.6**, the authors fabricated the <sup>1</sup>O<sub>2</sub>-responsive multilayer film by utilizing tellurium-containing micelles,

porphyrin (as a photosensitizer), and polystyrene sulfonate as building blocks. Upon exposure of the photosensitizer to visible light, the generated  $^1\text{O}_2$  not only played an important role in photodynamic therapy, but also oxidized the tellurium. Oxidizing the tellurium to  $\text{Te}=\text{O}$  increased the polarity of the micelles and led to an imbalance between the layers of the multilayer film, thus releasing the encapsulated drug (Nile red as a model drug).

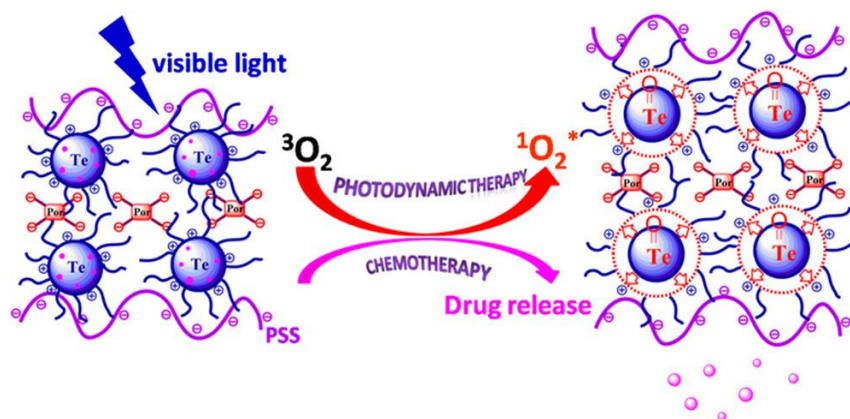


**Figure 1.6** The photosensitive tellurium-containing multilayer film was structured by utilizing tellurium-containing micelles, photosensitizer, and polystyrene sulfonate as building blocks. Under visible light, tellurium was oxidized to  $\text{Te}=\text{O}$  by exposure to generated  $^1\text{O}_2$ .  $\text{Te}=\text{O}$  increased the hydrophilicity of the micelles, followed by an imbalance between the layers of the multilayer film and the release of encapsulated drug. Reproduced with permission from Ref.<sup>239</sup>

The sensitivity of thioether-, selenoether- and telluroether-containing materials to multiple RONS make them candidates to be used as reactive species scavengers or responsive groups within drug delivery systems. Furthermore, their responsiveness toward  $^1\text{O}_2$  makes them great groups for photodynamic and cancer therapy. However, they remain unselective chemical bonds and are not able to distinguish between different reactive species. Additionally, the biological effect of selenoether- and telluroether-containing materials requires more evaluation *in vivo* as they are active electron donors that can potentially interfere with metabolic reactions.<sup>240</sup>

### 1.3.1.2 Disulfide and Diselenide

- **Disulfide**

Disulfide bonds have mainly been exploited as reducible groups due to their participation in thiol–disulfide exchange reactions. However, they equally exhibit some responsiveness towards oxidants and imply oxidation of their sulfur atoms. Furthermore, they exhibit less responsiveness towards  $\text{H}_2\text{O}_2$  than their thioether counterparts.<sup>241</sup> Biological disulfide bonds are oxidized in the

presence of RONS, including  $\text{H}_2\text{O}_2$ ,<sup>242</sup>  $\cdot\text{OH}$ ,<sup>243</sup>  $^1\text{O}_2$ ,<sup>244</sup>  $\text{O}_2^{\cdot-}$ ,<sup>245</sup>  $\text{ONOO}^-$ , and  $^-\text{OCl}$ .<sup>246</sup> In the presence of oxidants, disulfides can undergo several oxidation processes and eventually undergo cleavage. Thiosulfates ( $\text{R-S(O)-S-R}$ ), thiosulfonates ( $\text{R-S(O}_2\text{)-S-R}$ ), and sulfonates ( $\text{R-S(O}_2\text{)-OH}$ ) presented in **Figure 1.7** are the most common products of oxidation. Thiosulfates and thiosulfonates are more polar than the parent disulfides. They have been utilized for morphology switches or polarity transition (hydrophobicity to hydrophilicity) of the system, leading to the disassembly of nanocarriers. However, S-S cleavage may happen due to a third step of oxidation, leading to the production of sulfonates.<sup>95,246,247</sup> These chemical bonds can be presented in nanostructures as disulfide-linkers, in the main chain of the polymers,<sup>248</sup> side chains of polymers,<sup>249</sup> or as disulfide-crosslinked carriers.<sup>250,251</sup>

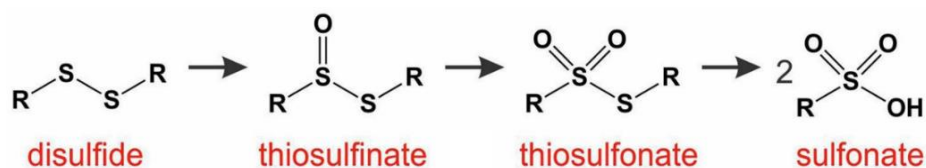


**Figure 1.7** Oxidation steps of disulfide bonds in oxidative environments. Disulfides bonds undergo oxidation in the presence of RONS and result in the generation of thiosulfates, thiosulfonates, and sulfonates. Thiosulfates and thiosulfonates lead to the polarity enhancement of nanocarriers. Reproduced with permission from Ref.<sup>95</sup>

Disulfide bonds have mainly been employed for drug delivery systems and mostly investigated in the presence of  $\text{H}_2\text{O}_2$ .<sup>163,164,172</sup> For instance, Xu *et al.* conjugated a hydrophobic PPS to hydrophilic poly(amidoamine)s through a disulfide bond. The resulting amphiphilic poly(amidoamine) dendrimer (PPS-SS-PAMAM) self-assembled into stable micelles.<sup>248</sup> Due to the high zeta potential of the micelles, DNA is trapped to the surface of the structure tightly. However, it was released after 24 h incubation with 10 mM  $\text{H}_2\text{O}_2$  due to the oxidation of sulfur-based groups of PPS to hydrophilic poly(propylene sulfone) and the cleavage of the disulfide bond of the complex. The nanomicelles exhibited high gene transfection efficacy and very low cytotoxicity *in vitro*. The system showed the potential of disulfide bonds in gene therapy by exposure to the intracellular ROS in cancer cells. In another example, Sun *et al.* utilized a specific strategy to achieve the faster degradation of disulfide bond in the presence of  $\text{H}_2\text{O}_2$ .<sup>247</sup> They conjugated PTX, an anticancer drug, and citronellol (CIT) through disulfide bond-containing carbon chain to form a prodrug nano-assembly (PTX-SS-CIT) for cancer therapy (**Figure 1.8a**). The authors utilized three different lengths of carbon chains with (n: 1, 2, 3) connected to ester bonds to produce  $\alpha$ -PTX-SS-CIT (n=1),  $\beta$ -PTX-SS-CIT (n=2),  $\gamma$ -PTX-SS-CIT (n=3). In the presence of 1, 5, 10 mM  $\text{H}_2\text{O}_2$ , the oxidation of the disulfide bond to a hydrophilic sulfoxide and sulfone facilitated the

hydrolysis of the neighbouring ester bonds and promoted the release of PTX (**Figure 1.8b**). Indeed, more than 90% PTX release was achieved in 8 hours incubation in the presence of 1 mM H<sub>2</sub>O<sub>2</sub> due to the oxidation of disulfide bond to thiosulfonates and thiosulfonates that led to the hydrolysis of ester bonds. Furthermore, the anticancer drug's release rate was inversely related to the distance between the sulfur atom and the ester bond ( $\alpha$ -PTX-SS-CIT >  $\beta$ -PTX-SS-CIT >  $\gamma$ -PTX-SS-CIT).

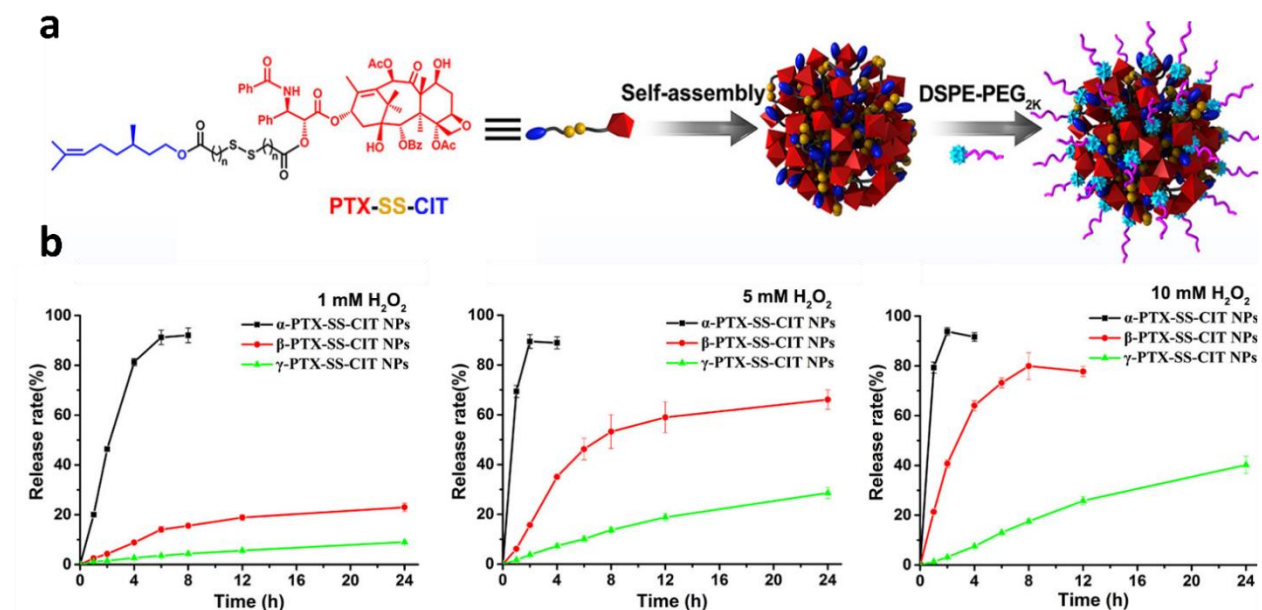


**Figure 1.8** A prodrug nano-assembly PTX-SS-CIT and its responsiveness toward H<sub>2</sub>O<sub>2</sub> for drug release in tumor cells. a) Three disulfide-bond-bridged prodrug nanoassemblies (PTX-SS-CIT) were formed by conjugation of PTX and CIT through 3 different lengths of the carbon chain that contained disulfide bond. b) *In vitro*, PTX release from H<sub>2</sub>O<sub>2</sub>-triggered PTX-SS-CIT contained 1, 2, or 3 carbon bonds ( $\alpha$ -PTX-SS-CIT,  $\beta$ -PTX-SS-CIT, and  $\gamma$ -PTX-SS-CIT, respectively) was increased by increasing the concentration of H<sub>2</sub>O<sub>2</sub> (1, 5, and 10 mM) and decreasing the length of carbon chains. Reproduced with permission from Ref.<sup>247</sup>

## • Diselenide

Similar to disulfide bonds, diselenide bonds are responsive to oxidizing and reducing reagents. However, their sensitivity and responsiveness are higher than that of disulfide bonds.<sup>241,253</sup> The reason can refer to the lower bond energy of Se–Se (172 kJ mol<sup>-1</sup>) compared to S–S (240 kJ mol<sup>-1</sup>).<sup>254–256</sup> Diselenide bonds can be reduced to selenols in the presence of reductant (e.g., GSH and thioredoxin reductase)<sup>257</sup> and oxidized in the presence of RONS, including H<sub>2</sub>O<sub>2</sub>, <sup>1</sup>O<sub>2</sub>, <sup>•</sup>OH, and ONOO<sup>-</sup>. For instance, diselenides of selenocysteine methyl ester [-SeCH<sub>2</sub>CH(NH<sub>2</sub>)C(=O)OCH<sub>3</sub>]<sub>2</sub> were found to react with ONOO<sup>-</sup> with high rate constants (0.72–1.3×10<sup>3</sup> M<sup>-1</sup> s<sup>-1</sup>).<sup>232</sup> Low-molecular-mass diselenides (0.5–1.25 mM) were reacted with 100  $\mu$ M ONOO<sup>-</sup> at 22 °C in less than 5 s, monitored with loss in the absorbance of ONOO<sup>-</sup> (at 302 nm).

The mechanism of diselenide bond oxidation in the presence of RONS is similar to that of disulfide bonds.<sup>12</sup> The oxidation leads to cleavage of diselenide bond and the production of seleninic acid (**Figure 1.9**).<sup>258–260</sup>

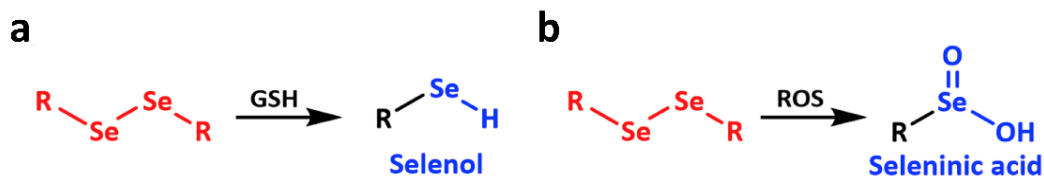


**Figure 1.9** Scheme of a) reduction and b) oxidation reactions of diselenide bonds in the presence of GSH and ROS, respectively. Reproduced with permission from Ref.<sup>261</sup>

The application of diselenide bond-containing materials has been restricted due to their general low solubility in water and instability in the presence of oxygen. However, Ma *et al.* improved the solubility by placing diselenide bond into a diol structure by conjugating an amphiphilic diselenide-containing polyurethane (PUSeSe) with two water-soluble PEG blocks (PEG-PUSeSe-PEG).<sup>262</sup> Afterwards, the diselenide-containing polymers were employed as ROS-responsive polymeric carriers, which are sensitive to relatively low concentrations of ROS<sup>253,254,263</sup> and exhibited almost 100% release of encapsulated fluorescent dye (i.e., rhodamine B) in response to diluted H<sub>2</sub>O<sub>2</sub> (~4.3 mM) over a 5-h period.<sup>263</sup>

The oxidation responsiveness of diselenide bonds has been utilized for different biomedical applications. Among all, they have mostly been used for drug delivery, chemotherapy, photodynamic therapy, and light therapy.<sup>221,238,243</sup> For instance Sun *et al.* utilized diselenide bonds not only for chemotherapy but also to compare the redox responsiveness of six different linkers (S, Se, S-S, Se-Se, C, and C-C) in the presence of GSH and H<sub>2</sub>O<sub>2</sub>.<sup>244</sup> As shown in **Figure 1.10a**, PTX, a chemotherapy medication, and CIT, monoterpene alcohol with antioxidant and anti-inflammatory properties,<sup>264</sup> were conjugated through linkers contained Se or Se-Se and compared their rate of release from each prodrug nano-assembly (PTX-Se-CIT and PTX-SeSe-CIT) different linkers (S, Se, S-S, Se-Se, C, and C-C) and PEGylated to form six prodrug nanoparticles. Upon exposure to H<sub>2</sub>O<sub>2</sub>, sulfur- and selenium-containing linkers underwent oxidation, followed by increasing the hydrophilicity of nanoparticles. The oxidation of linkers also resulted in the release of PTX by facilitating the hydrolysis of ester bonds placed in the neighbouring of the linkers. As shown in **Figure 1.10b,c**, the oxidation and H<sub>2</sub>O<sub>2</sub>-triggered drug release of conjugates followed the order of PTX-Se-CIT > PTX-S-CIT > PTX-SeSe-CIT > PTX-SS-CIT >>> PTX-CC-CIT and PTX-C-CIT, which inversely correlated to their electronegativity. Furthermore, selenoether/diselenide bond have been reported to have the ability to produce ROS *in vitro* due

to the toxicity of Se, which can induce apoptosis of tumor cells and promote the cytotoxicity of these prodrugs and the anticancer drug.

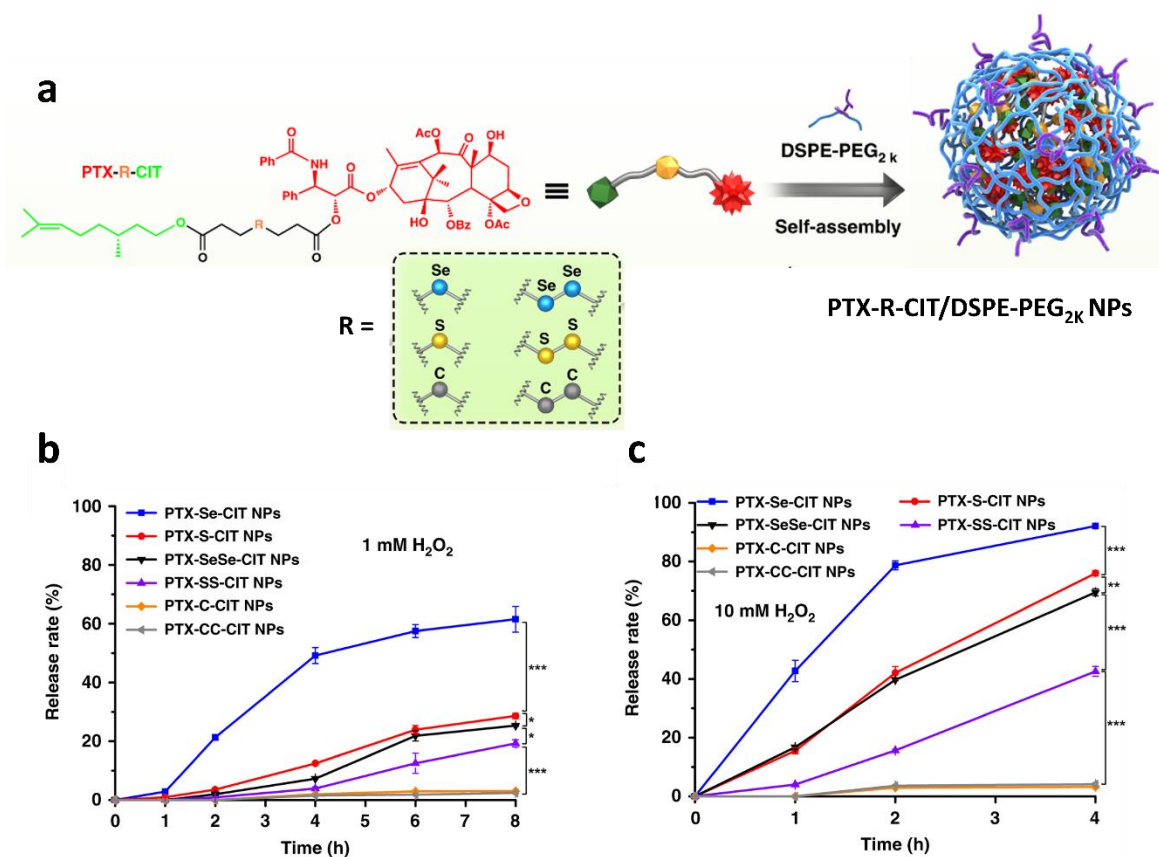


**Figure 1.10** (a) Scheme of prodrug nanoparticles preparation by utilizing different linkers between PTX and CIT for cancer therapy. The release of PTX from prodrug nanoparticles was achieved upon exposure to (b) 1 mM H<sub>2</sub>O<sub>2</sub> and (c) 10 mM H<sub>2</sub>O<sub>2</sub> due to the linker oxidation, which can facilitate the hydrolysis of adjacent ester bonds. The prodrugs nanoparticles contained Se exhibited the highest release rate in both conditions. Reproduced with permission from Ref.<sup>241</sup>

Furthermore, diselenide groups are responsive to ROS generated by  $\gamma$ -radiation<sup>259,265</sup> and light activates photosensitizers (visible light<sup>258</sup>, and red light<sup>266</sup>). For instance, Sun *et al.* developed a hyperbranched polymer by utilizing diselenide bonds and a porphyrin derivative, a fluorescent photosensitizer, as monomers that were polymerized with PEG.<sup>258</sup> Diselenide/porphyrin-containing hyperbranched polymer can self-assemble into nanoparticles through emulsification in an aqueous solution. Porphyrin can generate <sup>1</sup>O<sub>2</sub> upon irradiation with visible light. Accordingly, diselenide bonds started to oxidize after visible light irradiation of the porphyrin due to reaction with the produced <sup>1</sup>O<sub>2</sub>. 1-h visible light irradiation led to the degradation of the polymer into low-molecular-weight products due to the oxidation and cleavage of diselenide bonds. Furthermore,

the diselenide bonds could be oxidized to seleninic acid, which can exhibit cytotoxicity towards MDA-MB 231 human breast cancer cells and enhance the antitumor effect of PDT *in vitro*.  $\gamma$ -radiation also generates ROS, including  $\cdot\text{OH}$ ,  $\cdot\text{HO}_2$ , and  $\text{H}_2\text{O}_2$ , in an aqueous solution, leading to the oxidative cleavage of the diselenide bond.<sup>265</sup> For instance, Li *et al.* developed carrier-free nanoparticles that contain diselenide bonds for cancer radiotherapy combined with chemotherapy.<sup>259</sup> Upon mild  $\gamma$ -radiation with clinically doses of 2 or 5 Gy, the diselenide bonds were cleaved to form seleninic acids. Seleninic acid, as a chemotherapeutic drug,<sup>258</sup> increased the level of ROS in cancer cells, which leads to cell cytotoxicity and enhances the anticancer activity of radiotherapy in A549 lung cancer cells.

In general, disulfide and diselenide bonds are sensitive to high concentrations of RONS. When incorporating such bonds into nanocarriers, the system's stability should be considered in the biological environments to avoid any undesired linker breakages. Indeed, while being sensitive to reduction, disulfide and diselenide bonds do not exhibit rapid responses toward RONS. Moreover, diselenide bonds have been utilized for chemotherapy, radiotherapy and PDT due to the oxidation by  $^1\text{O}_2$  and  $\cdot\text{OH}$ , and the generation of seleninic acid *via* diselenide bond oxidation/breakage. However, the toxicity of released seleninic acid may limit their application. Last but not least, the responsiveness of diselenide bonds needs more investigation towards reactive species other than  $\text{H}_2\text{O}_2$ .

### 1.3.1.3 Vinyl disulfide

Vinyl disulfides (also referred to as *cis* (Z) bis(alkylthio)alkenes (BATAs)) have shown sensitivity toward  $^1\text{O}_2$ .<sup>267</sup> This group is usually synthesized through the nucleophilic reaction of thiolates with vinyl halides and is almost exclusively utilized in combination with type II photosensitizers, which produce  $^1\text{O}_2$  from molecular oxygen.<sup>268</sup> Among all reactive species,  $^1\text{O}_2$  reacts with the double bond of electron-rich vinyl disulfide through [2+2] cycloaddition and forms an unstable dioxetane intermediate, spontaneously followed by bond cleavage and generation of two carbonyl products (**Figure 1.11**).<sup>269</sup> However, the direct oxidation of sulfur is also possible, leading to the production of S-vinyl sulfoxide, which is no longer electron-rich. S-vinyl sulfoxide is not cleavable under exposure to  $^1\text{O}_2$  and affects the reactivity and efficiency of the vinyl disulfide-containing nanocarriers.<sup>270</sup>

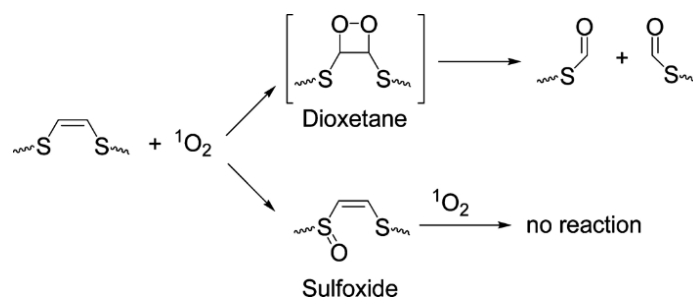


**Figure 1.11** Scheme of oxidation and transformation of vinyl in the presence of  $^1\text{O}_2$ .  $^1\text{O}_2$  can react with the double bond of vinyl disulfide and form unstable dioxetane intermediates, spontaneously followed by bond cleavage and generation of two carbonyl products. S-vinyl sulfoxide also can be generated from the direct reaction of a sulfur atom of vinyl disulfide with  $^1\text{O}_2$ . Reproduced with permission from Ref.<sup>270</sup>

Vinyl disulfide can functionalize polymer structures to construct  $^1\text{O}_2$ -responsive polymeric nanocarriers for photodynamic and cancer therapy.<sup>271,272</sup> Vinyl disulfide bonds can be utilized as the bridge between two different polymers, such as between PEG and poly( $\epsilon$ -caprolactone) (PCL)<sup>269</sup> or poly(D,L-lactic acid) (PDLLA).<sup>268</sup> For instance, amphiphilic diblock copolymers of PEG-b-PCL were designed as biocompatible visible-light responsive systems containing the  $^1\text{O}_2$ -sensitive vinyl disulfide linker between the blocks.<sup>269</sup> Self-assembled diblock copolymers were loaded with a long wavelength photosensitizer (i.e., Chlorin e6 (Ce6)) and a hydrophobic anticancer drug (i.e., DOX). Light irradiation ( $50 \text{ mW}\cdot\text{cm}^{-2}$ ; 660nm, 2 h) triggered photocleavage of the linker, and consequently, disassembly of the nanoparticles leading to enhancement of DOX release. Indeed, the release of loaded cargoes increased from ~35 to 45% over 25 h for the non-irradiated and irradiated samples, respectively. In another example, Dariva *et al.* developed two light-sensitive nanoparticles loaded with Ce6 and Dox based on copolymers of PEG (5 kDa) and PLA (1 or 10 kDa) connected to each other by the 1,2-bis(2-hydroxyethylthio)ethylene (BHETE), a vinyl disulfide moiety.<sup>268</sup> Accordingly, PEG<sub>5k</sub>-BHETE-PLA<sub>10k</sub> nanoparticles exhibited better Dox-controlled release by red-light irradiation compared to conjugate with PLA<sub>1k</sub> as a result of the tight PLA core. Vinyl disulfides can also be placed between mesoporous silica and a pore-blocking substrate for on-demand pore opening and drug release under light irradiation.<sup>267,273</sup> For instance, Yang *et al.* loaded the photosensitizer (i.e., Ce6) and a model therapeutic cargo (i.e., G3-Pt), within mesoporous silica nanorods.<sup>267</sup> Afterwards, nanorods were coated with bovine serum albumin through vinyl disulfide linkers to block the pores of nanorods and prevent undesirable drug release. The surface of the nanorods was then modified by attaching PEG to enhance the solubility and the physiological stability of nanorods. NIR light irradiation (1 h, 660 nm) induced the rapid release of loaded chemotherapeutic from the nanorods *in vitro* (6.5% vs. 31% for the

non-irritated and irritated samples, respectively). Furthermore, *in vivo*, the tumor growth was significantly inhibited after 2 weeks of therapy.

Overall, vinyl disulfides exhibit selectivity and sensitivity toward  $^1\text{O}_2$ , making it an option for photodynamic and cancer therapy. However, its efficiency and application are limited due S-vinyl sulfoxide production as a side reaction.

### 1.3.1.4 Thioketal

Thioketal groups have been shown to react with a broad spectrum of reactive species, including  $\text{H}_2\text{O}_2$ <sup>274</sup>,  $^1\text{O}_2$ <sup>275</sup>,  $\cdot\text{OH}$ <sup>276</sup>,  $\text{O}_2^{\cdot-}$ ,  $\text{ONOO}^-$ , and  $\cdot\text{OCl}$ .<sup>277</sup> Upon exposure to the oxidative environments, this group underwent the oxidation reaction that led to their cleavage and followed by the production of ketone or aldehyde and thiols by-products (**Figure 1.12**).<sup>278</sup> Zhang *et al.* have been the only group that compared the responsiveness of thioketal groups toward different RONS.<sup>277</sup> The authors investigated that the degradation of thioketal groups in the presence of RONS depends on the relative oxidation potency of these species ( $\cdot\text{OH} > \text{H}_2\text{O}_2 > \text{O}_2^{\cdot-}$ ). Furthermore, thioketal-containing materials underwent a faster degradation in the presence of  $\text{ONOO}^-$  and  $\cdot\text{OCl}$  compared to  $\cdot\text{OH}$ ,  $\text{H}_2\text{O}_2$ , and  $\text{O}_2^{\cdot-}$ . Thioketal groups can also be used to temporarily mask carbonyl groups (ketone, aldehyde), which are then exposed upon reaction with RONS and leading to the production of respective ketone or aldehydes.<sup>278,279</sup>

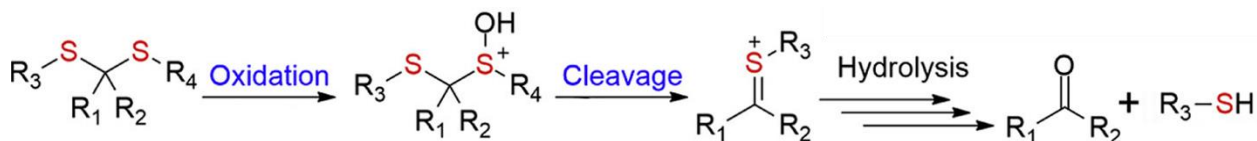


**Figure 1.12** Scheme of oxidation and degradation of thioketal bonds by RONS. RONS can oxidize a sulfur of thioketal bonds and lead to the generation of the respective ketones or aldehydes components by forming a thionium intermediate and its consequence hydrolysis. Adapted and modified from Ref.<sup>278</sup>

Thioketal groups have great potential for therapeutic applications<sup>280–282</sup> due to RONS-sensitivity and their known stability to acidic and basic conditions<sup>283</sup>. Thioketals can be placed in the main chain of polymers to form hydrophobic thioketal containing polymers, including poly(1,4-phenyleneacetone dimethylene thioketal) (PPADT)<sup>279,281,284</sup> or as a side chains of polymers to conjugate the drugs.<sup>285</sup> Kim *et al.* have investigated the degradation of PPADT in the presence of  $\cdot\text{OH}$  (generated by 10 mM  $\text{H}_2\text{O}_2$  and 20 mM ferrous perchlorate solution in PBS) and  $\text{O}_2^{\cdot-}$  (generated by 10 mM  $\text{KO}_2$  in degassed PBS).<sup>279</sup> The molecular weight of Nile red-loaded PPADT nanoparticles dropped to ~29% of its original value in the presence of 10 mM  $\text{KO}_2$  (containing

$O_2^{\cdot-}$ ) over a 24-h period, and ~44% drug release was equally observed. Drug release decreased to ~26% over 60 h in 10 mM  $H_2O_2$  solution (containing  $\cdot OH$ ). Based on their report, the thioketal group was more sensitive to  $O_2^{\cdot-}$  than to  $\cdot OH$ , due to the catalytic peroxidation-like chain reaction between  $O_2^{\cdot-}$  and the sulfur of PPADT.<sup>286</sup> Furthermore,  $\pi$ -conjugated thioketal moieties have attracted interest in cancer therapy not only because of RONS-sensitivity but also due to their potential in enhancing drug loading content by  $\pi$ - $\pi$  interactions between  $\pi$ -conjugated thioketal moieties and anticancer drug.<sup>287,288</sup> For instance, Sun *et al.* prepared block copolymer mPEG-thioketal-poly( $\epsilon$ -caprolactone) that could self-assemble into micelles. DOX was physically encapsulated into micelles *via*  $\pi$ - $\pi$  interactions between an aromatic thioketal and DOX.<sup>287</sup> The micelle showed high drug loading and encapsulation efficiency (12.8% and 64%, respectively) under physiological conditions. Afterwards, the release of DOX was reported around 50% and 30% within ~12 h at acidic condition (pH 5.5), with or without 10 mM  $H_2O_2$  incubation, respectively. In addition, Xu *et al.* compared the RONS sensitivity of three different amphiphilic copolymer micelles, including mPEG-poly(thioketal-ester), mPEG-poly(thioketal-ester-thioether) and mPEG-poly(ester-thioether).<sup>289</sup> Nile red was loaded into polymers as a model drug. The mPEG-poly(ester-thioether) nanoparticles showed the highest drug release (65%) in the presence of 500  $\mu M$   $H_2O_2$  within 72 h compared to poly(thioketal-ester-thioether) that exhibited 47% drug release in the same condition. Therefore, the authors showed that the thioketal bonds exhibited lower reactivity toward RONS than thioether bonds. Some works have also been proceeded based on Fenton reaction (an iron-mediated reaction that led to the conversion of  $H_2O_2$  to highly reactive and toxic  $\cdot OH$ ) and  $\cdot OH$ -responsive thioketal groups for cancer therapy.<sup>276,285</sup>

Thioketal bonds have also been widely applied for synergistic PDT in combination with chemotherapy, immunotherapy, and gene therapy due to the degradation of thioketals in response to  $^1O_2$ .<sup>290-292</sup> For instance, Wang *et al.* formed polyplexes by condensing thioketal-crosslinked polyethylenimine with plasmid DNA encoding p53 to obtain efficient gene delivery combined with photodynamic therapy.<sup>293</sup> Accordingly, a negatively charged photosensitizer, pheophytin a, was modified by hyaluronic acid and called HA-Pha. Afterward, HA-Pha was used to shield the positive charge of polyplexes, which enhanced colloidal stability and the cellular uptake in cancer cells. A non-toxic amount of ROS was produced by pheophytin a by a brief (8 min) far-red light irradiation, which promoted intracellular p53 gene release by decomposition of the thioketal cross-linker. However, prolonged exposure (30 min) produced lethal amounts of ROS, thus achieving cooperative anti-cancer efficacy by photodynamic therapy.

Overall, thioketal groups have been widely utilized for biomedical applications, including drug delivery, synergistic PDT in combination with chemotherapy, immunotherapy, and gene therapy. Notably, thioketal-containing materials are resistant to hydrolysis in different pH environments, making them interesting for applications involving harsh pH environments.<sup>281</sup> Furthermore, they do not show rapid degradation in the presence of H<sub>2</sub>O<sub>2</sub> but respond readily to <sup>1</sup>O<sub>2</sub> produced by photosensitizers.

### 1.3.1.5 Oxalate

The responsiveness of oxalate groups has been mainly investigated in the presence of H<sub>2</sub>O<sub>2</sub>. However, it exhibited sensitivity toward other RONS, including <sup>-</sup>OCl, <sup>•</sup>NO, <sup>•</sup>OH, and O<sub>2</sub><sup>•-</sup>.<sup>294</sup> As shown in **Figure 1.13**, oxalate bonds can be oxidized upon exposure to oxidants such as H<sub>2</sub>O<sub>2</sub>, leading to the generation of an intermediate 1,2-dioxetanediones and their corresponding alcohols or diols. Afterward, intermediate 1,2-dioxetanediones can be rapidly decomposed into CO<sub>2</sub> due to their high energy.<sup>295–297</sup> Energy from the degradation of 1,2-dioxetanediones can be transferred to various surrounding fluorescent dyes, leading to their excitation accompanied by light emission.

<sup>295,298,299</sup>

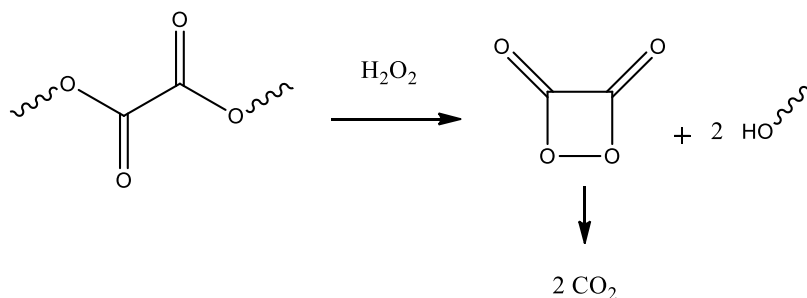


**Figure 1.13** Scheme for the oxidation of oxalate bonds upon exposure to H<sub>2</sub>O<sub>2</sub>. The oxidation of oxalate groups led to the generation of their corresponding alcohols or diols and intermediate dioxetanedione, followed by the generation of CO<sub>2</sub>. Adapted and modified from Ref.<sup>298</sup>

Peroxalate esters have been utilized for drug delivery as a linker between two block polymers,<sup>300</sup> side chains to link the drugs to different copolymers,<sup>297</sup> or monomers in the polymer backbones to produce hydrophobic polyoxalate.<sup>301</sup> Polyoxalate can degrade in response to H<sub>2</sub>O<sub>2</sub> and water, leading to nontoxic byproducts with low molecular weights.<sup>301,302</sup> Furthermore, polyoxalate exhibited highly potent for drug delivery due to their great biocompatibility and biodegradability with less cytotoxic than poly(lactic acid-co-glycolic acid) nanoparticles.<sup>301,302</sup> In addition, oxalate esters can be polymerized with a variety of diol/diphenol-containing antioxidants, such as curcumin, 4-vanillyl alcohol, and p-hydroxybenzyl alcohol, to develop the antioxidant polymeric

nanoparticles, including poly(oxalate-co-curcumin), vanillyl alcohol-incorporated copolyoxalate, and p-hydroxybenzyl alcohol-incorporated copolyoxalate (HPOX), respectively.<sup>303–307</sup> In oxidative microenvironments, the oxalate bond of these polymers underwent oxidation, resulting in the release of antioxidants for therapeutic effects in inflammatory diseases. For instance, HPOX nanoparticles can prevent the expression of inducible nitric oxide synthase and the production of pro-inflammatory mediators in LPS-activated RAW 264.7 macrophage cells.<sup>307</sup> HPOX also showed anti-asthmatic effects in a murine model of allergic asthma by releasing its monomer (p-hydroxybenzyl alcohol), a H<sub>2</sub>O<sub>2</sub> scavenger, which prevents the recruitment of inflammatory cells and the expression of pro-inflammatory mediators. Accordingly, HPOX can be applied as a therapeutic agent against airway inflammatory diseases.<sup>308</sup>

Different oxalate-containing fluorescent probes have been used to detect RONS, especially H<sub>2</sub>O<sub>2</sub>, *in vitro* and *in vivo*.<sup>294,295,309,310</sup> For this purpose, oxalate bonds were mainly employed as sources to excite fluorophores encapsulated into nanocarriers.<sup>295,309,310</sup> For example, Lee *et al.* synthesized fluorescent peroxalate nanoparticles for the sensitive and selective imaging of H<sub>2</sub>O<sub>2</sub> in the peritoneal cavity of mice experiencing inflammation.<sup>295</sup> The authors indicated that generated dioxetanedione excited the encapsulated fluorescent dyes (i.e., pentacene) *via* the chemically initiated electron-exchange luminescence mechanism.<sup>298</sup> Accordingly, the chemiluminescence emission intensity of dye increased in the presence of 10 μM H<sub>2</sub>O<sub>2</sub> around 50 times higher than with either tert-butyl peroxide or the ·OH. *In vivo*, the chemiluminescence intensity was almost 2 times higher in mice injected with LPS than in mice treated with saline and peroxalate nanoparticles. In another example, Yang *et al.* reported an oxalate–curcumin-based probe for near-IR fluorescence imaging and detection of RONS at sites of inflammation (Alzheimer's disease).<sup>294</sup> In contrast with the majority of articles, they investigated the responsiveness of oxalate-containing systems in the presence of a variety of RONS (250 nM), including H<sub>2</sub>O<sub>2</sub>, ·OCl, ·NO, ·OH, and O<sub>2</sub><sup>·-</sup>. Accordingly, oxalate–curcumin-based probe possessed a fast concentration-dependent response to all tested RONS with the highest and lowest responsiveness toward O<sub>2</sub><sup>·-</sup> and H<sub>2</sub>O<sub>2</sub>, respectively, during 15 min incubation. Oxalate bonds are also the options for theranostic applications due to their advantages in therapeutic and diagnostic applications.<sup>311,312</sup>

In summary, oxalate bonds have been employed for drug delivery, RONS detection, and theranostic applications. Polyoxalate moieties have been employed for drug delivery and antioxidant therapy due to their responsiveness toward RONS, biocompatibility, and biodegradability. Furthermore, the generated intermediate dioxetanedione can excite other fluorophores, facilitating ROS detection and imaging. They also generally exhibited slow

oxidative-oxalate breakage in the presence of physiologically-relevant concentrations of  $\text{H}_2\text{O}_2$ . One of the limitations of oxalate-based materials is the hydrolysis of peroxalate ester linkers in aqueous solvents. Therefore, oxalate-based materials require the protection of peroxalate linkers in aqueous solvents to achieve an efficient and more practical system.

### 1.3.1.6 Boronic acids/esters

Boronic acids/esters are highly electrophilic groups due to their  $\text{sp}^2$ -hybridized boron atom with an empty p orbital. A variety of RONS, including  $\text{H}_2\text{O}_2$ ,<sup>313</sup>  $\text{ONOO}^-$ ,<sup>313</sup>  $\text{OCl}^-$ ,<sup>314</sup>  $\cdot\text{OH}$ ,<sup>315</sup>  $\text{NO}$ ,  $^1\text{O}_2$ ,<sup>316</sup> and  $\text{O}_2^{\cdot-}$ <sup>313</sup> can oxidized boronic acids/esters groups. **Figure 1.14a** presented the oxidation reaction of boronic acids/esters groups in the presence of  $\text{H}_2\text{O}_2$  as a model of oxidizing agents. The nucleophile oxygen of  $\text{H}_2\text{O}_2$  inserts an oxygen atom into the C–B bond of boronic acids/esters, followed by R group migration to oxygen, resulting in hydrolysis into corresponding alcohol and boric acid.<sup>317–319</sup> In cases of participating arylboronic acids/esters, oxidation of the C–B bond will be followed by cleavage of the phenyl group from boron of arylboronic acids/esters *via* a quinone methide rearrangement (1,6-elimination) (**Figure 1.14b**). Accordingly, the process leads to the generation of corresponding alcohol, boric acid, and the generation of quinone methide, a toxic and active anticancer compound.<sup>318,320,321</sup>

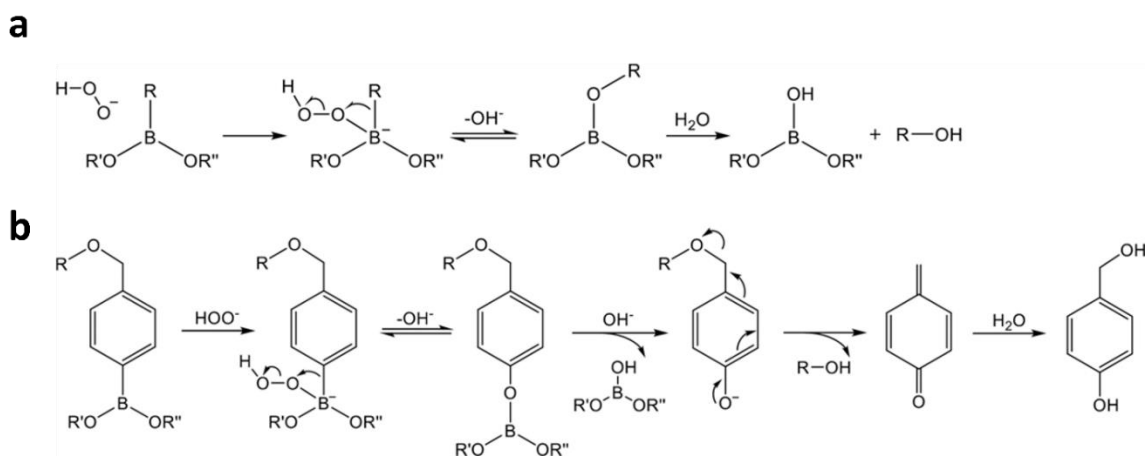


**Figure 1.14** Reaction mechanism of boronic acids/esters oxidation in the presence of  $\text{H}_2\text{O}_2$  as a model of RONS. (a) The nucleophile oxygen of  $\text{H}_2\text{O}_2$  can attack the boron atom of boronic acids/esters and lead to R migration to oxygen, followed by hydrolysis into corresponding alcohol and boric acid. (b) In arylboronic acids/esters, phenyl group will be cleaved from boron after oxidation of C–B bond by  $\text{H}_2\text{O}_2$ . The process leads to the release of ROH, boric acid, and quinone methide. Reproduced with permission from Ref.<sup>319</sup>

Among all boronic acids/esters derivatives, arylboronic acid/ester groups have attracted great attention due to their specificity and high selectivity to  $\text{H}_2\text{O}_2$ ,  $\text{OCl}^-$ , and  $\text{ONOO}^-$ .<sup>322</sup>  $\text{OCl}^-$  reacts

with aryl boronates around  $10^4$  times faster than  $\text{H}_2\text{O}_2$ .<sup>314</sup> However, in biological conditions,  $\text{OCl}^-$  reacts more rapidly with cellular thiols and amines compared to the oxidation of boronates.<sup>323</sup> At physiological pH, the reaction of  $\text{ONOO}^-$  with arylboronates is  $10^6$  times faster than the hydrogen peroxide-mediated oxidation, likely due to the anionic form of  $\text{ONOO}^-$  in comparison to neutral  $\text{H}_2\text{O}_2$ .<sup>314</sup>

Boronic acids/esters have been used widely in biomedical applications, including drug delivery, imaging probes, prodrugs, and vaccines.<sup>324–327</sup> For instance, Lux *et al.* synthesized a polyester with each monomer bearing arylboronic esters.<sup>317</sup> Afterward, hydrophobic Nile red was loaded into nanoparticles by the oil-in-water emulsion techniques to measure polymer degradation in the presence of  $\text{H}_2\text{O}_2$ . The arylboronic ester bonds located in the polymer's backbone underwent degradation in the presence of biologically relevant concentrations of  $\text{H}_2\text{O}_2$  (0.05 mM) due to oxidation and subsequent hydrolysis of arylboronic ester groups. This led to 40% cargo release over 25 h incubation. In another example, Zhao *et al.* designed caged thiocarbamate-functionalized arylboronates, a ROS-triggered  $\text{H}_2\text{S}$  donor, for  $\text{H}_2\text{S}$ -related therapies.<sup>313</sup>  $\text{H}_2\text{S}$  is a potential signalling compound that plays a vital role in mammalian biology.<sup>326</sup> The generation of  $\text{H}_2\text{S}$  was observed in 20 min incubation of prodrug (50  $\mu\text{M}$ ) with 500  $\mu\text{M}$  of various RONS, including  $\text{OCl}^-$ ,  $\text{OH}^\cdot$ ,  $^1\text{O}_2$ , Cys, GSH, GSSG,  $\text{NO}_2^-$ ,  $\text{NO}$ , or  $\text{HNO}$ . However, only incubation with  $\text{H}_2\text{O}_2$ ,  $\text{O}_2^{\cdot-}$ , or  $\text{ONOO}^-$  caused the oxidation of arylboronic ester, self-immolative reaction, and eventually led to the release of carbonyl sulfide (COS), which is quickly hydrolyzed to  $\text{H}_2\text{S}$ .

A variety of luminescent boronate-based probes have been developed for detection/imaging of the reactive species, including fluorescent,<sup>227,232</sup> chemiluminescent,<sup>328,329</sup> and bioluminescent<sup>330,331</sup> probes. Some boronate-based probes can accumulate in specific organelles such as the mitochondria,<sup>332</sup> nucleus,<sup>333</sup> or lysosome<sup>334</sup> via covalently attachment to an organelle-targeting moiety for RONS detection.<sup>335</sup> Boronate-based probes have emerged to detect exogenous and endogenous reactive species, including  $\text{H}_2\text{O}_2$ ,<sup>336</sup>  $\text{ONOO}^-$ ,<sup>337</sup> and  $\text{OCl}^-$ <sup>338</sup> *in vitro* and *in vivo*. For instance, Palanisamy *et al.* developed a boronate-based fluorescent probe, to detect the generated  $\text{ONOO}^-$  *in vitro* and *in vivo*.<sup>339</sup> Upon the addition of  $\text{ONOO}^-$  and elimination of the aryl boronate, a decrease in emission 385 nm and an increase at 450 nm were observed, suggesting its ability for ratiometric detection of  $\text{ONOO}^-$ . The probe's emission ratio  $I_{450}/I_{385}$  showed a linear relationship with  $\text{ONOO}^-$  concentration between 0–10  $\mu\text{M}$  with a detection limit of 29.8 nM. Furthermore, the reaction between boronate-based fluorescent probe (5  $\mu\text{M}$ ) and  $\text{ONOO}^-$  (1 eq.) finished in 5 min, and no response was observed in the presence of other RONS (20 eq.) such as  $\text{NO}^{2-}$ ,  $\text{NO}^{3-}$ ,  $\text{NO}$ ,  $\text{H}_2\text{O}_2$ ,  $\text{OCl}^-$ ,  $\text{OH}^\cdot$ ,  $\text{OtBu}$ , TBHP. Subsequently, endogenous  $\text{ONOO}^-$  was

detected in RAW 264.7 macrophages and EAhy926 cells that were treated with boronate-based fluorescent probe and stimulator of  $\text{ONOO}^-$ , including bacterial endotoxin LPS, pro-inflammatory cytokine interferon, 3-morpholininosydnonimine (SIN-1) and phorbol-12-myristate 13-acetate (PMA). Finally, the overproduction of  $\text{ONOO}^-$  in High-Fat-Diet-induced kidney injury was demonstrated in the High-Fat-Diet tissue model of male C57BL/6J mice *via* a considerable increase in emission. The obtained results proved the selectivity and sensitivity of 4-MB for  $\text{ONOO}^-$  *in vitro* and *in vivo*. In another example, Hou *et al.* prepared a NIR ratiometric fluorescent probe (AB1) in which a red fluorescent dye (DDAO) was attached to phenylboronic ester *via* an ether linkage for the imaging of  $\text{H}_2\text{O}_2$  *in vitro* and *in vivo*.<sup>340</sup> AB1 exhibited a relatively strong fluorescence emission at 620 nm by excitation at 480 nm. Upon exposure to  $\text{H}_2\text{O}_2$ , the phenyl boronic ester group underwent the oxidation and self-immolative cascade reaction resulting in a red-shifted emission wavelength due to the release of corresponding fluorophore DDAO with different excitation and emission wavelengths ( $\lambda_{\text{ex}}/\lambda_{\text{em}}$  600/660 nm) (Figure 1.15). AB1 exhibited high selectivity and sensitivity toward  $\text{H}_2\text{O}_2$  (100  $\mu\text{M}$ ) compared to the other RONS (1 mM), including  $\cdot\text{OH}$ ,  $\text{NO}$ ,  $\text{ROO}\cdot$ ,  $\text{O}_2^{\cdot-}$ , and  $^-\text{OCl}$ . Indeed, the emission wavelength of AB1 (5  $\mu\text{M}$ ) was almost completely shifted from 620 nm to 660 nm after 1 h incubation with  $\text{H}_2\text{O}_2$  (100  $\mu\text{M}$ ). Eventually, probe AB1 exhibited NIR fluorescence turn-on and a ratiometric response to  $\text{H}_2\text{O}_2$  in HeLa cells stimulated with PMA-induced ROS formation and in a murine model of acute inflammation.

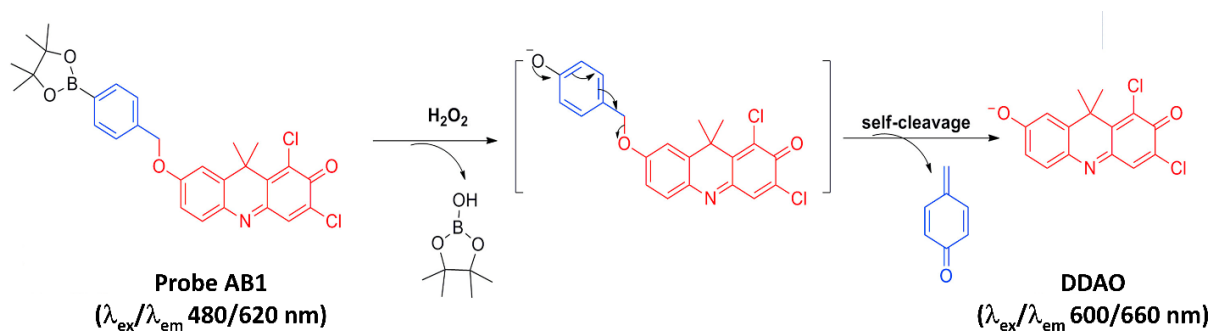


**Figure 1.15**  $\text{H}_2\text{O}_2$ -sensing mechanism of AB1. Under reaction with  $\text{H}_2\text{O}_2$ , the phenyl boronic ester group of AB1 underwent cleavage, resulting in the release of DDAO with red-shifted emission wavelength ( $\lambda_{\text{ex}}/\lambda_{\text{em}}$  600/660 nm) due to a strong intramolecular charge transfer (ICT) process. Adapted from Ref.<sup>340</sup>

Boronic acids/esters groups exhibited efficient and selective responses toward RONS. However, sometimes it is challenging to identify the reactive species involved. Accordingly, their sensitivity toward multiple RONS may limit the application of the probes to detect specific reactive species in biological systems. Moreover, the 1,6-elimination reaction may release the benzyl group in the

highly toxic quinone methide form, limiting its application *in vitro* and *in vivo*. However, quinone methide could be applied for anticancer therapy.<sup>341,342</sup> Furthermore, many of the current imaging probes are designed based on boronate structures due to the ease of functionalization, simple deprotection mechanism and high selectivity/sensitivity toward reactive species.

### 1.3.1.7 Ferrocene

Ferrocene (bis-cyclopentadienyl iron,  $\text{Cp}_2\text{Fe}$ ) is an organometallic compound with two  $\pi$ -bonded cyclopentadienyl (Cpa) ligands on an iron. As shown in **Figure 1.16**, ferrocene has a symmetrical structure with reversible oxidation properties and is frequently referred to as a “sandwich complex”.<sup>343</sup> Generally, the ferrocene moieties are non-toxic and water-stable, which can be quickly oxidized by oxygen under acidic conditions.<sup>344,345,346</sup> Ferrocene-containing nanosystems have shown responsiveness towards  $\text{H}_2\text{O}_2$ ,  $^-\text{OCl}$ ,  $^1\text{O}_2$ , and oxygen.<sup>347–349</sup> In general, ROS trigger the oxidation of the hydrophobic neutral ferrocene (Fc) into hydrophilic ferrocenium ( $\text{Fc}^+$ ) without changing its molecular structure.<sup>350,351</sup> The oxidation of ferrocene in ferrocene-containing nanoparticles depends on the oxidant's ability to diffuse in the shell. For instance, unipolar ( $\text{H}_2\text{O}_2$ ) molecules can more effectively oxidize the ferrocene side groups than negatively charged oxidants ( $\text{MnO}_4^-$ ) due to their ionic character and diffusion rate.<sup>350,352</sup>

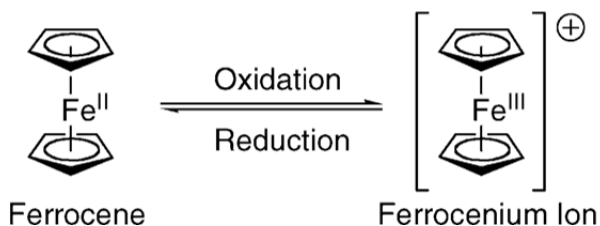


**Figure 1.16** Oxidation and reduction reactions of Ferrocene. Reproduced with permission from Ref.<sup>343</sup>

In general, most researchers have investigated the effect of  $\text{H}_2\text{O}_2$  on the ferrocene groups compared to other reactive species. However, some works reported the effect of  $^-\text{OCl}$ , oxygen, and  $^1\text{O}_2$  on nanocarriers containing ferrocene.<sup>347–349</sup> For instance, Xu *et al.* reported stimuli-responsive nanoparticles based on ferrocene-modified chitosan oligosaccharides to deliver 5-fluorouracil, an antitumor drug, under exposure to oxidants.<sup>347</sup>  $^-\text{OCl}$ ,  $\text{H}_2\text{O}_2$ , and oxygen were used model oxidants and showed the acceleration in nanoparticle disassembly due to oxidation of ferrocene in acidic solution (pH 3.8). It is worth mentioning that the oxidative power of oxygen rises significantly in the presence of acids. However, ferrocene is highly stable in oxygen without acids, as its redox potential is more than oxygen.<sup>348</sup>

Ferrocene has been used as a hydrophobic building block to synthesize self-assembled amphiphilic block copolymers for controlled drug release. For instance, Staff *et al.* prepared functional nanocapsules consisting of a poly(vinylferrocene)-block-poly(methyl methacrylate) copolymer shell and a hydrophobic liquid core contained that was selectively oxidized by H<sub>2</sub>O<sub>2</sub>.<sup>352</sup> This system was used to encapsulate fluorescent pyrene as a model of a hydrophobic substrate and then release it by hydrophobic to hydrophilic transition of ferrocene upon oxidation. Ferrocene also can be utilized as hydrophobic side chains within ferrocene-containing polymers in ROS-mediated drug delivery systems.<sup>273</sup> For instance, Liu *et al.* presented a ferrocene-containing self-assembled block copolymer (PEG-*b*-PMAEFc) for controlled release of a fluorescent dye (i.e., rhodamine B) in the presence of H<sub>2</sub>O<sub>2</sub> (**Figure 1.17**).<sup>350</sup> The release of rhodamine B from PEG-*b*-PMAEFc nanoparticles occurred due to ferrocene oxidation in the presence of ~0.6 M H<sub>2</sub>O<sub>2</sub>. In the presence of oxidants, the charge density and electrostatic repulsion between the side chains can be enhanced due to ferrocene oxidation, leading to the swelling of the micellar cores and followed by releasing the encapsulated drugs.<sup>347,352</sup> In another example, Na *et al.* prepared ferrocene-containing polymer nanocapsules for ROS-mediated delivery of the antioxidant  $\alpha$ -tocopherol to aid wound healing.<sup>353</sup> Accordingly, they utilized the ROS-scavenging advantage of ferrocene moieties<sup>354</sup> to enhance the antioxidant capacities of their system. Ferrocene polymer nanocapsules exhibited dissociation in the presence of ROS due to the oxidation of ferrocene, thereby releasing  $\alpha$ -tocopherol. Accordingly, 20% cumulative release was achieved within 2 h incubation in the presence of 100 mM H<sub>2</sub>O<sub>2</sub>, reaching ~80% after 24 h in PBS (pH 7.4). However, in the absence of H<sub>2</sub>O<sub>2</sub>, only 20% release was observed after 24 h. Finally, their system inhibited tissue damage of wounded sites *in vitro* (scratch assay) by promoting cell proliferation, migration and acceleration of the healing process due to their ROS scavenging activity.

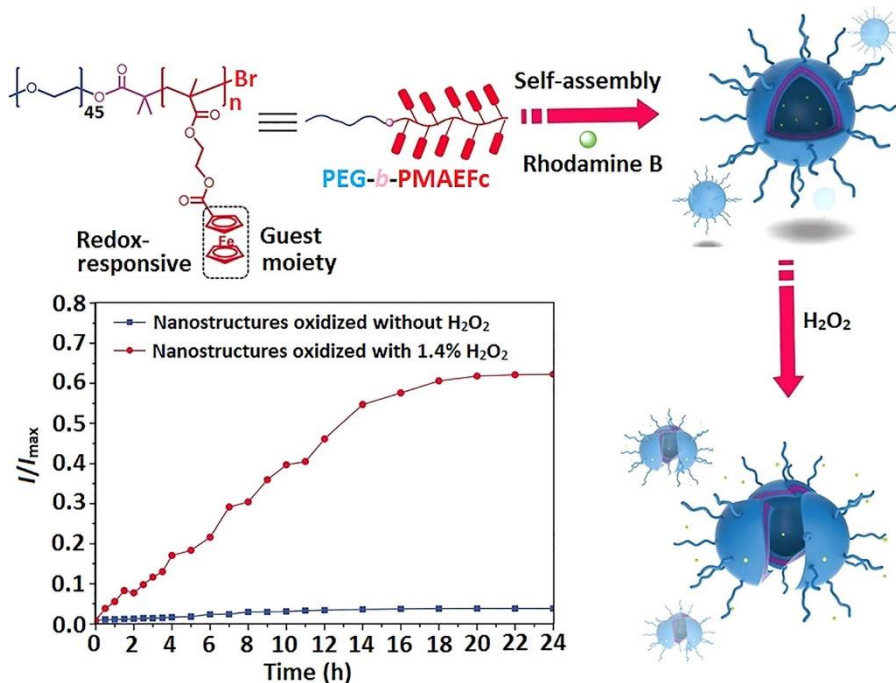


**Figure 1.17** Self-assembly of PEG-b-PMAEFC and responsiveness toward  $\sim 0.6$  M (1.4% v/v) H<sub>2</sub>O<sub>2</sub>, followed by releasing rhodamine B from nanoparticles, which was confirmed by enhancement in fluorescence intensity. Adapted from Ref.<sup>350</sup>

Ferrocene-based materials have also been utilized for  $\cdot\text{OCl}$  imaging and detection.<sup>355,356</sup> In 2010, a ferrocene-based fluorescent probe was reported for  $\cdot\text{OCl}$  fluorescence imaging in live cells (HeLa cells).<sup>356</sup> The probe was designed by connecting ferrocene and an anthracene fluorophore via a double bond as a linker. The probe strategy was based on the intramolecular charge-transfer (ICT) process between electron-donor ferrocene to an anthracene unit that led to the strong quenching effect of the ferrocene over the anthracene unit. The double bond of the linker was cleaved selectively just in 10 min presence of  $\cdot\text{OCl}$  (100  $\mu\text{M}$ ) but not in the presence of other ROS ( $\cdot\text{OH}$  (100  $\mu\text{M}$  Fe<sup>2+</sup> + 1 mM H<sub>2</sub>O<sub>2</sub>), O<sub>2</sub><sup>-</sup> (1 mM KO<sub>2</sub>), <sup>1</sup>O<sub>2</sub> (1 mM Na<sub>2</sub>MoO<sub>4</sub> + 2 mM H<sub>2</sub>O<sub>2</sub>), and H<sub>2</sub>O<sub>2</sub> (1 mM)) in pH 7.4, along with restoring the fluorescence of anthracene. Interestingly, the authors could not demonstrate the oxidation of ferrocene in the presence of  $\cdot\text{OCl}$ . However, they utilized the strong quenching effect of electron-donor ferrocene on anthracene fluorescence for  $\cdot\text{OCl}$  imaging. Furthermore, ferrocene-containing structures exhibited the potential to be used for PDT and cancer therapy due to the responsiveness of Ferrocene toward <sup>1</sup>O<sub>2</sub> and H<sub>2</sub>O<sub>2</sub>, respectively.<sup>349,357</sup>

In general, ROS-responsive nanosystems containing ferrocene groups have shown several advantages, including reversible redox properties, stability, ROS-scavenging, and a convenient synthesis process.<sup>343,358,359</sup> However, some studies have also reported various disadvantages

limiting their application, including low yield preparation due to multistep processes, poor solubility, and uncontrollable size and surface charges of nanoparticles.<sup>360,361</sup> Furthermore, it is still challenging to expand their therapeutic or diagnostic applications further as their responsiveness towards different reactive species has not been broadly investigated.

### 1.3.1.8 Cyanine and Hydrocyanine

- **Cyanine**

The absorbance and emission spectra of cyanine dyes can be adjusted from UV to infrared regions based on modifications to their molecular structure.<sup>362</sup> Cyanine dyes have been used as fluorescent labels, particularly in biomedical imaging.<sup>363,364</sup> However, it was discovered that cyanine dyes could be used to detect and image reactive species, especially  $\text{OCl}^-$ ,  $\text{ONOO}^-$ , and  $\cdot\text{OH}$ .<sup>365–367</sup> Indeed, the electron-deficient C=C bonds of polyenes are unstable in the presence of such reactive species. As a result, cyanine dyes go through oxidation and regioselective cleavage reactions that mainly happen at the  $\alpha$ -amine C=C bond position (**Figure 1.18**).<sup>368,369</sup>

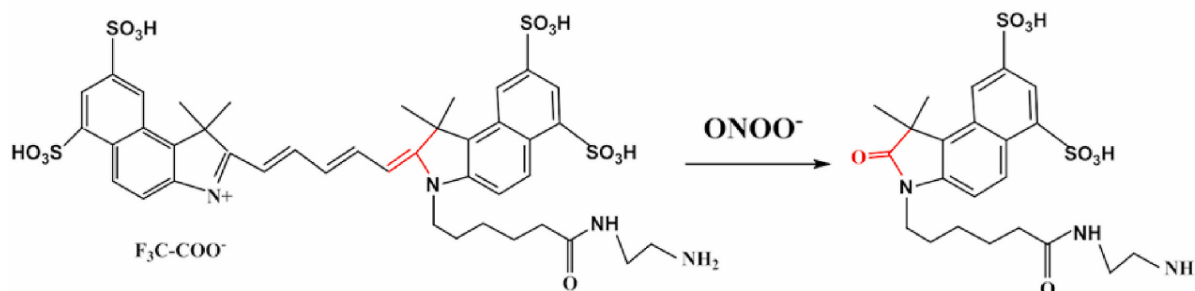


**Figure 1.18** The oxidation reaction of Cy5.5 in the presence of RONS, such as  $\text{ONOO}^-$  led to the breakage of the carbon-carbon double bond of the specific site of Cy5.5. Reproduced with permission from Ref.<sup>370</sup>

Different cyanine-dye-containing probes have been employed for the detection and quantification of reactive species in living organisms.<sup>365</sup> For instance, Karton-Lifshin *et al.* have developed a quinone-cyanine 7 probe that was used as a “turn-on” detector for  $\text{H}_2\text{O}_2$  detection with less than 1  $\mu\text{M}$  detection sensitivity.<sup>365</sup> In their report, the fluorescence intensity of probe was inhibited due to the attachment of phenylboronic acid to the quinone group of quinone-cyanine 7 through an ether linkage. Upon reaction with  $\text{H}_2\text{O}_2$ , the phenylboronic acid was removed and followed by  $\pi$ -electrons relocation that led to the formation of cyanine dye with strong NIR fluorescence. In another work, Oushiki *et al.* have designed a fluorescence probe, FOSCY-1, by attaching Cy5 and Cy7 through a linker to detect reactive species in HL60 cells and mouse models experiencing

oxidative stress.<sup>371</sup> Based on their observations, more potent oxidants such as  $^-\text{OCl}$  (10  $\mu\text{M}$ ),  $\text{ONOO}^-$  (10  $\mu\text{M}$ ), and  $^-\text{OH}$  ( $\text{H}_2\text{O}_2$  (1 mM) and  $\text{Fe}(\text{ClO}_4)_2$  (50  $\mu\text{M}$ )) were able to abolish the absorbance of cyanine dyes. However, in the presence of the weaker oxidants ( $\text{O}_2^{\cdot-}$  and  $\text{H}_2\text{O}_2$ ), fewer changes were observed in the absorption spectrum. Furthermore, introducing electron-donating groups such as thioethers into cyanine structures can enhance their reactivity toward RONS.<sup>371</sup> However, attaching electron-withdrawing molecules such as sulfonate, CN, or Br groups to the indolenine moiety can reduce the reactivity and enhance the photostability in the presence of RONS.<sup>371-373</sup> Cyanine has also been used as a reporter group in cyanine-dye-containing probes, while a dye or molecule with an insensitive signal has been employed as a reference.<sup>374</sup> Moreover, some works have explored the use of rare earth<sup>375</sup> or semiconducting<sup>376</sup> polymer-based fluorescent probes for ratiometric detection and quantitatively imaging the reactive species.

Cyanine-based materials have also been reported to quench  $^1\text{O}_2$  generation in the absence of oxidants for on-demand PDT.<sup>377</sup> It is well-known that the interaction of excited cyanine with  $\text{O}_2$  can produce  $^1\text{O}_2$  and  $\text{O}_2^{\cdot-}$ , which eventually cause decomposition and photofading of cyanine dyes through oxidative cleavage of their central polymethine chain.<sup>372,378,379</sup> As a result, the polymethine skeleton is inherently subjected to light-dependent decomposition.<sup>369,372,380</sup> Hence, some researchers have used cyanine dyes as photosensitizers in PDT,<sup>231,381</sup> while cyanine dyes were covered in hydrophobic cages to improve and protect their photostability in aqueous media.<sup>381,382</sup> Cyanine-dye-based materials also find applications in antioxidative therapy due to their ability to scavenge reactive species.<sup>383</sup>

- **Hydrocyanine**

Hydrocyanines have been employed to detect reactive species, including  $\text{O}_2^{\cdot-}$  and  $^-\text{OH}$ .<sup>384,385</sup> They have been synthesized for the first time by Kundu *et al.* in 2009 by reducing cyanine dyes with  $\text{NaBH}_4$ .<sup>386</sup> Hydrocyanines are in the class of non-fluorescent sensors due to disrupted  $\pi$  conjugation and the iminium cations reduction. However, they can switch on through the reaction with  $\text{O}_2^{\cdot-}$  and  $^-\text{OH}$  even *in vitro* and *in vivo*.<sup>386-388</sup> Corresponding reactions are presented in **Figure 1.19**.

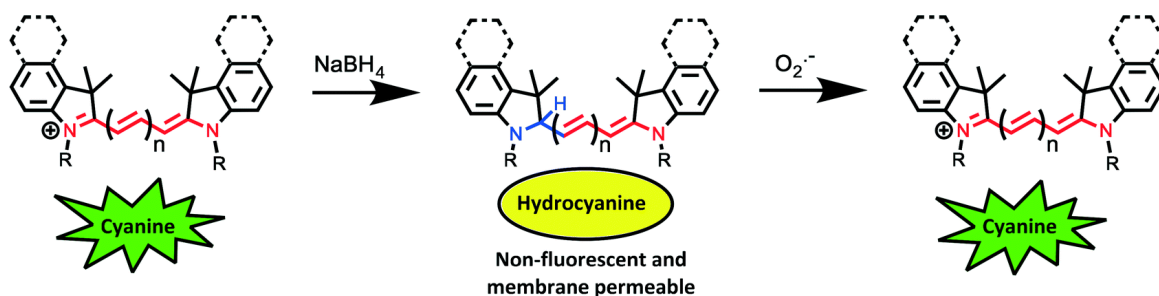


**Figure 1.19** Scheme of cyanine reduction and Hydrocyanine oxidation. Cyanine undergoes a reduction reaction in the presence of  $\text{NaBH}_4$  that leads to the generation of non-fluorescent and membrane-permeable hydrocyanine. While hydrocyanine can be oxidized in the presence of ROS, e.g.,  $\text{O}_2^{\cdot-}$  and  $\cdot\text{OH}$ , to turn on the fluorescence signal by producing cyanin. Reproduced with permission from Ref.<sup>388</sup>

Some hydrocyanine-containing probes for detecting reactive species have focused on building multi-functional systems to enhance the selectivity and functionality of the systems. For instance, Al-Karmi *et al.* placed an  $^{18}\text{F}$ -label on hydrocyanine (IR780) for quantitative and dynamic positron emission tomography (PET) imaging of reactive oxygen species *in vivo*.<sup>389</sup> The fluorescence intensity of the probe increased in the presence of  $20\ \mu\text{M}\ \text{O}_2^{\cdot-}$  and  $\cdot\text{OH}$ , but not for other reactive species, including  $\text{OCl}^-$ ,  $^1\text{O}_2$ , and  $\text{H}_2\text{O}_2$ . Some other works have been tracked the presence of  $\text{O}_2^{\cdot-}$  and  $\cdot\text{OH}$  in pathophysiological processes by developing ratiometric fluorescent or optoacoustic hydrocyanine-based nanoprobe.<sup>384,385</sup> For instance, Andina *et al.* designed a modular ratiometric fluorescent probe for extracellular detection of endogenous  $\text{O}_2^{\cdot-}$ .<sup>390</sup> The authors employed a fluorescent reference connected to hydro-Cy5 (as a ROS-sensitive dye) *via* a modular peptide-nucleic-acid-based linker to increase the modularity and versatility of the sensor. The use of a reference dye allowed them to detect the distribution differences using ratio-based readings. In another work, Ai *et al.* used a photon-upconverting nanoprobe (UCN) as a ratiometric PA probe to simultaneously screen various reactive species in living mice.<sup>384</sup> As shown in **Figure 1.20**, the probe was designed by encompassing an  $\text{O}_2^{\cdot-}$ -responsive hydrocyanic substrate (HCy5) and an  $\text{ONOO}^-$ -responsive cyanine substrate (Cy7) on the UCN surface. Upon radical stimulation, HCy5 regenerated the  $\pi$ -conjugation. However, Cy7 underwent degradation followed by ratiometric upconverted luminescence (UCL) and optoacoustic (OA) signal variations in NIR spectral region. The nanoprobe exhibited a detection limit of  $85\ \text{nM}$  for  $\text{O}_2^{\cdot-}$ .

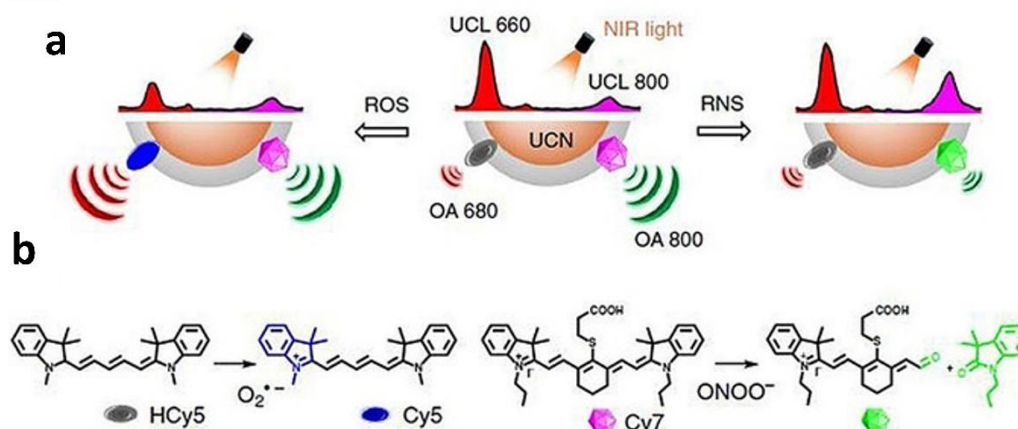


**Figure 1.20** (a) Scheme of a photon-upconverting nanoprobe (UCN) incorporating HCy5 and Cy7 onto the UCN surface. (b) Oxidation of HCy5 and Cy7 in the presence of O<sub>2</sub><sup>•-</sup> and ONOO<sup>-</sup>, respectively. Reproduced with permission from Ref.<sup>384</sup>

Cyanine- and hydrocyanine-based probes provide great opportunities to track and detect various reactive species with low detection limits. They exhibited relatively high selectivity as they do not react with all the reactive species at the same rate/concentration. These materials need more investigation to detect one specific reactive species in an environment experiencing oxidative and nitrosative stress. Furthermore, hydrocyanines have presented some limiting factors that restrict their application. For instance, they show high auto-oxidation that affects their half-life, small Stokes shifts that increase their background fluorescence, low water solubility, and turning into cyanine dyes that are not very stable in the presence of RONS, including <sup>-</sup>OCI, ONOO<sup>-</sup>, and <sup>•</sup>OH due to the oxidation reaction.<sup>391</sup>

### 1.3.1.9 Polypeptides

- **Poly-methionine**

Methionine residues are sensitive to reactive species through their thioether moiety. The thioether of methionine can undergo one or two steps of oxidation in the presence of ROS, including H<sub>2</sub>O<sub>2</sub>, and results in the production of sulfoxide and sulfone.<sup>392,393</sup>

Methionine has been mainly used in the form of poly-methionine for drug delivery applications.<sup>394–397</sup> Similar to PSS, the oxidation of methionine chains in the presence of ROS leads to a polarity change that can facilitate the drug release. For instance, Xu *et al.* synthesized methoxy poly(ethylene glycol)-poly(L-methionine) diblock copolymer (mPEG-PMet) to develop ROS-responsive thermogelling hydrogels.<sup>394</sup> By increasing the temperature, the copolymer transformed into a hydrogel, and the release of a model drug (i.e., rhodamine 6G) could be accelerated in the

presence of H<sub>2</sub>O<sub>2</sub> (30% and 100% release over 4 days in the absence or presence of 10 mM H<sub>2</sub>O<sub>2</sub>). The rapid release behavior was interpreted by oxidation of the thioether group of poly(L-methionine) to sulfoxide and sulfone by H<sub>2</sub>O<sub>2</sub>, concurrent with an increase of hydrophilicity, which eventually released the cargo. In another example, Hoang *et al.* utilized poly-methionine to develop ROS-responsive micelles for selectively disassembling and enhancing the preferable accumulation of drugs into tumor cells with high levels of intracellular ROS.<sup>398</sup> They encapsulated a hydrophobic pro-oxidant anticancer drug (i.e., piperlongumine), into self-assembled micelles formed by PEG-P(Met) copolymers. Around 97% and 65% drug release was observed within 48 h incubation in 1 mM and 50 μM H<sub>2</sub>O<sub>2</sub>, respectively, due to the oxidation of methionine residues. The piperlongumine-containing micelles also exhibited higher anticancer efficiency in MCF-7 human breast cancer cells than the incubation of free piperlongumine *in vitro*. Furthermore, Yu *et al.* reported poly(L-methionine)-based gel for immunotherapy by a triblock copolymer, including a PEG block located in the center and two polypeptide blocks (Me-D-1MT) on both flanks (**Figure 1.21**).<sup>399</sup> Me-D-1MT is built from the ROS-responsive L-methionine (Me) and dextro-1-methyl tryptophan (D-1-MT), which is the inhibitor of indoleamine-2,3-dioxygenase (IDO), an immunosuppressive enzyme. Furthermore, aPD-L1 antibody was encapsulated into the nanostructure by increasing the temperature, which led to the transformation of copolymer into the hydrogel. Similar to the rest of methionine-based nanostructures, oxidation of thioether group in the methionine and formation of sulfoxide and sulfone induced hydrophobic to hydrophilic changes, followed by releasing aPD-L1. At the same time, protease K degraded the polypeptide blocks and released the D-1MT. In conclusion, the bioresponsive gel scavenged and reduced ROS level and enhanced anti-melanoma efficacy *in vivo* by promoting the release of immunosuppressive enzyme.

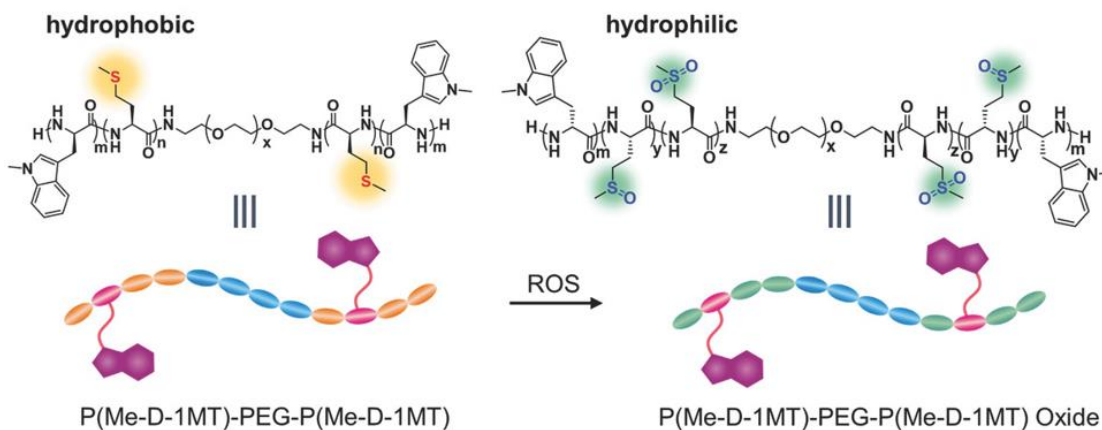


**Figure 1.21** Structure of poly(L-methionine)-based gel and ROS triggered polymeric hydrophobicity transition due to thioether oxidation. Reproduced with permission from Ref.<sup>399</sup>

### • Proline Oligomers

The free radical-mediated oxidation of amino acids and peptides was explored in the 1960s and has been highlighted recently. Proline residues in peptides are vulnerable to oxidation, followed by peptide backbone cleavage, leading to chain fragmentation (**Figure 1.22**).<sup>400–402</sup>

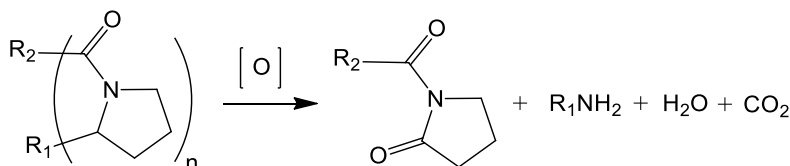


**Figure 1.22** Oxidants, such as  $\text{H}_2\text{O}_2$  and  $\text{ONOO}^-$ ,<sup>403</sup> can lead to the oxidation of proline residues and result in the cleavage of the parent polypeptide chain.

Proline oligomers or polyproline-containing materials have been developed as RONS-responsive materials for therapeutic applications.<sup>403–407</sup> For instance, Yu *et al.* developed a PCL-based scaffold crosslinked with oligoproline that experienced degradation by exposure to RONS.<sup>403</sup> In detail, diblock copolymers of PEG and PCL were carboxylated to form a terpolymer (4% PEG, 86% PCL, 10% cPCL). The polymers were then cross-linked with PEG-Proline<sub>n</sub>-PEG ( $n = 5–10$ ) to form scaffolds. After 6 days, all proline residues underwent cleavage in the reaction with 5 mM  $\text{H}_2\text{O}_2$  and 50  $\mu\text{M}$   $\text{Cu(II)}$  at 37 °C. Furthermore, the erosion of scaffolds was investigated in the presence of 1 mM of SIN-1 (a RONS generator that generates  $\cdot\text{NO}$  and  $\text{O}_2^{\cdot-}$  that can lead to the production of  $\text{ONOO}^-$  and  $\cdot\text{OH}$ ) for 28 days at 37 °C. The results confirmed about 30% of mass loss from the scaffold, while only minimal changes were observed in materials incubated without RONS. These results were consistent with those achieved *in vitro* on  $\gamma$ -interferon/LPS stimulated

bone marrow-derived macrophages, in which the scaffolds slowly degraded as a result of the increase in generated RONS by the stimulated cells. In a following study from the same group, the potential of this scaffold was investigated *in vivo* model for long-term tissue engineering and controlled release applications.<sup>405</sup> RONS-responsive drug delivery systems based on proline oligomers were mainly limited to the scaffold's design and physical characterization. However, pentaproline, cysteine–(proline)<sub>5</sub>–lysine (CP<sub>5</sub>K), has been applied for gene delivery *via* conjugation with mPEG and cationic poly(2-dimethylamino)ethyl methacrylate (PDMAEMA).<sup>406</sup> Pentaproline has also been utilized as a linker between chitosan, a linear polysaccharide, and mPEG to build a RONS-responsive carrier to release radioprotectant proteins.<sup>407</sup> Notably, the proline oligomers exhibited relatively slow degradation compared to sulfure-based materials, such as PPS, that degrades within a few hours of the oxidative environment.<sup>28,71,403</sup>

Overall, polypeptides have been widely applied as stimuli-responsive delivery agents due to their biocompatibility and biodegradability.<sup>408,409</sup> Proline oligomers exhibit very slow responses toward RONS (days to weeks), making them suitable options for sustained-release systems.<sup>104</sup>

### 1.3.2 RS<sup>•</sup>-responsive chemical bonds and materials

#### 1.3.2.1 BODIPY

BODIPY (4,4-difluoro-4-bora-3a,4a-diaza-s-indacene) dyes are the boron complex of dipyrromethene with intensive UV-absorption that emit high fluorescence quantum yields. These molecules exhibit reasonable stability in physiological conditions and relative insensitivity to pH and polarity of the environments.<sup>410</sup> Accordingly, BODIPY derivatives have been developed for different applications, such as fluorescent sensors/probes,<sup>411–413</sup> catalysts,<sup>414,415</sup> photosensitizers,<sup>416</sup> and others.<sup>417,418</sup> Among all, BODIPYs have mainly been utilized in developing fluorescent probes for GSH detection. However, more recently, it has been shown that RS<sup>•</sup> with high reactivity and strong bonding ability<sup>419–421</sup> could undergo a radical coupling reaction with BODIPYs in organic solvents, leading to changes in the photophysical properties of BODIPYs.<sup>422,423</sup> For instance, Ma *et al.* efficiently and selectively introduced thiophenol (ArS) units into BODIPY 1a by a one-step photocatalysis approach to functionalize BODIPYs through radical pathways.<sup>422</sup> BODIPY acted as a photosensitizer to promote the generation of ArS<sup>•</sup> *in situ* in THF upon exposure to the light. Subsequently, ArS<sup>•</sup> attacked the  $\alpha$ -positions of BODIPY, followed by the production of  $\alpha$ -ArS- and  $\alpha,\alpha'$ -(ArS)<sub>2</sub>-substituted BODIPY (BODIPY 1a and BODIPY 1aa, respectively) (**Figure 1.23a**). Eventually, the absorption and emission maxima of BODIPY 1a and

BODIPY 1aa were red-shifted by 32–37 nm and 77–84 nm, respectively, compared to the parent BODIPYs (Figure 1.23b,c).

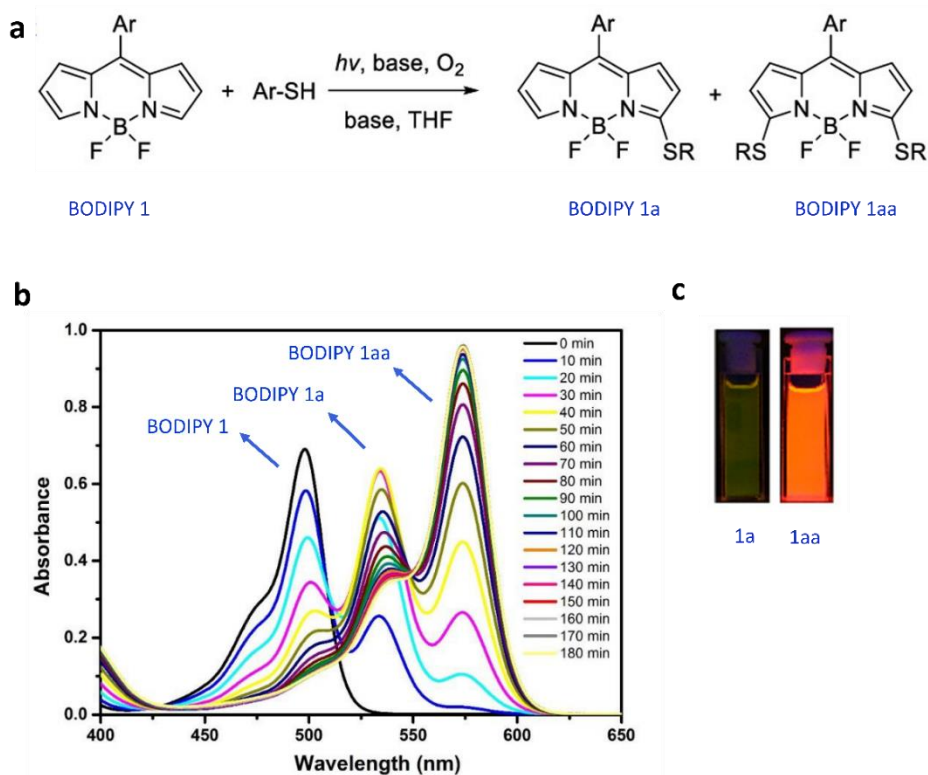


**Figure 1.23** An introduction of ArS units into boron-dipyrromethene (BODIPY) by a photocatalysis approach and through  $ArS^{\bullet}$ : (a) Under the light, BODIPY 1 acts as a photosensitizer, leading to  $ArS^{\bullet}$  generation and followed by the production of  $\alpha$ -ArS- and  $\alpha,\alpha'$ -(ArS)<sub>2</sub>-substituted BODIPY. (b) By increasing the reaction time of BODIPY 1 with ArSH (in THF under exposure to light), the decrease in the absorbance of BODIPY 1 simultaneously occurred with the increase in the absorbance of BODIPY 1a and 1aa. (c) Photographs of BODIPY 1a and BODIPY 1aa in THF upon exposure to a UV lamp at 365 nm. Adapted from Ref.<sup>422</sup>

Furthermore, the radical coupling reaction of  $RS^{\bullet}$  and BODIPY mainly occurred in organic solvents (e.g., THF and DMSO) with high temperature or prolonged reaction time,<sup>422–424</sup> limiting their application in  $RS^{\bullet}$  detection *in vitro* and *in vivo*. In 2021, Liu *et al.* modified BODIPY with  $\beta$ -cyclodextrin ( $\beta$ -CD), a macrocyclic compound with a hydrophobic interior and hydrophilic exterior, to prepare a ratiometric fluorescent probe (BODIPY- $\beta$ CD) for intracellular GSH radicals ( $GS^{\bullet}$ ) (Figure 1.24a).<sup>98</sup>  $\beta$ -CD was used to increase the water solubility of the probe, prevent the self-aggregation of BODIPY, and increase the biocompatibility of the system. Furthermore,  $GS^{\bullet}$  was generated through the reaction of GSH (1 mM) with  $\cdot OH$  produced from the Fenton-reaction ( $H_2O_2$  (10  $\mu M$ )/ $Fe^{2+}$ (10-150  $\mu M$ )). As shown in Figure 1.24b,c, upon addition of  $GS^{\bullet}$ , the absorbance (at 501 nm) and fluorescence intensity ( $\lambda_{ex}/\lambda_{em}$  491/520 nm) of BODIPY- $\beta$ CD decreased, followed by the appearance of two new red-shifted peaks related to the generated BODIPY- $\beta$ CD+ $GS^{\bullet}$  and

BODIPY- $\beta$ CD+2GS $\cdot$  within 10 min. In addition, BODIPY- $\beta$ CD didn't show any changes in fluorescence intensity toward intracellular amino acids and RONS (0.1 mM), including cysteine, homocysteine,  $\cdot$ OCl, H<sub>2</sub>O<sub>2</sub>, tBuCOO $\cdot$ , and NO<sub>2</sub> $\cdot$ . Moreover, BODIPY- $\beta$ CD (20  $\mu$ M  $\geq$ ) exhibited low cytotoxicity and was able to detect GS $\cdot$  in live cancer cells (A549 cells) after 3 h treatment with H<sub>2</sub>O<sub>2</sub>/Fe<sup>2+</sup>.

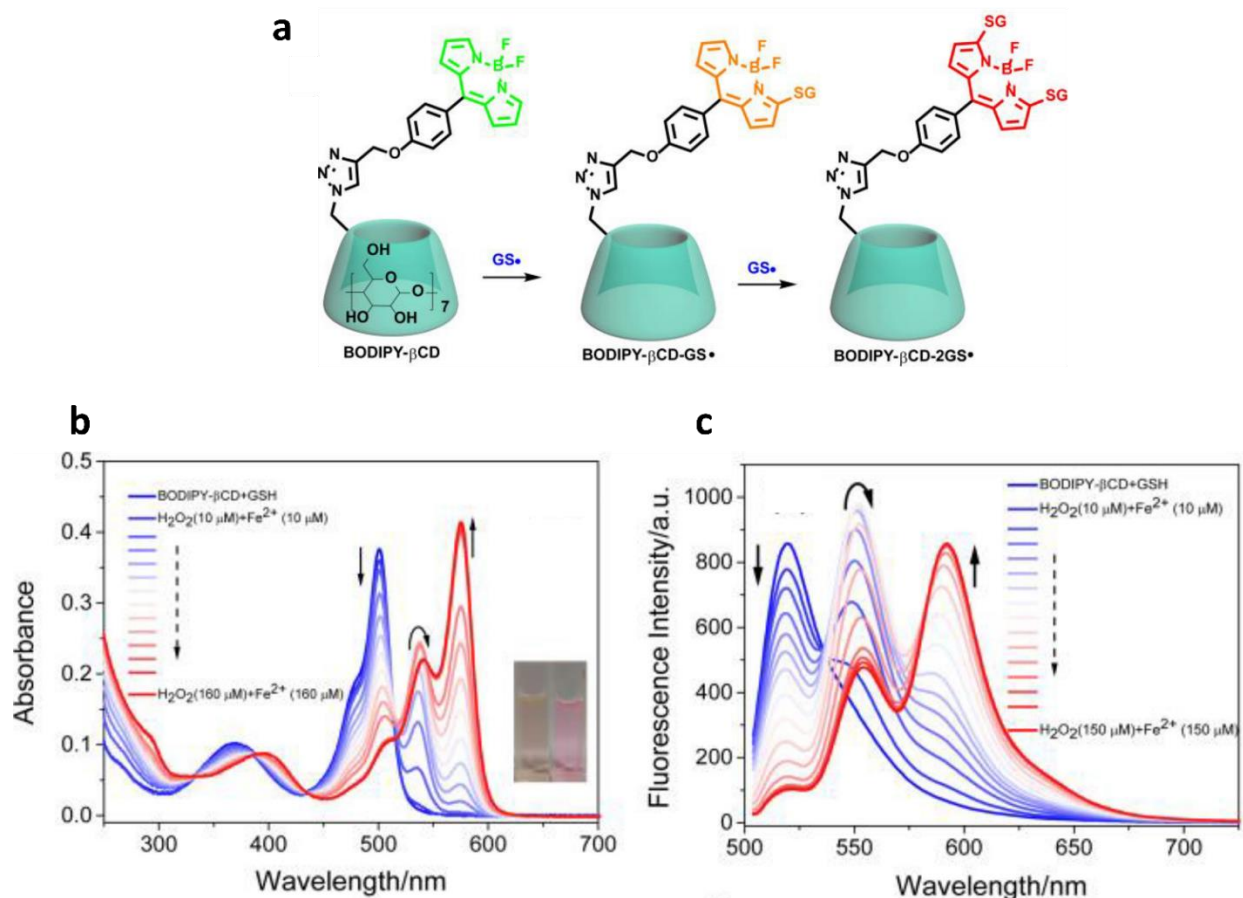


**Figure 1.24** BODIPY- $\beta$ CD for GS $\cdot$  fluorescence sensing. (a) BODIPY- $\beta$ CD probe was prepared by the modification of BODIPY with  $\beta$ CD. BODIPY- $\beta$ CD and GS $\cdot$  underwent the radical cross-coupling reaction at  $\alpha$ -positions of BODIPY. By increasing the concentration of GS $\cdot$  (H<sub>2</sub>O<sub>2</sub> (10  $\mu$ M)/Fe<sup>2+</sup> (10-160  $\mu$ M)) (b) the absorbance (at 501 nm) and (c) the fluorescence ( $\lambda_{\text{ex}}/\lambda_{\text{em}}$  491/520 nm) intensity of BODIPY decreased, accompanied by the appearance of two new red-shifted peaks related to BODIPY- $\beta$ CD+GS $\cdot$  and BODIPY- $\beta$ CD+2GS $\cdot$ . Adapted from Ref.<sup>98</sup>

### 1.3.2.2 Allyl sulfide

Allyl sulfide functional groups have been originally used as addition-fragmentation chain transfer (AFCT) agents for photopolymerization that provide stress and/or strain relaxation and equilibrium geometry modification mechanisms to polymers.<sup>425–427</sup> This chemical bond has also been utilized

as linkages in hydrogel networks to allow controlled and reversible exchange of biochemical moieties. As shown in **Figure 1.25**, photoinitiated  $RS^\bullet$  attack the double bond of allyl sulfide bonds, followed by the formation of an unstable intermediate and result in the regeneration of a new double bond and another  $RS^\bullet$  species.<sup>428</sup>

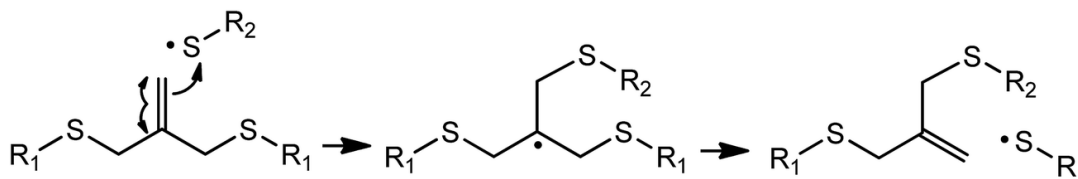


**Figure 1.25** Mechanism of  $RS^\bullet$ -initiated thiol-ene reactions implicating an allyl sulfide bond. The addition of  $RS^\bullet$  to the double bond of the allyl sulfide forms an unstable intermediate, which further undergoes a  $\beta$ -scission, followed by the generation of a new double bond and  $RS^\bullet$  species. Reproduced with permission from Ref.<sup>428</sup>

Sun *et al.* utilized allyl sulfide bonds as  $RS^\bullet$ -responsive linkers for a photoactivation drug delivery system in human colon carcinoma cell lines.<sup>429</sup> In their system, the allyl sulfide bond was formed using an isobutylene structure as a bridging graft to cage various thiol-containing materials, including cysteine, cyclic disulfide peptides, and histone deacetylase inhibitor (HDAC) largazole thiol. Upon UV irradiation at 365 nm in the presence of photoinitiator (2,2-dimethoxy-2-phenylacetophenone (DPAP)) and different thiol sources ( $\beta$ -mercaptoethanol, thiol-glucose, or GSH), the photoinitiated  $RS^\bullet$  and allyl sulfide bond of isobutylene-caged thiols underwent the thiol-ene decaging reactions, which were followed by releasing the stapled thiol-containing compounds (**Figure 1.26a**). The yield of thiol-ene decaging reaction was 37, 65, or 67% upon 120, 15, or 15 min UV irradiation of 1 eq. isobutylene-caged cysteine in organic solvents and in the presence of 3 eq.  $\beta$ -mercaptoethanol, thiol-glucose, or GSH, respectively. Furthermore, the growth-inhibitory activity of the stapled largazole thiol in HCT-116 colon carcinoma cells was significantly lower than free largazole and largazole thiol due to the protection of thiol groups by the isobutylene structure (**Figure 1.26b**). However, the UV-irradiated premixed group of stapled largazole and DPAP indicated considerably lowered cell viability than the corresponding non-irradiation group (**Figure 1.26c**). Therefore, the effective photoactivation decaging of isobutylene-caged largazole in HCT-116 cells represents the potential as an activation method and drug delivery for cancer therapy.

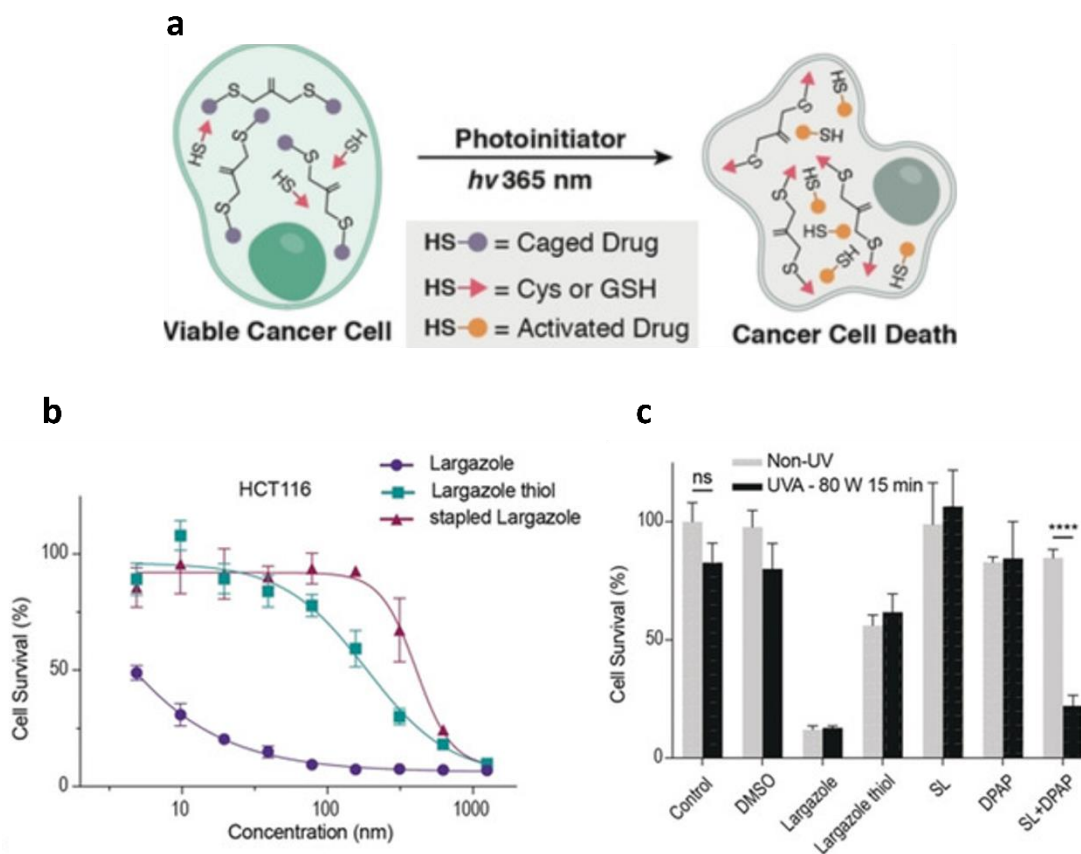


**Figure 1.26** Photoactivation of thiol-containing drugs in cancer cells due to  $RS^{\bullet}$ -mediated thiol-ene reactions. **a)** Thiol-containing drugs have been caged and deactivated by utilizing isobutylene structures as a bridge between thiol groups. Upon exposure to UV light, the generated radical thiols and allyl sulfide bonds underwent thiol-ene reaction, then released the activated drugs. **b)** The stapled largazole induced more cell survival in cancer cells than the corresponding largazole and largazole thiols due to the protection of thiols group by isobutylene structure that led to the deactivation of largazole. **c)** The UV irradiation of premixed stapled largazole (SL) and DPAP showed considerably lower cell survival than the corresponding non-irradiation group, which proved the photoactivation of largazole in cancer cells. Reproduced with permission from Ref.<sup>429</sup>

Overall, the development of  $RS^{\bullet}$ -responsive materials can be challenging due to short half-lives ( $\mu s$ )<sup>215</sup> and the high chemical reactivity of  $RS^{\bullet}$ <sup>430</sup>. While BODIPY groups and allyl sulfide bonds have been utilized for the  $RS^{\bullet}$  detection and  $RS^{\bullet}$ -responsive drug release, respectively, there is still a lack of investigation into the development of  $RS^{\bullet}$ -responsive chemical bonds and materials for biomedical applications.

## 1.4 Conclusion and outlook

Remarkable progress has been made to better understand the nature and reactivity of endogenous reactive species and to develop RONSS-responsive chemical bonds and materials over the past several years. Several payloads have been loaded into different nanocarriers containing RONSS-responsive chemical bonds and materials *via* hydrophobic interaction, electrostatic interaction, and covalent bonding for various biomedical applications. The responsiveness of the presented functional groups toward endogenous reactive species can yield RONSS scavenging and facilitate the release of payloads from their corresponding nanocarriers in the targeted sites.

Furthermore, each reported RONSS-responsive chemical bond and material exhibited different advantages, limitations, challenges, structures, solubility, toxicity, mechanisms of action, selectivity, and reactivity toward RONSS. In general, the potential of these materials for biological applications can be determined by their mechanism of action, selectivity, and reactivity toward RONSS. For instance, chalcogen-containing materials undergo a solubility switch upon oxidation, making them an option for drug delivery. However, vinyl disulfide groups can be utilized for photo-controlled drug release combined with PDT and cancer therapy due to their selectivity toward  $^1\text{O}_2$ . Peroxalate ester groups have been used for theranostic applications due to their oxidation responsiveness, leading to linker breakage with the advantage of exciting the surrounding fluorophores after oxidation. Disulfides and diselenides can be used for drug delivery and chemotherapy due to their responsiveness toward both oxidative and reductive biological species (e.g.,  $\text{H}_2\text{O}_2$  and GSH). The responsiveness of chemical bonds to multiple RONSS is beneficial for the therapy and diagnosis of disease associated with oxidative stress involving numerous redox reactive species. In contrast, these chemical bonds are not advantageous to target and/or diagnose the biological activity and pathological process of specific endogenous reactive species. Moreover, the reactivity of each chemical bond (sensitivity and response rates) varies from one species to another. Typically, the differential sensitivity of each RONSS-responsive bonds and materials is correlated with their bond energy, the oxidation/reduction potentials of the bonds, and the oxidation/reduction potentials of reactive species. Accordingly, the chemical bonds and materials with high sensitivity and response rates can be great for diagnostic applications and to understand/investigate biological and pathological processes. For instance, boronic acid/ester bonds exhibit higher sensitivity and rapid responsiveness toward  $\text{ONOO}^-$  compared to the rest of RONS, making them a great option for its detection *in vitro* and *in vivo*. However, the bonds with

lower response rates, such as polyproline and chalcogenides-based materials, can be employed for sustained-release systems.

Although significant progress has been made so far in the field, several critical issues remain to be addressed for future development. For instance, there are some conflicts between the observations of different groups when comparing the reactivity of some chemical bonds and materials (e.g., diselenide and disulfide bonds). However, to designate suitable bonds correlated with desired application, it is crucial to employ a united system to evaluate/compare the reactivity of different chemical bonds and materials toward RONSS. Furthermore, quite a few reports assess the sensitivity of their systems toward different RONSS. For instance, the majority of oxidation- and reduction-responsive systems are simply investigated in the presence of  $\text{H}_2\text{O}_2$  and GSH, respectively. However, various endogenous reactive species are involved in the onset and progress of the disease. Moreover, it is vital to design materials that distinguish between the low levels of RONSS from normal cellular activities and the increased levels of RONSS from pathologies. Indeed, most research has focused on evaluating RONS-responsive materials toward high concentrations of  $\text{H}_2\text{O}_2$  ( $>500 \mu\text{M}$ ). However, considering the biological concentration of  $\text{H}_2\text{O}_2$  and investigating the effect of all RONS on responsive groups are essential to better understanding the system's reactivity *in vitro* and *in vivo*. It is also essential to investigate the chemical bonds and materials with higher response rates to scavenge, target, and detect the reactive species, which have extremely short half-lives.<sup>103</sup> Furthermore, the presented bonds have exhibited the oxidizing potential of RNS. However, RNS, particularly  $\text{ONOO}^-$ , are oxidizing and nitrating agents. Therefore, to better understand the complex biological environments and the effects of RNS on biomolecules, it is vital to design a chemical bond that can indicate the nitrating potential of  $\text{ONOO}^-$ . Last but not least, until now,  $\text{RS}^\bullet$ -responsive chemical bonds and materials have been rarely investigated. Regarding the importance of  $\text{RS}^\bullet$  in physiological and pathological events, it would be interesting to develop and evaluate  $\text{RS}^\bullet$ -responsive chemical bonds and materials for different biomedical applications.

It is worth noting that, despite these challenges, it is anticipated that RONSS-responsive chemical bonds and materials will play significant roles in biological redox evaluation and the future of biomedical applications.

## 1.5 Research objectives

Based on the presented information above, chemical linkages that respond to biological stimuli are important for many pharmaceutical and biotechnological applications. Considering the diversity of applications foreseen for such chemical linkages, it is relevant to explore new variants with responsivity profiles that are different from those presently found in the literature. Hence, this thesis aims to develop a new responsive group, the sulfonium vinyl sulfide, and to explore its responsiveness towards physiologically-relevant levels of different categories of reactive species, including ROS, RNS, and RSS in conditions mimicking the cytosol of cells. In this context, the main objectives of this thesis are:

(1) To present a new chemical linkage, the sulfonium vinyl sulfide group, installed on the methionine residue of different peptides by selective alkylation of the methionine and subsequent Click reaction (nucleophilic thiol–allene addition) in order to provide a variety of bioconjugates (peptide–peptide, peptide–fluorophore, peptide–protein, and peptide–polymer). This work will be important to better understand the potential of sulfonium vinyl sulfide linkers in the preparation of a variety of bioconjugates. The specific objectives will be to synthesize, purify, and characterize a variety of bioconjugates containing sulfonium vinyl sulfide-containing linkers. Side-reactions will be scrutinized and the responsiveness of the bioconjugate towards a Click reaction (radical thiol–ene addition) will be explored. A variety of parameters will be explored, including the effect of pH, different categories of reactive species on Click reactions, UV light, the structure of radical thiols, and stability in the presence of biologically derived reactive species from bacteria.

(2) The objective of the third chapter is to further elucidate the identity of the reactive species that react with sulfonium vinyl sulfides in cell models of oxidative stress. The specific objectives are to design, synthesize, purify, and characterize a FRET-based probe containing a vinyl sulfonium sulfide linker group alongside a non-responsive control probe containing a thioether linker. The reactivity of these probes towards nucleophilic thiols, radical thiols, and peroxyxynitrite will be examined. Thereafter, the responsiveness of the probes in the presence of cells experiencing oxidative stress will be explored, and the responsiveness of the probe used to assess the identity of the reactive species with which it reacts.

## 1.6 Structure of the thesis

To achieve this overarching objective, the remainder of this thesis is divided into Chapters as follows:

**Chapter 1**, presented a brief overview of redox-responsive chemical bonds and materials for therapeutic, diagnostic, and theranostic applications. It also provides information about various endogenous reactive species, their equilibria, and their roles in physiological and pathological processes, including oxidative and nitrosative stress, within the human body. Furthermore, it summarizes information about endogenous reactive species-responsive chemical bonds and materials, including their structures, mechanism of action, selectivity, reactivity (sensitivity and rate of reaction), applications, opportunities, and limitations.

**Chapter 2**, is published as “Consecutive alkylation, “Click”, and “Clip” reactions for the traceless methionine-based conjugation and release of methionine-containing peptides” by Fatemeh Zare, Alessandro Potenza, Andrea A Greschner, Marc A Gauthier to the journal *Biomacromolecules* (2022). It provides a brief introduction specific to Click/Clip reactions and methionine-based bioconjugates, followed by experimental details, measurements, characterization, and discussion of Click reaction to prepare a variety of sulfonium vinyl sulfide linker-containing bioconjugates. This chapter also presents the stability and the responsiveness of the sulfonium vinyl sulfide linker in the presence of different biological reactive species, including ROS and RSS (i.e., H<sub>2</sub>O<sub>2</sub>, ·OH, GSH, and Cys) in model experimental conditions and in the presence of bacteria. It concludes that electron-deficient alkynes, conveniently installed on methionine residues, can participate in well-known Click (nucleophilic thiol–allene addition) and subsequent Clip reactions (radical thiol–ene addition), leading to the release of unmodified peptides (in minutes). This chapter contains the information that proves the potential of sulfonium vinyl sulfide linker in many applications in the biotechnological sector.

**Chapter 3**, prepared for submission as “Biological fate of sulfonium vinyl sulfides – A competition between reactive nitrogen species, radical thiols, and thiol nucleophiles” by Fatemeh Zare, Patrick Laplante, Jean-Francois Cailhier, and Marc A Gauthier. It provides a brief introduction specific to stimuli-responsive chemical bonds, and the chemistry and responsiveness of sulfonium vinyl sulfide toward ROS and RSS. Afterwards, it presents the synthesis and characterization of a responsive FRET-based probe (containing a vinyl sulfonium sulfide linker) and a control FRET-based probe (thioether linker). The discussion presents the responsiveness of sulfonium vinyl sulfide linker toward RNS and RSS in model experiments and indicates the competition reaction between thiol, RSS, and RNS in the reaction with sulfonium vinyl sulfide linker *in vitro*.

Accordingly, it concludes that these bonds preferentially respond to RNS in cell culture, which could be useful for achieving a change of polarity.

**Chapter 4**, presents a general discussion, conclusion, and perspective on possible future work based on the results obtained in this thesis.

**Chapter 5**, includes the bibliography used in this thesis

**Chapter 6**, presents Appendix contained additional information in order to complement the main text and provide elements that are essential for understanding and supporting its content. It includes:

- Appendix I, presents Supplementary information for Article 1.
- Appendix II presents Supplementary information for Article 2.
- Appendix III, includes the copyright permission of the presented Figures in Chapter 1.



## 2 ARTICLE 1

---

# Consecutive alkylation, “Click”, and “Clip” reactions for the traceless methionine-based conjugation and release of methionine-containing peptides

Fatemeh Zare<sup>1</sup>, Alessandro Potenza<sup>2</sup>, Andrea A Greschner<sup>1</sup>, Marc A Gauthier<sup>1,2,\*</sup>

<sup>1</sup> Institut National de la Recherche Scientifique (INRS), EMT Research Center, Varennes, Canada

<sup>2</sup> Swiss Federal Institute of Technology Zurich (ETHZ), Department of Chemistry and Applied Biosciences, Institute of Pharmaceutical Sciences, Zurich, Switzerland

### Corresponding author:

Marc A. Gauthier

Institut National de la Recherche Scientifique (INRS), EMT Research Center, 1650 boul. Lionel-Boulet, Varennes, J3X 1P7, Canada

E-mail: gauthier@emt.inrs.ca

Telephone: +1 514 228 69 32

Fax: +1 450 929 81 02

### Author contributions:

FZ carried out most experiments, responsible for data collection, analysis as well as manuscript composition and revision.

AP contributed by carrying out the data collection and analysis of some experiments, including the preparation of fluorescent peptide (Rho)FPAMAG, bioconjugation of (Rho)FPAMAG and human serum albumin, modification of FPAMAG by 1-bromo-2-butyne, and measuring the stability of 1b-gsh bioconjugates in the presence of 10 mM cysteine.

AAG contributed to manuscript writing and revision.

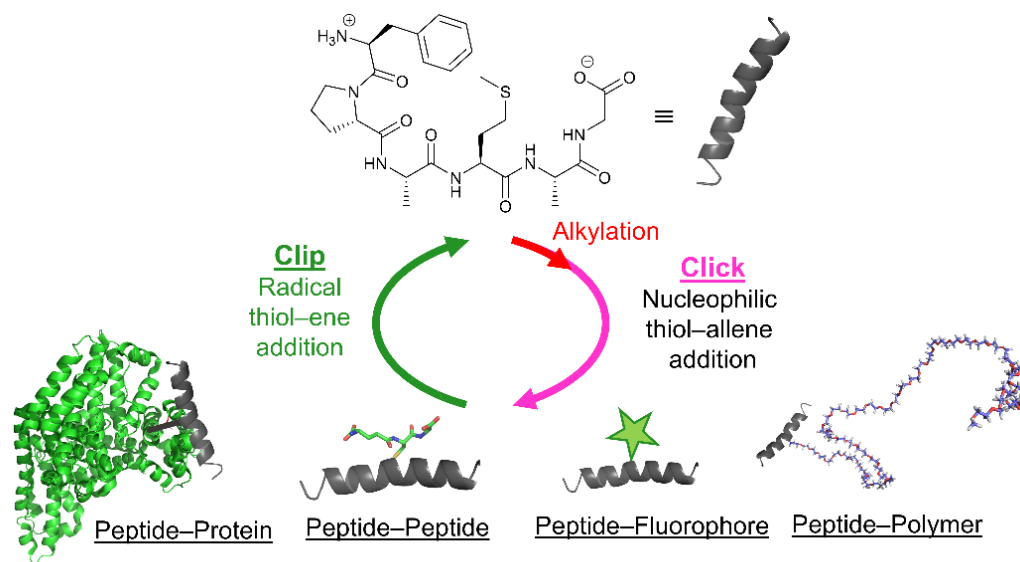
MAG was the supervisory author and involved with the designing of the experiments, data analysis, concept formation, manuscript composition and revision.

*Note: The work of this chapter is published in the ‘Biomacromolecules’. June 7, 2022. DOI: 10.1021/acs.biomac.2c00357*

## Abstract

“Click” reactions have revolutionized research in many areas of science. However, a consequence of Click product stability is that identifying simple treatments for cleanly dissociating the latter under the same guiding principles, i.e., a “Clip” reaction, remains a challenge. This study demonstrates that electron-deficient alkynes, conveniently installed on methionine residues, can participate in well-known Click (nucleophilic thiol–allene addition) and subsequent Clip reactions (radical thiol–ene addition). To illustrate this concept, a variety of bioconjugates (peptide–peptide; peptide–fluorophore; peptide–polymer) were prepared. Interestingly, the Clip of these bioconjugates releases the original peptides concurrent with regeneration of their unmodified methionine residue, in minutes. Moreover, the conjugates demonstrate substantial stability towards endogenous levels of reactive species in bacteria, illustrating the potential for this chemistry in the biosciences. The reaction conditions employed in the Click and Clip steps are compatible with the preservation of the integrity of biomolecules/fluorophores and involve readily accessible reagents and the natural functional groups on peptides/proteins.

## Graphical Abstract:



**Keywords** (9): Click chemistry; Radical thiol species; Bioconjugate; Polymer; Radical thiol; Linker; Thioether; Sulfonium; Clip chemistry

## 2.1 Introduction

So-called “Click” reactions have revolutionized research in many areas of chemistry, material science, and for the study of biological systems.<sup>34–37</sup> The guiding principle behind Click chemistry is that reactions should be high yielding with easily purified and safe by-products, be regio- and stereo-specific, and reactants should exhibit rapid coupling kinetics under mild conditions with high functional group and solvent tolerance.<sup>38</sup> Moreover, the process should ideally be insensitive to water or air with readily available starting materials and reagents, simple, wide in scope, and generate a chemically inert and stable product. Several chemical reactions display (most) of these characteristics, and important new variants continue to be discovered.<sup>39,40</sup> By far, the Cu(I)-catalyzed Huisgen 1,3-dipolar cycloaddition of alkynes and azides is the most popular Click reaction and is the standard to which the efficiency of new reactions is compared.<sup>38</sup> Unfortunately, a general consequence of the high stability of the Click product is that identifying simple treatments for cleanly dissociating the latter under the same guiding principles as above, i.e., a “Clip” reaction,<sup>431</sup> remains a challenge. For instance, Brantley *et al.* have demonstrated the possibility of reversing the Cu(I)-catalyzed Huisgen 1,3-dipolar cycloaddition reaction by ultrasound-induced cycloreversion.<sup>432</sup> Despite the innovative aspect of this work, this Clip reaction requires aggressive/prolonged exposure to ultrasounds and the presence of polymers for mechanotransduction of the energy to the triazole. In addition, a number of reversible Click reactions have been described in the literature and include Diels-Alder cycloadditions, Michael-addition (e.g., thiol–maleimide), non-aldol carbonyl reactions (e.g., hydrazone and oxime formation), and thiol–disulfide exchange reactions, amongst others.<sup>41–43</sup> These reversible reactions, however, are equilibrium processes that imply that while a rapid Click step may be possible, the corresponding Clip step is proportionately slower and may require interventions that can be inconvenient or destructive to biomolecules (dilution, prolonged heating, acidification, etc.). As such, to the extent of our knowledge, achieving conjugation *via* a Click reaction and release with a second distinct Clip reaction, *via* processes not relying on chemical equilibria and occurring under physiological conditions exploiting the natural functional groups on peptides/proteins, are rare. For instance, Sun *et al.* employed isobutylene as a bridging graft to cage various thiol-containing materials *via* a rapid and efficient radical-mediated thiol-ene reaction upon exposure to radical thiols.<sup>429</sup> A UV-triggered Clip reaction was used to release various thiol-containing materials from the polymer networks. However, their strategy was limited by long UV irradiation times (120 min). While the ‘decaging’ of thiols from a polymer network is well characterized, use of peptidic or protein starting materials in lieu of isobutylene was not explored.

Despite a low abundance of methionine in proteins (~2%), the functionalization of proteins through these residues has attracted some attention. In fact, the limited functional role of methionine residues in protein compared to other residues makes them a great option for protein labelling.<sup>44,45</sup> Therefore, several strategies have been developed for methionine-selective bioconjugation, including alkylation of methionine thioethers with cyanogen bromide (CNBr) or alkyl halide reagents,<sup>52</sup> imidation of methionine's thioether through oxaziridine reagents based on redox activated chemical tagging (ReACT),<sup>433</sup> methionine-selective modification using hypervalent iodine ( $\lambda$ 3-iodane) reagents,<sup>14,434</sup> and photoredox catalysis.<sup>435</sup> Chemoselective methionine bioconjugations have been applied for a broad range of pharmaceutical applications, including stapled peptides,<sup>436</sup> antibody-drug conjugates,<sup>437</sup> and optical<sup>438</sup> and positron emission tomography imaging.<sup>439</sup>

This study demonstrates that electron-deficient alkynes installed on the methionine residues of peptides are intriguing functional groups that can participate in well-known Click (nucleophilic thiol–allene addition) and subsequent Clip reactions (radical thiol–ene addition; **Figure 2.1**), both of which respect most of the guiding principles of Click chemistry. To illustrate the potential of these reactions, an electron-deficient alkyne was conveniently and selectively installed on the methionine residue of four model peptides and used to prepare a variety of bioconjugates by nucleophilic thiol–allene addition. To illustrate versatility, a variety of bioconjugates were prepared (peptide–peptide; peptide–fluorophore; peptide–polymer; peptide–protein). The subsequent Clip reaction is achieved by addition of a second thiol *via* the radical thiol–ene addition reaction. This second addition surprisingly induced the full release of the original peptides *via* a fragmentation process concurrent with regeneration of their unmodified methionine residue (in minutes). The reaction conditions employed in both steps are compatible with the preservation of the integrity of biomolecules/fluorophores, involve readily accessible reagents, and have many applications in biotechnology and material science. Moreover, the conjugates demonstrate substantial stability towards endogenous levels of reactive species in bacteria, illustrating the potential for this chemistry in the biosciences.

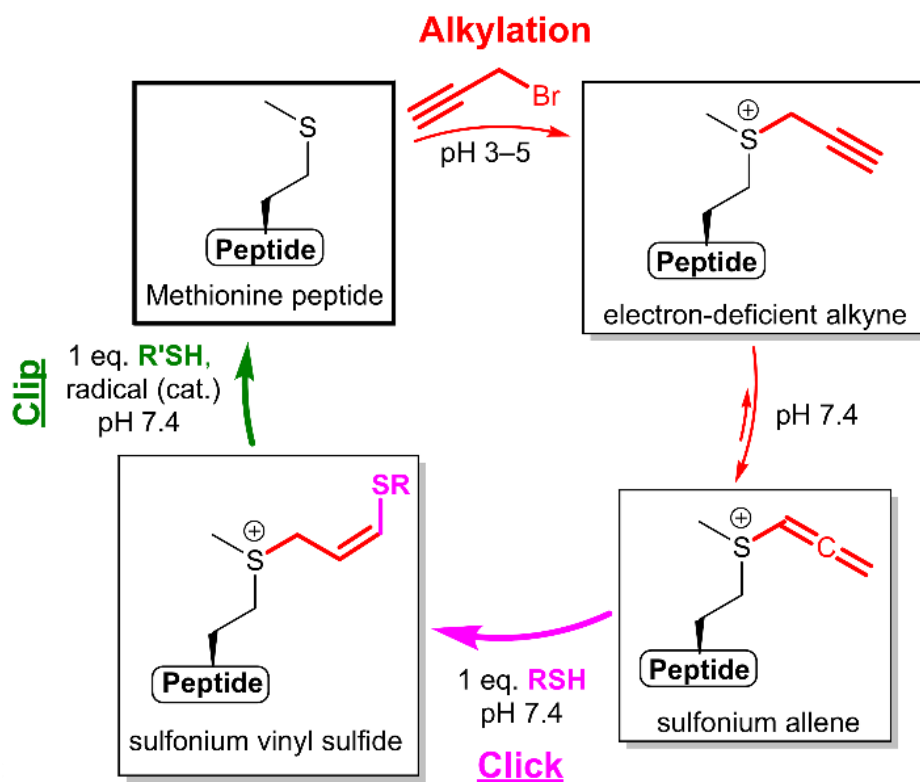


**Figure 2.1** Methionine (thioether)-containing peptides can be selectively and conveniently alkylated to produce a sulfonium allene. This entity may be modified by a Click reaction (nucleophilic thiol–allene addition), yielding a sulfonium vinyl sulfide. The latter can undergo a subsequent Clip reaction (radical thiol–ene addition) to regenerate the original methionine (thioether)-containing peptide. The details of each reaction (e.g., released materials) is provided in following pages.

## 2.2 Materials and Methods

### 2.2.1 Materials

All peptides were purchased commercially at >95% purity and were supplied with LC-MS validation of identity. Peptides sequences are given using single letter amino acid codes from the N- to the C-termini, which are free. FPAMAG (**1a**), HDMNKVLDL (**4a**; antinflammin-2), HDMNK(Cy5)VLDL (**5a**), and a fluorescent cell-penetrating peptide based on nona-arginine (Ac-CGK(Cy3)GKR<sub>9</sub>; CPP(Cy3)) were purchased from AnaSpec (Fremont Canada). *Escherichia coli* B (HER1024) obtained from the Felix d'Herelle Reference Center for Bacterial Viruses, Université Laval, Quebec. Poly(ethylene glycol) methyl ether thiol (mPEG–SH) 5 kDa was purchased from JenKem Technology (Plano, USA). 5-(and-6)-carboxy-X-rhodamine succinimidyl ester (5(6)-ROX-NHS) was purchased from Invitrogen (Paisley, UK). 5-((2-(and-3)-S-(acetylmercapto) succinoyl) amino) fluorescein (SAMSA fluorescein) were purchased from Thermo Fisher

Scientific. Glutathione (GSH), 2,2-dimethoxy-2-phenylacetophenone (DMPA), hydrogen peroxide (H<sub>2</sub>O<sub>2</sub>) 30% (w/w) in H<sub>2</sub>O, 2',7'-dichlorofluorescein diacetate (H<sub>2</sub>DCFDA), propargyl bromide (~80% solution in toluene), 2-mercaptoethanol (βME), 1-bromo-2-butyne, human serum albumin, and all buffer salts and solvents were purchased from Sigma-Aldrich at the highest grade possible and used as received. All buffers were prepared using MilliQ water (mean resistivity 18.2 MΩ·cm). The thiol group of SAMSA fluorescein is protected as a thioester and was deprotected prior to use as per the manufacturer's instructions (in brief: 2.06 mg of SAMSA fluorescein was dissolved in 1 mL NaOH (0.1 M) for 15 min at room temperature. The pH was then neutralized with 14 μL of 6 M HCl and 0.2 mL 200 mM phosphate buffer pH 7).

### 2.2.2 Equipment

Proton nuclear magnetic resonance spectra were recorded using a Bruker 300 MHz spectrometer (Ultrashield 300) or a Varian 600 MHz spectrometer (Inova). Liquid chromatography–mass spectrometry (LC-MS) was performed using an Agilent technologies 1260 high pressure liquid chromatography (HPLC) system equipped with a 1260 Infinity quaternary pump, a 1260 Infinity II multisampler, a 1260 Infinity VL+ diode array detector with a 3-mm flow cell, and a 6120 single quadrupole mass spectrometer. Analytical and preparative high-pressure liquid chromatography were performed with a second system consisting of a bio-inert 1260 Infinity quaternary pump, a bio-inert 1260 Infinity HiP autosampler, a 1260 Infinity VL+ diode array detector with a 3-mm flow cell, and an Agilent 1260 Infinity Fluorescence Detector. For both chromatography systems, an Agilent Zorbax 300SB-C18 (5 μm, 4.6 x 150 mm) column was used to separate analytes with gradients of H<sub>2</sub>O (+0.1% TFA) and acetonitrile (ACN; +0.1% TFA) as mobile phase. A typical elution profile was: 0 to 4 min 100% H<sub>2</sub>O + 0.1% TFA followed by a linear gradient of 0 to 95% ACN + 0.1% TFA over 25 min with a flow rate of 1 mL·min<sup>-1</sup>. Small differences in the retention time of identical compounds result for small variations of pump pressure, connective tubing, column age, etc., that occurred over the duration of the study. Preparative HPLC was performed using an Agilent Zorbax 300SB-C18 (5 μm, 9.4 x 250 mm) column and identical elution profiles, albeit with a flow rate of 3.3 mL·min<sup>-1</sup>. Fractions containing desired products were lyophilized using a FreeZone 4.5 Liter Benchtop Freeze Dry System from Labconco.

### 2.2.3 Preparation of sulfoxide FPAM(O)AG (**2a**)

A solution of **1a** (0.5 mg, 592.3 g·mol<sup>-1</sup>) in 1.7 mL of water was oxidized to a sulfoxide by addition of 1.7  $\mu$ L of a stock solution of 1M DMSO/ 2M HCl. After 3 h, **2a** was isolated by preparative HPLC and recovered by lyophilization. The mass spectrum of this compound is available in **Figure S3**.

### 2.2.4 Preparation of fluorescent peptide (Rho)FPAMAG (**3a**)

A solution of **1a** (0.66 mL, 2 mg·mL<sup>-1</sup>) in 100 mM sodium bicarbonate buffer pH 8.3 and a solution of 5(6)-ROX-NHS (0.66 mL, 3.62 mM in the same buffer) were combined in an eppendorf tube and the reaction monitored by LC-MS. After 3 h and 21 h, 2.59 mg 5(6)-ROX-NHS was added directly to the reaction mixture to increase conversion to the desired product. After 48 h, **3a** was isolated by preparative chromatography, recovered by lyophilization, and stored at -80 °C until used.

### 2.2.5 Alkylation of methionine-containing peptides

Solutions of peptides **1a–5a** (200  $\mu$ L, ~1.1 mg·mL<sup>-1</sup>) were prepared in 100 mM formic acid pH 3 at room temperature in an HPLC vial. Then, ~22.1, 21.5, 11.64, and 12.1  $\mu$ L (10 molar eq.) of propargyl bromide were added from a stock solution (80 vol% propargyl bromide in toluene diluted in ethanol to the final concentration of 0.17 M) to the solution of **1a**, **2a**, **3a**, and **4a**, respectively (final peptide concentration of 1 mg·mL<sup>-1</sup>). The reaction was gently mixed, and the progress of the reaction was monitored by LC-MS. Larger scale syntheses were also performed by scaling both the concentration and volume of these reactions ten-fold. The produced compounds, including FPAM(*allene*)AG (**1b**), (Rho)FPAM(*allene*)AG (**3b**), HDM(*allene*)NKVLDL (**4b**), and HDM(*allene*)NK(Cy5)VLDL (**5b**) were isolated by preparative HPLC, recovered by lyophilization, and stored at -80 °C until used. To evaluate stability, 1 mg·mL<sup>-1</sup> solutions of **1b** and **4b** in 100 mM phosphate buffer pH 7.4 were prepared in HPLC vials, and solution composition monitored by LC-MS for 15 h at room temperature. A lower concentration (0.3 mg·mL<sup>-1</sup>), buffer containing 10 vol% DMF, and 50 molar eq. propargyl bromide were used in the case of **5a**, to reduce loss due to adhesion to the vial and to promote conversion to **5b**. **1a** was also modified with 1-bromo-2-butyne rather than propargyl bromide according to the same procedure to investigate the influence of the terminal methyl group on the nucleophilic reaction with thiols (mass spectrum of product in **Figure S5e**). The mass spectra of **1b**, and **3b–5b**, as well as the products formed by incubation of **1b** and **4b** (hydration and [2,3]-sigmatropic rearrangement) in phosphate buffer can be found in **Figures S2,5**.

### 2.2.6 Click by nucleophilic thiol–allene addition with cysteine, peptide thiols, SAMSA fluorescein, and mPEG–SH

Different conditions were explored for this reaction, as listed explicitly in **Table S1**. As a representative example, allenic peptide (0.5 mg, 1 molar eq.) and thiol (1–10 molar eq.) were transferred to the same gas-tight HPLC vial. The mixture was then purged by N<sub>2</sub> for 10 min. Afterwards, 0.5 mL of N<sub>2</sub>-purged 100 mM phosphate buffer was added to the mixture to yield a final peptide concentration of 1 mg·mL<sup>-1</sup>. The reaction progress was monitored for 24 h by LC-MS and the resulting conjugate isolated by preparative HPLC, recovered by lyophilization, and stored at –80 °C until used. To investigate pH-dependency of the reaction, the pH of the N<sub>2</sub>-purged 100 mM phosphate buffer was adjusted to either 6.5 or 8.5 with concentrated HCl or NaOH solutions. A lower concentration (0.5 mg·mL<sup>-1</sup>) and buffer containing 10 vol% DMF were used to prepare **5b**–CPP(Cy3), to reduce losses. The mass spectra of **1b**–βME, **1b**–GSH, **1b**–SAMSA Fluorescein, , **1b**–mPEG, **4b**–βME, **4b**–GSH, **4b**–SAMSA Fluorescein, **5b**–CPP(Cy3) can be found in **Figures S9–12**.

### 2.2.7 Click by nucleophilic thiol–allene addition with human serum albumin

Solutions of human serum albumin (0.1 mL, 1 mg·mL<sup>-1</sup> in 100 mM phosphate buffer pH 8.5) and **3b** (63.1 μL, 0.24 mM in H<sub>2</sub>O + 0.1% TFA) were mixed in a gas-tight HPLC vial, and then 36.9 μL of 100 mM phosphate buffer pH 8.5 was added (Note: Cys-34 on HSA was ~61 ± 5% in its free reduced form in the starting material, as determined by titration using 2,2'-dipyridyldisulfide). Solution composition was monitored by LC-MS. As the retention time of the conjugate was identical to that of native human serum albumin, the increase of absorbance at 574 nm of this peak, associated with Rho ( $\epsilon_{574} = 78,000 \text{ cm}^{-1} \cdot \text{M}^{-1}$ ), was used to estimate conversion to **3b**–HSA. The identity of the conjugate was verified by mass spectrometry (**Figure S13**).

### 2.2.8 Stability towards nucleophilic substitution

Different conditions were explored for this reaction, as listed explicitly in **Table S2**. As an illustrative example, solutions of conjugate (50 μL, 2 mg·mL<sup>-1</sup>) were prepared in degassed 100 mM phosphate buffer (pH 7.4) in gas-tight HPLC vials. Then, an appropriate volume of thiol solution (50 μL, 20 mM of either GSH or cysteine in degassed 100 mM phosphate buffer) was added to reach a final peptide concentration of 1 mg·mL<sup>-1</sup> and a final thiol concentration of 10 mM. Solution composition was monitored by LC-MS over a 24-h period. Buffer containing 10 vol%

DMF was used in the case of **5b**-CPP(Cy3), to promote solubility. Full chromatograms and mass spectra to validate the identity of peaks are available in **Figures S16,17**.

### 2.2.9 Clip by radical thiol-ene addition

Different conditions were explored for this reaction, as listed explicitly in **Table S2**. As an illustrative protocol, solutions of bioconjugate (~90.6  $\mu\text{L}$ , ~1.1  $\text{mg}\cdot\text{mL}^{-1}$ ) containing 1.1–10 molar eq. of GSH or 10 molar eq. of cysteine were prepared in 100 mM phosphate buffer pH 7.4, 6.5, or 8.5 in a rectangular quartz cuvette. Then, DMPA (~9.4  $\mu\text{L}$ , 1.5 molar eq., from a 15 mM stock solution in methanol) was added at room temperature. Buffer containing 10 vol% DMF was used in the case of **5b**-CPP(Cy3), to reduce losses. The final concentration of **5b**-CPP(Cy3) in DMF/100 mM phosphate buffer pH 7.4 (10% v/v) was 0.1, 0.3, 0.8, or 1  $\text{mg}\cdot\text{mL}^{-1}$ . Samples were irradiated for up to 15 min at 365 nm using a 4 W UVGL-15 UV lamp (UVP, LLC) placed in contact with the cuvette. Solution composition was monitored by LC-MS. The fluorescence intensity of **5b**-CPP(Cy3) was monitored before and after irradiation with a Cytation 5 microplatereader (Biotek Instrument, VT) using the following parameters:  $\lambda_{\text{ex}}/\lambda_{\text{em}}$  549/595 nm (Cy3);  $\lambda_{\text{ex}}/\lambda_{\text{em}}$  646/672 nm (Cy5);  $\lambda_{\text{ex}}/\lambda_{\text{em}}$  549/672 nm (FRET). Spectra were also recorded  $\lambda_{\text{ex}}/\lambda_{\text{em}}$  549/585–700 nm. Full chromatograms and mass spectra to validate the identity of peaks are available in **Figures S18-22**.

#### 2.2.10 Stability of bioconjugates to $\text{H}_2\text{O}_2$ and UV light

Different conditions were explored for this reaction, as listed explicitly in **Table S2**. As an illustrative protocol, solutions of bioconjugate (90  $\mu\text{L}$ , 1.1  $\text{mg}\cdot\text{mL}^{-1}$  in 100 mM phosphate buffer) were incubated in the presence of 1–10 molar eq. of  $\text{H}_2\text{O}_2$  and 0–10 molar eq. of GSH in a quartz cuvette. The volume of the solution was then adjusted with the same buffer to yield a final peptide concentration of 0.1  $\text{mg}\cdot\text{mL}^{-1}$ . The samples were either incubated without or with external irradiation for up to 15 min at 365 nm using a 4 W UVGL-15 UV lamp (UVP, LLC) placed in contact with the cuvette. Sample composition was monitored by LC-MS (**Figure S23**).

#### 2.2.11 Responsiveness of **5b**-CPP(Cy3) in the presence of bacteria

*Escherichia coli* B (HER1024; obtained from the Felix d'Herelle Reference Center for Bacterial Viruses, Université Laval, Quebec) were cultured in Luria-Bertani medium (LB) at 37 °C (1 single colony in 10 mL LB). The next morning, the bacterial culture was diluted 1000-fold in fresh LB medium (i.e., 20  $\mu\text{L}$  culture in 20 mL LB). The bacteria were then grown until log phase (~4 h) at

37 °C on a shaking incubator. Growth was monitored by optical density at 600 nm until ~0.5 was reached (ca.  $\sim 5 \times 10^8$  cells·mL<sup>-1</sup>). Cells were then harvested by centrifugation for 15 minutes at 5000 rpm and then washed with 20 mL Dulbecco's phosphate buffered saline (DPBS) pH 7.4. The cells were then exposed to 20 mL of a 10  $\mu$ M solution of **5b**-CPP(Cy3) in 100 mM phosphate buffer pH 7.4 at 37 °C in the dark for 30 mins. The cells were recovered by centrifugation (15 min at 5000 rpm) and washed with DPBS to remove extracellular bioconjugate. The bacterial cells were suspended in 20 mL of a 100 mM phosphate buffer and 900- $\mu$ L aliquots were transferred into four eppendorf vials, to which was added 100  $\mu$ L of 0, 5, 10, or 50 mM of H<sub>2</sub>O<sub>2</sub> (final concentration of H<sub>2</sub>O<sub>2</sub> was 0  $\mu$ M, 500  $\mu$ M, 1 mM and 5 mM, respectively). Afterwards, the fluorescence intensity of each sample was monitored over 2 h at 37 °C with a microplate reader ( $\lambda_{\text{ex}}/\lambda_{\text{em}}$  550/672 nm; 550/595 nm; 646/672 nm). The level of H<sub>2</sub>O<sub>2</sub>-induced R was estimated using 10  $\mu$ M H<sub>2</sub>DCFDA (1 mg in 200  $\mu$ L DMSO diluted 1000-fold in 100 mM phosphate buffer) instead of **5b**-CPP(Cy3) and the fluorescence intensity of samples were monitored over 2 h at 37 °C with a microplate reader ( $\lambda_{\text{ex}}/\lambda_{\text{em}}$  485/528 nm) (**Figure S24**).

## 2.3 Results and discussion

### 2.3.1 Peptide-based electron-deficient alkyne

The selective alkylation of methionine residues in peptides/proteins is a common tool in chemical biology and enzymology for assessing the potential role of these residues in binding and catalytic events.<sup>46</sup> It is therefore generally considered non-destructive to protein structure and to the integrity of residues other than solvent-exposed methionine. Below pH ~5, the thioether of methionine is the only nucleophilic functional group on proteins and can be selectively modified with alkylating agents. Deming, Li, and their co-workers have exploited this approach to selectively modify methionine-containing peptides with a variety of alkylating agents, including propargyl bromide.<sup>52,440,441</sup> The resulting alkyne grafted to methionine is electron-deficient owing to the adjacent sulfonium group, and such functional groups have been discussed some 40 years ago in the work of Stirling and co-workers.<sup>442,443</sup> While Deming exploited the alkyne to conjugate azide-containing molecules via copper-catalyzed 1,2-dipolar cycloaddition under slightly acidic conditions, the sulfonium naturally induces an isomerization of the alkyne to an allene under neutral conditions, which makes it susceptible to nucleophilic addition. Hou *et al.*<sup>441</sup> have exploited this concept to staple peptides by nucleophilic thiol-allene addition involving a cysteine residue present elsewhere on the same peptide. Inspired by these pioneering works, and to illustrate the potential of this second reaction for bioconjugation purposes, four model methionine-containing

peptides were modified with propargyl bromide to produce electron-deficient alkynes (**Figure 2.2**). To test peptides with different hydrophilicity and pendant functional groups, the model peptide **1a** (592.71 Da) as well as **4a** (1084.25 Da) were chosen for analysis. Analogs of both of these peptides bearing different fluorophores (Rhodamine, Rho; Cyanine 5, Cy5) at different locations were also tested to evaluate compatibility with optical probes (**3a** and **5a** in **Figure 2.2a**).<sup>47,48</sup> The reaction between propargyl bromide and these peptides was quantitative and selective to methionine, and the resulting peptides were easily isolated from reagents with the expected molecular weights (**Figure 2.2b**; **Figures S1,2** and **Table S3** of the Supplementary Information). Prior oxidation of the methionine on **1a** to a **2a** prevented alkylation (**Figure S3** of the Supplementary Information), further supporting that the modification was selective to methionine (**Figure 2.2b**). The resulting adducts **1b** and **4b** were stable at the acidic pH used for alkylation, though hydration<sup>49</sup> and [2,3]-sigmatropic rearrangement<sup>50,51</sup> were observed upon prolonged incubation at near-neutral pH (**1b** and **4b** remained 40 and 70% intact, respectively, after 15 h of incubation; **Figure 2.2a,c** and **Figures S4,5** of the Supplementary Information). This stability was entirely sufficient considering the rate of the subsequent reaction (*vide infra*), and differences in stability were attributed to peptide sequence near the methionine that may influence alkyne/allene isomerization and accessibility of the electron-deficient alkyne. Indeed, the structure of the sulfonium can play a major role in the stability of the allene, presumably by influencing alkyne/allene isomerization. For instance, Bothwell *et al.* observed that the half-life of propargylic S-adenosyl-L-methionine towards hydration was less than one minute at pH 8, which is substantially lower than that observed herein.<sup>49</sup> In this example however, the S-adenosyl group is very different from the S-methyl group of methionine. It is important to mention, however, that the proposed strategy is most appropriate for peptides and compounds that can be handled/purified at acidic pH, which prevents hydration. Indeed, while a successful attempt was made to alkylate the active-site methionine residue of the protein  $\alpha$ -chymotrypsin, handling of the alkylated protein at near neutral pH for purification led to hydration of the sulfonium allene, as evidenced by mass spectrometry (data not shown). Hence, it is important to recognize this limitation of the present concept, or take precautions to handle the sulfonium allene under acidic conditions to preserve its integrity for subsequent reaction with thiols (*vide infra*). Regarding other side-reactions, prior work has shown that modifications to the allene had little effect on the rate or efficiency of [2,3]-sigmatropic rearrangement.<sup>50</sup> Replacing propargyl bromide with 2-butyric bromide prevented isomerization to an allene as well as the subsequent reactions described below and therefore modifications beyond those naturally produced by reaction of propargyl bromide with methionine were not considered in this study.

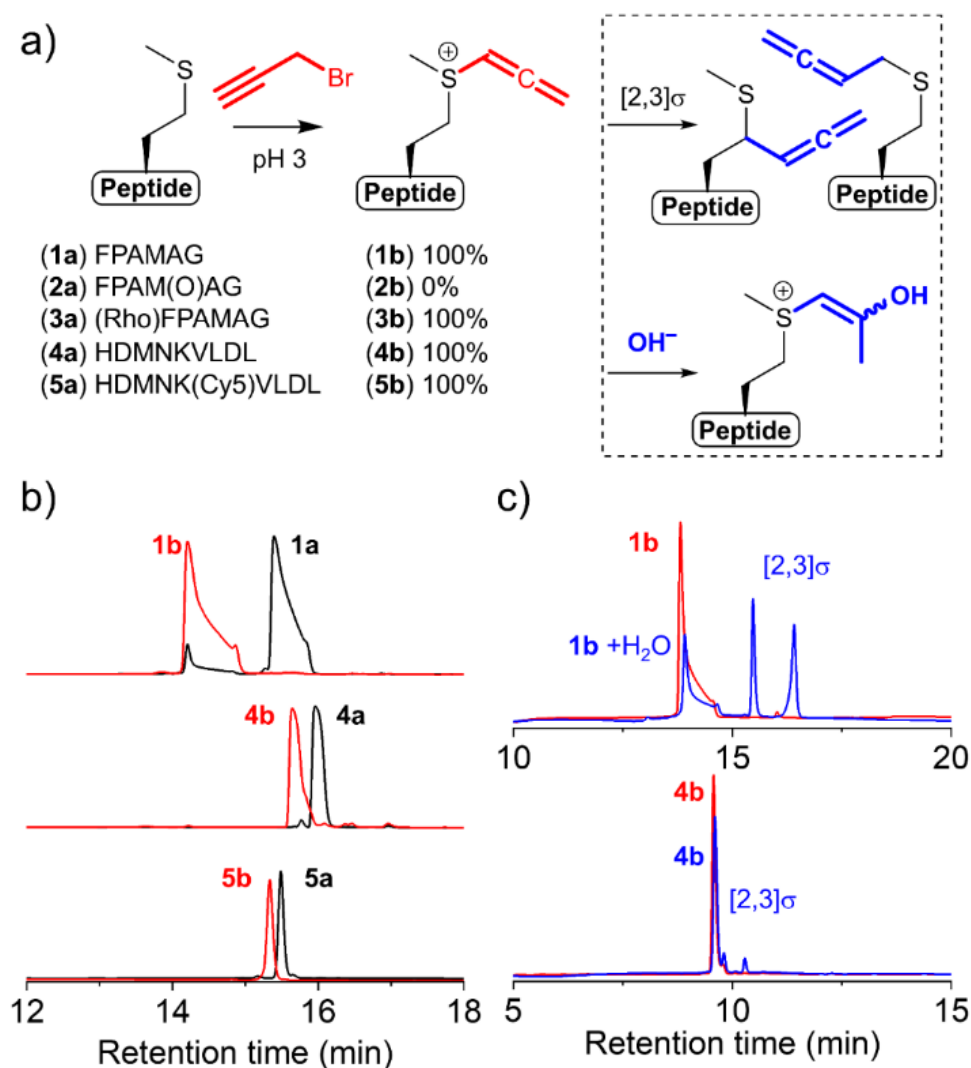


**Figure 2.2** Alkylation of methionine-containing peptides. (a,b) Reaction of propargyl bromide is selective to the thioether of methionine below pH ~5 and occurs without side reactions. (a,c) Incubation of the adduct at neutral pH induces an isomerization from the alkyne to an allene, which can undergo [2,3]-sigmatropic rearrangement or hydration upon prolonged incubation. 1b is more susceptible to these reactions than 4b. Full chromatograms, the mechanism of the reaction, and mass spectra are provided in the Supplementary Information (Figures S1–5).

### 2.3.2 Click – Nucleophilic thiol–allene addition

The four allenic peptides above were reacted with thiols to illustrate the scope of this reaction within the biotechnological sector. These included  $\beta$ ME, GSH, mPEG–SH, deprotected SAMSA fluorescein, human serum albumin, and CPP(Cy3) to cover molecules with a broad range of molecular weights, functional groups, and physical properties. All reactions proceeded smoothly at pH 7.4 and >80% conversion was generally achieved within 1–2 h, using stoichiometric amounts of reagents (**Table S1**). Reaction progress was monitored by liquid chromatography–mass spectrometry, and did not reveal any significant side-reactions (**Figure 2.3a,b** and **Figures**

**S6–13**, of the Supplementary Information). One apparent exception was conjugate formation with human serum albumin, which reached ~64% conversion within 12 h. This likely reflects the fact that cysteine-34 of human serum albumin is (naturally) 30–40% oxidized in this biologically-derived material, which affects the accessibility of free thiols required for the nucleophilic thiol-allene addition reaction.<sup>444</sup> Thus, ~64% conversion in the conjugation of human serum albumin represented the complete conversion of its free thiols. Product formation should be mainly driven by the basicity of the nucleophile: thiolate > hydroxide > ylide (hydroxide and ylide leading to side-reactions of hydration and [2,3]-sigmatropic rearrangement, respectively, which were not observed in the chromatograms).<sup>28</sup> Thus, pH and reactant concentrations/ratios were expected to play a large role in maximizing conversion and minimizing side-reactions (should these be observed). This trend was confirmed experimentally based on the available pK<sub>a</sub> data (e.g., ~8 and ~8.7 for cysteine and glutathione, respectively) for the thiols employed, as well as an acceleration of the reaction by basification and a deceleration by acidification (**Table S1**, **Figure S14**). Such trends were consistent with the observations of others.<sup>445</sup> All the fluorophores tested (Rho, fluorescein, Cy3, and Cy5) maintained their fluorescent properties following activation of methionine to an allene as well as conjugation *via* thiol–allene Click chemistry.

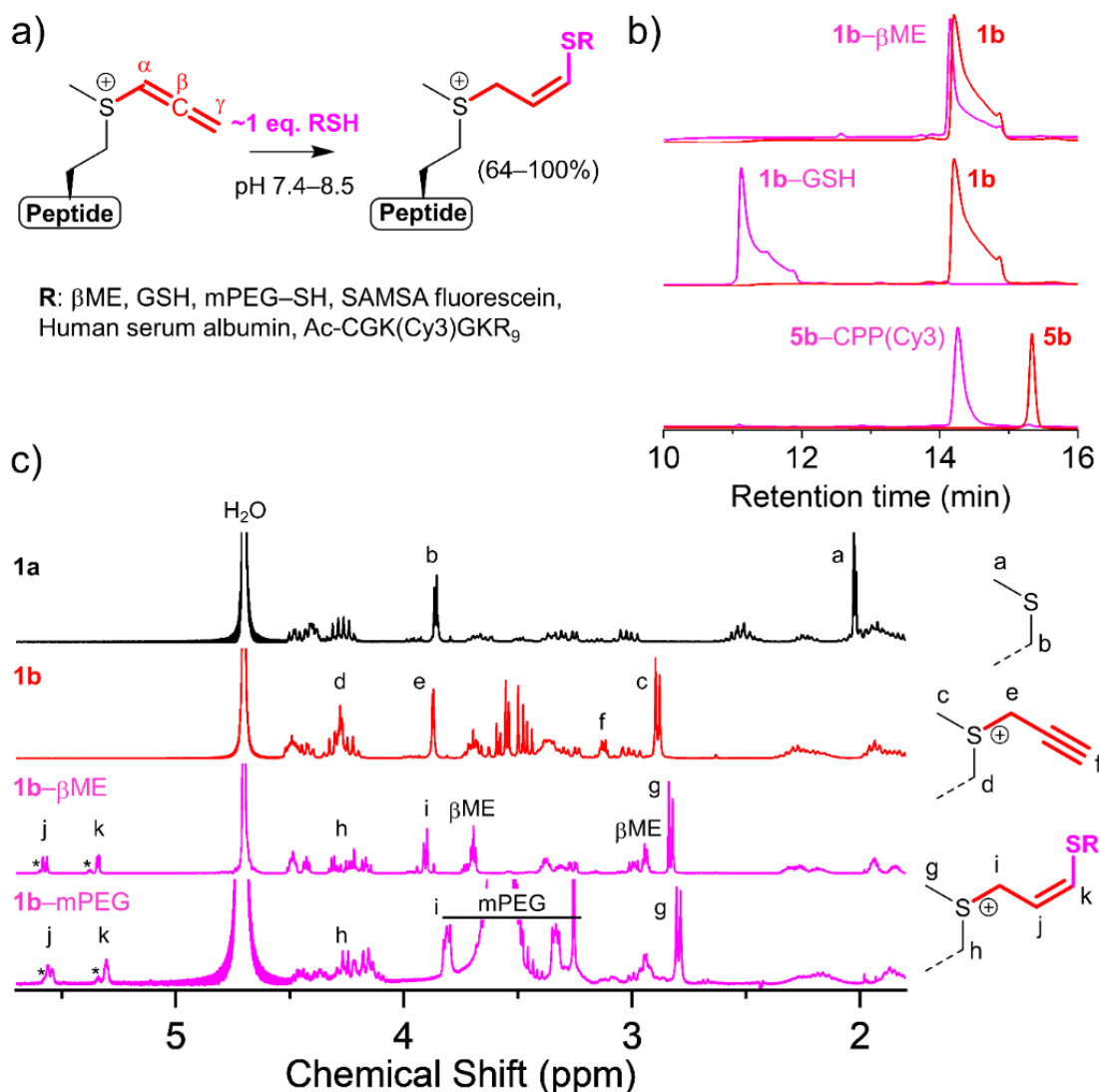


**Figure 2.3** Bioconjugate preparation by Click nucleophilic thiol–allene addition. (a,b) Representative chromatograms showing that reaction of allenic peptides with thiols proceeds with high conversion and without side-reaction. Quantitative data in Table S1. Full chromatograms and mass spectra are provided in the Supplementary Information (Figures S6,7). (c) Selected assigned <sup>1</sup>H NMR spectra demonstrating successful conjugation to the thioether side-chain of methionine. Minor peaks annotated with “\*” represent the *trans* isomer of the sulfonium vinyl sulfide (structure not shown). Note that **1b** is present in its propargylic rather than allenic form due to acidification of the solvent by trace trifluoroacetic acid.

To examine the regioselectivity of the reaction, <sup>1</sup>H NMR spectroscopy was employed. As illustrated in **Figure 2.3c**, one set of major peaks was observed at  $\sim 5.5$  and  $\sim 5.3$  ppm for the sulfonium vinyl sulfide of **1b**– $\beta$ ME (selected because it is the least structurally-complex conjugate), alongside another set of minor peaks at  $\sim 5.6$  and  $\sim 5.4$  ppm accounting for  $\sim 15\%$  of the total. Both *cis* and *trans* isomers are formed, with a strong dominance of the *cis* stereoisomer, as evidenced by <sup>1</sup>H–<sup>1</sup>H Nuclear Overhauser Effect spectroscopy (**Figure S15** of the Supplementary Information). The *trans* isomer also represented  $\sim 20\%$  of **1b**–mPEG, prepared

with the much larger thiol nucleophile. In contrast to Hou *et al.*,<sup>441</sup> who observed addition to the  $\beta$ -position of the allene (and two singlets at 5.8 and 5.6 ppm), in the present work the peaks are both doublets and shifted up field, which suggests addition of the thiol to the  $\gamma$ -position of the allene (**Figure 2.3a**). These results, which diverge from those of Hou *et al.* in terms of regioselectivity, very likely result from differences in solvent (i.e., polarity of the reaction mixture) and catalyst, as discussed in detail by Truong and Dove.<sup>100</sup> Addition to the  $\beta$ -position of the allene in Hou *et al.* occurred in mixed aqueous/organic solution in the presence of triethylamine, while in the present work addition to the  $\gamma$ -position of the allene occurred in near neutral phosphate buffer without catalyst. In fact, in our investigation, we observed the nucleophilic addition of  $RS^-$  to alkyne of alkylated peptides, which is in equilibrium with allene form in near natural pH. The inter- versus intra-molecular nature of the reactions investigated (i.e., this work vs. Hou *et al.*,<sup>441</sup> respectively) may have also played a role but was not explored herein.

To evaluate the stability of the formed conjugates, **1b**-GSH, **4b**-GSH, and **5b**-CPP(Cy3) were incubated in 10 mM GSH pH 7.4, which mimics the thiol concentration of the intracellular space. In agreement with Kramer *et al.*,<sup>52</sup> the prolonged incubation with the thiol nucleophile (under an inert atmosphere) led to a very slow recovery of the native peptides, reaching ~20–30% conversion after 1 day (**Figure 2.4a,b** and **Table S2**). The expected mechanism of this reaction involves nucleophilic addition of a thiol to the carbon adjacent the sulfonium, and side-reactions were not observed (**Figure 2.4b**). Interestingly, due to the strongly electrophilic nature of the sulfonium ion, this reaction results in the release of the fully unmodified peptides **1a**, **4a**, and **5a** with recovery of the original thioether of methionine and no other alterations to the peptide. Thus, this bioconjugation strategy is particularly interesting for slowly releasing native peptides from the bioconjugates in the presence of thiols. In 10 mM cysteine, the rate of release of **1a** from **1b**-GSH remained slow, but was faster owing to the lower thiol  $pK_a$  of cysteine vs. GSH (66% after 22 h; 84% after ~6 days; **Table S2** of the Supplementary Information). These results are interesting because the physiologically relevant concentrations of thiols in the blood are roughly three orders of magnitude lower (in the micromolar range), hinting to the long-term stability of these bonds in the blood. Intriguingly, Hou *et al.*,<sup>441</sup> for whom the thiol is present on the  $\beta$ -position rather than the  $\gamma$ -position of the allene, did not observe reaction with several nucleophiles. This demonstrates the importance of regioselectivity of the thiol–allene reaction on the stability of the resulting bioconjugate. Modification of the allene at the  $\gamma$ -position by reaction in neutral phosphate buffer therefore appears beneficial and necessary to achieve slow peptide release by nucleophilic addition of thiols (and other Clip processes discussed in the next section). Overall, the inter-

molecular thiol–allene reaction studied herein is regioselective under the conditions employed and quantitative conversion can be rapidly achieved with stoichiometric amounts of easily accessible thiol reagents (including small molecules, fluorophores, peptides, polymers, and proteins). Moreover, the resulting adduct is very stable, even towards concentrations of thiols vastly superior to those found in blood.

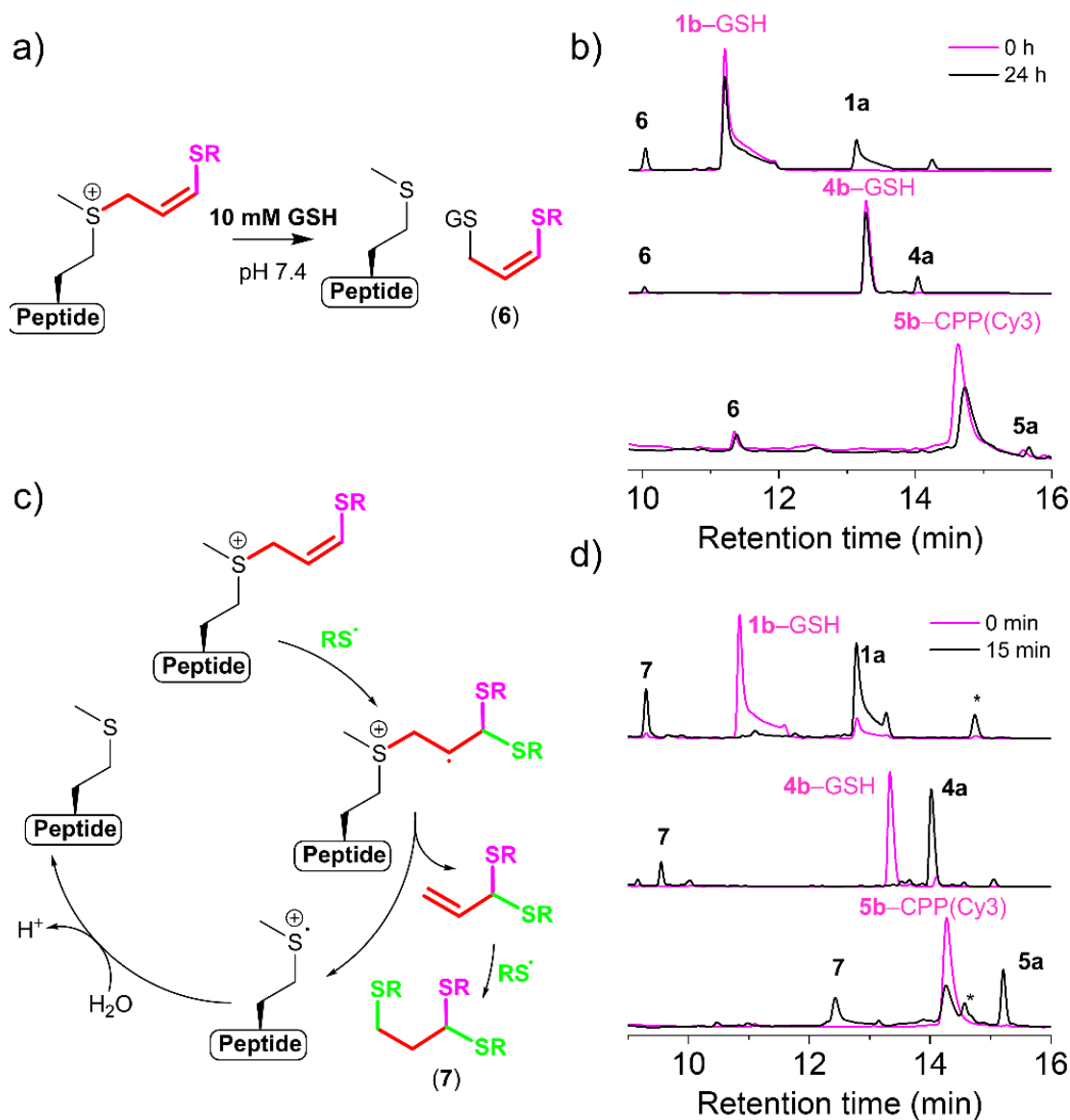


**Figure 2.4** Stability of bioconjugates towards nucleophiles and Clip of bioconjugates by radical thiol-ene addition. (a) Thiol nucleophiles can react at the carbon adjacent the sulfonium, thereby releasing the original thioether of methionine. The mechanism of the reaction is provided in the Supplementary information (Figure S16a). (b) This process occurred slowly without side-reactions, as evidenced in the representative chromatograms for three bioconjugates. (c) Radical thiols induce a fragmentation reaction that releases the original thioether of methionine in minutes. (d) This process occurred rapidly (<15 min) without side-reactions, as evidenced in the representative chromatograms for three bioconjugates. “\*” denotes peaks

from the photo-radical generator. Full chromatograms and mass spectra are provided in the Supplementary information (Figures S16b–19).

### 2.3.3 Clip – Radical thiol–ene addition

Considering the relative stability of the Click adducts above in the presence of large amounts of thiols and for prolonged periods, an exploratory attempt was made to add a second thiol molecule to three sulfonium vinyl sulfide bioconjugates **1b**–GSH, **4b**–GSH, and **5b**–CPP(Cy3) by radical thiol–ene addition, another well-known Click reaction.<sup>53</sup> Surprisingly, rather than observing the expected addition of a second thiol, the very rapid degradation of conjugates **1b**–GSH, **4b**–GSH, and **5b**–CPP(Cy3) was observed alongside the regeneration of the original methionine-containing peptide, **1a**, **4a**, and **5a**, respectively (**Figure 2.4c,d**). As illustrated in **Table S2**, this reaction was very efficient (generally 70–100% conversion within 15 min), took place in neutral aqueous media, and occurred in the presence of near stoichiometric amounts of thiol and source of free radicals. It is anticipated that radical thiol–ene addition initiates a fragmentation process akin to that reported for allylic sulfonium salts, consistent with the mechanism known for cationic polymerization using allyl sulfonium salts (**Figure 2.4c**).<sup>54</sup> In brief, the radical thiol adds to the vinyl group and produces an unstable radical cation that decomposes to a thioether (the original methionine-containing peptide), a dithioacetal, and a proton, the first two of which are observed chromatographically (**Figure 2.4d**). As this process is *a priori* compatible with maintaining the structure/function of biomolecules and the fluorescence of Cy3/Cy5, it could be used for various biotechnological applications. While the aqueous stability of the dithioacetal was not examined further in this work, release of both thiol molecules and acrolein should occur slowly under acidic conditions. The toxicity of the byproducts of the Clip reaction would warrant investigation in future *in vivo* work.

Radical thiols are highly self-reactive and thus short-lived. Therefore, it stands to reason that disulfide bond formation achieved by self-reactivity would compete with the desired thiol–ene reaction and that this competition will strongly influence the efficiency of the Clip reaction. Indeed, it was observed that the Clip reaction was more efficient when increasing the absolute concentration of the bioconjugate, thiol, and radical source, to promote the radical thiol–ene reaction (**Table S2**, **Figure S20**). Furthermore, the conversion of the Clip reaction was not influenced by either the pH of environment or the radical thiol structure (**Table S2**, **Figure S21**), achieving more than >90% conversion in the presence of different thiol sources (GSH or cysteine) at different pH (6.5, 7.4, and 8.5) within 15 min. In contrast, when radical thiols were produced much more slowly, such as by UV-exposure of H<sub>2</sub>O<sub>2</sub> (rather than photo-radical generator DMPA)

in the presence of thiols, very little reaction was observed (<6%; **Figure S23**). Exposure of bioconjugates to H<sub>2</sub>O<sub>2</sub> alone in the dark or under exposure to UV light to generate hydroxyl radicals did not affect the stability of the bioconjugate. In light of these results, it was considered that radical thiols generated naturally in the intracellular space of cells when thiols scavenge reactive-oxygen species could potentially initiate the thiol–ene Clip reaction. However, their low expected abundance and short lifetime (which makes their concentration very difficult to assess) alongside the high concentration of thiol species in the intracellular space would disfavor the Clip reaction versus disulfide bond formation.

To gain some preliminary insight into the stability of sulfonium vinyl sulfide linkages towards biologically-derived thiols and radical thiols (at their natural concentrations), **5b**–CPP(Cy3) was incubated with *E. coli* experiencing different degrees of oxidative stress (induced by incubation with 0–5 mM H<sub>2</sub>O<sub>2</sub>; **Figure S24** of the Supplementary Information). While testing the stability of the probe in blood/serum and cell lysate was considered, it was believed that the known rapid oxidation of the small amounts of thiols in such samples (caused by air, dilution, as well as oxidized biomolecules)<sup>446</sup> would yield a false sense of stability. Moreover, considering the slow expected rate of reaction of the probe with thiols, bacteria were chosen over mammalian cells owing to their significantly higher rate of division and slightly higher intracellular thiol concentration (~20 mM).<sup>447,448</sup> Indeed, this experiment was performed to complement the stability data obtained in model solutions above (e.g., 10 mM GSH) in view of future use in biotechnological applications, and not specifically designed to elucidate the implication of thiols or radical thiols in a reaction. In fact, the very low expected abundance of radical thiols (even if their levels are altered by H<sub>2</sub>O<sub>2</sub>) as well as the high expected concentration of intracellular thiols (~20 mM in the case of *E. coli*) inherently strongly disfavor the radical thiols-induced Clip reaction on the basis of kinetic arguments, as discussed above. As illustrated in **Figure 2.5a,b**, the Clip reaction of this probe under model conditions produced a 70% cleavage of the bioconjugate alongside a corresponding ~70% decrease in the intensity of the fluorescence-resonance energy transfer (FRET) signal between Cy3/Cy5. It was thus considered that FRET intensity could be used to monitor the integrity of the bioconjugate spectroscopically in complex environments. In the presence of *E. coli*, FRET remained relatively constant over the 2-h period investigated (~25% decrease of signal; **Figure 2.5c**) and did not depend to any great extent on exposure to H<sub>2</sub>O<sub>2</sub>. These results suggest that that release of **5a** most likely occurs by reaction with nucleophilic thiols, and not with radical thiols. However, considering the very low abundance and short lifetime of thiol species, which makes them very difficult to characterize, as well as cross-reactivity of blocking agents for thiols/thiyl radicals, it was not possible to completely disregard the implications of radical thiols at

this stage. Ultimately, the stability of the sulfonium vinyl sulfide remains very relevant for labelling experiments (short exposure time) as well as for intracellular drug delivery applications (release over longer times). However, future work should scrutinize the non-trivial question of characterizing the location and species involved in release of methionine peptides from sulfonium vinyl sulfide bioconjugates, which likely depends on the structure of the conjugate itself.

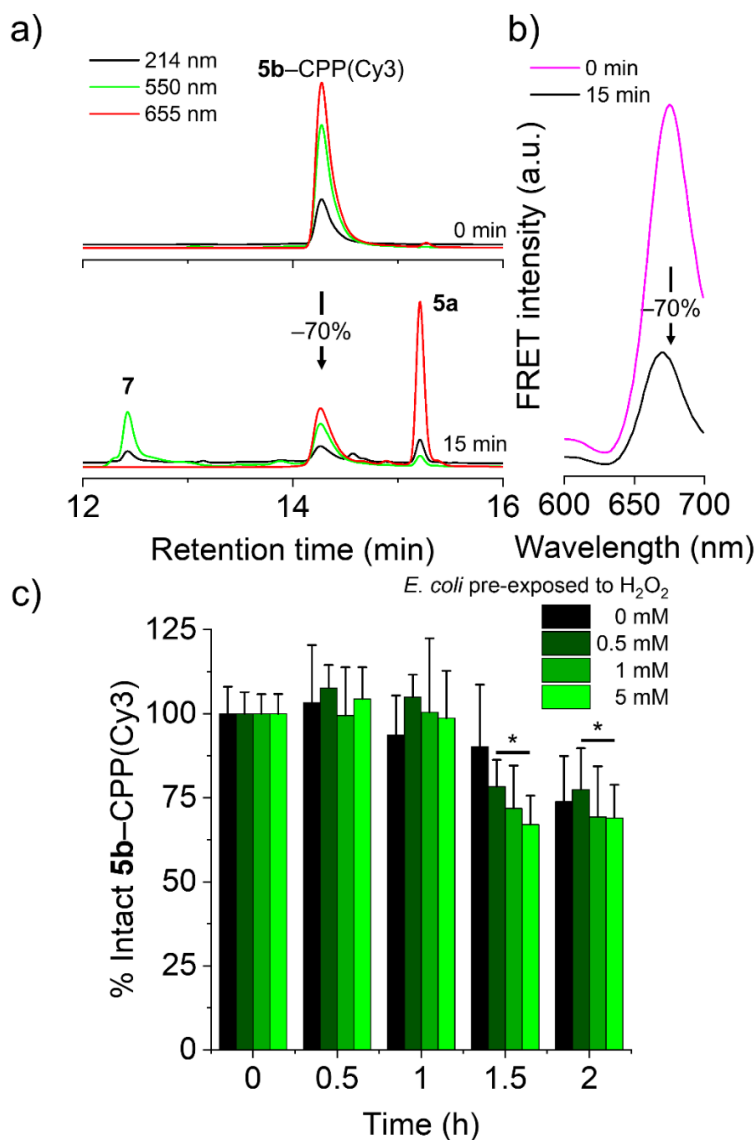


**Figure 2.5** Stability of a sulfonium vinyl sulfide bioconjugate in the presence of reactive species from bacterial cells. (a) The exposure of 5b-CPP(Cy3) to radical thiols yields a ~70% release of the methionine-containing peptide 5a. Chromatograms shown at three absorbance wavelengths before and after a 15-min Clip reaction. (b) Clip occurred concurrently with a ~70% reduction in the intensity of FRET, illustrating that this parameter can be used to track the stability of the bioconjugate in more complex environments. (c) Incubation of 5b-CPP(Cy3) with bacterial cells experiencing different levels of oxidative stress from H<sub>2</sub>O<sub>2</sub> produces very little or no change to FRET over a 1-h period, with some small differences appearing at 1.5 h (Mean + SD, n = 3). “\*” denotes statistically significant difference relative to value at time zero (Repeated measures ANOVA, Tukey, p < 0.05).

## 2.4 Conclusions

Overall, this study reports a combination of two well-known reactions that obey most of the criteria of Click chemistry and that could unexpectedly be used to prepare and disassemble bioconjugates in a Click/Clip manner. Methionine is naturally present in many biomolecules and, in general, thioethers can be conveniently introduced into synthetic molecules, peptides, nucleic acids, polymers, fluorophores, etc. Compared to other reactive handles, such as thiols, thioethers are generally more stable to oxidation and are easily handled. The thiol–allene Click reaction enabled the high-yielding preparation of a variety of peptide–peptide, peptide–fluorophore, peptide–protein, and peptide–polymer conjugates without side-reactions and the process was not harmful to fluorophores from different families. The conjugates were relatively stable to high concentrations of thiols (mimicking the cytosol), and in the presence of cells, yet underwent a radical thiol–ene Clip reaction in a matter of minutes in the presence of radical thiols, again without side-reactions. This reaction released the original methionine-containing peptide with full recovery of its thioether side-chain. Considering the convenience of this Click/Clip strategy, the readily accessible nature of the reactants/reagents and the biological relevance of the latter, this concept has many applications in the biotechnological sector.

### Acknowledgement

MAG is a Research Scholar of the Fonds de Recherche Québec (FRQ) – Santé. AAG acknowledges postdoctoral scholarships from the Fonds de Recherche du Québec Nature et Technologies (FRQNT) and the Canadian Institutes for Health Research (CIHR). Further, she acknowledges the Chu Family Scholarship for a career award. Prof. Jean-Christophe Leroux is thanked for scientific advice.

### Supporting Information

Full chromatograms and mass spectra of all presented data in the main manuscript and in **Table S1, and S2**.  $^1\text{H}$ – $^1\text{H}$  NOESY of sulfonium vinyl sulfide. Analysis of oxidative stress in *E. coli* cells exposed to  $\text{H}_2\text{O}_2$ .

### 3 ARTICLE 2

---

## Biological fate of sulfonium vinyl sulfides – A competition between reactive nitrogen species, radical thiols, and thiol nucleophiles

Fatemeh Zare<sup>1</sup>, Patrick Laplante<sup>2</sup>, Jean-François Cailhier<sup>2</sup>, and Marc A Gauthier<sup>1\*</sup>

<sup>1</sup> Institut National de la Recherche Scientifique (INRS), EMT Research Center, Varennes, Canada

<sup>2</sup> Centre Hospitalier de l'Université de Montréal and Montreal Cancer Institute, Montreal, Canada

#### Corresponding author:

Marc A. Gauthier

Institut National de la Recherche Scientifique (INRS), EMT Research Center, 1650 boul. Lionel-Boulet, Varennes, J3X 1P7, Canada

E-mail: gauthier@emt.inrs.ca

Telephone: +1 514 228 69 32

Fax: +1 450 929 81 02

#### Author contributions:

FZ carried out the most experiments, responsible for the designing of the experiments, data collection, analysis, as well as manuscript composition and revision.

PL trained FZ for *in vitro* experiments and provided guidance, and prepared the cell cultures (RAW 264.7 and THP-1).

JFC provided supports and guidance for cells experiments.

MAG was the supervisory author, involved with the designing of the experiments, concept formation, manuscript composition and revision.

*Note: The work of this chapter is prepared for submission to a scientific journal.*

## Abstract

Chemical linkages that respond to biological stimuli are important for many pharmaceutical and biotechnological applications. Considering the diversity of applications foreseen for such chemical linkages, it is relevant to explore new variants with responsivity profiles that are different from those presently found in the literature. This work explores the responsiveness of a sulfonium vinyl sulfide linker towards physiologically-relevant levels of different categories of reactive species and elucidates the competitive nature of this process in cells. Results indicate that these linkers respond to nucleophilic thiols (hours/days), radical thiols (minutes), and reactive nitrogen species (RNS; minutes) under model conditions leading to the release of a methionine-containing peptide in the first two cases and to hydroxynitration in the third case. In the presence of cells and hence biologically-relevant concentrations of various reactive species, RNS outcompeted radical thiols for reaction with the sulfonium vinyl sulfide, while reaction with nucleophilic thiols remained expected at longer times (hours/days). This work therefore sets the stage for predictably using such linkages in the biotechnological and pharmaceutical sectors.

**Keywords:** Linker; Bioconjugate; Drug delivery system; Thioether; Methionine.

### 3.1 Introduction

The development of chemical linkages that respond to biological stimuli is an important area of research in the pharmaceutical and biotechnological sectors. The latter can be exploited for releasing drug molecules from carriers, as sensitive elements for chemical sensors, as polarity changing groups to alter the physical/chemical properties of drug delivery systems, amongst many other applications.<sup>33</sup> A variety of such linkages exist and respond to stimuli such as pH, over-expression of certain biomolecules, redox status, as well as various nucleophilic and radical species.<sup>449–451</sup> Considering the diversity of applications foreseen of such chemical linkages, it is relevant to explore new variants with responsivity profiles that are different from those presently found in the literature. In this context, our group has recently reported that sulfonium vinyl sulfides could be installed on thioether molecules such as methionine-containing peptides, and that these bonds respond very rapidly to down to equimolar amounts of radical thiols (Chapter 2). This reaction leads to the release of the thioether in minutes. The sulfonium could equally react with nucleophilic thiols, albeit the release of the thioether was slow even in the presence of high concentrations of thiols. Finally, these linkages were insensitive to physiologically-relevant concentrations of reactive oxygen species (ROS) such as hydrogen peroxide, and were stable for

at least 1.5 h in the presence of reactive species produced by bacteria, though slow peptide release was observed in the longer term. However, the identity of the cell-produced reactive species involved in thioether release for sulfonium vinyl sulfide bioconjugates was not fully elucidated. Answering such a question is challenging in view of the concurrent high diversity, reactivity, low concentration, and short lifetime of many of the various reactive species within cells.<sup>452,215</sup>

This study complements our group's previous efforts to characterize the sulfonium vinyl sulfide linkage by preparing a probe that surprisingly produced an orthogonal fluorescence resonance energy transfer (FRET) response to radical thiols and peroxyxynitrite (a model reactive nitrogen species, RNS), thereby enabling us to characterize the competition between these species for the linkage in cells. Results obtained under model conditions indicate that sulfonium vinyl sulfides respond to nucleophilic thiols (hours/days), radical thiols (minutes), and RNS (minutes), leading to the release of methionine-containing peptides in the first two cases and to hydroxynitration in the third case. In the presence of cells and hence biologically-relevant concentrations of various reactive species, RNS outcompeted radical thiols for reaction with the sulfonium vinyl sulfide, while reaction with nucleophilic thiols remained expected upon much longer incubation (hours/days). This work therefore establishes new perspectives on how best to exploit such linkages for biotechnological applications (e.g., *ex cellulo/ex vivo*), as well as applications involving exposure to physiological mixes of reactive species and nucleophiles.

## 3.2 Materials and Methods

### 3.2.1 Materials

Peptides (Ac-K(N<sub>3</sub>)-GSGMGGRKKRRQRRR-NH<sub>2</sub> (**1a**) and Ac-K(N<sub>3</sub>)-GSGCGGRKKRRQRRR-NH<sub>2</sub> (**2a**)) were purchased from Biotechnologies (Zhejiang, China). H<sub>2</sub>DCFDA – Cellular ROS Assay Kit was purchased from Abcam (Toronto, Ontario). ThiolTracker™ Violet (Glutathione Detection Reagent) was purchased from Invitrogen (Waltham, USA). Glutathione (GSH), 5-((2-(and-3)-S-(acetylmercapto) succinoyl) amino) fluorescein (SAMSA fluorescein), and fluorescein-5-maleimide were purchased from Thermo Fisher Scientific. 2,2-Dimethoxy-2-phenylacetophenone (DMPA), tert-butyl hydroperoxide (tBHP), hydrogen peroxide (H<sub>2</sub>O<sub>2</sub>; 30 wt% in H<sub>2</sub>O), propargyl bromide solution (~80% in toluene), hydrochloric acid (HCl), sodium hydroxide (NaOH), sodium nitrite (NaNO<sub>2</sub>), 5,5'-dithiobis(2-nitrobenzoic acid) (DTNB), and N-ethylmaleimide (NEM) were purchased from Sigma Aldrich (Oakville, Canada). Mouse

macrophage RAW 264.7 (ATCC® TIB-71™) and human monocyte THP-1 (ATCC® TIB-202™) cell lines were obtained from ATCC. Fetal bovine serum (FBS) was purchased from Wisent Bioproducts (Quebec, Canada). All chemicals were purchased at the highest grade possible and used as received. All buffers were prepared using MilliQ water (mean resistivity 18.2 MΩ·cm). The thiol group of SAMSA fluorescein is protected as a thioester and was deprotected prior to use as per the manufacturer's instructions (in brief: 2.06 mg of SAMSA fluorescein was dissolved in 1 mL NaOH (0.1 M) for 15 min at room temperature. The pH was then neutralized with 14 µL of 6 M HCl and 0.2 mL 200 mM phosphate buffer pH 7).

### 3.2.2 Equipment

Fluorescence spectra were recorded with either a Synergy 2, Synergy 4, or Cytation 5 microplate reader. A UVGL-15 UV lamp (256/365 nm, 4W) was used for UV light irradiation. Liquid chromatography–mass spectrometry (LC-MS) was performed using an Agilent technologies 1260 high-pressure liquid chromatography (HPLC) system equipped with a 1260 Infinity quaternary pump, a 1260 Infinity II multisampler, a 1260 Infinity VL+ diode array detector with a 3-mm flow cell, and a 6120 single quadrupole mass spectrometer. Analytical and preparative high-pressure liquid chromatography was performed with a second system consisting of a bio-inert 1260 Infinity quaternary pump, a bio-inert 1260 Infinity HiP autosampler, a 1260 Infinity VL+ diode array detector with a 3-mm flow cell, and an Agilent 1260 Infinity Fluorescence Detector. For both chromatography systems, an Agilent Zorbax 300SB-C18 (5 µm, 4.6 x 150 mm) column was used to separate analytes with gradients of H<sub>2</sub>O (+0.1% TFA) and acetonitrile (ACN; +0.1% TFA) as mobile phase. A typical elution profile was: 0 to 4 min 100% H<sub>2</sub>O + 0.1% TFA followed by a linear gradient of 0 to 95% ACN + 0.1% TFA over 25 min with a flow rate of 1 mL·min<sup>-1</sup>. Preparative HPLC was performed using an Agilent Zorbax 300SB-C18 (5 µm, 9.4 x 250 mm) column and identical elution profiles, albeit with a flow rate of 3.3 mL·min<sup>-1</sup>. Fractions containing desired products were lyophilized using a FreeZone 4.5 Liter Benchtop Freeze Dry System from Labconco.

### 3.2.3 Preparation of the sulfonium vinyl sulfide probe (1d)

A solution of **1a** (880.7 µL, ~5.7 mg·mL<sup>-1</sup>) was prepared in 100 mM formic acid pH 3 at room temperature in an HPLC vial. Then, 119.3 µL (10 molar eq.) of propargyl bromide was added from a stock solution (80 vol% propargyl bromide in toluene diluted in ethanol to the final concentration of 0.2 M). This yielded a final peptide concentration of 5 mg·mL<sup>-1</sup>. The reaction was gently mixed

and the progress of the reaction was monitored by LC-MS. Afterwards, **1b** was isolated by preparative chromatography, recovered by lyophilization, and stored at  $-80\text{ }^{\circ}\text{C}$  until used. In the second step, the purified **1b** (1 mg, 1 molar eq.) in 100 mM phosphate buffer pH 7.4 (712.4  $\mu\text{L}$ ) was purged by  $\text{N}_2$  for 10 min and then reacted with 2 molar eq. of a  $\text{N}_2$ -purged deprotected SAMSA fluorescein solution (284.6  $\mu\text{L}$ , 3.36 mM) in the dark. Afterwards, the sample was sealed and purged by  $\text{N}_2$  for 5 more minutes. The reaction progress was monitored and characterized by LC-MS. After  $\sim 4$  h, the produced **1c** was isolated by preparative chromatography, recovered by lyophilization, and stored at  $-80\text{ }^{\circ}\text{C}$  until used. In the third step, the purified **1c** (1 mg, 1 molar eq.) was mixed with 2 molar eq. AFDye<sub>647</sub> DBCO ( $\sim 0.90$  mg) and added to 2 mL phosphate buffer (100 mM, pH 7.4) containing 5 vol% DMF. The mixture was left to react in the dark for  $\sim 3$  h. Eventually, the produced **1d** was isolated by preparative chromatography, confirmed by mass spectrometry, recovered by lyophilization, and stored at  $-80\text{ }^{\circ}\text{C}$  until used.

### 3.2.4 Preparation of the control probe (**2c**)

1.05 mg of peptide **2a** (Ac-K(N<sub>3</sub>)-GSGCGGRKKRRQRRR-NH<sub>2</sub>, 1952.11 g/mol) and 4.27 mg fluorescein-5-maleimide were dissolved separately in 1 mL of  $\text{N}_2$ -purged phosphate buffer (100 mM, pH 7) and 1 mL of  $\text{N}_2$ -purged DMF at room temperature, respectively. Thereafter, 2 molar eq. of fluorescein-5-maleimide (51.7  $\mu\text{L}$ , 10 mM in DMF) was added to the solution of **2a** and left in the dark to react overnight. The produced **2b** was then isolated by preparative chromatography, recovered by lyophilization, and stored at  $-80\text{ }^{\circ}\text{C}$  until used. In the next step, the purified **2b** (1 mg, 1 molar eq.) was mixed with 2 molar eq. AFDye<sub>647</sub> DBCO ( $\sim 0.95$  mg) and added to 2 mL phosphate buffer (100 mM, pH 7.4) containing 5 vol% DMF. The mixture was left to react in the dark for  $\sim 3$  h. Eventually, the produced **2c** was isolated by preparative chromatography, recovered by lyophilization, and stored at  $-80\text{ }^{\circ}\text{C}$  until used.

### 3.2.5 Stability towards nucleophilic substitution

Solutions of **1d** (100  $\mu\text{L}$ , 2 mg·mL<sup>-1</sup>) were prepared in  $\text{N}_2$ -purged phosphate buffer containing 2 vol% DMF (100mM, pH 7.4) in gas-tight HPLC vials. Then, 100  $\mu\text{L}$  GSH solution (20 mM) in  $\text{N}_2$ -purged phosphate buffer (100 mM, pH 7.4) was added to reach the **1d** solution to reach a final peptide concentration of 1 mg·mL<sup>-1</sup> and a final thiol concentration of 10 mM. Afterward, Solution composition was monitored by LC-MS over a 24-h period.

### 3.2.6 Clip by radical thiol–ene addition

The reaction of sulfonium vinyl sulfide bond and radical thiols was explored in different conditions. Solutions of **1d** (~192.0  $\mu\text{L}$ , ~1.04  $\text{mg}\cdot\text{mL}^{-1}$ ) or **2c** (~191.7  $\mu\text{L}$ , ~1.04  $\text{mg}\cdot\text{mL}^{-1}$ ) containing 10 molar eq. of GSH were separately prepared in 100 mM phosphate buffer containing 2 vol% DMF (100mM, pH 7.4) in a rectangular quartz cuvette. Afterwards, ~8.0  $\mu\text{L}$  or ~8.3  $\mu\text{L}$  of a DMPA solution (1.5 molar eq., from a 10 mM stock solution in methanol) was added to **1d** or **2c** solution at room temperature, respectively. An appropriate volume of 100 mM phosphate buffer (pH 7.4) containing 2 vol% DMF was then added to each sample to reach a final **1d** or **2c** concentration of 1  $\text{mg}\cdot\text{mL}^{-1}$ . Samples were irradiated for up to 15 min at 365 nm using a 4 W UVGL-15 UV lamp (UVP, LLC) placed in intimate contact with the cuvette. Solution composition was monitored by LC-MS. The fluorescence intensity of each sample was monitored at each 2 min of UV-light irradiation with a Cytation 5 microplate reader (Biotek Instrument, VT) using the following parameters:  $\lambda_{\text{ex}}/\lambda_{\text{em}}$  480/673 nm (FRET);  $\lambda_{\text{ex}}/\lambda_{\text{em}}$  480/519 nm (fluorescein);  $\lambda_{\text{ex}}/\lambda_{\text{em}}$  643/672 nm (AFDye<sub>647</sub>).

### 3.2.7 Peroxynitrite solution preparation

In a refrigerated beaker under constant stirring, 100 mL of  $\text{NaNO}_2$  600 mM, 100 mL of  $\text{H}_2\text{O}_2$  600 mM in HCl 0.6 M, and 100 mL of NaOH 3.6 M are mixed to prepare the  $\text{ONOO}^-$  standard solutions. The yellow solution indicates the formation of  $\text{ONOO}^-$ . Stirring was maintained until bubble formation ceased. The concentration of peroxynitrite was estimated using its extinction coefficient of 1670  $\text{cm}^{-1}\text{M}^{-1}$  at 302 nm in a 0.5 M sodium hydroxide solution. Calibration standards were prepared by dilution of the  $\text{ONOO}^-$  solution in NaOH 0.1 M.

### 3.2.8 Stability in the presence of peroxynitrite

FPAM(vinyl sulfide–GSH)AG, a model of peptide containing a sulfonium vinyl sulfide group, was prepared as described in our previous paper (Chapter 2; Article 1). 0.13 mg of FPAM(vinyl sulfide–GSH)AG was dissolved in 0.9 mL phosphate buffer (100 mM, pH 7.4). Different molar eq. of peroxynitrite (0, 1, and 5 eq.) were then added to the solution of each sample. An appropriate volume of phosphate buffer (100 mM, pH 7.4) was added to each sample to reach a final FPAM(vinyl sulfide–GSH)AG concentration of 0.1  $\text{mg}\cdot\text{mL}^{-1}$ . Solution composition was monitored by LC-MS over a 3-h period.

### 3.2.9 The effect of peroxyxynitrite on fluorophores

0.5 mg of either AFDye<sub>647</sub> DBCO or SAMSA fluorescein were separately dissolved in 1 mL phosphate buffer (100 mM, pH 7.4) containing 5 vol% DMF. The relevant volume of different molar eq. of ONOO<sup>-</sup> (0, 1, 2, 5, and 10 eq.) and an appropriate volume of phosphate buffer pH 7.4 were then quickly added to each fluorophore solution to reach a final fluorophore concentration of 0.3 mg·mL<sup>-1</sup> in phosphate buffer (100 mM, pH 7.4). Solution composition was monitored by LC-MS. The fluorescence intensity of each sample was immediately monitored with a Cytation 5 microplate reader (Biotek Instrument, VT) using the following parameters:  $\lambda_{ex}/\lambda_{em}$  480/673 nm (FRET);  $\lambda_{ex}/\lambda_{em}$  480/519 nm (Fluorescein);  $\lambda_{ex}/\lambda_{em}$  643/672 nm (AFDye<sub>647</sub>).

### 3.2.10 The effect of peroxyxynitrite on 1d and 2c

0.5 mg of **1d** or **2c** were separately dissolved in 1 mL phosphate buffer containing 0.5 vol% DMF (100 mM, pH 7.4). The relevant volume of different molar eq. of ONOO<sup>-</sup> (0, 1, 2, 5, and 10 eq.) and an appropriate volume of phosphate buffer (100 mM, pH 7.4) were then quickly added to the probe solutions to reach a final probe concentration of 10  $\mu$ M in phosphate buffer containing 0.5 vol% DMF (100 mM, pH 7.4). Solution composition was monitored by LC-MS. The fluorescence intensity of each sample was immediately read with a Cytation 5 microplate reader (Biotek Instrument, VT) using the following parameters:  $\lambda_{ex}/\lambda_{em}$  480/673 nm (FRET);  $\lambda_{ex}/\lambda_{em}$  480/519 nm (Fluorescein);  $\lambda_{ex}/\lambda_{em}$  643/672 nm (AFDye<sub>647</sub>). Spectra were also recorded  $\lambda_{ex}/\lambda_{em}$  480/499–800 nm;  $\lambda_{ex}/\lambda_{em}$  640/660–800 nm.

### 3.2.11 Cell culture preparation

Mouse macrophage RAW 264.7 and human monocyte THP-1 cell lines were used. RAW 264.7 cells were cultured in Dulbecco minimal Eagle's medium (DMEM) supplemented with 10 vol% fetal bovine serum (FBS) and the base medium for THP-1 in RPMI-1640 supplemented with 10 vol% FBS. Cells were kept separately in a humidified incubator at 37 °C and 5% CO<sub>2</sub> in 75 cm<sup>2</sup> tissue culture flasks. THP-1 (suspensions) and RAW 264.7 (adherent) were seeded in 96-well microplates at a concentration of 5 × 10<sup>5</sup> and 2 × 10<sup>5</sup> cells·mL<sup>-1</sup>, respectively. Experiments were designed for adherent cells. Therefore THP-1 cells were differentiated into macrophages-like cells by incubation with the solution of phorbol 12-myristate 13-acetate (PMA) in media culture (160 nM) and seeded in the 96-well plates for 3 days.

### 3.2.12 Cellular ROS Assay

A cell-permeant reagent 2',7'-dichlorodihydrofluorescein diacetate (H<sub>2</sub>DCFDA) was used to measure the levels of intracellular ROS. H<sub>2</sub>DCFDA is a cell-permeable, non-fluorescent molecule that is deacetylated by cellular esterases after diffusion into the cells. Later, it can be oxidized by ROS into 2',7'-dichlorofluorescein (DCF), a highly fluorescent compound. Hence, relative ROS levels can be monitored by fluorescence ( $\lambda_{ex}/\lambda_{em}$  485/528 nm).<sup>453</sup> Accordingly, cells were washed with phosphate-buffered saline (1×, pH 7.2–7.4) to remove the media and then exposed to 100  $\mu$ L H<sub>2</sub>DCFDA solution (20  $\mu$ M solution, which was prepared by dissolving 1.9 mg in 200  $\mu$ L DMSO diluted 1000-fold in phosphate-buffered saline (1×, pH 7.2–7.4) containing 2 vol% FBS) at 37 °C in the dark for 30 mins. Afterwards, cells were washed with phosphate-buffered saline (1×, pH 7.2–7.4) to remove extracellular H<sub>2</sub>DCFDA. Finally, cells were treated with 100  $\mu$ L tBHP solution (50  $\mu$ M and 250  $\mu$ M) or LPS solution (0, 1, and 10  $\mu$ g·mL<sup>-1</sup>) in phosphate-buffered saline (1×, pH 7.2–7.4) containing 2 vol% FBS. The fluorescence intensity of each sample was monitored over 2 h at 37 °C with a microplate reader ( $\lambda_{ex}/\lambda_{em}$  485/528 nm).

### 3.2.13 Cellular Thiol assay

The relative levels of reduced thiols were detected using the ThiolTracker™ Violet (TTV) kit using the manufacturer's protocol.<sup>454</sup> Reduced GSH represents the majority of intracellular free thiols, so this probe can be used to estimate its levels in cells. Briefly, each well containing RAW 264.7 and THP-1 cells was washed with 100  $\mu$ L phosphate-buffered saline (1×, pH 7.2–7.4) to remove the media. Afterwards, cells were incubated with 100  $\mu$ L tBHP (50  $\mu$ M and 250  $\mu$ M) or LPS (0, 10  $\mu$ g·mL<sup>-1</sup>) solution in phosphate-buffered saline (1×, pH 7.2–7.4) containing 2 vol% FBS. After 0, 15, 30, and 120 minutes of incubation, each well-containing RAW 264.7 and THP-1 cells was washed twice with 100  $\mu$ L Dulbecco's phosphate buffered saline, containing Ca<sup>2+</sup> and Mg<sup>2+</sup>, glucose, and sodium pyruvate (D-PBS C/M) and were then incubated with 100  $\mu$ L of prewarmed 20  $\mu$ M TTV solution (prepared by diluting 12  $\mu$ L of 20 mM ThiolTracker™ Violet stock solution (15  $\mu$ L DMSO to each vial of ThiolTracker™ Violet dye (Invitrogen, Catalog nos. T10095, T10096)) into 12 mL of D-PBS C/M containing 2 vol% FBS at 37 °C for 30 minutes in a dark place. Following incubation, the dye was washed out and replaced with phosphate-buffered saline (1X, pH 7.2–7.4) containing 2 vol% FBS. Eventually, the fluorescence intensity of each well was measured in a microplate reader ( $\lambda_{ex}/\lambda_{em}$  404/526 nm).

### 3.2.14 Exposure of 1d/2c to cells

RAW 264.7 and THP1 cells were seeded in 96-well plates to reach the desired population of  $2 \times 10^5$  and  $5 \times 10^5$  cells·mL<sup>-1</sup>, respectively. After that, they were washed with phosphate-buffered saline (1×, pH 7.2–7.4) and incubated with a 100 μL solution containing 10 μM **1d** or **2c**, tBHP (50 μM and 250 μM), or LPS (0, 10 μg·mL<sup>-1</sup>) in phosphate-buffered saline (1×, pH 7.2–7.4) containing 2% v/v FBS at 37 °C. The fluorescence intensity was measured over 2 h incubation by a microplate reader using the following parameters:  $\lambda_{\text{ex}}/\lambda_{\text{em}}$  480/673 nm (FRET);  $\lambda_{\text{ex}}/\lambda_{\text{em}}$  480/519 nm (Fluorescein);  $\lambda_{\text{ex}}/\lambda_{\text{em}}$  643/672 nm (AFDye<sub>647</sub>).

### 3.2.15 Cellular thiol blocking treatments by DTNB or NEM

The membrane-impermeable compound 5,5'-dithio-bis-(2-nitrobenzoic acid) (DTNB) and membrane-permeable compound N-ethylmaleimide (NEM) were used to inactivate cellular thiol functional groups and evaluate the impact of GSH and radical thiols on sulfonium vinyl sulfide bond breakage in cells experiencing oxidative stress. Accordingly, the seeded living cells (RAW 264.7 and THP-1 cells) in 96-well plates were washed with phosphate-buffered saline (1×, pH 7.2–7.4) to remove the media. Each well-containing cell was then incubated with **1d** or **2c** solution (10 μL, 0.1 mM) in phosphate-buffered saline (1×, pH 7.2–7.4) containing 5 vol% DMF and 2% FBS, NEM solution (10 μL, 10 mM) or DTNB solution (10 μL, 25 mM) in phosphate-buffered saline (1×, pH 7.2–7.4) containing 2% FBS, tBHP solution (10 μL of 0, 0.5, and 2.5 mM) or LPS solution (10 μL, 0.1 mg·mL<sup>-1</sup>) phosphate-buffered saline (1×, pH 7.2–7.4) containing 2% FBS, and an appropriate volume of phosphate-buffered saline (1×, pH 7.2–7.4) containing 2% FBS to reach 100 μL solution per each well with a desired final concentration of compounds (10 μM **1d**, 10 μM **2c**, 1 mM NEM, 2.5 mM DTNB, 0, 50, or 250 μM tBHP, and 0 or 10 μg·mL<sup>-1</sup> LPS). It is worth mentioning that the final vol% of DMF and FBS were 0.5% and 2% at each well. Afterwards, the fluorescence intensity of each well was immediately measured over 2.5 h at 37 °C by a microplate reader ( $\lambda_{\text{ex}}/\lambda_{\text{em}}$  480/673 nm (FRET);  $\lambda_{\text{ex}}/\lambda_{\text{em}}$  480/519 nm (fluorescein);  $\lambda_{\text{ex}}/\lambda_{\text{em}}$  643/672 nm (AFDye<sub>647</sub>).

### 3.2.16 Cell viability assay

The cell viability of each cell line was evaluated using the crystal violet assay. Each well containing RAW 264.7 and THP-1 cells was rinsed with phosphate-buffered saline (1×, pH 7.2–7.4) after 3 h exposure to **1d** and **2c** solution (100 μL, 10 μM). Furthermore, each well was incubated with 50 μL of 0.5% crystal violet staining solution and incubated for 10 min at room temperature.

Subsequently, cells were washed extensively with distilled water to remove the excess dye. Finally, the optical density (OD) of each well was measured by a microplate reader at 570 nm.

### 3.3 Results and discussion

#### 3.3.1 Design and synthesis of sulfonium vinyl sulfide and control FRET probes

In order to monitor the stability of sulfonium vinyl sulfide linkages in the presence of cells, a FRET-based probe was designed based on a cell-penetrating peptide, Tat<sub>49–57</sub>, extended on its N-terminal side with a short peptide sequence containing azidolysine (for conjugation of the acceptor fluorophore AFDye<sub>647</sub> via copper-free Click chemistry) and a methionine residue. This cell-penetrating peptide sequence was chosen in favor of nona-arginine used in our previous work, owing to the reported propensity of the latter for self-aggregation,<sup>55</sup> which complicated subsequent analyses from a technical standpoint. To prepare the responsive probe (**1d**), the methionine residue of peptide (**1a**) was first alkylated to a sulfonium allene (**1b**) with propargyl bromide under acidic conditions and subsequently modified with the donor fluorophore (SAMSA fluorescein; deprotected to its thiol form) by nucleophilic thiol–allene addition to yield the fluorescent sulfonium vinyl sulfide peptide (**1c**). Thereafter, the acceptor fluorophore (DBCO–AFDye<sub>647</sub>) was introduced onto the azido group of the peptide by copper-free Click chemistry to yield **1d** (**Figure 3.1a,c**). A control probe (**2c**) containing a thioether rather than a sulfonium vinyl sulfide linkage was prepared by a similar approach but by substituting the methionine residue on **1a** for a cysteine (**2a** in **Figure 3.1b,d**). The thiol group on this peptide was alkylated with fluorescein-5-maleimide to produce a stable thioether bond. Both probes were analytically pure by high-performance liquid chromatography (HPLC), exhibited the expected optical properties based on the appended fluorophores, and their identity validated by mass spectrometry (**Figures S1–3**). Moreover, both probes exhibited FRET upon excitation to the donor fluorophore ( $\lambda_{\text{ex}}/\lambda_{\text{em}}$  485/625–800 nm) (**Figure 3.1e**).

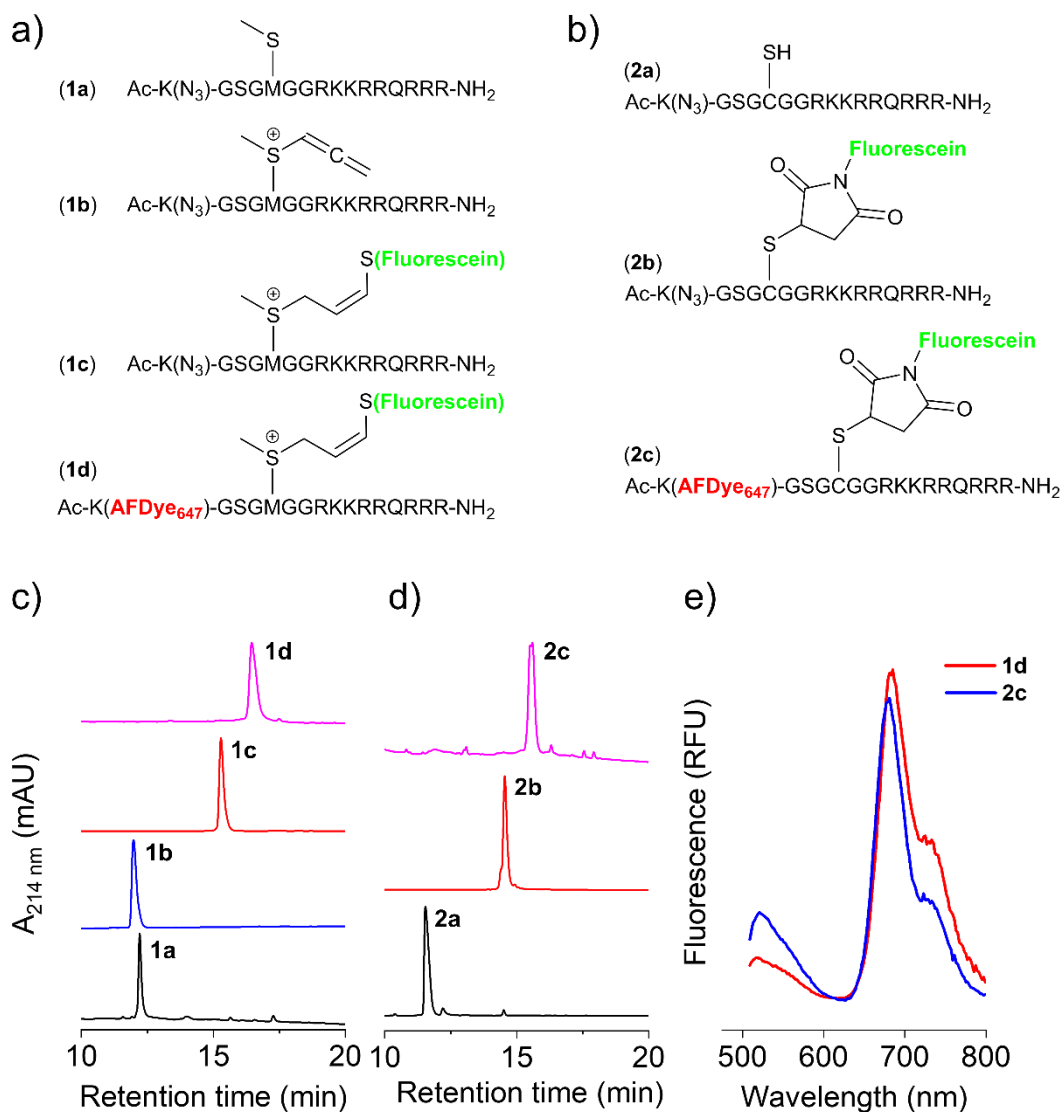


**Figure 3.1** FRET-based sulfonium vinyl sulfide and thioether probes. (a,b) Synthetic scheme to prepare **1d** and **2c** from methionine-containing peptide **1a** and cysteine-containing peptide **2a**, respectively. (c,d) Representative chromatograms of purified compounds. (e) Fluorescence spectra ( $\lambda_{\text{ex}}$  485 nm) demonstrate FRET for **1d** and **2c**.

### 3.3.2 Reaction with radical thiols and thiol nucleophiles

In agreement with our previous work, the sulfonium vinyl sulfide bond of **1d** was very stable in the presence of thiols upon prolonged incubation in conditions mimicking the cytosol (i.e., 10 mM GSH, pH 7.4). As shown in **Figure 3.2a**, **1d** remained >92% intact over 24 h, based on the integration of the peak of the original conjugate. Over this period, the slow nucleophilic addition of GSH to the carbon adjacent to the sulfonium on **1d** produced a peptide fragment with the recovery of the original methionine residue (**1e**) as well as a fluorescent adduct of GSH (**1f**), without side reactions. Both **1e** and **1f** were evidenced by HPLC and mass spectrometry (**Figures**

**S4,5**). To validate the responsiveness of the sulfonium vinyl sulfide **1d** towards a radical thiol-ene “Clip” reaction (with a concurrent effect on the intensity of the FRET signal), **1d** was reacted with radical thiols generated from 10 molar eq. of GSH and 1.5 eq. of photo-radical initiator in neutral phosphate buffer. The scheme illustrating the reaction is presented in **Figure 3.2b**. Results shown in **Figure 3.2c** illustrate that after a 15-min exposure to UV light at 366 nm, ~60% of the sulfonium vinyl sulfide fragmented to release the AFDye<sub>647</sub> modified peptide (**1e**, with the original methionine residue intact) alongside another fluorescent adduct of GSH (**1g**), as identified chromatographically by their optical properties and mass spectrometry (**Figure S6,7**). Moreover, the intensity of the FRET signal dropped by ~60% with this transformation (**Figure 3.2d**), indicating that this parameter can be used to quantitatively monitor the stability of the sulfonium vinyl sulfide linkage in cell culture. In parallel, a ~350% increase in fluorescence intensity of the fluorescein channel ( $\lambda_{\text{ex}}/\lambda_{\text{em}}$  480/519 nm) was observed over the same period due to discontinuation of FRET. The fluorescence intensity of the AFDye<sub>647</sub> channel ( $\lambda_{\text{ex}}/\lambda_{\text{em}}$  643/672 nm) did not change significantly from its initial value. In contrast to the results above, **2c** was insensitive to radical thiols as evidenced by the insensitivity of the intensity of its FRET signal after exposure to radical thiols (**Figure S6b**).

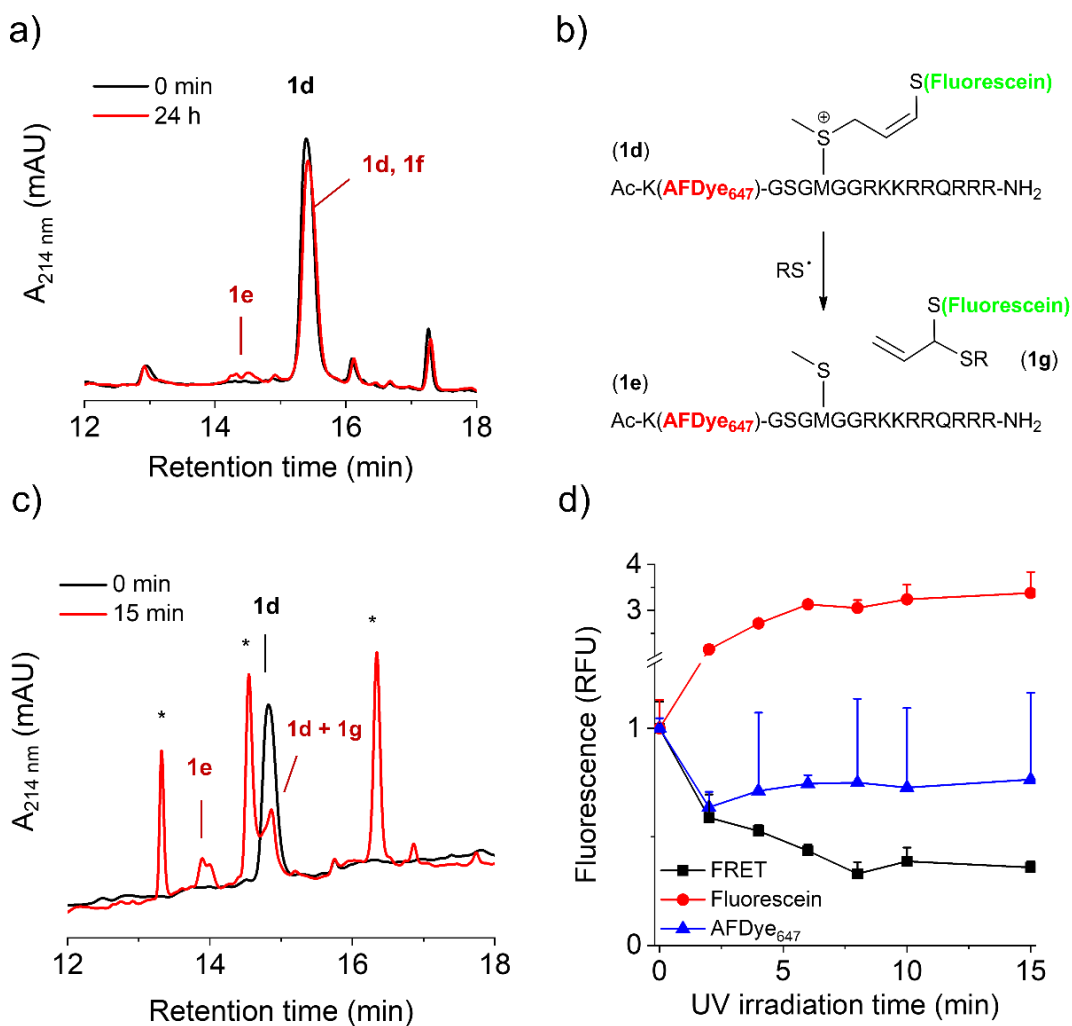


**Figure 3.2** Reaction with radical thiols and thiol nucleophiles. (a) Chromatogram illustrating the stability of 1d/2c in 10 mM GSH over 24 h. (b) Scheme illustrating the products formed by reaction of 1d with a radical thiol (15 min UV irradiation of 10 eq. GSH and 1.5 eq. photoinitiator). (c,d) Illustrative chromatogram and evolution of optical properties of 1d exposed to radical thiols. Data in pane d is presented as Mean + SD (n = 3). “\*” denotes peaks from photo-radical generator.

### 3.3.3 Nitration with peroxynitrite (ONOO<sup>-</sup>) as a model RNS

To assess the reactivity of sulfonium vinyl sulfides towards RNS, **1d** and **2c** were incubated with 0–5 molar eq. of peroxynitrite. Peroxynitrite (ONOO<sup>-</sup>) is a potent nitrating agent for biomolecules (e.g., proteins, nucleic acids, lipids, and sugars)<sup>455</sup> and is involved in many physiological and pathological processes.<sup>178,179</sup> It is an unstable molecule (half-life of ~10–20 ms)<sup>12</sup> that transforms at physiological pH to other highly reactive molecules such as peroxynitrous acid (ONOOH, pK<sub>a</sub> 6.8) or the unstable nitrosoperoxocarbonate anion (ONOCO<sub>2</sub><sup>-</sup>).<sup>178,456</sup> Both ONOOH and

ONOOCO<sub>2</sub><sup>-</sup> decompose to <sup>•</sup>NO<sub>2</sub>, which is the primary species expected to react with **1d/2c**.<sup>178,179</sup> As illustrated in **Figure 3.3a,c**, **2c** remained relatively stable in the presence of up to 2 eq. peroxyxynitrite, as evidenced by only a small change in the chromatogram and fluorescent signals (FRET channel and channels of both fluorophores). Curiously, when **1d** was exposed to up to 2 eq. peroxyxynitrite, the intensity of the FRET signal increased by 160% and was equally accompanied by a 350% increase of intensity from the fluorescein channel (**Figure 3.3b,d**). Upon exposure to higher molar eq. of peroxyxynitrite (5 and 10 eq.), substantial degradation of both **1d** and **2c** was observed by chromatography as well as by a decrease of all fluorescent signals (FRET and individual fluorophores). To better understand the nature of this increase and subsequent decrease of fluorescent signals for **1d** (and only decrease for **2c**), a smaller model peptide, SAMSA fluorescein, and AFDye<sub>647</sub> were separately exposed to peroxyxynitrite under identical conditions to facilitate analysis by mass spectrometry. The results, shown in **Figure S8**, reveal that both fluorophores were relatively stable in the presence of up to ~2 eq. of peroxyxynitrite (0–15% loss of fluorescence intensity), though degraded rapidly thereafter with concomitant substantial loss of fluorescence intensity. This was due to nitration and/or oxidation of these entities and some of these species were evidenced by mass spectrometry (**Figures S9,10**). Indeed, these observations are in line with those of other groups, who have reported the mechanism of oxidation of cyanine polyenes by peroxyxynitrite.<sup>457,458</sup> However, this result does not explain the pronounced increase of fluorescence of **1d** (both fluorescein and FRET channels) in the presence of <2 eq. of peroxyxynitrite. Indeed, while the fluorophores themselves are relatively stable in the presence of up to ~2 eq. of peroxyxynitrite, analysis of the model peptide revealed hydroxynitration of the sulfonium vinyl sulfide (**Figures S11,12**). As such, the increase of fluorescence observed for **1d** (both fluorescein and FRET channels) upon hydroxy nitrosylation of the sulfonium vinyl sulfide can be ascribed to a change of chemical structure and local polarity near fluorescein. As this process occurs more rapidly than the degradation of either fluorophore, probe **1d** first exhibits an increase of fluorescence due to this phenomenon and is followed by a decrease in the presence of higher amounts of peroxyxynitrite. Therefore, this probe system is very interesting for characterizing the competition between radical thiols and RNS in complex biological milieu – something that is challenging to accomplish – owing to the orthogonal changes to its fluorescence properties resulting from reaction with either species.

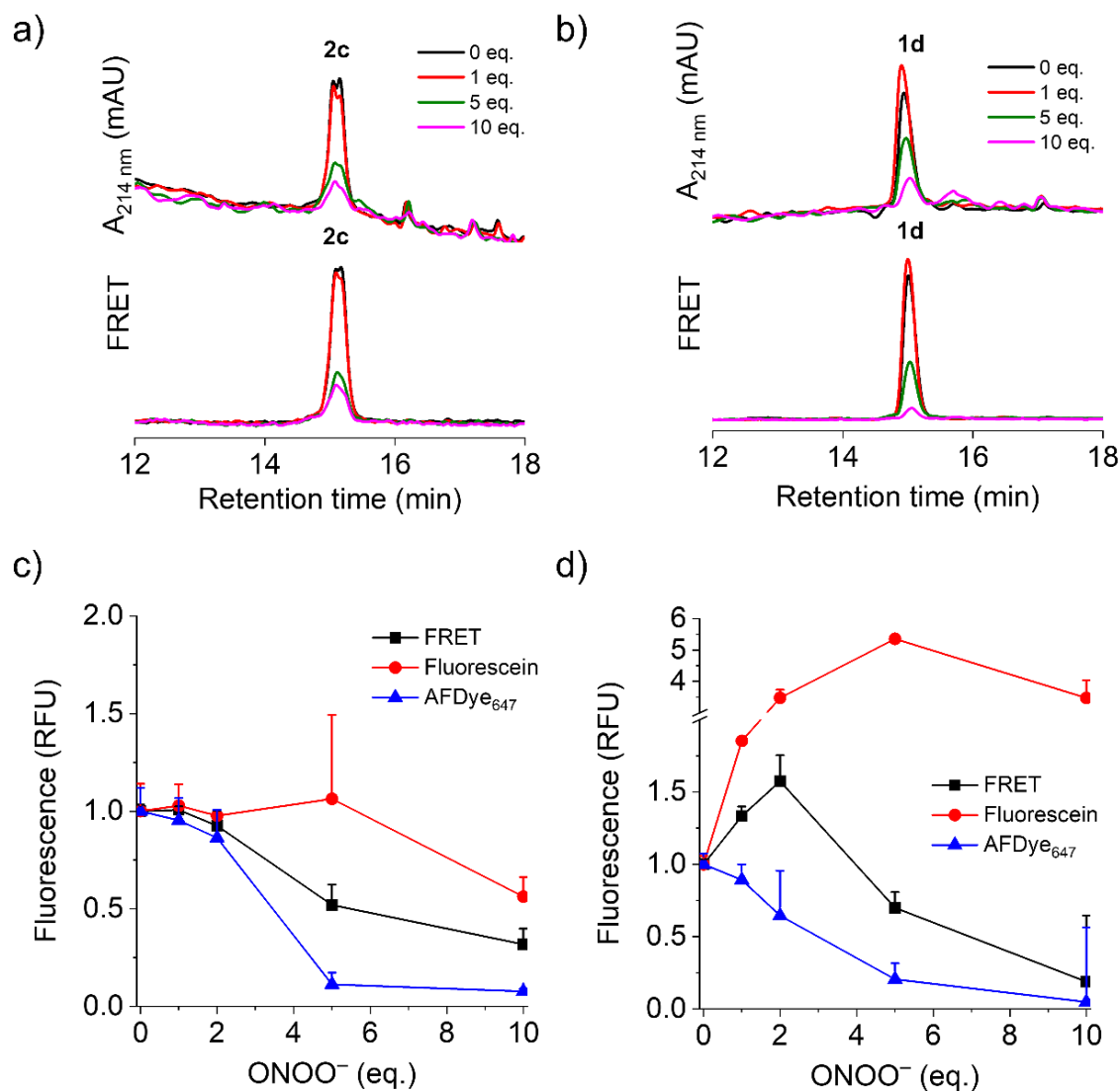


**Figure 3.3** Stability of 2c/1d in the presence of peroxynitrite. (a,c) 2c is stable towards ~2 eq. of peroxynitrite, above which loss of fluorescence intensity is observed. (b,d) Exposure of 1d to peroxynitrite first leads to an increase of fluorescein and FRET intensity, then to a subsequent decrease. For panes c and d, values are given as Mean + SD (n = 3).

### 3.3.4 Reactivity of sulfonium vinyl sulfides in cell culture models of oxidative stress

To evaluate the competition RNS and radical thiols for sulfonium vinyl sulfide linkages in cell culture, permanent mouse macrophages RAW 264.7 and adherent human monocyte THP-1 cell lines were chosen as *in vitro* models owing to the substantial amount of reactive species they generate upon activation compared to other cell types.<sup>459–461</sup> To modify the amount of reactive species naturally generated by these cells, cultures were exposed to the ROS tert-butyl hydroperoxide (tBHP) and lipopolysaccharide (LPS), a cell-wall component of gram-negative

bacteria known to influence the activation of monocytes and macrophages by the production of pro-inflammatory mediators and cytokines.<sup>462–465</sup> To characterize oxidative stress, the levels of ROS were quantified using H<sub>2</sub>DCFDA, and the concentration of intracellular thiols was measured using thiol tracker violet, both as a function of tBHP/LPS concentration and time (**Figure S13**). In general, exposure of both cell lines to the stressors resulted in an increase in ROS concentration as a function of concentration and time, and a more dramatic effect was observed for tBHP, probably as it is itself a ROS. Concurrently, and in line with previous reports,<sup>198,466</sup> a reduction in the concentration of intracellular thiols was observed for both cell lines after a two-hour exposure to the stressors. As thiols are known scavengers for ROS and RNS, decreased thiol concentration suggests the transient formation of radical thiols that recombine to form disulfide compounds.

22,208,453

The sulfonium vinyl sulfide **1d** and thioether **2c** were added to the cells at a concentration that was minimally cytotoxic (**Figure S14**) and changes to FRET intensity and individual fluorophore channels were monitored with time (**Figure 3.4**). As expected, the FRET signal of the thioether probe **2c** remained constant over the 150-minute experiment, indicating the stability of the peptidic probe and its constituents. In contrast, the FRET signal of **1d** increased with time to reach a plateau at ~200% of its initial value over a ~2-h period, which is suggestive of hydroxynitration of the sulfonium vinyl sulfide by RNS. Very little to no effect of LPS or tBHP on the kinetics of fluorescence increase was observed, which suggests that ROS are not involved in the changes affecting **1d** (or at most contribute to a minor extent). Moreover, the addition of DTNB and NEM to block extracellular and total thiols, respectively, equally did not have a great effect on the kinetics of the evolution of the FRET signal from **1d**, indicating the lack of (or at most minimal) participation of thiols or RSS in the changes affecting **1d**, over the short timeframe of the experiment (**Figure 3.4**). Nonetheless, the plateau FRET signal reached in the presence of NEM was lower than for the other experiments, suggesting the scavenging of radical species by the latter. Similar results were observed for both cell lines and only modest differences in kinetics were observed. In line with the experiments from previous sections, the AFDye<sub>647</sub> channel of both **1d** and **2c** was stable over the entire 150-min incubation period (**Figure S15**), while the intensity of the fluorescein channel increased slightly over this same timeframe, and in both cell lines (**Figure S16**). The small progressive increase of intensity from the fluorescein channel was insensitive to any of the stressors applied to the cells, suggesting that it reflects changes to the local environment (pH, polarity) associated with interaction and cellular trafficking.<sup>467</sup> Hence, the global analysis of the results above indicate that hydroxynitration of the sulfonium vinyl sulfide

outcompetes other reactions, in particular the radical thiol–ene “Clip” reaction that would lead to the release of **1a** from **1d**.

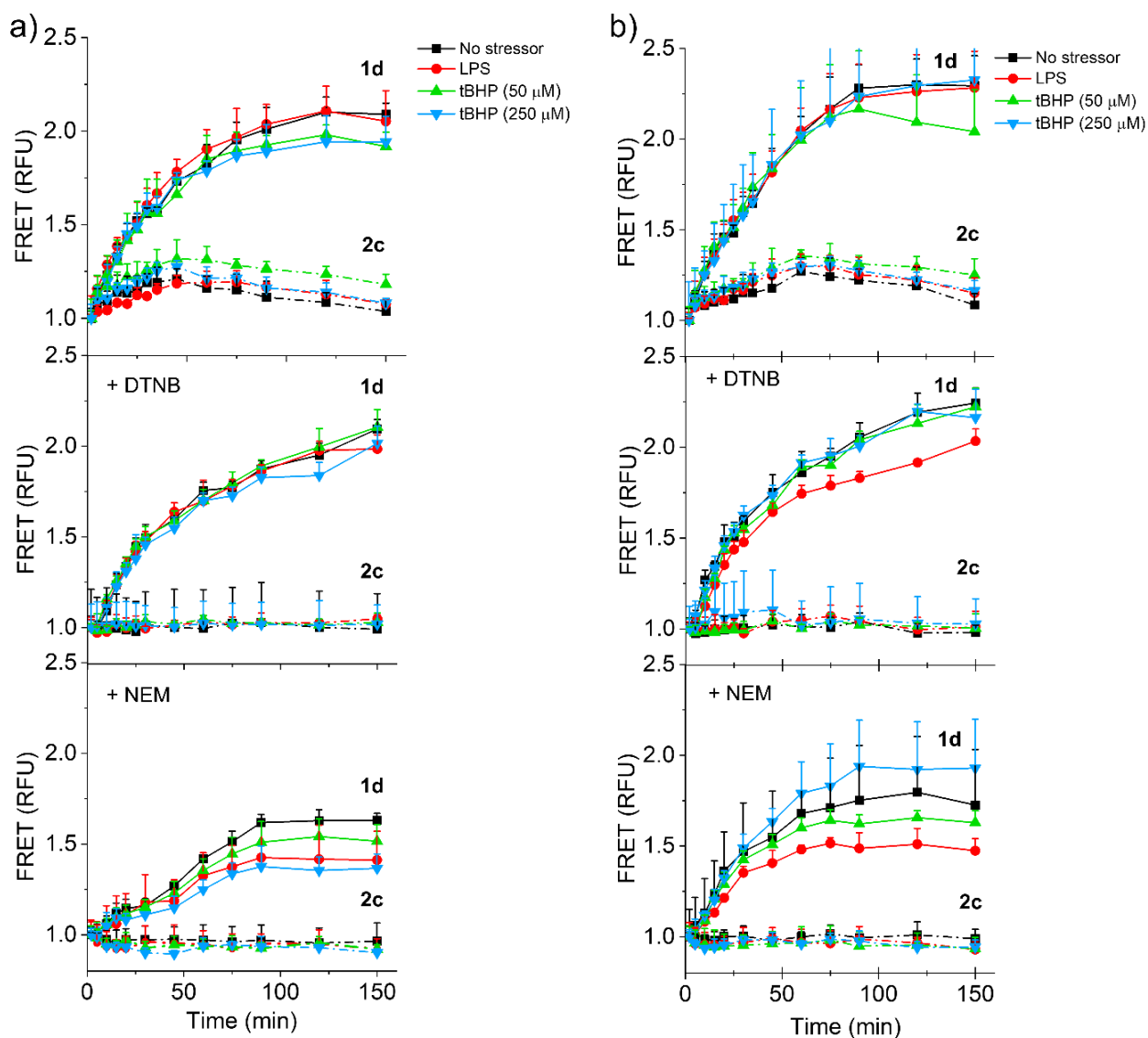


**Figure 3.4** Responsiveness of sulfonium vinyl sulfides in cell culture. Evolution of the FRET signal of **1d/2c** in the presence of RAW 264.7 (a) and THP-1 (b) cells exposed to different stressors and thiol quenching agents. Data presented as Mean + SD (n = 3).

### 3.4 Discussion

One particular challenge associated with developing stimuli-responsive linkers designed for drug delivery applications is the characterization of their biological fate.<sup>97</sup> This challenge becomes exacerbated when the linker can respond to different types of reactive molecules, and when the

concentration/half-life of these species are low. A previous report from Zare *et al.* (Chapter 2; Article 1) showcased the preparation of various bioconjugates containing sulfonium vinyl sulfide linkers as well as their high sensitivity to radical thiols and general low sensitivity to nucleophilic thiols. This type of functional group could be considered interesting as linker chemistry for releasing methionine-containing peptides (or thioether-containing molecules in a more general context) in a traceless manner within the body. Indeed, release could be triggered either by radical thiols or nucleophilic thiols, by two different mechanisms and at very different rates. In fact, a FRET-based probe exposed to bacteria in Zare *et al.* demonstrated a great deal of stability over 1.5 h, and a small progressive loss of FRET signal with time reaching 75% of its original value within 2 h. This behavior was interpreted as the linker being stable to biologically-relevant levels of radical thiols, and the slight decrease after prolonged incubation was interpreted as the release of the methionine-containing peptide owing to reaction with thiol nucleophiles. The present study complements these findings by developing a probe able to differentiate the effects of RNS and radical thiols on the sulfonium vinyl sulfide group, knowing from past work that this linker is insensitive to biologically-relevant concentrations ROS within the timeframe explored. In fact, the current work suggests that the sulfonium vinyl sulfide is not stable during the initial 1.5-h period reported previously, but rather undergoes relatively rapid hydroxynitration by RNS over a ~2 h period. This phenomenon is elucidated herein by an increase of the FRET channels for **1d** with time and was invisible to the previous probe design used in Zare *et al.* (Chapter 2; Article 1) because of the insensitivity of the donor fluorophore (Cy3) to changes in local chemical structure/polarity. Hence, this work provides new insight into the early biological fate of such linkages, even if the long-term fate of the sulfonium is known (sulfoniums are unstable upon prolonged incubation with thiol nucleophiles to ultimately release methionine-containing peptides over the period of many hours, as shown in **Figure 3.2a** for **1d**).

### 3.5 Conclusions

This study demonstrates that sulfonium vinyl sulfides respond, under model conditions, to nucleophilic thiols (hours/days), radical thiols (minutes), and RNS (minutes), leading the release of methionine-containing peptides in the first two cases and to hydroxynitration in the third case. In the presence of cells and hence biologically-relevant concentrations of these three reactive species, RNS outcompeted radical thiols for reaction with the sulfonium vinyl sulfide (presumably due to a combination of reactivity, half-life, and concentration), while reaction with nucleophilic thiols remains expected upon much longer incubation (hours/days). These combined results suggest that sulfonium vinyl sulfide functional groups, when designed for exposure to cells or the

body, could be exploited for e.g., preparing polarity changing biodegradable nanocarriers for various applications owing to their responsiveness to biologically-relevant levels of RNS. Moreover, these materials would remain biodegradable due to slow reaction with nucleophilic thiols. Hence, the combined ease of synthesis and responsiveness to radical thiols, RNS, nucleophilic thiols, under different conditions, make sulfonium vinyl sulfides versatile new functional groups for creating responsive and biodegradable entities. Of course, these linkers could be exploited for other applications not involving biologically-derived reactive species (i.e., *ex cellulo/ex vivo*), whereby exposure to radical thiols could be used to trigger degradation of the linker and release of methionine-containing peptides. Ultimately, this work highlights the complexity of developing responsive chemical bonds, owing to the concurrent high diversity, reactivity, low concentration and lifetime of the various reactive species within cells.

### **Supporting Information**

Full chromatograms and mass spectra of purified FRET-based responsive probe and FRET-based control probes and all presented data in the main manuscript. Scheme illustrating the products formed by reaction of FRET-based responsive probe with nucleophilic thiols. The stability of AFDye<sub>647</sub> and Fluorescein upon exposure to ONOO<sup>-</sup>. The stability of sulfonium vinyl sulfide-containing model peptide (FPAM(vinyl sulfide–GSH)AG) upon exposure to ONOO<sup>-</sup>. Analysis of ROS level and the concentration of intracellular thiols in cell lines (THP-1 and RAW 264.7) exposed to different stressors. Cell viability of THP-1 and RAW 264.7 cells treated with FRET-based responsive probe and FRET-based control probe. Evolution of the AFDye<sub>647</sub> and fluorescein signals of FRET-based responsive probe and FRET-based control probe in the presence of RAW 264 and THP-1 cells.



## 4 GENERAL DISCUSSION, CONCLUSION, AND PERSPECTIVES

---

In light of the importance of biological stimuli-responsive chemical linkages in many pharmaceutical and biotechnological applications and due to the implication of various endogenous reactive species in the onset and development of various diseases,<sup>5,6</sup> this thesis aims to provide a new chemical bond, sulfonium vinyl sulfide, which can be applied as a responsive linkage toward biological reactive species for various biomedical applications. While the specific conclusions and guidelines have been discussed and presented in each relevant Chapter, in this section, we provide a general discussion about the most significant achievements of this thesis, what makes this work different from the work of others, limitations and the future perspective of this thesis, and how this thesis will benefit society.

### 4.1 The most significant achievement of this thesis

GSH is the most abundant intracellular reducing thiol (1–10 mM intracellular and 2–20  $\mu$ M extracellular) and in equilibrium with its oxidized form (GSSG).<sup>19,20</sup> GSH is an essential antioxidant reagent under normal physiological conditions and prevents cell damages caused by RONS.<sup>21,22</sup> Under oxidative stress and elevated level of RONS, the intracellular level of GSH increases around four times compared to normal cells.<sup>23,25</sup> On one hand, this process can lead to the alteration of cellular redox balance (GSH: GSSG ratios), which can cause the oxidation and disulfide exchange reactions at specific cysteine residues of proteins.<sup>23</sup> On the other hand, radical thiols ( $RS^{\cdot}$ ), an oxidizing agent,<sup>14</sup> are produced during the radical scavenging of GSH in the cellular metabolic process.<sup>15</sup> Radical thiols are an important mediator in the intracellular redox process, leading to cell damage by reacting with unsaturated acyl chains of phospholipids and protein thiols.<sup>16,17</sup> Therefore, radical thiols play a significant role in the intracellular redox process. Since the GSH is the highest concentration non-protein thiol molecule in the cytosol and due to the importance of radical thiols and increased level of GSH in pathophysiological events, it is interesting to design chemical bonds that can respond to radical thiols. However, to the best of our knowledge and based on the presented introduction content (Chapter 1), there is a lack of radical thiol-responsive chemical bonds in the literature.

In the first part of our work (Chapter 2), we designed a chemical bond that can respond to radical thiols. For this purpose, a combination of two well-known reactions, including Click reaction (nucleophilic thiol–allene addition) and Clip reactions (radical thiol–ene addition) were utilized for the preparation and disassembly of bioconjugates in a Click/Clip manner. The utilized Click

reaction obeys the most of the criteria of Click chemistry and resulted in the preparation of bioconjugates by the formation of sulfonium vinyl sulfide bond between methionine residue-containing peptides and a variety of molecules containing thiol functional groups, including peptides, a fluorophore, a polymer, and a protein. In this thesis, three different methionine residue-containing peptides were utilized, including FPAMAG (a model peptide), HDMNKVLDL (Antiflammin-2), and Ac-K(N<sub>3</sub>)-GSGCGGRKKRRQRRR-NH<sub>2</sub> (a designed cell-penetrating peptide (Tat<sub>49-57</sub>)). HDMNKVLDL and Ac-K(N<sub>3</sub>)-GSGCGGRKKRRQRRR-NH<sub>2</sub> were chosen due to their anti-inflammatory properties<sup>48</sup> and to facilitate the cellular uptake,<sup>468,469</sup> respectively. It was demonstrated that electron-deficient alkynes, conveniently and selectively installed on methionine residues of peptides, can participate in the thiol–allene Click reaction, leading to formation of a sulfonium vinyl sulfide bond in various bioconjugations and enabled the high-yielding preparation of a variety of peptide–peptide, peptide–fluorophore, peptide–protein, and peptide–polymer conjugates without side-reactions. The process was not harmful to fluorophores from different families. As a control experiment, it was also shown that oxidation of the methionine residue prevented the alkylation reaction. Furthermore, the regioselectivity of Click reaction and the structure of the sulfonium vinyl sulfide bond was determined by <sup>1</sup>H NMR spectroscopy and <sup>1</sup>H–<sup>1</sup>H Nuclear Overhauser Effect spectroscopy, which demonstrated the addition of thiol group to the  $\gamma$ -position of the allene, leading to the formation of both *cis* and *trans* isomers with a strong dominance of the *cis* stereoisomer. Moreover, this work evaluated the responsiveness of sulfonium vinyl sulfide bond towards various reactive species, including radical thiols, nucleophilic thiol, ONOO<sup>-</sup>, H<sub>2</sub>O<sub>2</sub>, and UV-exposure of H<sub>2</sub>O<sub>2</sub> (<sup>•</sup>OH). Accordingly, our presented linkage underwent the very rapid dissociation in the presence of equimolar amounts of radical thiols (in minutes) with more than >90% conversion due to radical thiol–ene Click reaction, leading to the release of the original methionine-containing peptide with full recovery of its thioether side-chain and without side-reactions. It was also shown that the conversion of the Click reaction was not influenced by either the pH of the environment or the radical thiol structure. Under model conditions, the sulfonium vinyl sulfide-containing bioconjugates exhibited relatively high stability to high concentrations of thiols at pH 7.4 (mimicking the cytosol). However, the prolonged incubation of sulfonium vinyl sulfide-containing bioconjugates with the thiol nucleophile (under an inert atmosphere) led to a very slow recovery of the native peptides and without side-reactions due to nucleophilic addition of a thiol to the carbon adjacent the sulfonium. Despite the linkage dissociation in the presence of radical thiols (minutes) and nucleophilic thiols (hours/days), exposure of bioconjugates to H<sub>2</sub>O<sub>2</sub> alone in the dark or under exposure to UV light to generate hydroxyl radicals did not affect the stability of the bioconjugate.

On the other hand, RNS are another important group of reactive species associated with pathophysiological events. These reactive species can significantly affect cellular mechanisms of redox regulations due to their oxidation and nitration potential.<sup>11</sup> Therefore, in the next part of this thesis (Chapter 3), the reactivity of sulfonium vinyl sulfides towards ONOO<sup>-</sup> (a model RNS) was investigated. Accordingly, it was demonstrated that the equimolar amounts of ONOO<sup>-</sup> led to hydroxynitration of the sulfonium vinyl sulfide in a short period of time. Therefore, the results indicated that sulfonium vinyl sulfide bond of bioconjugates did not undergo the clip reaction in the presence of ONOO<sup>-</sup>.

In general, this work introduced 3 different probes with fluorescence resonance energy transfer (FRET) signal, including two sulfonium vinyl sulfide-containing probes with Cy3/Cy5 or fluorescein/AFDye<sub>647</sub> fluorophore pair and one control probe (fluorescein/AFDye<sub>647</sub>) containing a thioether rather than a sulfonium vinyl sulfide linkage. The responsiveness of sulfonium vinyl sulfide bond and consequence effect on the FRET signal of probes were evaluated in the model conditions and in cell cultures, including *E. coli*, permanent mouse macrophages RAW 264.7, and adherent human monocyte THP-1 cell lines experiencing oxidative stress. Bacteria were chosen over mammalian cells owing to their significantly higher rate of division and slightly higher intracellular thiol concentration (~20 mM).<sup>447,448</sup> RAW 264.7 and THP-1 cell lines were selected as *in vitro* models owing to the substantial amount of reactive species they generate upon activation compared to other cell types.<sup>459-461</sup> Under model conditions, the reduction in the FRET signal of sulfonium vinyl sulfide-containing probes was observed in the presence of radical thiol and nucleophilic thiols due to the linkage dissociation that occurred by radical thiol-ene and thiol-ene Clip reactions, respectively, regardless of applied donor/acceptor fluorophores. However, hydroxynitration of the sulfonium vinyl sulfide in the presence of ONOO<sup>-</sup> led to an enhancement in the FRET signal of probe (fluorescein/AFDye<sub>647</sub>), which can be ascribed to a change of chemical structure and local polarity near fluorescein (the donor fluorophore).

Finally, this thesis studied the competition between RNS, radical thiols, and nucleophilic thiols to react with sulfonium vinyl sulfide linkage in cell lines. According to Chapter 2, sulfonium vinyl sulfide-containing probe (Cy3/Cy5) exposed to bacteria demonstrated a great deal of stability over 1.5 h, and a small progressive loss of FRET signal with time reaching 75% of its original value within 2 h. This behavior was interpreted as the linker being stable to biologically-relevant levels of radical thiols, and the slight decrease after prolonged incubation was interpreted as the release of the methionine-containing peptide owing to reaction with thiol nucleophiles. In Chapter 3, we complement these findings by developing a probe able to differentiate the effects of RNS and

radical thiols on the sulfonium vinyl sulfide group. In fact, this chapter suggests that the sulfonium vinyl sulfide is not stable during the initial 1.5-h period reported previously, but rather undergoes relatively rapid hydroxynitration by RNS over a ~2 h period. This phenomenon is elucidated herein by an increase of the FRET channels for sulfonium vinyl sulfide-containing probe (fluorescein/AFDye<sub>647</sub>) with time and was invisible to the previous probe design used in the first article because of the insensitivity of the donor fluorophore (Cy3) to changes in local chemical structure/polarity.

## 4.2 The most significant limitation of this work

Despite the achievements mentioned above, this work faced some challenges that should be considered in future work. For instance, this work's main limitation is the difficulty of unambiguously and precisely establishing which reactive species are involved in reacting with sulfonium vinyl sulfide linkers in complex environments. While Chapter 3 demonstrated that RNS outcompeted radical thiols for reaction with the sulfonium vinyl sulfide, it is still possible that multiple reactive species react with our presented linker at the same time or over time. Another limitation of this thesis is related to the natural abundance of radical thiol species and competitive scavengers for these. As mentioned previously, endogenous radical thiols cannot competitively react with the linker in a complex environment, eliminating the application of the linker for the rapid release of methionine-containing peptides under presented conditions for drug delivery systems.

## 4.3 How this work is different from the work of others

This study reports a combination of two well-known reactions that obey most of the criteria of Click chemistry and could unexpectedly be used to prepare and disassemble bioconjugates in a Click/Clip manner by utilizing the methionine residue of the peptides. Furthermore, to the best of our knowledge, RS<sup>•</sup>-responsive chemical bonds and materials have been rarely investigated. Regarding the importance of radical thiols in physiological and pathological events, it would be interesting to develop and evaluate RS<sup>•</sup>-responsive chemical bonds and materials for different biomedical applications. Regarding the detection of the ONOO<sup>-</sup> in living cells, the majority of ONOO<sup>-</sup>-responsive chemical bonds, including selenium or tellurium-based derivatives,<sup>470–473</sup> boronic acid/esters,<sup>474,475</sup> double carbon bonds,<sup>458,476–478</sup> and others,<sup>479–482</sup> exhibited the oxidizing potential of ONOO<sup>-</sup>. However, sulfonium vinyl sulfide linkers provide the opportunity to represent and understand better the nitration potential of ONOO<sup>-</sup> in living cells. Considering the potential of ONOO<sup>-</sup> in nitration of various biomolecules,<sup>455</sup> including proteins, DNA, sugars, and carbon-

carbon double bonds of monounsaturated and unsaturated fatty acids,<sup>483–485</sup> our presented linker can be useful for future therapeutic and diagnostic applications. Furthermore, FRET-based probes have been used for the detection of ONOO<sup>-</sup>,<sup>458,486</sup> due to their ability to regulate emission signals in two channels.<sup>467,487–489</sup> However, synthesizing the FRET-based probes is often complicated due to the existence of two different fluorophores in the probe.<sup>458,486</sup> In this project, we simply synthesized a FRET-based responsive probe and a FRET-based control probe by employing fluorescein and AFDye<sub>647</sub> that exhibited an enhancement and relative stability of FRET signals in living cells. Last but not least, the current ONOO<sup>-</sup>-responsive systems are able to detect ONOO<sup>-</sup> in macrophages upon interferon-gamma (IFN-γ)/LPS stimulation and/or SIN-1 (ONOO<sup>-</sup> donor) incubation to increase the level of endogenous ONOO<sup>-</sup> in living cells.<sup>370,384,458,477,490</sup> However, in this project, we presented the effects of ONOO<sup>-</sup> on FRET-based responsive probe in cells in the presence and absence of only LPS stimulation. Such a response may provide opportunities to detect the short-lived endogenous ONOO<sup>-</sup> in biological systems in the absence of additional stimulants.

#### **4.4 What is left to be done (future perspectives)**

Future experimental studies could investigate the local generation of radical thiols by photoinitiation using an appropriate system (e.g., photodynamic therapy). This increase in the concentration of radical thiols may make the rapid release of from sulfonium vinyl sulfide linkers possible using light. Future experiments can also be designed and performed by a variety of fluorophore pair-based bioconjugates to better understand the effect of ONOO<sup>-</sup> on sulfonium vinyl sulfide linkers and FRET signals in the absence of fluorophore degradation. It is also quite helpful to perform some additional investigation, e.g., exploring the reactivity of sulfonium vinyl sulfide linker in the presence of other reactive species, in various cell lines, within several incubation times, and many others, to understand better the potential limitation, and possible future applications of this linker. Moreover, the potential of sulfonium vinyl sulfide linkers can be explored for the bioconjugation of methionine-containing proteins. Indeed, the limited functional role of methionine residues in protein compared to other residues makes them a great option for protein labelling,<sup>44,45</sup> which can be applied for a broad range of pharmaceutical applications. Last but not least, sulfonium vinyl sulfide linkers can be employed as repeatable functional groups in methionine- or thioether-containing polymers and be used for its polarity changing characteristics for future applications.

#### **4.5 How will this work benefit society?**

Considering the convenience of Click/Clip strategy, the readily accessible nature of the reactants/reagents and the biological relevance of the latter, this concept can have many applications in the biotechnological sector. In addition, the combined results suggest that sulfonium vinyl sulfide functional groups, when designed for exposure to cells or the body, could be exploited for, e.g., preparing polarity changing biodegradable nanocarriers for various applications owing to their responsiveness to biologically-relevant levels of RNS. Furthermore, sulfonium vinyl sulfide linkers could be exploited for other applications not involving biologically-derived reactive species (i.e., *ex cellulo/ex vivo*), whereby exposure to radical thiols could be used to trigger degradation of the linker and release of methionine-containing peptides. Ultimately, this work highlights the complexity of developing responsive chemical bonds, owing to the concurrent high diversity, reactivity, low concentration and lifetime of the various reactive species within cells.

## 5 BIBLIOGRAPHIE

---

1. Weidinger, A. & Kozlov, A. V. Biological activities of reactive oxygen and nitrogen species: Oxidative stress versus signal transduction. *Biomolecules* **5**, 472–484 (2015).
2. Gruhlke, M. C. H. & Slusarenko, A. J. The biology of reactive sulfur species (RSS). *Plant Physiol. Biochem.* **59**, 98–107 (2012).
3. Winterbourn, C. C. Reconciling the chemistry and biology of reactive oxygen species. *Nat. Chem. Biol.* **4**, 278–286 (2008).
4. Kwon, N., Kim, D., Swamy, K. M. K. & Yoon, J. Metal-coordinated fluorescent and luminescent probes for reactive oxygen species ( ROS ) and reactive nitrogen species ( RNS ). *Coord. Chem. Rev.* **427**, 213581 (2021).
5. Valko, M. *et al.* Free radicals and antioxidants in normal physiological functions and human disease. *Int. J. Biochem. Cell Biol.* **39**, 44–84 (2007).
6. Giles, G. I., Tasker, K. M. & Jacob, C. Hypothesis: The role of reactive sulfur species in oxidative stress. *Free Radic. Biol. Med.* **31**, 1279–1283 (2001).
7. Bindoli, A. & Rigobello, M. P. Principles in redox signaling: From chemistry to functional significance. *Antioxidants Redox Signal.* **18**, 1557–1593 (2013).
8. Quiney, C., Finnegan, S., Groeger, G. & Cotter, T. G. Protein oxidation. *Protein Rev.* **13**, 57–78 (2011).
9. Marnett, L. J. Oxyradicals and DNA damage. *Carcinogenesis* **21**, 361–370 (2000).
10. Phaniendra, A., Jestadi, D. B. & Periyasamy, L. Free Radicals: Properties, Sources, Targets, and Their Implication in Various Diseases. *Indian J. Clin. Biochem.* **30**, 11–26 (2015).
11. Martínez, M. C. & Andriantsitohaina, R. Reactive Nitrogen Species: Molecular Mechanisms and Potential Significance in Health and Disease. *Antioxid. Redox Signal.* **11**, 669–702 (2009).
12. Ferrer-Sueta, G. & Radi, R. Chemical biology of peroxynitrite: Kinetics, diffusion, and radicals. *ACS Chem. Biol.* **4**, 161–177 (2009).
13. Beckman, J. S. & Koppenol, W. H. Nitric oxide, superoxide, and peroxynitrite: the good, the bad, and ugly. *Am. J. Physiol. Physiol.* **271**, C1424–C1437 (1996).

14. Winterbourn, C. C. Are free radicals involved in thiol-based redox signaling? *Free Radic. Biol. Med.* **80**, 164–170 (2015).
15. Moldéus, P., O'Brien, P. J., Thor, H., Berggren, M. & Orrenius, S. Oxidation of glutathione by free radical intermediates formed during peroxidase-catalysed N -demethylation reactions. *FEBS Lett.* **162**, 411–415 (1983).
16. Borisenko, G. G., Martin, I., Zhao, Q., Amoscato, A. A. & Kagan, V. E. Nitroxides Scavenge Myeloperoxidase-Catalyzed Thiyl Radicals in Model Systems and in Cells. *J. Am. Chem. Soc.* **126**, 9221–9232 (2004).
17. Schöneich, C., Dillinger, U., von Bruchhausen, F. & Asmus, K.-D. Oxidation of polyunsaturated fatty acids and lipids through thiyl and sulfonyl radicals: Reaction kinetics, and influence of oxygen and structure of thiyl radicals. *Arch. Biochem. Biophys.* **292**, 456–467 (1992).
18. Kleinman, W. A. & Richie, J. P. Status of glutathione and other thiols and disulfides in human plasma. *Biochem. Pharmacol.* **60**, 19–29 (2000).
19. Cheng, R., Meng, F., Deng, C., Klok, H.-A. & Zhong, Z. Dual and multi-stimuli responsive polymeric nanoparticles for programmed site-specific drug delivery. *Biomaterials* **34**, 3647–3657 (2013).
20. Chiang, Y.-T., Yen, Y.-W. & Lo, C.-L. Reactive oxygen species and glutathione dual redox-responsive micelles for selective cytotoxicity of cancer. *Biomaterials* **61**, 150–161 (2015).
21. Lee, M. H. *et al.* Disulfide-Cleavage-Triggered Chemosensors and Their Biological Applications. *Chem. Rev.* **113**, 5071–5109 (2013).
22. Augusto, O., Gatti, R. M. & Radi, R. Spin-Trapping Studies of Peroxynitrite Decomposition and of 3-Morpholinopyridone N-Ethylcarbamide Autooxidation: Direct Evidence for Metal-Independent Formation of Free-Radical Intermediates. *Arch. Biochem. Biophys.* **310**, 118–125 (1994).
23. Townsend, D. M., Tew, K. D. & Tapiero, H. The importance of glutathione in human disease. *Biomed. Pharmacother.* **57**, 145–155 (2003).
24. Schafer, F. Q. & Buettner, G. R. Redox environment of the cell as viewed through the redox state of the glutathione disulfide/glutathione couple. *Free Radic. Biol. Med.* **30**, 1191–1212 (2001).
25. Estrela, J. M., Ortega, A. & Obrador, E. Glutathione in Cancer Biology and Therapy. *Crit.*

- Rev. Clin. Lab. Sci.* **43**, 143–181 (2006).
26. Vijayakameswara Rao, N., Ko, H., Lee, J. & Park, J. H. Recent progress and advances in stimuli-responsive polymers for cancer therapy. *Front. Bioeng. Biotechnol.* **6**, (2018).
  27. Monteiro, P. F., Travanut, A., Conte, C. & Alexander, C. Reduction-responsive polymers for drug delivery in cancer therapy—Is there anything new to discover? *Wiley Interdisciplinary Reviews: Nanomedicine and Nanobiotechnology* **13**, (2021).
  28. El-Mohtadi, F., d’Arcy, R. & Tirelli, N. Oxidation-Responsive Materials: Biological Rationale, State of the Art, Multiple Responsiveness, and Open Issues. *Macromol. Rapid Commun.* **40**, 1–24 (2019).
  29. Guo, X. *et al.* Advances in redox-responsive drug delivery systems of tumor microenvironment. *J. Nanobiotechnology* **16**, 74 (2018).
  30. Hsu, P. H. & Almutairi, A. Recent progress of redox-responsive polymeric nanomaterials for controlled release. *J. Mater. Chem. B* **9**, 2179–2188 (2021).
  31. Lou, Z., Li, P. & Han, K. Redox-responsive fluorescent probes with different design strategies. *Acc. Chem. Res.* **48**, 1358–1368 (2015).
  32. Chen, M. *et al.* Recent advances of redox-responsive nanoplatfoms for tumor theranostics. *J. Control. Release* **332**, 269–284 (2021).
  33. Ramasamy, T. *et al.* Smart chemistry-based nanosized drug delivery systems for systemic applications: A comprehensive review. *J. Control. Release* **258**, 226–253 (2017).
  34. Iha, R. K. *et al.* Applications of Orthogonal “Click” Chemistries in the Synthesis of Functional Soft Materials. *Chem. Rev.* **109**, 5620–5686 (2009).
  35. Moses, J. E. & Moorhouse, A. D. The growing applications of click chemistry. *Chem. Soc. Rev.* **36**, 1249–1262 (2007).
  36. Gauthier, M. A., Gibson, M. I. & Klok, H.-A. Synthesis of Functional Polymers by Post-Polymerization Modification. *Angew. Chemie Int. Ed.* **48**, 48–58 (2009).
  37. Hou, J., Liu, X., Shen, J., Zhao, G. & Wang, P. G. The impact of click chemistry in medicinal chemistry. *Expert Opin. Drug Discov.* **7**, 489–501 (2012).
  38. Kolb, H. C., Finn, M. G. & Sharpless, K. B. Click Chemistry: Diverse Chemical Function from a Few Good Reactions. *Angew. Chemie Int. Ed.* **40**, 2004–2021 (2001).
  39. Yu, Z., Ho, L. Y. & Lin, Q. Rapid, Photoactivatable Turn-On Fluorescent Probes Based on

- an Intramolecular Photoclick Reaction. *J. Am. Chem. Soc.* **133**, 11912–11915 (2011).
40. Becer, C. R., Hoogenboom, R. & Schubert, U. S. Click Chemistry beyond Metal-Catalyzed Cycloaddition. *Angew. Chemie Int. Ed.* **48**, 4900–4908 (2009).
  41. Tasdelen, M. A. Diels–Alder “click” reactions: recent applications in polymer and material science. *Polym. Chem.* **2**, 2133 (2011).
  42. Gauthier, M. A. & Klok, H.-A. Peptide/protein–polymer conjugates: synthetic strategies and design concepts. *Chem. Commun.* 2591 (2008). doi:10.1039/b719689j
  43. Brülisauer, L., Gauthier, M. A. & Leroux, J.-C. Disulfide-containing parenteral delivery systems and their redox-biological fate. *J. Control. Release* **195**, 147–154 (2014).
  44. Taylor, M. T., Nelson, J. E., Suero, M. G. & Gaunt, M. J. A protein functionalization platform based on selective reactions at methionine residues. *Nature* **562**, 563–568 (2018).
  45. Cowie, D. B., Cohen, G. N., Bolton, E. T. & De Robichon-Szulmajster, H. Amino acid analog incorporation into bacterial proteins. *BBA - Biochim. Biophys. Acta* **34**, 39–46 (1959).
  46. Lawson, W. B. & Schrammt, H. J. Modification of a Methionine Residue near the Active Site of Chymotrypsin by p-Nitrophenyl Bromoacetyl- $\alpha$ -aminoisobutyrate. *Biochemistry* **4**, 377–386 (1965).
  47. Miele, L., Cordella-Miele, E., Facchiano, A. & Mukherjee, A. B. Novel anti-inflammatory peptides from the region of highest similarity between uteroglobin and lipocortin I. *Nature* **335**, 726–730 (1988).
  48. Kamal, A. M. *et al.* Antiflammin-2 activates the human formyl-peptide receptor like 1. *ScientificWorldJournal*. **6**, 1375–84 (2006).
  49. Bothwell, I. *et al.* Se-Adenosyl- L- selenomethionine Cofactor Analogue as a Reporter of Protein Methylation. *J. Am. Chem. Soc.* **134**, 14905–14912 (2012).
  50. Prabharasuth, R. & Van Vranken, D. L. Iron-catalyzed reaction of propargyl sulfides and trimethylsilyldiazomethane. *J. Org. Chem.* **66**, 5256–5258 (2001).
  51. Yan, X., Li, C., Xu, X., Zhao, X. & Pan, Y. Hemin Catalyzed Dealkylative Intercepted [2, 3]-Sigmatropic Rearrangement Reactions of Sulfonium Ylides with 2, 2, 2-Trifluorodiazoethane. *Advanced Synthesis and Catalysis* **362**, 2005–2011 (2020).
  52. Kramer, J. R. & Deming, T. J. Reversible chemoselective tagging and functionalization of methionine containing peptides. *Chem. Commun.* **49**, 5144–5146 (2013).

53. Hoyle, C. E. & Bowman, C. N. Thiol-ene click chemistry. *Angew. Chemie - Int. Ed.* **49**, 1540–1573 (2010).
54. Denizligil, S., Resul, R., Yagci, Y., Mc Ardle, C. & Fouassier, J.-P. Photosensitized cationic polymerization using allyl sulfonium salt. *Macromol. Chem. Phys.* **197**, 1233–1240 (1996).
55. Tesei, G. *et al.* Self-association of a highly charged arginine-rich cell-penetrating peptide. *Proc. Natl. Acad. Sci.* **114**, 11428–11433 (2017).
56. Caldorera-Moore, M. E., Liechty, W. B. & Peppas, N. A. Responsive Theranostic Systems: Integration of Diagnostic Imaging Agents and Responsive Controlled Release Drug Delivery Carriers. *Acc. Chem. Res.* **44**, 1061–1070 (2011).
57. Liu, D., Yang, F., Xiong, F. & Gu, N. The Smart Drug Delivery System and Its Clinical Potential. *Theranostics* **6**, 1306–1323 (2016).
58. Tayo, L. L. Stimuli-responsive nanocarriers for intracellular delivery. *Biophys. Rev.* **9**, 931–940 (2017).
59. Mura, S., Nicolas, J. & Couvreur, P. Stimuli-responsive nanocarriers for drug delivery. *Nature Materials* **12**, 991–1003 (2013).
60. Kelley, E. G., Albert, J. N. L., Sullivan, M. O. & Epps, III, T. H. Stimuli-responsive copolymer solution and surface assemblies for biomedical applications. *Chem. Soc. Rev.* **42**, 7057 (2013).
61. LI, D.-Z., CHEN, H.-D., BI, F. & WANG, Z.-X. Progress of Multimodal Molecular Imaging Technology in Diagnosis of Tumor. *Chinese J. Anal. Chem.* **44**, 1609–1618 (2016).
62. Zhang, N. *et al.* Recent advances in near-infrared II imaging technology for biological detection. *J. Nanobiotechnology* **19**, 132 (2021).
63. Zhang, J., Ning, L., Huang, J., Zhang, C. & Pu, K. Activatable molecular agents for cancer theranostics. *Chem. Sci.* **11**, 618–630 (2020).
64. Raza, A., Hayat, U., Rasheed, T., Bilal, M. & Iqbal, H. M. N. Redox-responsive nano-carriers as tumor-targeted drug delivery systems. *Eur. J. Med. Chem.* **157**, 705–715 (2018).
65. Li, R., Peng, F., Cai, J., Yang, D. & Zhang, P. Redox dual-stimuli responsive drug delivery systems for improving tumor-targeting ability and reducing adverse side effects. *Asian J. Pharm. Sci.* **15**, 311–325 (2020).
66. Liu, J. *et al.* Biomedical Application of Reactive Oxygen Species – Responsive

- Nanocarriers in Cancer , Inflammation , and Neurodegenerative Diseases. **8**, 1–24 (2020).
67. Deng, Z., Hu, J. & Liu, S. Reactive Oxygen, Nitrogen, and Sulfur Species (RONSS)-Responsive Polymersomes for Triggered Drug Release. *Macromolecular Rapid Communications* **38**, (2017).
  68. Joshi-Barr, S., De Gracia Lux, C., Mahmoud, E. & Almutairi, A. Exploiting oxidative microenvironments in the body as triggers for drug delivery systems. *Antioxidants Redox Signal.* **21**, 730–754 (2014).
  69. Paulsen, C. E. & Carroll, K. S. Cysteine-mediated redox signaling: Chemistry, biology, and tools for discovery. *Chem. Rev.* **113**, 4633–4679 (2013).
  70. Giles, G. I., Nasim, M. J., Ali, W. & Jacob, C. The reactive sulfur species concept: 15 years on. *Antioxidants* **6**, 1–29 (2017).
  71. Napoli, A., Valentini, M., Tirelli, N., Müller, M. & Hubbell, J. A. Oxidation-responsive polymeric vesicles. *Nat. Mater.* **3**, 183–189 (2004).
  72. Lee, S. H., Gupta, M. K., Bang, J. B., Bae, H. & Sung, H. J. Current progress in reactive oxygen species (ROS)-Responsive materials for biomedical applications. *Adv. Healthc. Mater.* **2**, 908–915 (2013).
  73. Sun, H., Meng, F., Cheng, R., Deng, C. & Zhong, Z. Reduction-responsive polymeric micelles and vesicles for triggered intracellular drug release. *Antioxidants Redox Signal.* **21**, 755–767 (2014).
  74. Liu, L. & Liu, P. Synthesis strategies for disulfide bond-containing polymer-based drug delivery system for reduction-responsive controlled release. *Front. Mater. Sci.* **9**, 211–226 (2015).
  75. Wu, L. *et al.* Reaction-Based Fluorescent Probes for the Detection and Imaging of Reactive Oxygen, Nitrogen, and Sulfur Species. *Acc. Chem. Res.* **52**, 2582–2597 (2019).
  76. Li, D., Zhang, R., Liu, G., Kang, Y. & Wu, J. Redox- Responsive Self- Assembled Nanoparticles for Cancer Therapy. *Adv. Healthc. Mater.* **9**, 2000605 (2020).
  77. Zhang, P., Chen, D., Li, L. & Sun, K. Charge reversal nano-systems for tumor therapy. *J. Nanobiotechnology* **20**, 31 (2022).
  78. Oh, J. K. Disassembly and tumor-targeting drug delivery of reduction-responsive degradable block copolymer nanoassemblies. *Polym. Chem.* **10**, 1554–1568 (2019).

79. Wang, Q., Guan, J., Wan, J. & Li, Z. Disulfide based prodrugs for cancer therapy. *RSC Adv.* **10**, 24397–24409 (2020).
80. Nagy, P. Kinetics and Mechanisms of Thiol–Disulfide Exchange Covering Direct Substitution and Thiol Oxidation-Mediated Pathways. *Antioxid. Redox Signal.* **18**, 1623–1641 (2013).
81. Jensen, K. S., Hansen, R. E. & Winther, J. R. Kinetic and Thermodynamic Aspects of Cellular Thiol–Disulfide Redox Regulation. *Antioxid. Redox Signal.* **11**, 1047–1058 (2009).
82. McNulty, J., Krishnamoorthy, V., Amoroso, D. & Moser, M. Tris(3-hydroxypropyl)phosphine (THPP): A mild, air-stable reagent for the rapid, reductive cleavage of small-molecule disulfides. *Bioorg. Med. Chem. Lett.* **25**, 4114–4117 (2015).
83. Li, Y. *et al.* Tailored Trojan horse nanocarriers for enhanced redox-responsive drug delivery. *J. Control. Release* **342**, 201–209 (2022).
84. Jia, Z., Wong, L., Davis, T. P. & Bulmus, V. One-Pot Conversion of RAFT-Generated Multifunctional Block Copolymers of HPMA to Doxorubicin Conjugated Acid- and Reductant-Sensitive Crosslinked Micelles. *Biomacromolecules* **9**, 3106–3113 (2008).
85. Rajes, K. *et al.* Redox-responsive nanocarrier for controlled release of drugs in inflammatory skin diseases. *Pharmaceutics* **13**, 1–15 (2021).
86. Scales, S. J. *et al.* Development of a Cysteine-Conjugatable Disulfide FRET Probe: Influence of Charge on Linker Cleavage and Payload Trafficking for an Anti-HER2 Antibody Conjugate. *Bioconjug. Chem.* **30**, 3046–3056 (2019).
87. Mortera, R. *et al.* Cell-induced intracellular controlled release of membrane impermeable cysteine from a mesoporous silica nanoparticle-based drug delivery system. *Chem. Commun.* 3219 (2009). doi:10.1039/b900559e
88. Wu, C., Belenda, C., Leroux, J.-C. & Gauthier, M. A. Interplay of Chemical Microenvironment and Redox Environment on Thiol-Disulfide Exchange Kinetics. *Chem. - A Eur. J.* **17**, 10064–10070 (2011).
89. Bulaj, G., Kortemme, T. & Goldenberg, D. P. Ionization–Reactivity Relationships for Cysteine Thiols in Polypeptides. *Biochemistry* **37**, 8965–8972 (1998).
90. Wei, C. *et al.* Enhanced bioreduction-responsive biodegradable diselenide-containing poly(ester urethane) nanocarriers. *Biomater. Sci.* **5**, 669–677 (2017).

91. Pang, Z., Zhou, J. & Sun, C. Ditelluride-Bridged PEG-PCL Copolymer as Folic Acid-Targeted and Redox-Responsive Nanoparticles for Enhanced Cancer Therapy. *Front. Chem.* **8**, 1–12 (2020).
92. Chivers, T. & Laitinen, R. S. Tellurium: a maverick among the chalcogens. *Chem. Soc. Rev.* **44**, 1725–1739 (2015).
93. Wang, Y. *et al.* Ultrasensitive GSH-Responsive Ditelluride-Containing Poly(ether-urethane) Nanoparticles for Controlled Drug Release. *ACS Appl. Mater. Interfaces* **8**, 35106–35113 (2016).
94. Xia, X. *et al.* Biodegradable and self-fluorescent ditelluride-bridged mesoporous organosilica / polyethylene glycol-curcumin nanocomposite for dual-responsive drug delivery and enhanced therapy efficiency. **23**, (2022).
95. Geven, M. *et al.* Sulfur-based oxidation-responsive polymers. Chemistry, (chemically selective) responsiveness and biomedical applications. *Eur. Polym. J.* **149**, 110387 (2021).
96. Gao, F. & Xiong, Z. Reactive Oxygen Species Responsive Polymers for Drug Delivery Systems. *Front. Chem.* **9**, 1–17 (2021).
97. Zhao, C. *et al.* Oxidative-Species-Selective Materials for Diagnostic and Therapeutic Applications. *Angew. Chemie Int. Ed.* **60**, 9804–9827 (2021).
98. Liu, Z., Dai, X., Xu, Q., Sun, X. & Liu, Y. Fluorescence Sensing of Glutathione Thiyl Radical by BODIPY-Modified  $\beta$ -Cyclodextrin. *Chinese J. Chem.* **40**, 493–499 (2022).
99. Cao, Z., Li, D., Wang, J. & Yang, X. Reactive oxygen species-sensitive polymeric nanocarriers for synergistic cancer therapy. *Acta Biomater.* **130**, 17–31 (2021).
100. Truong, V. X. & Dove, A. P. Organocatalytic, regioselective nucleophilic ‘click’ addition of thiols to propionic acid esters for polymer-polymer coupling. *Angew. Chemie - Int. Ed.* **52**, 4132–4136 (2013).
101. Xu, Q., He, C., Xiao, C. & Chen, X. Reactive Oxygen Species (ROS) Responsive Polymers for Biomedical Applications. *Macromol. Biosci.* **16**, 635–646 (2016).
102. Giorgio, M., Trinei, M., Migliaccio, E. & Pelicci, P. G. Hydrogen peroxide: a metabolic by-product or a common mediator of ageing signals? *Nat. Rev. Mol. Cell Biol.* **8**, 722–728 (2007).
103. Parvez, S., Long, M. J. C., Poganik, J. R. & Aye, Y. Redox signaling by reactive

- electrophiles and oxidants. *Chem. Rev.* **118**, 8798–8888 (2018).
104. Ye, H. *et al.* Recent Advances on Reactive Oxygen Species-Responsive Delivery and Diagnosis System. *Biomacromolecules* **20**, 2441–2463 (2019).
  105. Hou, J. T. *et al.* Fluorescent Imaging of Reactive Oxygen and Nitrogen Species Associated with Pathophysiological Processes. *Chem* **6**, 832–866 (2020).
  106. D’Autréaux, B. & Toledano, M. B. ROS as signalling molecules: Mechanisms that generate specificity in ROS homeostasis. *Nat. Rev. Mol. Cell Biol.* **8**, 813–824 (2007).
  107. Murphy, M. P. How mitochondria produce reactive oxygen species. *Biochem. J.* **417**, 1–13 (2009).
  108. Maghzal, G. J., Krause, K. H., Stocker, R. & Jaquet, V. Detection of reactive oxygen species derived from the family of NOX NADPH oxidases. *Free Radic. Biol. Med.* **53**, 1903–1918 (2012).
  109. Halliwell, B. Free Radicals and Other Reactive Species in Disease. in *eLS* 1–7 (Wiley, 2005). doi:10.1038/npg.els.0003913
  110. Kohen, R. & Nyska, A. Oxidation of biological systems: Oxidative stress phenomena, antioxidants, redox reactions, and methods for their quantification. *Toxicol. Pathol.* **30**, 620–650 (2002).
  111. Genestra, M. Oxyl radicals, redox-sensitive signalling cascades and antioxidants. *Cell. Signal.* **19**, 1807–1819 (2007).
  112. Nordberg, J. & Arnér, E. S. J. Reactive oxygen species, antioxidants, and the mammalian thioredoxin system. *Free Radic. Biol. Med.* **31**, 1287–1312 (2001).
  113. Dröge, W. Free radicals in the physiological control of cell function. *Physiol. Rev.* **82**, 47–95 (2002).
  114. Arthur, M. J. P. *et al.* Reduction of ferricytochrome C may underestimate superoxide production by monocytes. *J. Immunol. Methods* **98**, 63–69 (1987).
  115. Farías, J. G. *et al.* Antioxidant therapeutic strategies for cardiovascular conditions associated with oxidative stress. *Nutrients* **9**, 1–23 (2017).
  116. Sies, H. Oxidative stress: Concept and some practical aspects. *Antioxidants* **9**, 1–6 (2020).
  117. Heinzelmanna, S. & Bauer, G. Multiple protective functions of catalase against intercellular apoptosis-inducing ROS signaling of human tumor cells. *Biol. Chem.* **391**, 675–693 (2010).

118. Andersen, J. K. Oxidative stress in neurodegeneration: Cause or consequence? *Nat. Rev. Neurosci.* **10**, S18 (2004).
119. Kuppusamy, P. & Zweier, J. L. Characterization of free radical generation by xanthine oxidase. Evidence for hydroxyl radical generation. *J. Biol. Chem.* **264**, 9880–9884 (1989).
120. Kontos, H. A. *et al.* Appearance of superoxide anion radical in cerebral extracellular space during increased prostaglandin synthesis in cats. *Circ. Res.* **57**, 142–151 (1985).
121. Fridovich, I. Superoxide radicals, superoxide dismutases and the aerobic lifestyle. *Photochem. Photobiol.* **28**, 733–41 (1978).
122. Bielski, B. H. J., Cabelli, D. E., Arudi, R. L. & Ross, A. B. Reactivity of HO<sub>2</sub>/O<sub>2</sub><sup>-</sup> Radicals in Aqueous Solution. *J. Phys. Chem. Ref. Data* **14**, 1041–1100 (1985).
123. Naik, E. & Dixit, V. M. Mitochondrial reactive oxygen species drive proinflammatory cytokine production. *J. Exp. Med.* **208**, 417–420 (2011).
124. Bastow, E. L. *et al.* New links between SOD1 and metabolic dysfunction from a yeast model of amyotrophic lateral sclerosis. *J. Cell Sci.* **129**, 4118–4129 (2016).
125. Di Marzo, N., Chisci, E. & Giovannoni, R. The Role of Hydrogen Peroxide in Redox-Dependent Signaling: Homeostatic and Pathological Responses in Mammalian Cells. *Cells* **7**, 156 (2018).
126. Halliwell, B., Clement, M. V. & Long, L. H. Hydrogen peroxide in the human body. *FEBS Lett.* **486**, 10–13 (2000).
127. Matés, J. M., Pérez-Gómez, C. & De Castro, I. N. Antioxidant enzymes and human diseases. *Clin. Biochem.* **32**, 595–603 (1999).
128. Winterbourn, C. C. The Biological Chemistry of Hydrogen Peroxide. in *Methods in Enzymology* **528**, 3–25 (Elsevier Inc., 2013).
129. Burgoyne, J. R., Oka, S. I., Ale-Agha, N. & Eaton, P. Hydrogen peroxide sensing and signaling by protein kinases in the cardiovascular system. *Antioxidants Redox Signal.* **18**, 1042–1052 (2013).
130. Bedwell, S., Dean, R. T. & Jessup, W. The action of defined oxygen-centred free radicals on human low-density lipoprotein. *Biochem. J.* **262**, 707–712 (1989).
131. Halliwell, B. Oxidants and human disease: some new concepts 1. *FASEB J.* **1**, 358–364 (1987).

132. Kehrer, J. P. The Haber-Weiss reaction and mechanisms of toxicity. *Toxicology* **149**, 43–50 (2000).
133. Koppenol, W. H. The centennial of the Fenton reaction. *Free Radic. Biol. Med.* **15**, 645–651 (1993).
134. Biemond, P., van Eijk, H. G., Swaak, A. J. G. & Koster, J. F. Iron mobilization from ferritin by superoxide derived from stimulated polymorphonuclear leukocytes. Possible mechanism in inflammation diseases. *J. Clin. Invest.* **73**, 1576–9 (1984).
135. Ye, J. & Zhai, H. Z. Oxidative stress and Alzheimer disease. *Chinese J. Clin. Rehabil.* **9**, 117–119 (2005).
136. Hojo, Y., Okado, A., Kawazoe, S. & Mizutani, T. In vivo singlet-oxygen generation in blood of chromium(VI)-treated mice: An electron spin resonance spin-trapping study. *Biol. Trace Elem. Res.* **76**, 85–93 (2000).
137. Hampton, M. B., Kettle, A. J. & Winterbourn, C. C. Inside the Neutrophil Phagosome: Oxidants, Myeloperoxidase, and Bacterial Killing. *Blood* **92**, 3007–3017 (1998).
138. Kanofsky, J. R. Singlet oxygen production by biological systems. *Chem. Biol. Interact.* **70**, 1–28 (1989).
139. Kanofsky, J. R. Singlet oxygen production by lactoperoxidase. *J. Biol. Chem.* **258**, 5991–5993 (1983).
140. Chan, H. W. S. Singlet oxygen analogs in biological systems. Coupled oxygenation of 1,3-dienes by soybean lipoxidase. *J. Am. Chem. Soc.* **93**, 2357–2358 (1971).
141. Sies, H. & Menck, C. F. M. Singlet oxygen induced DNA damage. *Mutat. Res. DNAGing* **275**, 367–375 (1992).
142. Davies, M. J. Singlet oxygen-mediated damage to proteins and its consequences. *Biochem. Biophys. Res. Commun.* **305**, 761–770 (2003).
143. Winterbourn, C. C. & Kettle, A. J. Biomarkers of myeloperoxidase-derived hypochlorous acid. *Free Radic. Biol. Med.* **29**, 403–409 (2000).
144. Morris, J. C. The Acid Ionization Constant of HOCl from 5 to 35°. *J. Phys. Chem.* **70**, 3798–3805 (1966).
145. Winterbourn, C. C. Comparative reactivities of various biological compounds with myeloperoxidase-hydrogen peroxide-chloride, and similarity of oxidant to hypochlorite.

- BBA - Gen. Subj.* **840**, 204–210 (1985).
146. Prütz, W. A. Hypochlorous acid interactions with thiols, nucleotides, DNA, and other biological substrates. *Arch. Biochem. Biophys.* **332**, 110–120 (1996).
  147. Stamp, L. K. *et al.* Myeloperoxidase and oxidative stress in rheumatoid arthritis. *Rheumatol. (United Kingdom)* **51**, 1796–1803 (2012).
  148. Valko, M., Rhodes, C. J., Moncol, J., Izakovic, M. & Mazur, M. Free radicals, metals and antioxidants in oxidative stress-induced cancer. *Chem. Biol. Interact.* **160**, 1–40 (2006).
  149. Adams, L., Franco, M. C. & Estevez, A. G. Reactive nitrogen species in cellular signaling. *Exp. Biol. Med.* **240**, 711–717 (2015).
  150. Karoui, H., Hogg, N., Fréjaville, C., Tordo, P. & Kalyanaraman, B. Characterization of sulfur-centered radical intermediates formed during the oxidation of thiols and sulfite by peroxynitrite: ESR-spin trapping and oxygen uptake studies. *J. Biol. Chem.* **271**, 6000–6009 (1996).
  151. Whiteman, M. & Halliwell, B. Thiols and disulphides can aggravate peroxynitrite-dependent inactivation of  $\alpha$ 1-antiproteinase. *FEBS Lett.* **414**, 497–500 (1997).
  152. Zhao, J. Interplay among nitric oxide and reactive oxygen species: A complex network determining cell survival or death. *Plant Signal. Behav.* **2**, 544–547 (2007).
  153. Wang, F., Yuan, Q., Chen, F. & Pang, J. Fundamental Mechanisms of the Cell Death Caused by Nitrosative Stress. **9**, 1–10 (2021).
  154. Di Meo, S., Reed, T. T., Venditti, P. & Victor, V. M. Role of ROS and RNS Sources in Physiological and Pathological Conditions. *Oxid. Med. Cell. Longev.* **2016**, (2016).
  155. Costa, N. T., Iriyoda, T. M. V., Alfieri, D. F., Simão, A. N. C. & Dichi, I. Influence of disease-modifying antirheumatic drugs on oxidative and nitrosative stress in patients with rheumatoid arthritis. *Inflammopharmacology* **26**, 1151–1164 (2018).
  156. Beckmann, J. S. *et al.* Extensive nitration of protein tyrosines in human atherosclerosis detected by immunohistochemistry. *Biol. Chem. Hoppe. Seyler.* **375**, 81–88 (1994).
  157. Thomson, L. 3-Nitrotyrosine Modified Proteins in Atherosclerosis. *Dis. Markers* **2015**, (2015).
  158. Patel, R. P. *et al.* Biological aspects of reactive nitrogen species. *Biochim. Biophys. Acta - Bioenerg.* **1411**, 385–400 (1999).

159. Nash, K. M., Rockenbauer, A. & Villamena, F. A. Reactive nitrogen species reactivities with nitrones: Theoretical and experimental studies. *Chem. Res. Toxicol.* **25**, 1581–1597 (2012).
160. Zhou, S. *et al.* Heme-biosynthetic porphobilinogen deaminase protects *Aspergillus nidulans* from nitrosative stress. *Appl. Environ. Microbiol.* **78**, 103–109 (2012).
161. Sawa, T. *et al.* Protein S-guanylation by the biological signal 8-nitroguanosine 3',5'-cyclic monophosphate. *Nat. Chem. Biol.* **3**, 727–735 (2007).
162. Baker, P. R. S., Schopfer, F. J., O'Donnell, V. B. & Freeman, B. A. Convergence of nitric oxide and lipid signaling: Anti-inflammatory nitro-fatty acids. *Free Radic. Biol. Med.* **46**, 989–1003 (2009).
163. Zmijewski, J. W. *et al.* Cell signalling by oxidized lipids and the role of reactive oxygen species in the endothelium. *Biochem. Soc. Trans.* **33**, 1385 (2005).
164. White, P. J., Charbonneau, A., Cooney, G. J. & Marette, A. Nitrosative modifications of protein and lipid signaling molecules by reactive nitrogen species. *Am. J. Physiol. - Endocrinol. Metab.* **299**, 868–878 (2010).
165. Missall, T. A., Lodge, J. K. & McEwen, J. E. Mechanisms of resistance to oxidative and nitrosative stress: Implications for fungal survival in mammalian hosts. *Eukaryot. Cell* **3**, 835–846 (2004).
166. Stern, A. M., Liu, B., Bakken, L. R., Shapleigh, J. P. & Zhu, J. A novel protein protects bacterial iron-dependent metabolism from nitric oxide. *J. Bacteriol.* **195**, 4702–4708 (2013).
167. Doi, Y. & Takaya, N. A Novel A3 Group Aconitase Tolerates Oxidation and Nitric Oxide. *J. Biol. Chem.* **290**, 1412–1421 (2015).
168. Tharmalingam, S., Alhasawi, A., Appanna, V. P., Lemire, J. & Appanna, V. D. Reactive Nitrogen Species (RNS)-resistant microbes: Adaptation and medical implications. *Biol. Chem.* **398**, 1193–1208 (2017).
169. Andrew, P. J. & Mayer, B. Enzymatic function of nitric oxide synthases. *Cardiovasc. Res.* **43**, 521–531 (1999).
170. Rauhala, P., Andoh, T. & Chiueh, C. C. Neuroprotective properties of nitric oxide and S-nitrosoglutathione. *Toxicol. Appl. Pharmacol.* **207**, 91–95 (2005).
171. Guyer, R. L. & Koshland, D. E. The molecule of the year. *Science (80-. )*. **246**, 1543–1546

- (1989).
172. Knott, A. B. & Bossy-Wetzel, E. Nitric oxide in health and disease of the nervous system. *Antioxidants Redox Signal.* **11**, 541–553 (2009).
  173. Bove, P. F. & van der Vliet, A. Nitric oxide and reactive nitrogen species in airway epithelial signaling and inflammation. *Free Radic. Biol. Med.* **41**, 515–527 (2006).
  174. Khojah, H. M., Ahmed, S., Abdel-Rahman, M. S. & Hamza, A. B. Reactive oxygen and nitrogen species in patients with rheumatoid arthritis as potential biomarkers for disease activity and the role of antioxidants. *Free Radic. Biol. Med.* **97**, 285–291 (2016).
  175. Haklar, G., Sayin-Özveri, E., Yüksel, M., Aktan, A. Ö. & Yalçın, A. S. Different kinds of reactive oxygen and nitrogen species were detected in colon and breast tumors. *Cancer Lett.* **165**, 219–224 (2001).
  176. Eiján, A. M. *et al.* Nitric oxide in patients with transitional bladder cancer. *J. Surg. Oncol.* **81**, 203–208 (2002).
  177. Smulik, R. *et al.* Nitroxyl (HNO) Reacts with Molecular Oxygen and Forms Peroxynitrite at Physiological pH. *J. Biol. Chem.* **289**, 35570–35581 (2014).
  178. Augusto, O. *et al.* Carbon dioxide-catalyzed peroxynitrite reactivity – The resilience of the radical mechanism after two decades of research. *Free Radic. Biol. Med.* **135**, 210–215 (2019).
  179. Pryor, W. A. & Squadrito, G. L. The chemistry of peroxynitrite: A product from the reaction of nitric oxide with superoxide. *Am. J. Physiol. - Lung Cell. Mol. Physiol.* **268**, (1995).
  180. Denicola, A., Freeman, B. A., Trujillo, M. & Radi, R. Peroxynitrite reaction with carbon dioxide/bicarbonate: Kinetics and influence on peroxynitrite-mediated oxidations. *Arch. Biochem. Biophys.* **333**, 49–58 (1996).
  181. Augusto, O. *et al.* Nitrogen dioxide and carbonate radical anion: two emerging radicals in biology. *Free Radic. Biol. Med.* **32**, 841–859 (2002).
  182. Sabadashka, M., Nagalievskaa, M. & Sybirna, N. Tyrosine nitration as a key event of signal transduction that regulates functional state of the cell. *Cell Biol. Int.* **45**, 481–497 (2021).
  183. Ferrer-Sueta, G. *et al.* Biochemistry of Peroxynitrite and Protein Tyrosine Nitration. *Chem. Rev.* **118**, 1338–1408 (2018).
  184. Dickinson, B. C. & Chang, C. J. Chemistry and biology of reactive oxygen species in

- signaling or stress responses. *Nat. Chem. Biol.* **7**, 504–511 (2011).
185. Touyz, R. M. Reactive oxygen species, vascular oxidative stress, and redox signaling in hypertension: What is the clinical significance? *Hypertension* **44**, 248–252 (2004).
  186. Liaudet, L. Role of peroxynitrite in the redox regulation of cell signal transduction pathways. *Front. Biosci.* **Volume**, 4809 (2009).
  187. Allen, R. G. *et al.* Stressor-induced increase in microbicidal activity of splenic macrophages is dependent upon peroxynitrite production. *Infect. Immun.* **80**, 3429–3437 (2012).
  188. Alvarez, M. N., Peluffo, G., Piacenza, L. & Radi, R. Intrapagosomal peroxynitrite as a macrophage-derived cytotoxin against internalized *Trypanosoma cruzi*: Consequences for oxidative killing and role of microbial peroxiredoxins in infectivity. *J. Biol. Chem.* **286**, 6627–6640 (2011).
  189. Fukuto, J. M., Dutton, A. S. & Houk, K. N. The chemistry and biology of nitroxyl (HNO): A chemically unique species with novel and important biological activity. *ChemBioChem* **6**, 612–619 (2005).
  190. Miranda, K. M. *et al.* Unique oxidative mechanisms for the reactive nitrogen oxide species, nitroxyl anion. *J. Biol. Chem.* **276**, 1720–1727 (2001).
  191. Ohshima, H., Gilibert, I. & Bianchini, F. Induction of DNA strand breakage and base oxidation by nitroxyl anion through hydroxyl radical production. *Free Radic. Biol. Med.* **26**, 1305–1313 (1999).
  192. Bai, P. Partial protection by poly(ADP-ribose) polymerase inhibitors from nitroxyl-induced cytotoxicity in thymocytes. *Free Radic. Biol. Med.* **31**, 1616–1623 (2001).
  193. Ohshima, H., Celan, I., Chazotte, L., Pignatelli, B. & Mower, H. F. Analysis of 3-nitrotyrosine in biological fluids and protein hydrolyzates by high-performance liquid chromatography using a postseparation, on-line reduction column and electrochemical detection: Results with various nitrating agents. *Nitric Oxide - Biol. Chem.* **3**, 132–141 (1999).
  194. Bazylnski, D. A. & Hollocher, T. C. Evidence from the reaction between trioxodinitrate(II) and nitrogen-15-labeled nitric oxide that trioxodinitrate(II) decomposes into nitrosyl hydride and nitrite in neutral aqueous solution. *Inorg. Chem.* **24**, 4285–4288 (1985).
  195. Reisz, J. A., Zink, C. N. & King, S. B. Rapid and selective nitroxyl (HNO) trapping by phosphines: Kinetics and new aqueous ligations for HNO detection and quantitation. *J. Am. Chem. Soc.* **133**, 11675–11685 (2011).

196. Ulrich, K. & Jakob, U. The role of thiols in antioxidant systems. *Free Radic. Biol. Med.* **140**, 14–27 (2019).
197. Lesslie, M. *et al.* Hydrogen atom transfer in metal ion complexes of the glutathione thiyl radical. *Int. J. Mass Spectrom.* **429**, 39–46 (2018).
198. Masella, R., Di Benedetto, R., Vari, R., Filesi, C. & Giovannini, C. Novel mechanisms of natural antioxidant compounds in biological systems: Involvement of glutathione and glutathione-related enzymes. *J. Nutr. Biochem.* **16**, 577–586 (2005).
199. Hwang, C., Sinskey, A. & Lodish, H. Oxidized redox state of glutathione in the endoplasmic reticulum. *Science (80-. ).* **257**, 1496–1502 (1992).
200. Galaris, D., Cadenas, E. & Hochstein, P. Glutathione-dependent reduction of peroxides during ferryl- and met-myoglobin interconversion: A potential protective mechanism in muscle. *Free Radic. Biol. Med.* **6**, 473–478 (1989).
201. Mieyal, J. J., Gallogly, M. M., Qanungo, S., Sabens, E. A. & Shelton, M. D. Molecular Mechanisms and Clinical Implications of Reversible Protein S -Glutathionylation. *Antioxid. Redox Signal.* **10**, 1941–1988 (2008).
202. Winterbourn, C. C. Superoxide as an intracellular radical sink. *Free Radic. Biol. Med.* **14**, 85–90 (1993).
203. D'Aquino, M. *et al.* [3] Sulfhydryl free radical formation enzymatically by sonolysis, by radiolysis, and thermally: Vitamin A, curcumin, muconic acid, and related conjugated olefins as references. in *Methods in Enzymology* **233**, 34–46 (1994).
204. Fernandes, D. D. C., Bonatto, D. & Laurindo, F. R. M. *Studies on Cardiovascular Disorders. Studies on Cardiovascular Disorders* (Humana Press, 2010). doi:10.1007/978-1-60761-600-9
205. Chae, H. Z., Chung, S. J. & Rhee, S. G. Thioredoxin-dependent peroxide reductase from yeast. *J. Biol. Chem.* **269**, 27670–27678 (1994).
206. Galaris, D. & Evangelou, A. The role of oxidative stress in mechanisms of metal-induced carcinogenesis. *Crit. Rev. Oncol. Hematol.* **42**, 93–103 (2002).
207. Gatti, R. M., Radi, R. & Augusto, O. Peroxynitrite-mediated oxidation of albumin to the protein-thiyl free radical. *FEBS Lett.* **348**, 287–290 (1994).
208. Balazy, M., Kaminski, P. M., Mao, K., Tan, J. & Wolin, M. S. S-nitroglutathione, a product

- of the reaction between peroxyxynitrite and glutathione that generates nitric oxide. *J. Biol. Chem.* **273**, 32009–32015 (1999).
209. Kalyanaraman, B. Thiyl radicals in biological systems: significant or trivial? *Biochem. Soc. Symp.* **61**, 55–63 (1995).
  210. Sun, J., Steenbergen, C. & Murphy, E. S -Nitrosylation: NO-Related Redox Signaling to Protect Against Oxidative Stress. *Antioxid. Redox Signal.* **8**, 1693–1705 (2006).
  211. Wu, C. *et al.* Redox Regulatory Mechanism of Transnitrosylation by Thioredoxin. *Mol. Cell. Proteomics* **9**, 2262–2275 (2010).
  212. Nakamura, T. & Lipton, S. A. Emerging Role of Protein-Protein Transnitrosylation in Cell Signaling Pathways. *Antioxid. Redox Signal.* **18**, 239–249 (2013).
  213. Anand, P. & Stamler, J. S. Enzymatic mechanisms regulating protein S-nitrosylation: implications in health and disease. *J. Mol. Med.* **90**, 233–244 (2012).
  214. Lushchak, V. I. Glutathione Homeostasis and Functions: Potential Targets for Medical Interventions. *J. Amino Acids* **2012**, 1–26 (2012).
  215. Stoyanovsky, D. A., Maeda, A., Atkins, J. L. & Kagan, V. E. Assessments of thiyl radicals in biosystems: Difficulties and new applications. *Anal. Chem.* **83**, 6432–6438 (2011).
  216. Wu, L. *et al.* Photostable Ratiometric Pdot Probe for in Vitro and in Vivo Imaging of Hypochlorous Acid. *J. Am. Chem. Soc.* **139**, 6911–6918 (2017).
  217. Gupta, M. K., Meyer, T. A., Nelson, C. E. & Duvall, C. L. Poly(PS-b-DMA) micelles for reactive oxygen species triggered drug release. *J. Control. Release* **162**, 591–598 (2012).
  218. Zhou, Z. *et al.* Synchronous Chemoradiation Nanovesicles by X-Ray Triggered Cascade of Drug Release. *Angew. Chemie - Int. Ed.* **57**, 8463–8467 (2018).
  219. Deng, H., Zhao, X., Deng, L., Liu, J. & Dong, A. Reactive oxygen species activated nanoparticles with tumor acidity internalization for precise anticancer therapy. *J. Control. Release* **255**, 142–153 (2017).
  220. Fuhrmann, K. *et al.* Modular design of redox-responsive stabilizers for nanocrystals. *ACS Nano* **7**, 8243–8250 (2013).
  221. Herzberger, J. *et al.* Oxidation-Responsive and ‘clickable’ Poly(ethylene glycol) via Copolymerization of 2-(Methylthio)ethyl Glycidyl Ether. *J. Am. Chem. Soc.* **138**, 9212–9223 (2016).

222. Rehor, A., Hubbell, J. A. & Tirelli, N. Oxidation-Sensitive Polymeric Nanoparticles. *Langmuir* **21**, 411–417 (2005).
223. Wu, T. *et al.* Aortic plaque-targeted andrographolide delivery with oxidation-sensitive micelle effectively treats atherosclerosis via simultaneous ROS capture and anti-inflammation. *Nanomedicine Nanotechnology, Biol. Med.* **14**, 2215–2226 (2018).
224. Hu, P. & Tirelli, N. Scavenging ROS: Superoxide dismutase/catalase mimetics by the use of an oxidation-sensitive nanocarrier/enzyme conjugate. *Bioconjug. Chem.* **23**, 438–449 (2012).
225. Yi, S. *et al.* An Injectable Hydrogel Platform for Sustained Delivery of Anti-inflammatory Nanocarriers and Induction of Regulatory T Cells in Atherosclerosis. **8**, 1–10 (2020).
226. Allen, B. L., Johnson, J. D. & Walker, J. P. Encapsulation and enzyme-mediated release of molecular cargo in polysulfide nanoparticles. *ACS Nano* **5**, 5263–5272 (2011).
227. Carampin, P. *et al.* Oxidant-dependent REDOX responsiveness of polysulfides. *Macromol. Chem. Phys.* **213**, 2052–2061 (2012).
228. Kim, K., Lee, C. S. & Na, K. Light-controlled reactive oxygen species (ROS)-producible polymeric micelles with simultaneous drug-release triggering and endo/lysosomal escape. *Chem. Commun.* **52**, 2839–2842 (2016).
229. Bobbala, S. *et al.* Employing bicontinuous-to-micellar transitions in nanostructure morphology for on-demand photo-oxidation responsive cytosolic delivery and off-on cytotoxicity. *Nanoscale* **12**, 5332–5340 (2020).
230. Zhao, C. *et al.* Reactive oxygen species-responsive theranostic nanoparticles for enhanced hypoxic tumor photodynamic therapy: Via synchronous HIF-1 $\alpha$  inhibition and ATP depletion. *Materials Chemistry Frontiers* **3**, 1793–1799 (2019).
231. Wang, K. *et al.* Self-assembled IR780-loaded transferrin nanoparticles as an imaging, targeting and PDT/PTT agent for cancer therapy. *Sci. Rep.* **6**, 27421 (2016).
232. Storkey, C., Pattison, D. I., Ignasiak, M. T., Schiesser, C. H. & Davies, M. J. Kinetics of reaction of peroxyxynitrite with selenium- and sulfur-containing compounds: Absolute rate constants and assessment of biological significance. *Free Radic. Biol. Med.* **89**, 1049–1056 (2015).
233. Tan, X. *et al.* Single-molecule force spectroscopy of selenium-containing amphiphilic block copolymer: Toward disassembling the polymer micelles. *Langmuir* **28**, 9601–9605 (2012).

234. Fang, R., Xu, H., Cao, W., Yang, L. & Zhang, X. Reactive oxygen species (ROS)-responsive tellurium-containing hyperbranched polymer. *Polym. Chem.* **6**, 2817–2821 (2015).
235. Zhang, W. *et al.* Te-containing carbon dots for fluorescence imaging of superoxide anion in mice during acute strenuous exercise or emotional changes. *Chem. Sci.* **9**, 721–727 (2018).
236. Ma, N. *et al.* Selenium-containing block copolymers and their oxidation-responsive aggregates. *Polym. Chem.* **1**, 1609–1614 (2010).
237. Yang, X.-L. *et al.* Enzymatic synthesis of selenium-containing amphiphilic aliphatic polycarbonate as an oxidation-responsive drug delivery vehicle. *RSC Adv.* **9**, 6003–6010 (2019).
238. Wang, Y. *et al.* Light-Responsive Nanoparticles for Highly Efficient Cytoplasmic Delivery of Anticancer Agents. *ACS Nano* **11**, 12134–12144 (2017).
239. Fan, F., Wang, L., Li, F., Fu, Y. & Xu, H. Stimuli-Responsive Layer-by-Layer Tellurium-Containing Polymer Films for the Combination of Chemotherapy and Photodynamic Therapy. *ACS Appl. Mater. Interfaces* **8**, 17004–17010 (2016).
240. Wang, H., Chai, L., Xie, Z. & Zhang, H. Recent Advance of Tellurium for Biomedical Applications. *Chem. Res. Chinese Univ.* **36**, 551–559 (2020).
241. Sun, B. *et al.* Probing the impact of sulfur/selenium/carbon linkages on prodrug nanoassemblies for cancer therapy. *Nat. Commun.* **10**, 1–10 (2019).
242. Brandes, N., Schmitt, S. & Jakob, U. Thiol-Based Redox Switches in Eukaryotic Proteins. *Antioxid. Redox Signal.* **11**, 997–1014 (2009).
243. Bonifacic, M., Schaefer, K., Moeckel, H. & Asmus, K. D. Primary steps in the reactions of organic disulfides with hydroxyl radicals in aqueous solution. *J. Phys. Chem.* **79**, 1496–1502 (1975).
244. Jiang, S., Carroll, L., Mariotti, M., Per, H. & Davies, M. J. Redox Biology Formation of protein cross-links by singlet oxygen-mediated disulfide oxidation. **41**, (2021).
245. WEFERS, H. & SIES, H. Oxidation of glutathione by the superoxide radical to the disulfide and the sulfonate yielding singlet oxygen. *Eur. J. Biochem.* **137**, 29–36 (1983).
246. Carroll, L. *et al.* Free Radical Biology and Medicine Oxidant-induced glutathionylation at

- protein disulfide bonds. *Free Radic. Biol. Med.* **160**, 513–525 (2020).
247. Sun, B. *et al.* Disulfide Bond-Driven Oxidation- and Reduction-Responsive Prodrug Nanoassemblies for Cancer Therapy. *Nano Lett.* **18**, 3643–3650 (2018).
  248. Xu, C.-T. *et al.* Low generation PAMAM-based nanomicelles as ROS-responsive gene vectors with enhanced transfection efficacy and reduced cytotoxicity in vitro. *New J. Chem.* **41**, 3273–3279 (2017).
  249. Zhou, Z. *et al.* Linear-dendritic drug conjugates forming long-circulating nanorods for cancer-drug delivery. *Biomaterials* **34**, 5722–5735 (2013).
  250. Ryu, J.-H. *et al.* Self-Cross-Linked Polymer Nanogels: A Versatile Nanoscopic Drug Delivery Platform. *J. Am. Chem. Soc.* **132**, 17227–17235 (2010).
  251. Xing, T., Mao, C., Lai, B. & Yan, L. Synthesis of disulfide-cross-linked polypeptide nanogel conjugated with a near-infrared fluorescence probe for direct imaging of reduction-induced drug release. *ACS Appl. Mater. Interfaces* **4**, 5662–5672 (2012).
  252. Wang, J. *et al.* Comparison of Redox Responsiveness and Antitumor Capability of Paclitaxel Dimeric Nanoparticles with Different Linkers. *Chem. Mater.* **32**, 10719–10727 (2020).
  253. Xia, J., Li, T., Lu, C. & Xu, H. Selenium-Containing Polymers: Perspectives toward Diverse Applications in Both Adaptive and Biomedical Materials. *Macromolecules* **51**, 7435–7455 (2018).
  254. Xu, H., Cao, W. & Zhang, X. Selenium-containing polymers: Promising biomaterials for controlled release and enzyme mimics. *Acc. Chem. Res.* **46**, 1647–1658 (2013).
  255. Kildahl, N. K. Bond energy data summarized. *J. Chem. Educ.* **73**, 423–424 (1995).
  256. Zhang, L., Liu, Y., Zhang, K., Chen, Y. & Luo, X. Redox-responsive comparison of diselenide micelles with disulfide micelles. *Colloid Polym. Sci.* **297**, 225–238 (2019).
  257. Carroll, L. *et al.* Interaction kinetics of selenium-containing compounds with oxidants. *Free Radic. Biol. Med.* **155**, 58–68 (2020).
  258. Sun, C., Ji, S., Li, F. & Xu, H. Diselenide-Containing Hyperbranched Polymer with Light-Induced Cytotoxicity. *ACS Appl. Mater. Interfaces* **9**, 12924–12929 (2017).
  259. Li, T., Pan, S., Zhuang, H., Gao, S. & Xu, H. Selenium-Containing Carrier-Free Assemblies with Aggregation-Induced Emission Property Combine Cancer Radiotherapy with

- Chemotherapy. *ACS Appl. Bio Mater.* **3**, 1283–1292 (2020).
260. Ma, N. *et al.* Radiation-Sensitive Diselenide Block Co-polymer Micellar Aggregates: Toward the Combination of Radiotherapy and Chemotherapy. *Langmuir* **27**, 5874–5878 (2011).
  261. Zhai, S., Hu, X., Hu, Y., Wu, B. & Xing, D. Visible light-induced crosslinking and physiological stabilization of diselenide-rich nanoparticles for redox-responsive drug release and combination chemotherapy. *Biomaterials* **121**, 41–54 (2017).
  262. Ma, N., Li, Y., Xu, H., Wang, Z. & Zhang, X. Dual redox responsive assemblies formed from diselenide block copolymers. *J. Am. Chem. Soc.* **132**, 442–443 (2010).
  263. Sun, C., Tan, Y. & Xu, H. From Selenite to Diselenide-Containing Drug Delivery Systems. *ACS Mater. Lett.* **2**, 1173–1177 (2020).
  264. Xue, P. *et al.* Redox-Sensitive Citronellol-Cabazitaxel Conjugate: Maintained in Vitro Cytotoxicity and Self-Assembled as Multifunctional Nanomedicine. *Bioconjug. Chem.* **27**, 1360–1372 (2016).
  265. Cao, W., Zhang, X., Miao, X., Yang, Z. & Xu, H.  $\Gamma$ -Ray-Responsive Supramolecular Hydrogel Based on a Diselenide-Containing Polymer and a Peptide. *Angewandte Chemie - International Edition* **52**, 6233–6237 (2013).
  266. Han, P. *et al.* Red light responsive diselenide-containing block copolymer micelles. *J. Mater. Chem. B* **1**, 740–743 (2013).
  267. Yang, G., Sun, X., Liu, J., Feng, L. & Liu, Z. Light-Responsive, Singlet-Oxygen-Triggered On-Demand Drug Release from Photosensitizer-Doped Mesoporous Silica Nanorods for Cancer Combination Therapy. *Adv. Funct. Mater.* **26**, 4722–4732 (2016).
  268. Dariva, C. G. *et al.* Development of red-light cleavable PEG-PLA nanoparticles as delivery systems for cancer therapy. *Colloids Surfaces B Biointerfaces* **196**, (2020).
  269. Saravanakumar, G., Lee, J., Kim, J. & Kim, W. J. Visible light-induced singlet oxygen-mediated intracellular disassembly of polymeric micelles co-loaded with a photosensitizer and an anticancer drug for enhanced photodynamic therapy. *Chem. Commun.* **51**, 9995–9998 (2015).
  270. Arian, D., Kovbasyuk, L. & Mokhir, A. 1,9-Dialkoxyanthracene as a  $^{1}O_2$ -Sensitive Linker. *J. Am. Chem. Soc.* **133**, 3972–3980 (2011).

271. Baugh, S. D. P., Yang, Z., Leung, D. K., Wilson, D. M. & Breslow, R. Cyclodextrin dimers as cleavable carriers of photodynamic sensitizers. *J. Am. Chem. Soc.* **123**, 12488–12494 (2001).
272. Liu, J. *et al.* Light-controlled drug release from singlet-oxygen sensitive nanoscale coordination polymers enabling cancer combination therapy. *Biomaterials* **146**, 40–48 (2017).
273. Lee, J., Park, J., Singha, K. & Kim, W. J. Mesoporous silica nanoparticle facilitated drug release through cascade photosensitizer activation and cleavage of singlet oxygen sensitive linker. *Chem. Commun.* **49**, 1545–1547 (2013).
274. Zhang, Y. *et al.* Reactive Oxygen Species (ROS)-Degradable Polymeric NanoplatforM for Hypoxia-Targeted Gene Delivery: Unpacking DNA and Reducing Toxicity. *Biomacromolecules* **20**, 1899–1913 (2019).
275. Zhou, F. *et al.* Theranostic Prodrug Vesicles for Reactive Oxygen Species-Triggered Ultrafast Drug Release and Local-Regional Therapy of Metastatic Triple-Negative Breast Cancer. *Adv. Funct. Mater.* **27**, (2017).
276. Wang, S. *et al.* Enhanced Antitumor Efficacy by a Cascade of Reactive Oxygen Species Generation and Drug Release. *Angew. Chemie* **131**, 14900–14905 (2019).
277. Zhang, W., Hu, X., Shen, Q. & Xing, D. Mitochondria-specific drug release and reactive oxygen species burst induced by polyprodrug nanoreactors can enhance chemotherapy. *Nat. Commun.* **10**, 1704 (2019).
278. Liu, B. & Thayumanavan, S. Mechanistic Investigation on Oxidative Degradation of ROS-Responsive Thioacetal/Thioacetal Moieties and Their Implications. *Cell Reports Phys. Sci.* **1**, 100271 (2020).
279. Kim, J. S., Jo, S. D., Seah, G. L., Kim, I. & Nam, Y. S. ROS-induced biodegradable polythioacetal nanoparticles for intracellular delivery of anti-cancer therapeutics. *J. Ind. Eng. Chem.* **21**, 1137–1142 (2015).
280. Shim, M. S. & Xia, Y. A Reactive Oxygen Species (ROS)-Responsive Polymer for Safe, Efficient, and Targeted Gene Delivery in Cancer Cells. *Angew. Chemie* **125**, 7064–7067 (2013).
281. Wilson, D. S. *et al.* Orally delivered thioacetal nanoparticles loaded with TNF- $\alpha$ -siRNA target inflammation and inhibit gene expression in the intestines. *Nature Materials* **9**, 923–928

- (2010).
282. Yuan, Y., Liu, J. & Liu, B. Conjugated-polyelectrolyte-based polyprodrug: Targeted and image-guided photodynamic and chemotherapy with on-demand drug release upon irradiation with a single light source. *Angew. Chemie - Int. Ed.* **53**, 7163–7168 (2014).
  283. Saravanakumar, G., Kim, J. & Kim, W. J. Reactive-Oxygen-Species-Responsive Drug Delivery Systems: Promises and Challenges. *Adv. Sci.* **4**, 1600124 (2017).
  284. Zhang, Y., Zhang, H., Mao, Z. & Gao, C. ROS-Responsive Nanoparticles for Suppressing the Cytotoxicity and Immunogenicity Caused by PM2.5 Particulates. *Biomacromolecules* **20**, 1777–1788 (2019).
  285. Ke, W. *et al.* Therapeutic polymersome nanoreactors with tumor-specific activable cascade reactions for cooperative cancer therapy. *ACS Nano* **13**, 2357–2369 (2019).
  286. Winterbourn, C. C. & Metodiewa, D. Reactivity of biologically important thiol compounds with superoxide and hydrogen peroxide. *Free Radic. Biol. Med.* **27**, 322–328 (1999).
  287. Sun, C. *et al.* A ROS-responsive polymeric micelle with a  $\pi$ -conjugated thioketal moiety for enhanced drug loading and efficient drug delivery. *Organic and Biomolecular Chemistry* **15**, 9176–9185 (2017).
  288. Xu, L. *et al.* A reactive oxygen species (ROS)-responsive low molecular weight gel co-loaded with doxorubicin and Zn(II) phthalocyanine tetrasulfonic acid for combined chemophotodynamic therapy. *J. Mater. Chem. B* **5**, 9157–9164 (2017).
  289. Xu, L. *et al.* Polymeric nanoparticles responsive to intracellular ROS for anticancer drug delivery. *Colloids Surfaces B Biointerfaces* **181**, 252–260 (2019).
  290. Chen, B. *et al.* Reactive oxygen species-responsive nanoparticles based on a thioketal-containing poly( $\beta$ -amino ester) for combining photothermal/photodynamic therapy and chemotherapy. *Polym. Chem.* **10**, 4746–4757 (2019).
  291. Xu, C., Xu, L., Han, R., Zhu, Y. & Zhang, J. Blood circulation stable doxorubicin prodrug nanoparticles containing hydrazone and thioketal moieties for antitumor chemotherapy. *Colloids Surfaces B Biointerfaces* **201**, 111632 (2021).
  292. Yue, C. *et al.* ROS-responsive mitochondria-targeting blended nanoparticles: Chemo- and photodynamic synergistic therapy for lung cancer with on-demand drug release upon irradiation with a single light source. *Theranostics* **6**, 2352–2366 (2016).

293. Wang, J. *et al.* Far-red light-mediated programmable anti-cancer gene delivery in cooperation with photodynamic therapy. *Biomaterials* **171**, 72–82 (2018).
294. Yang, J. *et al.* Oxalate-curcumin–based probe for micro- and macroimaging of reactive oxygen species in Alzheimer’s disease. *Proc. Natl. Acad. Sci. U. S. A.* **114**, 12384–12389 (2017).
295. Lee, D. *et al.* In vivo imaging of hydrogen peroxide with chemiluminescent nanoparticles. *Nat. Mater.* **6**, 765–769 (2007).
296. Kwon, J. *et al.* Inflammation-responsive antioxidant nanoparticles based on a polymeric prodrug of vanillin. *Biomacromolecules* **14**, 1618–1626 (2013).
297. Li, J. *et al.* Self-sufficing H<sub>2</sub>O<sub>2</sub>-responsive nanocarriers through tumor-specific H<sub>2</sub>O<sub>2</sub> production for synergistic oxidation-chemotherapy. *J. Control. Release* **225**, 64–74 (2016).
298. Arnous, A., Petrakis, C., Makris, D. P. & Kefalas, P. A peroxyoxalate chemiluminescence-based assay for the evaluation of hydrogen peroxide scavenging activity employing 9,10-diphenylanthracene as the fluorophore. *J. Pharmacol. Toxicol. Methods* **48**, 171–177 (2002).
299. Xu, Y., Yang, W. & Zhang, B. ROS-responsive probes for low-background optical imaging: a review. *Biomed. Mater.* **16**, 022002 (2021).
300. Wu, Y. *et al.* Novel multi-sensitive pseudo-poly(amino acid) for effective intracellular drug delivery. *RSC Adv.* **5**, 31972–31983 (2015).
301. Kim, S. *et al.* Polyoxalate nanoparticles as a biodegradable and biocompatible drug delivery vehicle. *Biomacromolecules* **11**, 555–560 (2010).
302. Ballance, W. C., Qin, E. C., Chung, H. J., Gillette, M. U. & Kong, H. Reactive oxygen species-responsive drug delivery systems for the treatment of neurodegenerative diseases. *Biomaterials* **217**, (2019).
303. Berwin Singh, S. V. *et al.* Hydrogen peroxide-activatable polymeric prodrug of curcumin for ultrasound imaging and therapy of acute liver failure. *Nanomedicine Nanotechnology, Biol. Med.* **16**, 45–55 (2019).
304. Jung, E. *et al.* Ultrasound imaging and on-demand therapy of peripheral arterial diseases using H<sub>2</sub>O<sub>2</sub>-Activated bubble generating anti-inflammatory polymer particles. *Biomaterials* **179**, 175–185 (2018).

305. Cho, B. R. *et al.* P-Hydroxybenzyl alcohol-containing biodegradable nanoparticle improves functional blood flow through angiogenesis in a mouse model of hindlimb ischemia. *Biomaterials* **53**, 679–687 (2015).
306. Park, H. *et al.* Antioxidant and anti-inflammatory activities of hydroxybenzyl alcohol releasing biodegradable polyoxalate nanoparticles. *Biomacromolecules* **11**, 2103–2108 (2010).
307. Kim, S. *et al.* Reduction of oxidative stress by p-hydroxybenzyl alcohol-containing biodegradable polyoxalate nanoparticulate antioxidant. *Biomaterials* **32**, 3021–3029 (2011).
308. Yoo, D. *et al.* Antioxidant polymeric nanoparticles as novel therapeutics for airway inflammatory diseases. *Int. J. Pharm.* **450**, 87–94 (2013).
309. Shuhendler, A. J., Pu, K., Cui, L., Uetrecht, J. P. & Rao, J. Real-time imaging of oxidative and nitrosative stress in the liver of live animals for drug-toxicity testing. *Nat. Biotechnol.* **32**, 373–380 (2014).
310. Lee, I.-J., Hwang, O., Yoo, D., Khang, G. & Lee, D. Detection of Hydrogen Peroxide in vitro and in vivo Using Peroxalate Chemiluminescent Micelles. *Bull. Korean Chem. Soc.* **32**, 2187–2192 (2011).
311. Lee, J. *et al.* Thrombus targeting aspirin particles for near infrared imaging and on-demand therapy of thrombotic vascular diseases. *J. Control. Release* **304**, 164–172 (2019).
312. Ma, B. *et al.* Reactive Oxygen Species Responsive Theranostic Nanoplatfrom for Two-Photon Aggregation-Induced Emission Imaging and Therapy of Acute and Chronic Inflammation. *ACS Nano* **14**, 5862–5873 (2020).
313. Zhao, Y. & Pluth, M. D. Hydrogen Sulfide Donors Activated by Reactive Oxygen Species. *Angew. Chemie* **128**, 14858–14862 (2016).
314. Sikora, A., Zielonka, J., Lopez, M., Joseph, J. & Kalyanaraman, B. Direct oxidation of boronates by peroxyxynitrite: Mechanism and implications in fluorescence imaging of peroxyxynitrite. *Free Radic. Biol. Med.* **47**, 1401–1407 (2009).
315. Chang, M. C. Y., Pralle, A., Isacoff, E. Y. & Chang, C. J. A Selective, Cell-Permeable Optical Probe for Hydrogen Peroxide in Living Cells. *J. Am. Chem. Soc.* **126**, 15392–15393 (2004).
316. Miller, E. W., Tulyathan, O., Isacoff, E. Y. & Chang, C. J. Molecular imaging of hydrogen

- peroxide produced for cell signaling. *Nat. Chem. Biol.* **3**, 263–267 (2007).
317. de Gracia Lux, C. *et al.* Biocompatible Polymeric Nanoparticles Degrade and Release Cargo in Response to Biologically Relevant Levels of Hydrogen Peroxide. *J. Am. Chem. Soc.* **134**, 15758–15764 (2012).
  318. Maslah, H., Skarbek, C., Pethe, S. & Labruère, R. Anticancer boron-containing prodrugs responsive to oxidative stress from the tumor microenvironment. *Eur. J. Med. Chem.* **207**, (2020).
  319. Stubelius, A., Lee, S. & Almutairi, A. The Chemistry of Boronic Acids in Nanomaterials for Drug Delivery. *Acc. Chem. Res.* **52**, 3108–3119 (2019).
  320. Kashfi, K. & Rigas, B. The mechanism of action of nitric oxide-donating aspirin. *Biochem. Biophys. Res. Commun.* **358**, 1096–1101 (2007).
  321. Han, E. *et al.* Dual Stimuli-Activatable Oxidative Stress Amplifying Agent as a Hybrid Anticancer Prodrug. *Bioconjug. Chem.* **28**, 968–978 (2017).
  322. Zielonka, J. *et al.* Boronate probes as diagnostic tools for real time monitoring of peroxynitrite and hydroperoxides. *Chem. Res. Toxicol.* **25**, 1793–1799 (2012).
  323. Folkes, L. K., Candeias, L. P. & Wardman, P. Kinetics and mechanisms of hypochlorous acid reactions. *Arch. Biochem. Biophys.* **323**, 120–126 (1995).
  324. Han, J. *et al.* A simple boronic acid-based fluorescent probe for selective detection of hydrogen peroxide in solutions and living cells. *Bioorg. Chem.* **81**, 362–366 (2018).
  325. Previtali, V., Petrovic, K., Peiró Cadahía, J., Troelsen, N. S. & Clausen, M. H. Auxiliary in vitro and in vivo biological evaluation of hydrogen peroxide sensitive prodrugs of methotrexate and aminopterin for the treatment of rheumatoid arthritis. *Bioorganic Med. Chem.* **28**, 115247 (2020).
  326. Predmore, B. L., Lefer, D. J. & Gojon, G. Hydrogen sulfide in biochemistry and medicine. *Antioxidants Redox Signal.* **17**, 119–140 (2012).
  327. Broaders, K. E., Grandhe, S. & Fréchet, J. M. J. A biocompatible oxidation-triggered carrier polymer with potential in therapeutics. *J. Am. Chem. Soc.* **133**, 756–758 (2011).
  328. Calabria, D. *et al.* Selective chemiluminescent TURN-ON quantitative bioassay and imaging of intracellular hydrogen peroxide in human living cells. *Anal. Biochem.* **600**, 113760 (2020).

329. Seven, O., Sozmen, F. & Simsek Turan, I. Self immolative dioxetane based chemiluminescent probe for H<sub>2</sub>O<sub>2</sub> detection. *Sensors Actuators B Chem.* **239**, 1318–1324 (2017).
330. Wu, W. *et al.* Bioluminescent probe for hydrogen peroxide imaging in vitro and in vivo. *Anal. Chem.* **86**, 9800–9806 (2014).
331. Szala, M. *et al.* Characterization of the reactivity of luciferin boronate - A probe for inflammatory oxidants with improved stability. *Dye. Pigment.* **183**, (2020).
332. Shen, Y. *et al.* A mitochondria-targeted colorimetric and ratiometric fluorescent probe for hydrogen peroxide with a large emission shift and bio-imaging in living cells. *Sensors Actuators, B Chem.* **255**, 42–48 (2018).
333. Wen, Y. *et al.* A highly sensitive ratiometric fluorescent probe for the detection of cytoplasmic and nuclear hydrogen peroxide. *Anal. Chem.* **86**, 9970–9976 (2014).
334. Kim, D., Kim, G., Nam, S. J., Yin, J. & Yoon, J. Visualization of endogenous and exogenous hydrogen peroxide using a lysosome-targetable fluorescent probe. *Sci. Rep.* **5**, 2–7 (2015).
335. Zhu, H., Fan, J., Du, J. & Peng, X. Fluorescent Probes for Sensing and Imaging within Specific Cellular Organelles. *Acc. Chem. Res.* **49**, 2115–2126 (2016).
336. Liu, K. *et al.* A novel near-infrared fluorescent probe for H<sub>2</sub>O<sub>2</sub> in alkaline environment and the application for H<sub>2</sub>O<sub>2</sub> imaging in vitro and in vivo. *Biomaterials* **100**, 162–171 (2016).
337. Shu, W. *et al.* A highly selective fluorescent probe for monitoring exogenous and endogenous ONOO<sup>-</sup> fluctuations in HeLa cells. *Dyes and Pigments* **175**, (2020).
338. Tong, H. *et al.* A pinacol boronate caged NIAD-4 derivative as a near-infrared fluorescent probe for fast and selective detection of hypochlorous acid. *Chinese Chem. Lett.* **29**, 139–142 (2018).
339. Palanisamy, S. *et al.* In vitro and in vivo imaging of peroxynitrite by a ratiometric boronate-based fluorescent probe. *Biosens. Bioelectron.* **91**, 849–856 (2017).
340. Hou, J. *et al.* A near-infrared ratiometric/turn-on fluorescent probe for in vivo imaging of hydrogen peroxide in a murine model of acute inflammation. *Anal. Chim. Acta* **1024**, 169–176 (2018).
341. Hernandez, C. *et al.* Anticancer Activities of the Quinone-Methide Triterpenes Maytenin and 22-β-hydroxymaytenin Obtained from Cultivated Maytenus ilicifolia Roots Associated

- with Down-Regulation of miRNA-27a and miR-20a/miR-17-5p. *Molecules* **25**, 760 (2020).
342. Basaric, N., Mlinaric-Majerski, K. & Kralj, M. Quinone Methides: Photochemical Generation and its Application in Biomedicine. *Curr. Org. Chem.* **18**, 3–18 (2014).
343. Gasser, G., Ott, I. & Metzler-Nolte, N. Organometallic anticancer compounds. *J. Med. Chem.* **54**, 3–25 (2011).
344. Hanzlik, R. P. & Soine, W. H. Enzymic hydroxylation of ferrocene. *J. Am. Chem. Soc.* **100**, 1290–1291 (1978).
345. van Staveren, D. R. & Metzler-Nolte, N. Bioorganometallic chemistry of ferrocene. *Chem. Rev.* **104**, 5931–5985 (2004).
346. Zotti, G., Schiavon, G., Zecchin, S., Berlin, A. & Pagani, G. Adsorption of ferrocene compounds on indium-tin-oxide electrodes. Enhancement of adsorption by decomposition of ferrocenium molecules by oxygen. *Langmuir* **14**, 1728–1733 (1998).
347. Xu, Y., Wang, L., Li, Y. K. & Wang, C. Q. Oxidation and pH responsive nanoparticles based on ferrocene-modified chitosan oligosaccharide for 5-fluorouracil delivery. *Carbohydr. Polym.* **114**, 27–35 (2014).
348. Fomin, V. M. Common relationships of ferrocene oxidation with oxygen and sulfur dioxide in acid solutions and of its direct oxidation with carboxylic acids. *Russ. J. Gen. Chem.* **77**, 954–960 (2007).
349. Zhang, N. *et al.* Oxidation-Responsive Nanoassemblies for Light-Enhanced Gene Therapy. *Small* **15**, 1–11 (2019).
350. Liu, L., Rui, L., Gao, Y. & Zhang, W. Self-assembly and disassembly of a redox-responsive ferrocene-containing amphiphilic block copolymer for controlled release. *Polym. Chem.* **6**, 1817–1829 (2015).
351. Na, Y. *et al.* Reactive oxygen species (ROS)-responsive ferrocene-polymer-based nanoparticles for controlled release of drugs. *J. Mater. Chem. B* **8**, 1906–1913 (2020).
352. Staff, R. H. *et al.* Patchy Nanocapsules of Poly(vinylferrocene)-Based Block Copolymers for Redox-Responsive Release. *ACS Nano* **6**, 9042–9049 (2012).
353. Na, Y. *et al.*  $\alpha$ -Tocopherol-loaded reactive oxygen species-scavenging ferrocene nanocapsules with high antioxidant efficacy for wound healing. *International Journal of Pharmaceutics* **596**, (2021).

354. Liu, Z.-Q. Potential Applications of Ferrocene as a Structural Feature in Antioxidants. *Mini-Reviews Med. Chem.* **11**, 345–358 (2011).
355. Zheng, M. H., Hu, X., Wang, X. W., Liu, X. L. & Jin, J. Y. Fluorescence-Enhanced Sensing of Hypochlorous Acid Based on 2-Pyridylthiazole Unit. *J. Fluoresc.* **26**, 593–598 (2016).
356. Chen, S., Lu, J., Sun, C. & Ma, H. A highly specific ferrocene-based fluorescent probe for hypochlorous acid and its application to cell imaging. *Analyst* **135**, 577–582 (2010).
357. Lei, Z., Zhang, X., Zheng, X., Liu, S. & Xie, Z. Porphyrin-ferrocene conjugates for photodynamic and chemodynamic therapy. *Org. Biomol. Chem.* **16**, 8613–8619 (2018).
358. Fouda, M. F. R., Abd-Elzaher, M. M., Abdelsamaia, R. A. & Labib, A. A. On the medicinal chemistry of ferrocene. *Appl. Organomet. Chem.* **21**, 613–625 (2007).
359. Connelly, N. G. & Geiger, W. E. Chemical redox agents for organometallic chemistry. *Chem. Rev.* **96**, 877–910 (1996).
360. Mu, S., Liu, W., Ling, Q., Liu, X. & Gu, H. Ferrocenyl amphiphilic Janus dendrimers as redox-responsive micellar carriers. *Appl. Organomet. Chem.* **33**, 1–14 (2019).
361. Qiu, G., Liu, X., Wang, B., Gu, H. & Wang, W. Ferrocene-containing amphiphilic polynorbornenes as biocompatible drug carriers. *Polym. Chem.* **10**, 2527–2539 (2019).
362. Ernst, L. A., Gupta, R. K., Mujumdar, R. B. & Waggoner, A. S. Cyanine dye labeling reagents for sulfhydryl groups. *Cytometry* **10**, 3–10 (1989).
363. Heilemann, M. *et al.* Subdiffraction-resolution fluorescence imaging with conventional fluorescent probes. *Angew. Chemie - Int. Ed.* **47**, 6172–6176 (2008).
364. Rye, H. S. *et al.* Stable fluorescent complexes of double-stranded DNA with bis-intercalating asymmetric cyanine dyes: properties and applications. *Nucleic Acids Res.* **20**, 2803–2812 (1992).
365. Karton-Lifshin, N. *et al.* A unique paradigm for a turn-ON near-infrared cyanine-based probe: Noninvasive intravital optical imaging of hydrogen peroxide. *J. Am. Chem. Soc.* **133**, 10960–10965 (2011).
366. Peng, J. *et al.* Real-Time In Vivo Hepatotoxicity Monitoring through Chromophore-Conjugated Photon-Upconverting Nanoprobes. *Angewandte Chemie - International Edition* **56**, 4165–4169 (2017).
367. Thekkan, S. *et al.* A DNA-based fluorescent reporter maps HOCl production in the maturing

- phagosome. *Nat. Chem. Biol.* **15**, 1165–1172 (2019).
368. Zhang, W. *et al.* A ruthenium(ii) complex-cyanine energy transfer scaffold based luminescence probe for ratiometric detection and imaging of mitochondrial peroxynitrite. *Chem. Commun.* **54**, 13698–13701 (2018).
369. Nani, R. R., Kelley, J. A., Ivanic, J. & Schnermann, M. J. Reactive species involved in the regioselective photooxidation of heptamethine cyanines. *Chem. Sci.* **6**, 6556–6563 (2015).
370. Yang, K. *et al.* A mitochondria-targeted ratiometric fluorescent nanoprobe for imaging of peroxynitrite in living cells. *Talanta* **231**, 122421 (2021).
371. Oushiki, D. *et al.* Development and application of a near-infrared fluorescence probe for oxidative stress based on differential reactivity of linked cyanine dyes. *J. Am. Chem. Soc.* **132**, 2795–2801 (2010).
372. Chen, X. *et al.* Photostabilities of novel heptamethine 3H-indolenine cyanine dyes with different N-substituents. *J. Photochem. Photobiol. A Chem.* **181**, 79–85 (2006).
373. Schwechheimer, C., Röncke, F., Schepers, U. & Wagenknecht, H. A. A new structure-activity relationship for cyanine dyes to improve photostability and fluorescence properties for live cell imaging. *Chem. Sci.* **9**, 6557–6563 (2018).
374. Qin, X. *et al.* In Vivo Photoacoustic Detection and Imaging of Peroxynitrite. *Anal. Chem.* **90**, 9381–9385 (2018).
375. Wang, S. *et al.* In Vivo High-resolution Ratiometric Fluorescence Imaging of Inflammation Using NIR-II Nanoprobes with 1550 nm Emission. *Nano Lett.* **19**, 2418–2427 (2019).
376. Yang, Z. *et al.* Activatable Semiconducting Theranostics: Simultaneous Generation and Ratiometric Photoacoustic Imaging of Reactive Oxygen Species In Vivo. *Adv. Mater.* **30**, 1–8 (2018).
377. Wu, W. *et al.* ONOO- and ClO- Responsive Organic Nanoparticles for Specific in Vivo Image-Guided Photodynamic Bacterial Ablation. *Chem. Mater.* **30**, 3867–3873 (2018).
378. Chen, C., Zhou, B., Lu, D. & Xu, G. Electron transfer events in solutions of cyanine dyes. *J. Photochem. Photobiol. A Chem.* **89**, 25–29 (1995).
379. Toutchkine, A., Nguyen, D. V. & Hahn, K. M. Merocyanine dyes with improved photostability. *Org. Lett.* **9**, 2775–2777 (2007).
380. Guo, Z. *et al.* Photocaged prodrug under NIR light-triggering with dual-channel

- fluorescence: in vivo real-time tracking for precise drug delivery. *Sci. China Chem.* **61**, 1293–1300 (2018).
381. Jiao, L. *et al.* Constructing a Local Hydrophobic Cage in Dye-Doped Fluorescent Silica Nanoparticles to Enhance the Photophysical Properties. *ACS Cent. Sci.* **6**, 747–759 (2020).
382. Zhang, Y. *et al.* Harnessing Hypoxia-Dependent Cyanine Photocages for In Vivo Precision Drug Release. *Angewandte Chemie - International Edition* **60**, 9553–9561 (2021).
383. Chan, M. S. *et al.* Cyanine fluorophores for cellular protection against ROS in stimulated macrophages and two-photon ROS detection. *Org. Biomol. Chem.* **13**, 7307–7312 (2015).
384. Ai, X. *et al.* Multispectral optoacoustic imaging of dynamic redox correlation and pathophysiological progression utilizing upconversion nanoprobes. *Nat. Commun.* **10**, 1–11 (2019).
385. Liu, R. *et al.* Design of a New Near-Infrared Ratiometric Fluorescent Nanoprobe for Real-Time Imaging of Superoxide Anions and Hydroxyl Radicals in Live Cells and in Situ Tracing of the Inflammation Process in Vivo. *Anal. Chem.* **90**, 4452–4460 (2018).
386. Kundu, K. *et al.* Hydrocyanines: A class of fluorescent sensors that can image reactive oxygen species in cell culture, tissue, and in vivo. *Angew. Chemie - Int. Ed.* **48**, 299–303 (2009).
387. Kundu, K., Knight, S. F., Lee, S., Taylor, W. R. & Murthy, N. A significant improvement of the efficacy of radical oxidant probes by the kinetic isotope effect. *Angew. Chemie - Int. Ed.* **49**, 6134–6138 (2010).
388. Sadlowski, C. M., Maity, S., Kundu, K. & Murthy, N. Hydrocyanines: A versatile family of probes for imaging radical oxidants: In vitro and in vivo. *Mol. Syst. Des. Eng.* **2**, 191–200 (2017).
389. Al-Karmi, S. *et al.* Preparation of an<sup>18</sup>F-Labeled Hydrocyanine Dye as a Multimodal Probe for Reactive Oxygen Species. *Chem. - A Eur. J.* **23**, 254–258 (2017).
390. Andina, D. *et al.* Development of a Modular Ratiometric Fluorescent Probe for the Detection of Extracellular Superoxide. *Chem. - A Eur. J.* **23**, 4765–4769 (2017).
391. Maity, S. *et al.* Thiophene bridged hydrocyanine-a new fluorogenic ROS probe. *Chem. Commun.* **53**, 10184–10187 (2017).

392. Drazic, A. & Winter, J. The physiological role of reversible methionine oxidation. *Biochim. Biophys. Acta - Proteins Proteomics* **1844**, 1367–1382 (2014).
393. Moskovitz, J., Berlett, B. S., Poston, J. M. & Stadtman, E. R. The yeast peptide-methionine sulfoxide reductase functions as an antioxidant in vivo. *Proceedings of the National Academy of Sciences of the United States of America* **94**, 9585–9589 (1997).
394. Xu, Q., He, C., Ren, K., Xiao, C. & Chen, X. Thermosensitive Polypeptide Hydrogels as a Platform for ROS-Triggered Cargo Release with Innate Cytoprotective Ability under Oxidative Stress. *Adv. Healthc. Mater.* **5**, 1979–1990 (2016).
395. Rodriguez, A. R., Kramer, J. R. & Deming, T. J. Enzyme-Triggered Cargo Release from Methionine Sulfoxide Containing Copolypeptide Vesicles. *Biomacromolecules* **14**, 3610–3614 (2013).
396. Zhao, D. *et al.* An Injectable ROS-Responsive Self-Healing Hydrogel Based on tetra-poly(ethylene glycol)-b-oligo(l-methionine). *Macromol. Chem. Phys.* **220**, 1–8 (2019).
397. Yoo, J., Sanoj Rejinold, N., Lee, D. Y., Jon, S. & Kim, Y. C. Protease-activatable cell-penetrating peptide possessing ROS-triggered phase transition for enhanced cancer therapy. *J. Control. Release* **264**, 89–101 (2017).
398. Truong Hoang, Q., Lee, D. Y., Choi, D. G., Kim, Y. C. & Shim, M. S. Efficient and selective cancer therapy using pro-oxidant drug-loaded reactive oxygen species (ROS)-responsive polypeptide micelles. *J. Ind. Eng. Chem.* **95**, 101–108 (2021).
399. Yu, S. *et al.* Injectable Bioresponsive Gel Depot for Enhanced Immune Checkpoint Blockade. *Adv. Mater.* **30**, 1–8 (2018).
400. Garrison, W. M. Reaction mechanisms in the radiolysis of peptides, polypeptides, and proteins. *Chem. Rev.* **87**, 381–398 (1987).
401. Stadtman, E. R. & Levine, R. L. Free radical-mediated oxidation of free amino acids and amino acid residues in proteins. *Amino Acids* **25**, 207–218 (2003).
402. Amici, A., Levine, R. L., Tsai, L. & Stadtman, E. R. Conversion of amino acid residues in proteins and amino acid homopolymers to carbonyl derivatives by metal-catalyzed oxidation reactions. *J. Biol. Chem.* **264**, 3341–3346 (1989).
403. Yu, S. S. *et al.* Physiologically relevant oxidative degradation of oligo(proline) cross-linked polymeric scaffolds. *Biomacromolecules* **12**, 4357–4366 (2011).

404. Tapeinos, C. & Pandit, A. Physical, Chemical, and Biological Structures based on ROS-Sensitive Moieties that are Able to Respond to Oxidative Microenvironments. *Advanced Materials* **28**, 5553–5585 (2016).
405. Lee, S. H. *et al.* ROS-cleavable proline oligomer crosslinking of polycaprolactone for pro-angiogenic host response. *J. Mater. Chem. B* **2**, 7109–7113 (2014).
406. Gupta, M. K. *et al.* Oligoproline-derived nanocarrier for dual stimuli-responsive gene delivery. *J. Mater. Chem. B* **3**, 7271–7280 (2015).
407. Zhang, H. *et al.* A strategy for high radioprotective activity via the assembly of the Pprl protein with a ROS-sensitive polymeric carrier. *J. Mater. Chem. B* **6**, 3297–3304 (2018).
408. Jana, S., Biswas, Y. & Mandal, T. K. Methionine-based cationic polypeptide/polypeptide block copolymer with triple-stimuli responsiveness: DNA polyplexation and phototriggered release. *Polym. Chem.* **9**, 1869–1884 (2018).
409. Tao, W. & He, Z. ROS-responsive drug delivery systems for biomedical applications. *Asian J. Pharm. Sci.* **13**, 101–112 (2018).
410. Loudet, A. & Burgess, K. BODIPY Dyes and Their Derivatives: Syntheses and Spectroscopic Properties. *Chem. Rev.* **107**, 4891–4932 (2007).
411. Boens, N., Leen, V. & Dehaen, W. Fluorescent indicators based on BODIPY. *Chem. Soc. Rev.* **41**, 1130–1172 (2012).
412. Kowada, T., Maeda, H. & Kikuchi, K. BODIPY-based probes for the fluorescence imaging of biomolecules in living cells. *Chem. Soc. Rev.* **44**, 4953–4972 (2015).
413. Wang, Q., Wei, X., Li, C. & Xie, Y. A novel p -aminophenylthio- and cyano- substituted BODIPY as a fluorescence turn-on probe for distinguishing cysteine and homocysteine from glutathione. *Dye. Pigment.* **148**, 212–218 (2018).
414. Magagnano, G. *et al.* Photocatalytic ATRA reaction promoted by iodo-Bodipy and sodium ascorbate. *Chem. Commun.* **53**, 1591–1594 (2017).
415. Duret, G., Quinlan, R., Bissere, P. & Blanchard, N. Boron chemistry in a new light. *Chem. Sci.* **6**, 5366–5382 (2015).
416. Turksoy, A., Yildiz, D. & Akkaya, E. U. Photosensitization and controlled photosensitization with BODIPY dyes. *Coord. Chem. Rev.* **379**, 47–64 (2019).
417. Xu, L. *et al.* Strategic Construction of Directly Linked Porphyrin-BODIPY Hybrids. *Angew.*

- Chemie* **129**, 12490–12494 (2017).
418. Yin, B. *et al.* Porphyrin–Azobenzene–Bodipy Triads: Syntheses, Structures, and Photophysical Properties. *Org. Lett.* **19**, 2654–2657 (2017).
419. Dénès, F., Pichowicz, M., Povie, G. & Renaud, P. Thiyl Radicals in Organic Synthesis. *Chem. Rev.* **114**, 2587–2693 (2014).
420. Ahangarpour, M., Kavianinia, I., Harris, P. W. R. & Brimble, M. A. Photo-induced radical thiol–ene chemistry: a versatile toolbox for peptide-based drug design. *Chem. Soc. Rev.* **50**, 898–944 (2021).
421. Studer, A. & Curran, D. P. Catalysis of Radical Reactions: A Radical Chemistry Perspective. *Angew. Chemie Int. Ed.* **55**, 58–102 (2016).
422. Ma, F., Zhou, L., Liu, Q., Li, C. & Xie, Y. Selective Photocatalysis Approach for Introducing ArS Units into BODIPYs through Thiyl Radicals. *Org. Lett.* **21**, 733–736 (2019).
423. Lv, F. *et al.* Transition-metal-free regioselective cross-coupling of BODIPYs with thiols. *Chem. Commun.* **55**, 1639–1642 (2019).
424. Lv, F. *et al.* Direct sulfonylation of BODIPY dyes with sodium sulfinates through oxidative radical hydrogen substitution at the  $\alpha$ -position. *Chem. Commun.* **56**, 15577–15580 (2020).
425. Scott, T. F., Schneider, A. D., Cook, W. D. & Bowman, C. N. Photoinduced Plasticity in Cross-Linked Polymers. *Science (80- )*. **308**, 1615–1617 (2005).
426. Kloxin, C. J., Scott, T. F. & Bowman, C. N. Stress Relaxation via Addition–Fragmentation Chain Transfer in a Thiol-ene Photopolymerization. *Macromolecules* **42**, 2551–2556 (2009).
427. Kloxin, C. J., Scott, T. F., Park, H. Y. & Bowman, C. N. Mechanophotopatterning on a Photoresponsive Elastomer. *Adv. Mater.* **23**, 1977–1981 (2011).
428. Gandavarapu, N. R., Azagarsamy, M. A. & Anseth, K. S. Photo-Click Living Strategy for Controlled, Reversible Exchange of Biochemical Ligands. *Adv. Mater.* **26**, 2521–2526 (2014).
429. Sun, S., Oliveira, B. L., Jiménez-Osés, G. & Bernardes, G. J. L. Radical-Mediated Thiol-Ene Strategy: Photoactivation of Thiol-Containing Drugs in Cancer Cells. *Angew. Chemie Int. Ed.* **57**, 15832–15835 (2018).
430. Nauser, T., Koppenol, W. H. & Schöneich, C. Protein thiyl radical reactions and product

- formation: a kinetic simulation. *Free Radic. Biol. Med.* **80**, 158–163 (2015).
431. Shieh, P., Hill, M. R., Zhang, W., Kristufek, S. L. & Johnson, J. A. Click Chemistry: Diverse (Bio)(macro)molecular and Material Function through Breaking Covalent Bonds. *Chem. Rev.* **121**, 7059–7121 (2021).
  432. Brantley, J. N., Wiggins, K. M. & Bielawski, C. W. Unclicking the Click: Mechanically Facilitated 1,3-Dipolar Cycloreversions. *Science (80-. )*. **333**, 1606–1609 (2011).
  433. Lin, S. *et al.* Redox-based reagents for chemoselective methionine bioconjugation. *Science (80-. )*. **355**, 597–602 (2017).
  434. Maruyama, K. & Kanai, M. Synthetic methodology-driven chemical protein modifications. *Chem. Lett.* **48**, 1421–1432 (2019).
  435. Kim, J. *et al.* Site-Selective Functionalization of Methionine Residues via Photoredox Catalysis. *J. Am. Chem. Soc.* **142**, 21260–21266 (2020).
  436. Christian, A. H. *et al.* A Physical Organic Approach to Tuning Reagents for Selective and Stable Methionine Bioconjugation. *J. Am. Chem. Soc.* **141**, 12657–12662 (2019).
  437. Elledge, S. K. *et al.* Systematic identification of engineered methionines and oxaziridines for efficient, stable, and site-specific antibody bioconjugation. *Proc. Natl. Acad. Sci.* **117**, 5733–5740 (2020).
  438. Ohata, J. *et al.* An Activity-Based Methionine Bioconjugation Approach to Developing Proximity-Activated Imaging Reporters. *ACS Cent. Sci.* **6**, 32–40 (2020).
  439. Lin, D. *et al.* Chemoselective Methionine Bioconjugation: Site-Selective Fluorine-18 Labeling of Proteins and Peptides. *Bioconjug. Chem.* **31**, 1908–1916 (2020).
  440. Kramer, J. R. & Deming, T. J. Preparation of multifunctional and multireactive polypeptides via methionine alkylation. *Biomacromolecules* **13**, 1719–1723 (2012).
  441. Hou, Z. *et al.* A Sulfonium Triggered Thiol-yne Reaction for Cysteine Modification. *J. Org. Chem.* **85**, 1698–1705 (2020).
  442. Ellis, B. S., Griffiths, G., Howes, P. D., Stirling, C. J. M. & Fishwick, B. R. Elimination and addition reactions. Part 28. Nucleophilic addition–displacement reactions with allenic sulphonium salts. *J. Chem. Soc., Perkin Trans. 1* 286–292 (1977). doi:10.1039/P19770000286
  443. Batty, J. W., Howes, P. D. & Stirling, C. J. M. Elimination–addition. Part XXI. Addition–

- dealkylation reactions of acetylenic sulphonium salts with oxygen, sulphur, and nitrogen nucleophiles. *J. Chem. Soc., Perkin Trans. 1* 59–65 (1973). doi:10.1039/P19730000059
444. Torres, M. J. *et al.* Modulation of the reactivity of the thiol of human serum albumin and its sulfenic derivative by fatty acids. *Arch. Biochem. Biophys.* **521**, 102–110 (2012).
445. Shiu, H. Y. *et al.* Electron-deficient alkynes as cleavable reagents for the modification of cysteine-containing peptides in aqueous medium. *Chem. - A Eur. J.* **15**, 3839–3850 (2009).
446. Rossi, R. *et al.* Blood glutathione disulfide: In vivo factor or in vitro artifact? *Clin. Chem.* **48**, 742–753 (2002).
447. Bennett, B. D. *et al.* Absolute metabolite concentrations and implied enzyme active site occupancy in *Escherichia coli*. *Nat. Chem. Biol.* **5**, 593–599 (2009).
448. Montero, D., Tachibana, C., Rahr Winther, J. & Appenzeller-Herzog, C. Intracellular glutathione pools are heterogeneously concentrated. *Redox Biol.* **1**, 508–513 (2013).
449. Taresco, V., Alexander, C., Singh, N. & Pearce, A. K. Stimuli-Responsive Prodrug Chemistries for Drug Delivery. *Adv. Ther.* **1**, 1800030 (2018).
450. Xie, A. *et al.* Stimuli-responsive prodrug-based cancer nanomedicine. *EBioMedicine* **56**, 102821 (2020).
451. Hu, J. *et al.* Recent advances in stimuli-responsive theranostic systems with aggregation-induced emission characteristics. *Aggregate* **2**, 48–65 (2021).
452. Hardy, M. *et al.* Detection and Characterization of Reactive Oxygen and Nitrogen Species in Biological Systems by Monitoring Species-Specific Products. *Antioxid. Redox Signal.* **28**, 1416–1432 (2018).
453. Eruslanov, E., K. Identification of ROS using DCFDA and flow-cytometry. *Oxidative Stress* // **24**, 6 (2010).
454. Catalog, T. & Violet, T. ThiolTracker™ Violet ( Glutathione Detection Reagent ). *Imaging* 1–6 (2008).
455. Radi, R. Peroxynitrite Reactions and Diffusion in Biology. *Chem. Res. Toxicol.* **11**, 720–721 (1998).
456. Radi, R. Peroxynitrite, a Stealthy Biological Oxidant. *J. Biol. Chem.* **288**, 26464–26472 (2013).
457. Oushiki, D. *et al.* Development and application of a near-infrared fluorescence probe for

- oxidative stress based on differential reactivity of linked cyanine dyes. *J. Am. Chem. Soc.* **132**, 2795–2801 (2010).
458. Jia, X. *et al.* FRET-Based Mito-Specific Fluorescent Probe for Ratiometric Detection and Imaging of Endogenous Peroxynitrite: Dyad of Cy3 and Cy5. *J. Am. Chem. Soc.* **138**, 10778–10781 (2016).
459. Prolo, C., Álvarez, M. N. & Radi, R. Peroxynitrite, a potent macrophage-derived oxidizing cytotoxin to combat invading pathogens. *BioFactors* **40**, 215–225 (2014).
460. Begum, R. *et al.* Molecular hydrogen protects against oxidative stress - induced RAW 264 . 7 macrophage cells through the activation of Nrf2 and inhibition of MAPK signaling pathway. *Mol. Cell. Toxicol.* **16**, 103–118 (2020).
461. Chanput, W., Mes, J. J. & Wichers, H. J. THP-1 cell line: An in vitro cell model for immune modulation approach. *Int. Immunopharmacol.* **23**, 37–45 (2014).
462. Nicholas, C. *et al.* Apigenin Blocks Lipopolysaccharide-Induced Lethality In Vivo and Proinflammatory Cytokines Expression by Inactivating NF- $\kappa$ B through the Suppression of p65 Phosphorylation. *J. Immunol.* **179**, 7121–7127 (2007).
463. Zhan, Z., Zhang, K., Zhang, L., Li, Q. & Lv, Y. Development of iridium(III) phosphorescent probe for hypochlorous acid detection in macrophages cells and cancer cells co-culture system and application in inflamed mouse model. *Sensors Actuators, B Chem.* **303**, (2020).
464. García-Mendoza, D., Han, B., Berg, H. J. H. J. & Brink, N. W. Cell-specific immune-modulation of cadmium on murine macrophages and mast cell lines in vitro. *J. Appl. Toxicol.* **39**, 992–1001 (2019).
465. Brown, D. M. *et al.* The effect of oxidative stress on macrophages and lung epithelial cells: The role of phosphodiesterases 1 and 4. *Toxicol. Lett.* **168**, 1–6 (2007).
466. Alvariño, R. *et al.* Evaluation of the Protective Effects of Sarains on H<sub>2</sub>O<sub>2</sub>-Induced Mitochondrial Dysfunction and Oxidative Stress in SH-SY5Y Neuroblastoma Cells. *Neurotox. Res.* **32**, 368–380 (2017).
467. Fan, J., Hu, M., Zhan, P. & Peng, X. Energy transfer cassettes based on organic fluorophores: construction and applications in ratiometric sensing. *Chem. Soc. Rev.* **42**, 29–43 (2013).
468. Massodi, I., Bidwell, G. L. & Raucher, D. Evaluation of cell penetrating peptides fused to

- elastin-like polypeptide for drug delivery. *J. Control. Release* **108**, 396–408 (2005).
469. Longoria-García, S., Sánchez-Domínguez, C. N. & Gallardo-Blanco, H. Recent applications of cell-penetrating peptide guidance of nanosystems in breast and prostate cancer (Review). *Oncol. Lett.* **23**, 103 (2022).
470. Yu, F., Li, P., Wang, B. & Han, K. Reversible Near-Infrared Fluorescent Probe Introducing Tellurium to Mimetic Glutathione Peroxidase for Monitoring the Redox Cycles between Peroxynitrite and Glutathione in Vivo. *J. Am. Chem. Soc.* **135**, 7674–7680 (2013).
471. Yu, F. *et al.* A near-IR reversible fluorescent probe modulated by selenium for monitoring peroxynitrite and imaging in living cells. *J. Am. Chem. Soc.* **133**, 11030–11033 (2011).
472. Wang, B., Yu, F., Li, P., Sun, X. & Han, K. A BODIPY fluorescence probe modulated by selenoxide spirocyclization reaction for peroxynitrite detection and imaging in living cells. *Dye. Pigment.* **96**, 383–390 (2013).
473. Koide, Y. *et al.* A reversible near-infrared fluorescence probe for reactive oxygen species based on Te-rhodamine. *Chem. Commun.* **48**, 3091–3093 (2012).
474. Sedgwick, A. C. *et al.* The development of a novel AND logic based fluorescence probe for the detection of peroxynitrite and GSH. *Chem. Sci.* **9**, 3672–3676 (2018).
475. Kim, J., Park, J., Lee, H., Choi, Y. & Kim, Y. A boronate-based fluorescent probe for the selective detection of cellular peroxynitrite. *Chem. Commun.* **50**, 9353–9356 (2014).
476. Zhou, X., Kwon, Y., Kim, G., Ryu, J. H. & Yoon, J. A ratiometric fluorescent probe based on a coumarin-hemicyanine scaffold for sensitive and selective detection of endogenous peroxynitrite. *Biosens. Bioelectron.* **64**, 285–291 (2015).
477. Zhan, Z., Liu, R., Chai, L., Dai, Y. & Lv, Y. Visualization of Lung Inflammation to Pulmonary Fibrosis via Peroxynitrite Fluctuation. *Anal. Chem.* **91**, 11461–11466 (2019).
478. Zhou, D.-Y. *et al.* A ratiometric fluorescent probe for the detection of peroxynitrite with simple synthesis and large emission shift and its application in cells image. *Dye. Pigment.* **161**, 288–295 (2019).
479. Yang, D., Wang, H. L., Sun, Z. N., Chung, N. W. & Shen, J. G. A highly selective fluorescent probe for the detection and imaging of peroxynitrite in living cells. *J. Am. Chem. Soc.* **128**, 6004–6005 (2006).
480. Sun, Q. *et al.* Ultrafast Detection of Peroxynitrite in Parkinson's Disease Models Using a

- Near-Infrared Fluorescent Probe. *Anal. Chem.* **92**, 4038–4045 (2020).
481. Shen, Y. *et al.* A fluorescent sensor for fast detection of peroxyxynitrite by removing of C=N in a benzothiazole derivative. *Anal. Chim. Acta* **1014**, 71–76 (2018).
482. Peng, T. *et al.* Molecular imaging of peroxyxynitrite with HKGreen-4 in live cells and tissues. *J. Am. Chem. Soc.* **136**, 11728–11734 (2014).
483. Woodcock, S. R., Bonacci, G., Gelhaus, S. L. & Schopfer, F. J. Nitrated fatty acids: synthesis and measurement. *Free Radic. Biol. Med.* **59**, 14–26 (2013).
484. Rubbo, H., Trostchansky, A. & O'Donnell, V. B. Peroxyxynitrite-mediated lipid oxidation and nitration: Mechanisms and consequences. *Arch. Biochem. Biophys.* **484**, 167–172 (2009).
485. Fazzari, M. *et al.* Endogenous generation of nitro-fatty acid hybrids having dual nitrate ester (RONO<sub>2</sub>) and nitroalkene (RNO<sub>2</sub>) substituents. *Redox Biol.* **41**, 101913 (2021).
486. Cheng, D. *et al.* Selective Visualization of the Endogenous Peroxyxynitrite in an Inflamed Mouse Model by a Mitochondria-Targetable Two-Photon Ratiometric Fluorescent Probe. *J. Am. Chem. Soc.* **139**, 285–292 (2017).
487. Demchenko, A. P. The Concept of  $\lambda$ -Ratiometry in Fluorescence Sensing and Imaging. *J. Fluoresc.* **20**, 1099–1128 (2010).
488. Huang, C. *et al.* Selective and Ratiometric Fluorescent Trapping and Quantification of Protein Vicinal Dithiols and in Situ Dynamic Tracing in Living Cells. *J. Am. Chem. Soc.* **136**, 14237–14244 (2014).
489. Zhai, Q., Yang, S., Fang, Y., Zhang, H. & Feng, G. A new ratiometric fluorescent probe for the detection of thiophenols. *RSC Adv.* **5**, 94216–94221 (2015).
490. Rios, N. *et al.* Sensitive detection and estimation of cell-derived peroxyxynitrite fluxes using fluorescein-boronate. *Free Radic. Biol. Med.* **101**, 284–295 (2016).

### 6.1 APPENDIX I: Supplementary Information of Article 1

#### **Consecutive alkylation, “Click”, and “Clip” reactions for the traceless methionine-based conjugation and release of methionine-containing peptides**

Fatemeh Zare<sup>1</sup>, Alessandro Potenza<sup>2</sup>, Andrea A Greschner<sup>1</sup>, Marc A Gauthier<sup>1,2,\*</sup>

<sup>1</sup> Institut National de la Recherche Scientifique (INRS), EMT Research Center, Varennes, Canada

<sup>2</sup> Swiss Federal Institute of Technology Zurich (ETHZ), Department of Chemistry and Applied Biosciences, Institute of Pharmaceutical Sciences, Zurich, Switzerland

#### **Corresponding author:**

Marc A. Gauthier

Institut National de la Recherche Scientifique (INRS), EMT Research Center, 1650 boul. Lionel-Boulet, Varennes, J3X 1P7, Canada

E-mail: gauthier@emt.inrs.ca

Telephone: +1 514 228 69 32

Fax: +1 450 929 81 02

#### **Author contributions:**

FZ carried out most experiments, responsible for data collection, analysis as well as manuscript composition and revision.

AP contributed by carrying out the data collection and analysis of some experiments, including the preparation of fluorescent peptide (Rho)FPAMAG, bioconjugation of (Rho)FPAMAG and human serum albumin, modification of FPAMAG by 1-bromo-2-butyne, and measuring the stability of 1b-gsh bioconjugates in the presence of 10 mM cysteine.

AAG contributed to manuscript writing and revision.

MAG was the supervisory author and involved with the designing the experiments, concept formation, manuscript composition and revision.

*Note: The work of this chapter is published in the ‘Biomacromolecules’. June 7, 2022. DOI: 10.1021/acs.biomac.2c00357*

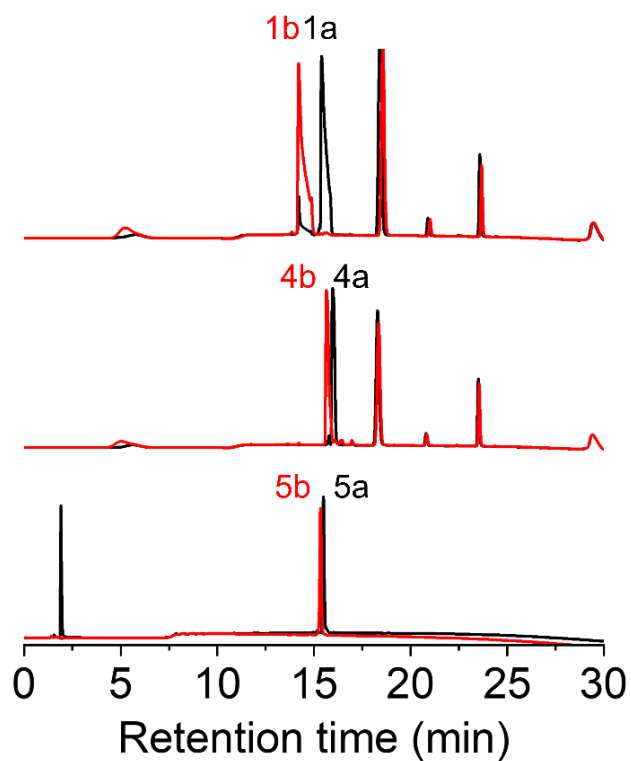


**Figure S1.** Full chromatograms (absorbance at 214 nm) presented in Figure 2.2b of the main manuscript. Representative chromatograms used to monitor the progress of the alkylation of methionine-containing peptides 1a, 4a, and 5a by propargyl bromide into 1b, 4b, and 5b, respectively. Unidentified peaks relate to propargyl bromide and trace solvents in the crude reaction mixtures. Black and red chromatograms represent the samples at 0 and 24 h of the reaction, respectively.

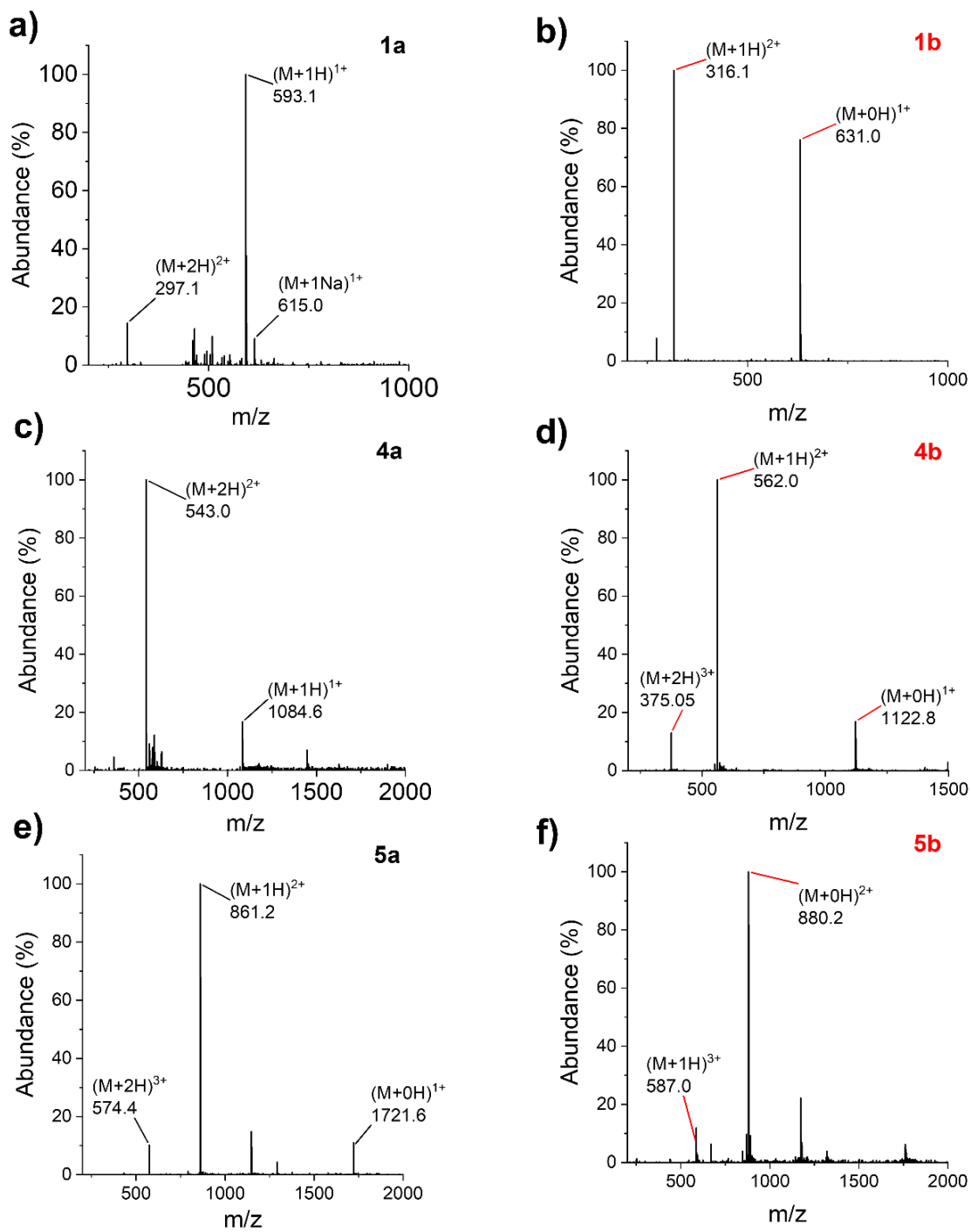
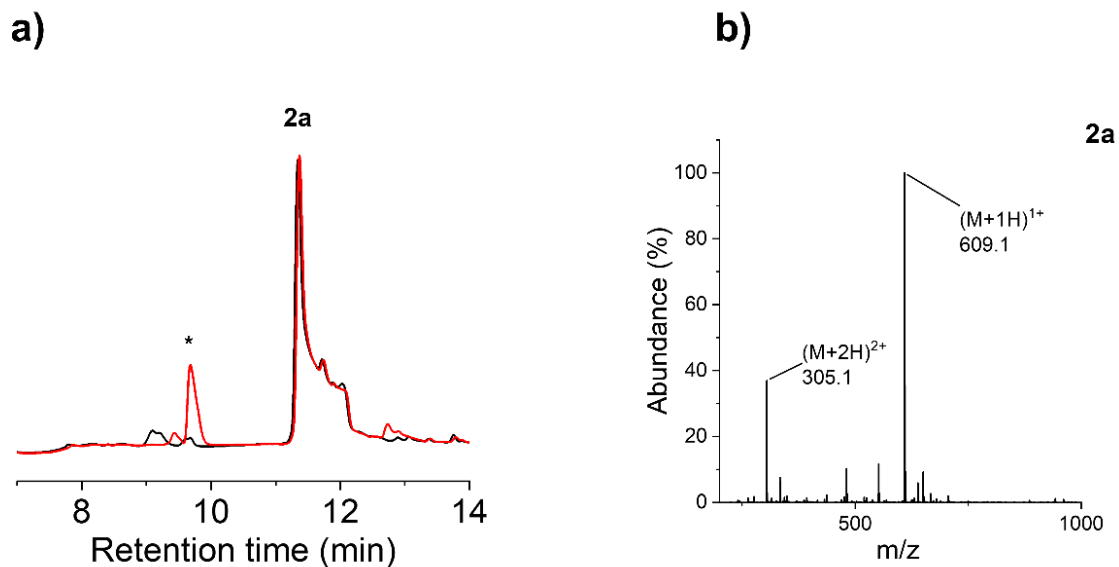
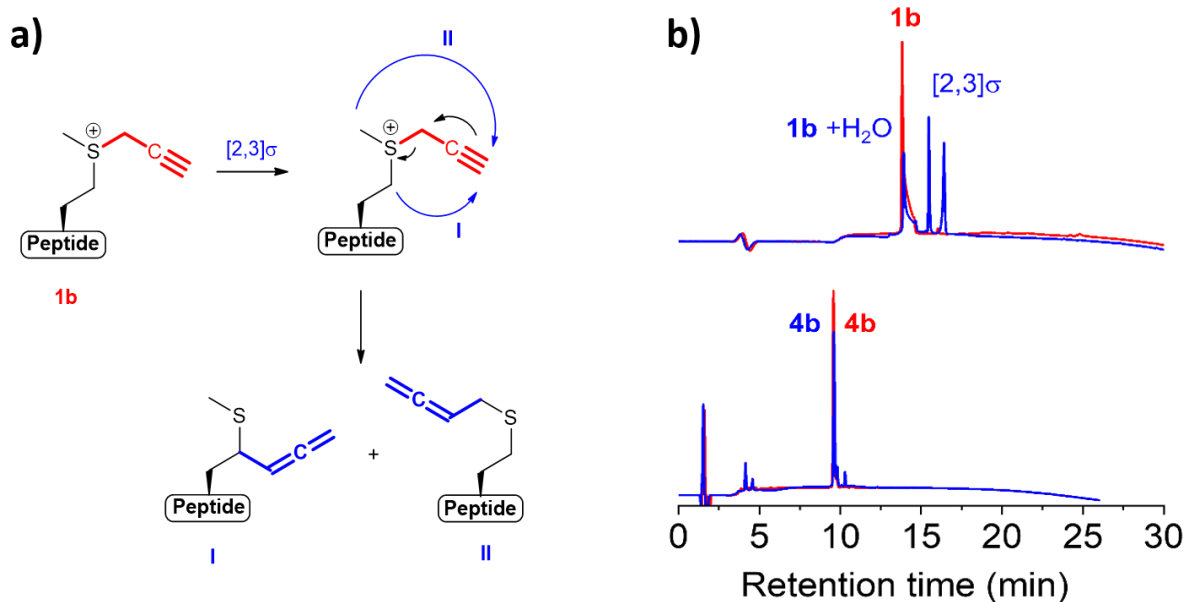


Figure S2. Mass spectra of conjugates presented in Figure S1 and Figure 2.2b of the main manuscript.



**Figure S3.** Alkylation of 2a by propargyl bromide. (a) Representative chromatograms (absorbance at 214 nm) showing that no changes in the intensity of the peak of 2a was observed over a 24 h period. Lack of reactivity was associated to the absence of thioether in 2a, for which the side-chain of methionine is present as a sulfoxide. Black and red chromatograms represent the samples at 0 and 24 h of the reaction, respectively. \* Relates to propargyl bromide and trace solvents in the crude reaction mixtures. (b) Mass spectra of 2a.



**Figure S4.** Stability of sulfonium activated allene in aqueous media pH 7.4. (a) Mechanism of [2,3] sigmatropic rearrangement of 1b presented in Figure 2.2a of the main manuscript. (b) Full chromatograms (absorbance at 214 nm) presented in Figure 2.2c of the main manuscript. Prolonged incubation of 1b and 4b at near-neutral pH resulted in hydration and [2,3]-sigmatropic rearrangement. Red and blue chromatograms represent the samples at 0 and 15 h, respectively.

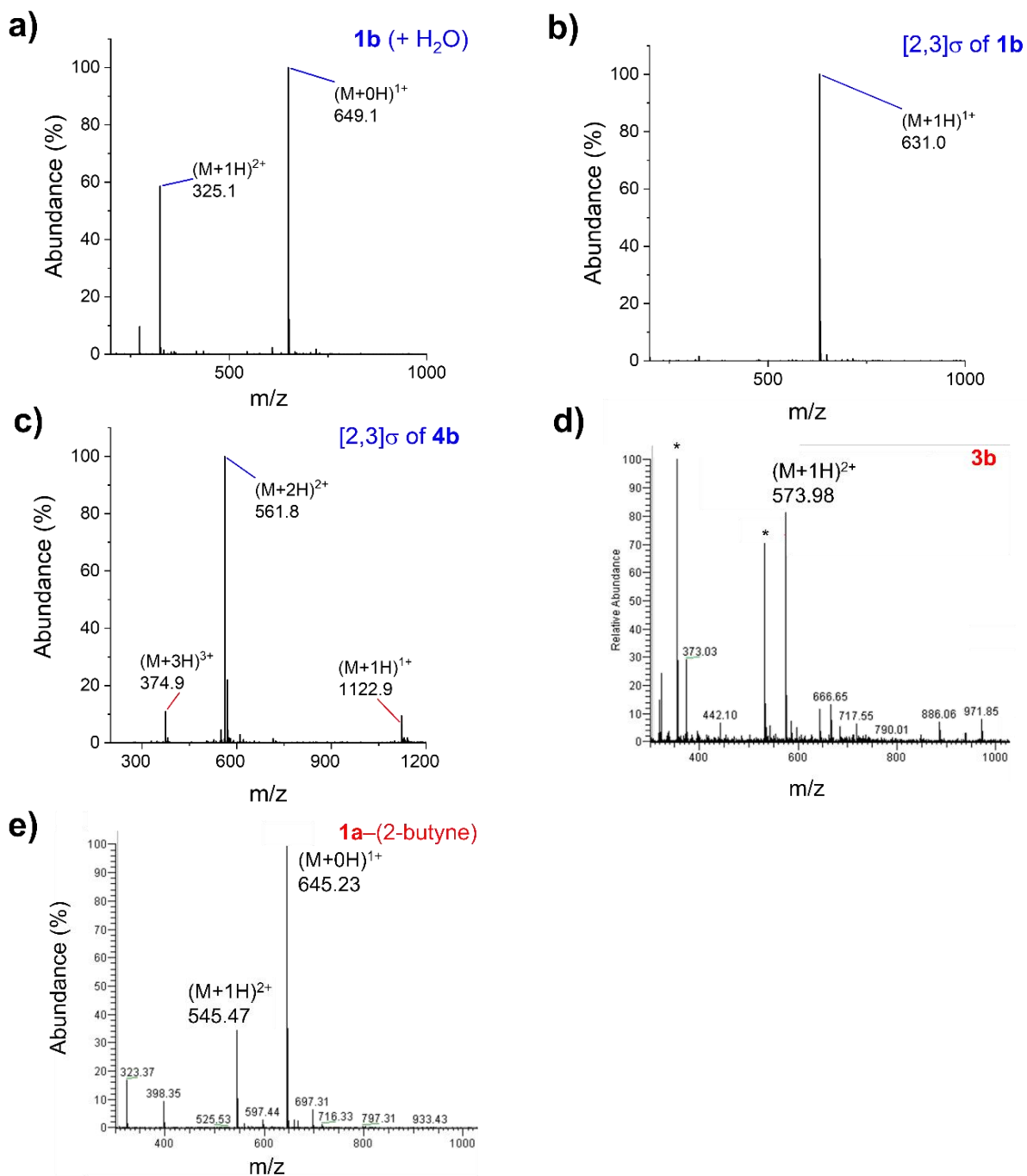


**Figure S5.** Mass spectra of oxidized and alkylated peptides. Mass spectra of hydration and [2,3]σ products of 1b, 2a, [2,3]σ product of 4b, 1a-(2-butyne), and 3b.

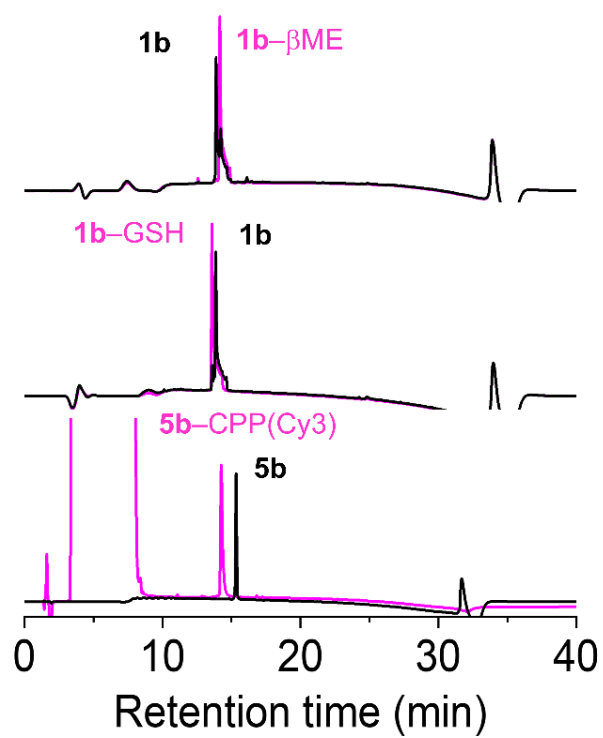


**Figure S6.** Full chromatograms (absorbance at 214 nm) presented in Figure 2.3b of the main manuscript. Representative chromatograms used to monitor the reaction of allenic peptides of 1b and 5b with thiols proceeds with high conversion and without side-reaction.

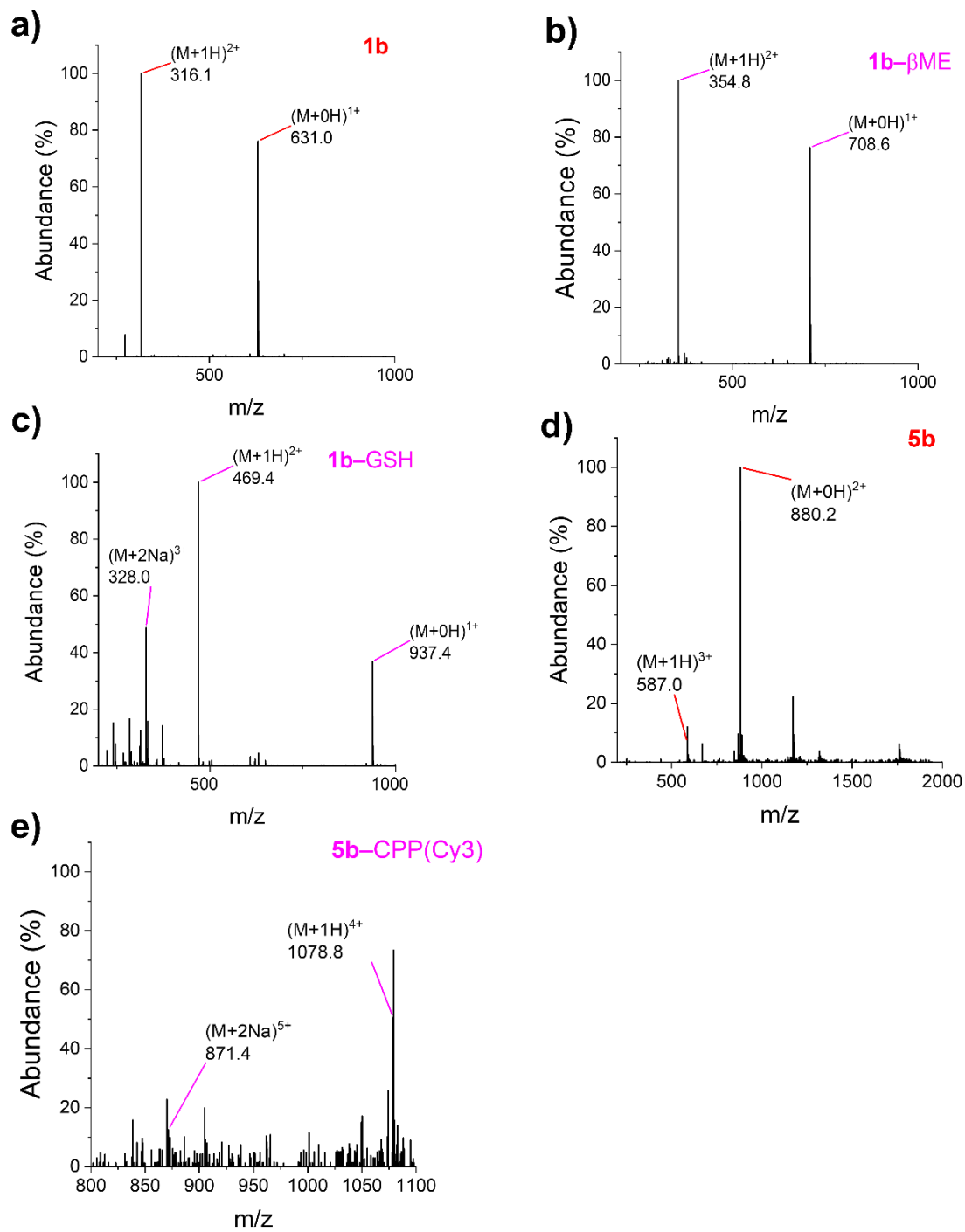


**Figure S7.** Mass spectra of conjugates presented in Figure S6 and Figure 2.3b of the main manuscript.

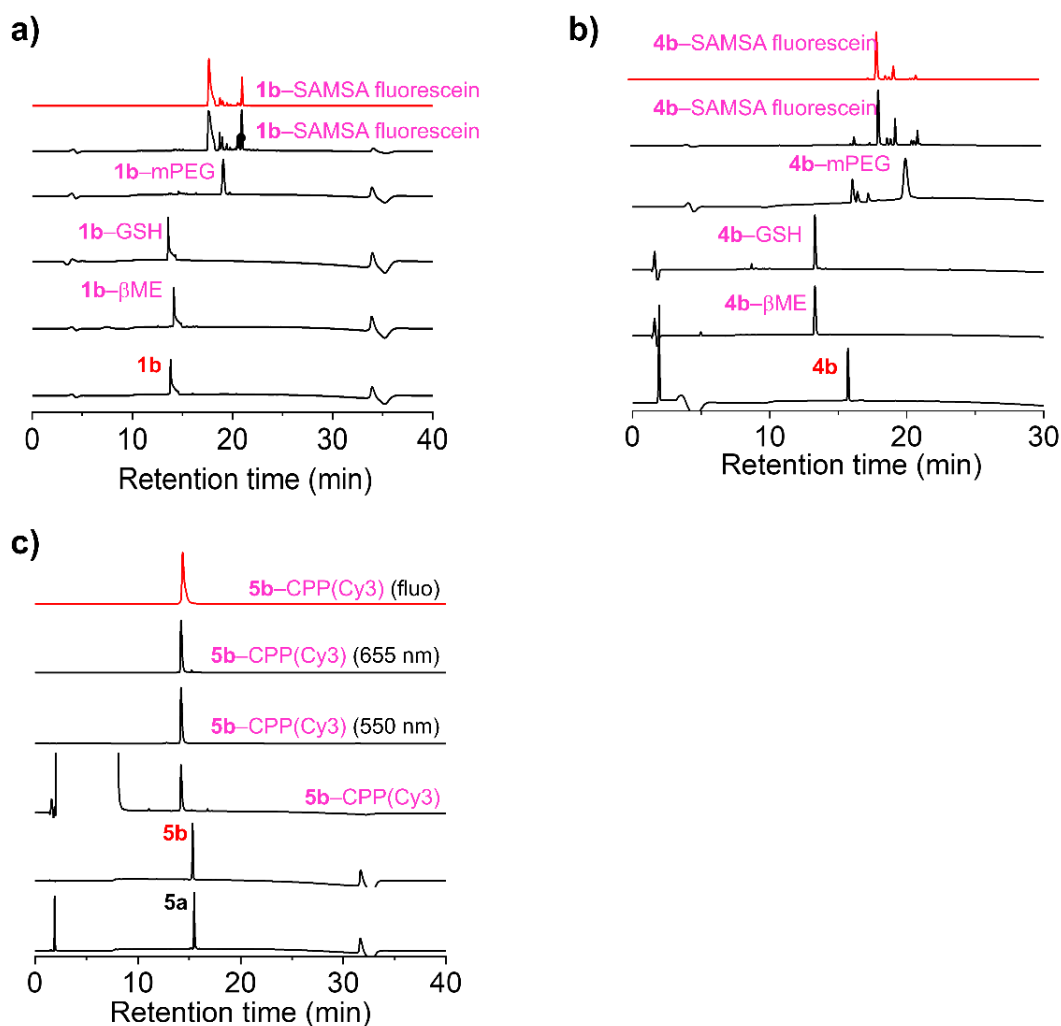


**Figure S8.** Full chromatograms of 1b, 4b, 5b and their bioconjugates produced by the nucleophilic thiol–allene reaction. (a) Representative full HPLC chromatograms of 1b– $\beta$ ME, 1b–GSH, 1b–mPEG, and 1b–SAMSA fluorescein (black: absorbance at 214 nm; red: fluorescence  $\lambda_{ex}/\lambda_{em}$  490/520 nm) produced by the thiol–allene click reaction at pH 7.4. Extra peaks in the chromatograms of 1b–SAMSA fluorescein correspond to unreacted SAMSA fluorescein present in the crude reaction mixture. (b) Representative full HPLC chromatograms of 4b, 4b– $\beta$ ME, 4b–GSH, 4b–mPEG, and 4b–SAMSA fluorescein (black: absorbance at 214 nm; red: fluorescence  $\lambda_{ex}/\lambda_{em}$  490/520 nm) produced by the thiol–allene click reaction at pH 7.4. Extra peaks in the chromatograms of 4b–SAMSA fluorescein correspond to unreacted SAMSA fluorescein present in the crude reaction mixture. (c) Representative full HPLC chromatograms (Black: absorbance at 214 nm unless otherwise indicated; Red: Fluorescence  $\lambda_{ex}/\lambda_{em}$  550/655 nm (FRET between Cy3/Cy5)). Large peak that saturates the detector (0–8 min) in the chromatogram of 5b–CPP(Cy3) is from DMF in the sample.

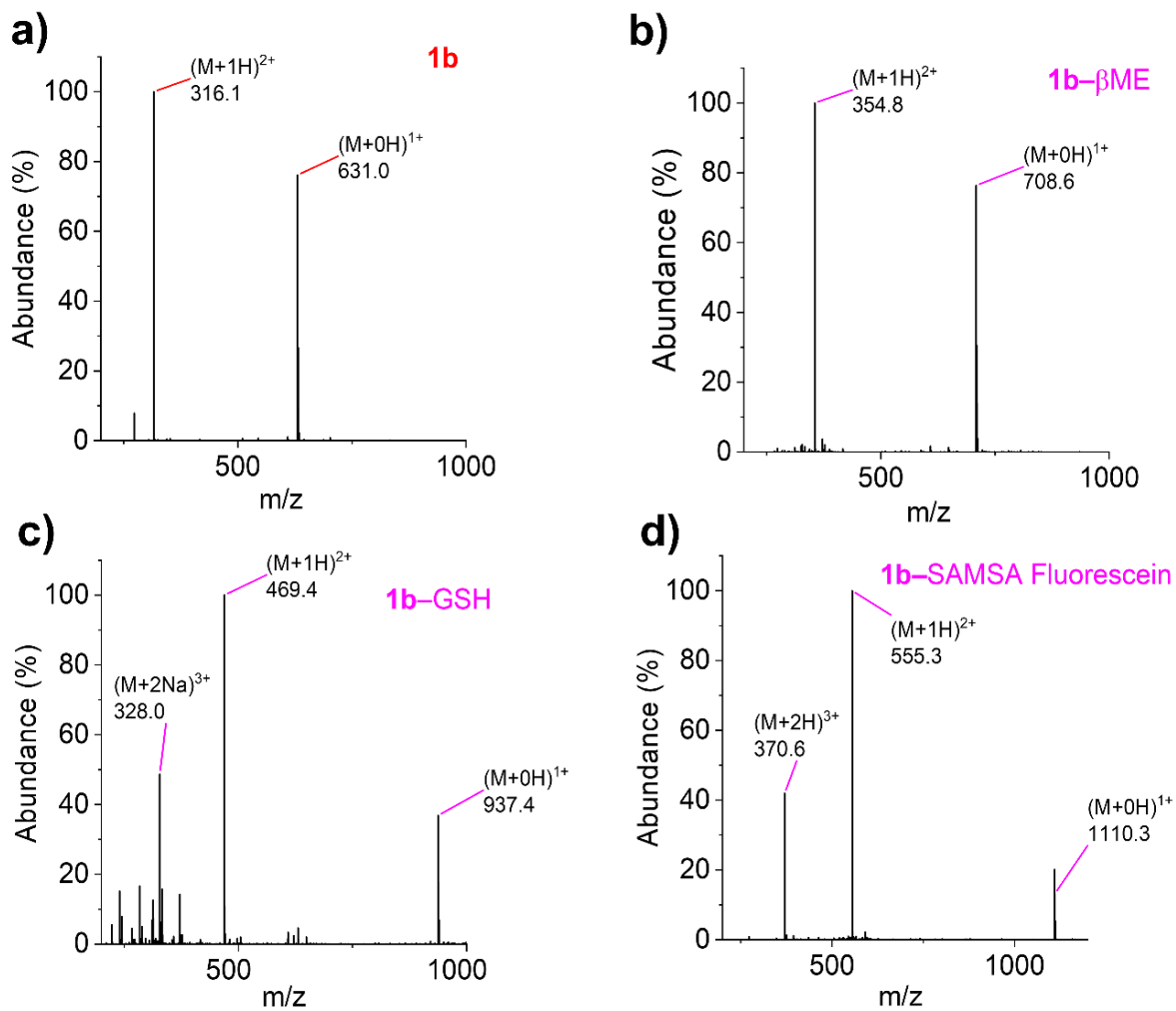


Figure S9. Mass spectra of conjugates presented in Figure S8a.

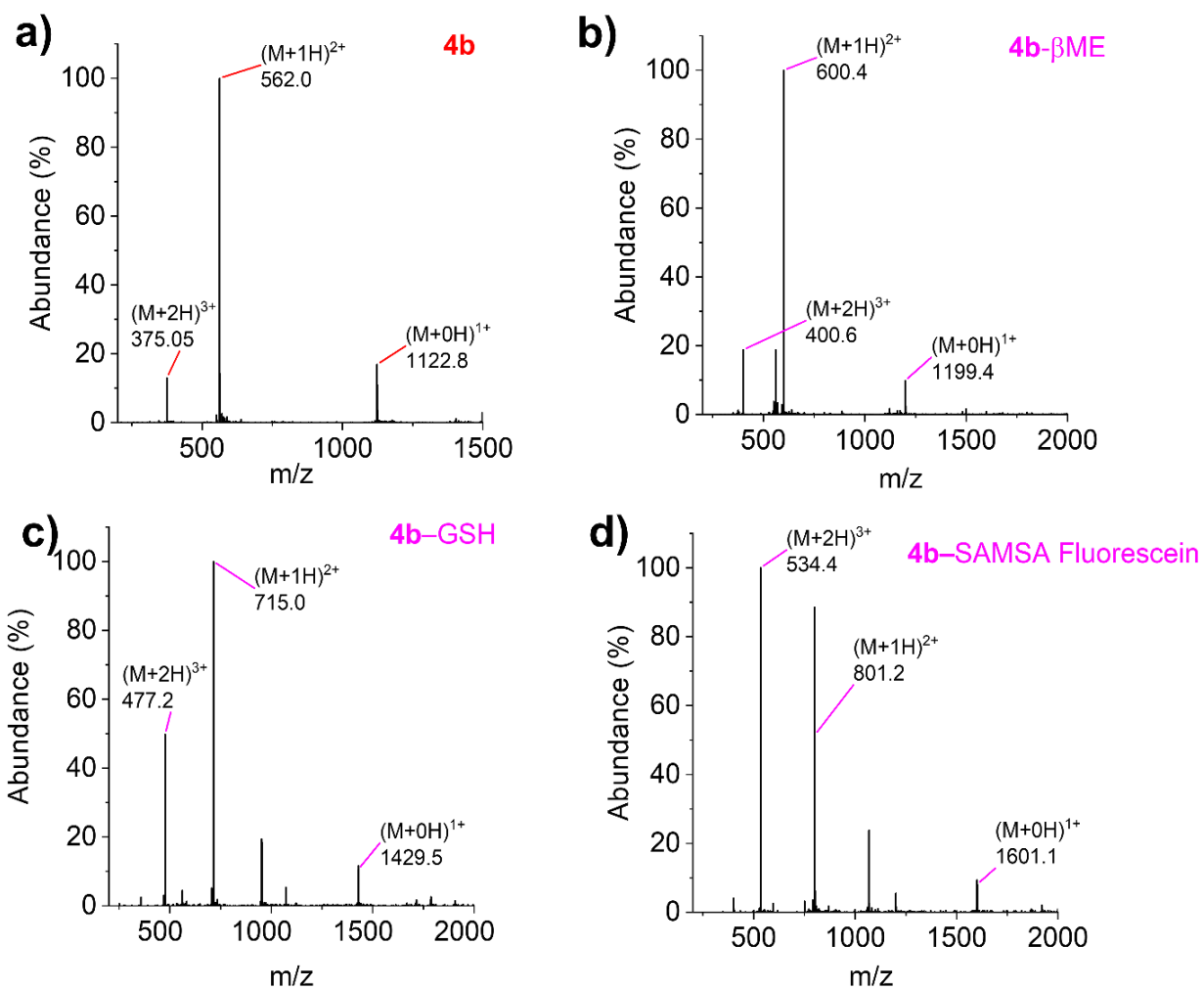


Figure S10. Mass spectra of conjugates presented in Figure S8b.

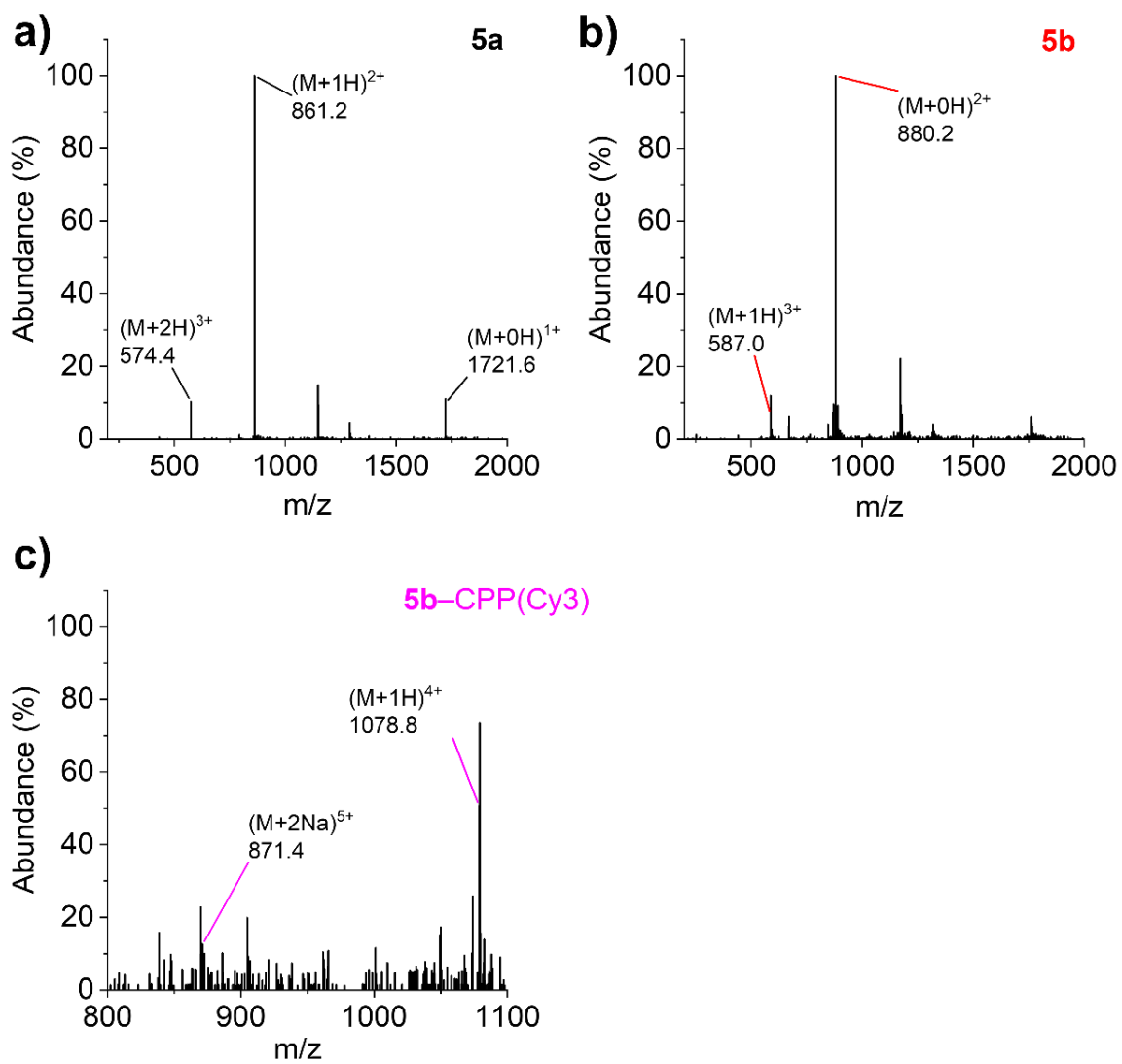
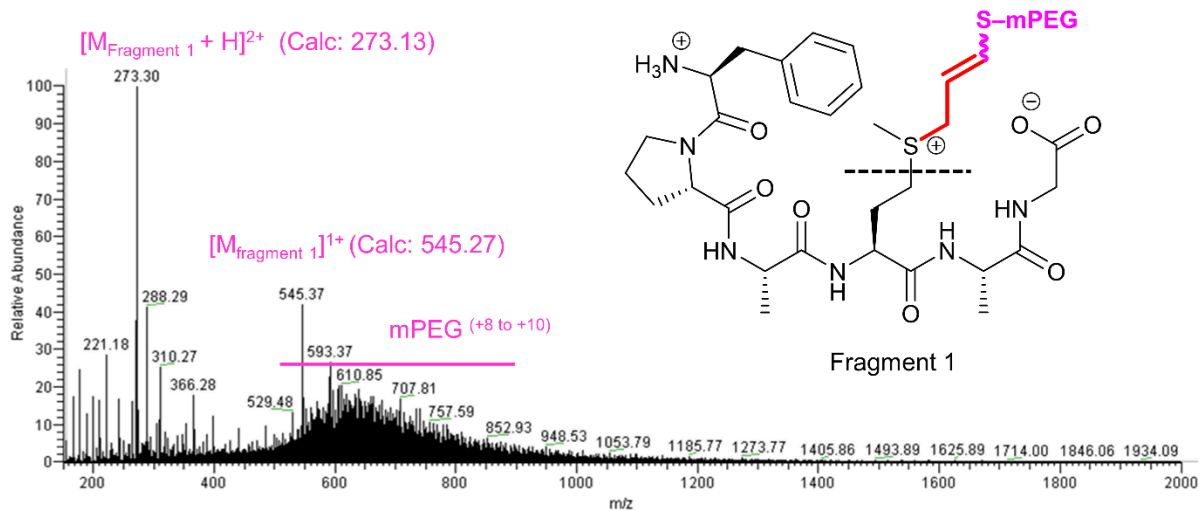
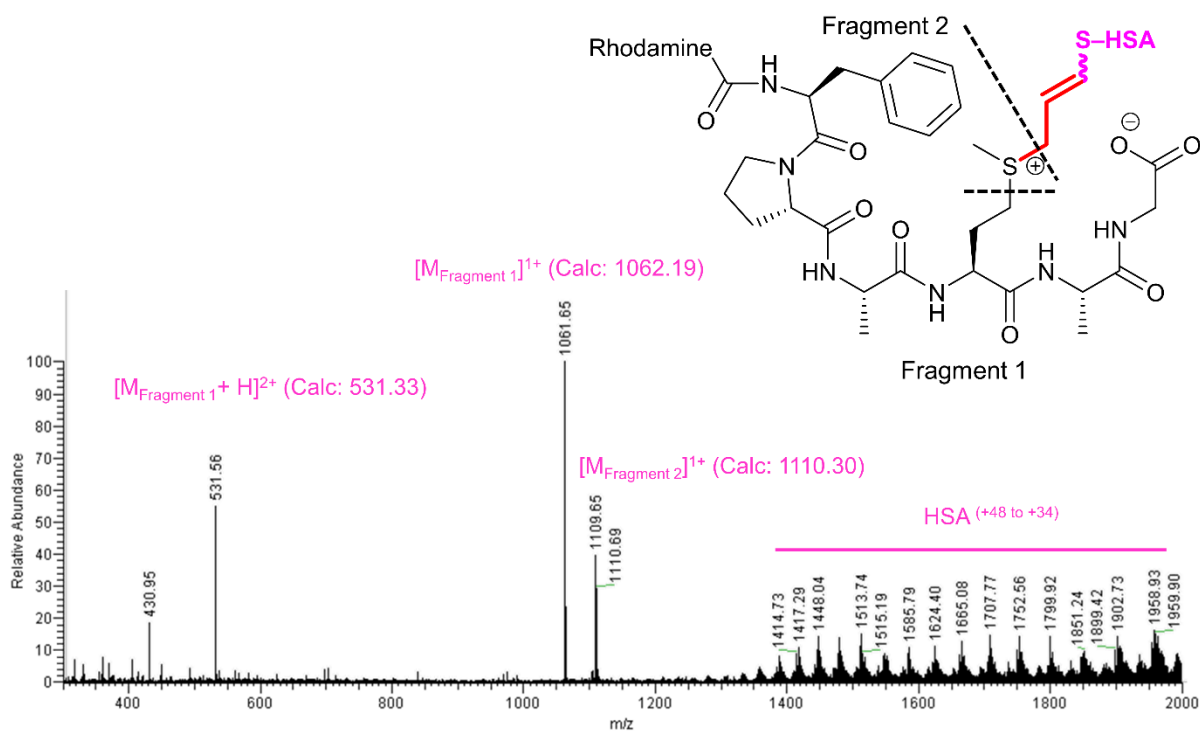


Figure S11. Mass spectra of conjugates presented in Figure S8c.



**Figure S12.** Mass spectrum of purified 1b-mPEG. This spectrum was acquired with a Thermo Scientific LTQ XL linear ion trap mass spectrometer and illustrates a broad series of peaks between m/z 500–1000 associated with the mPEG component of the bioconjugate, as well as peaks associated with fragmentation of the sulfonium and release of a truncated form of 3b (structure shown in inset).



**Figure S13.** The mass spectra of 3b-HSA. 3b-HSA cannot be identified directly due to fragmentation of the sulfonium salt. However, the sulfonium fragmentation  $M_{\text{Fragment 1}}$  and  $M_{\text{Fragment 2}}$  of 3b-HSA are distinguishable.

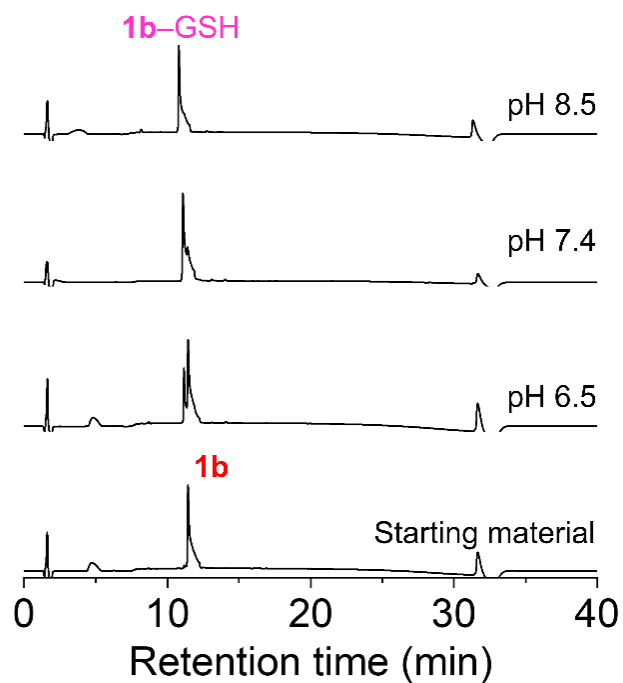


Figure S14. Full chromatograms of 1b and 1b-containing bioconjugates produced by the nucleophilic thiol–allene reaction. HPLC chromatograms (absorbance at 214 nm) of 1b, and 1b reacting with 1.1 molar eq. of GSH for 90 min at pH 6.5, 7.4, and 8.5, illustrating that the reaction is faster by basification.

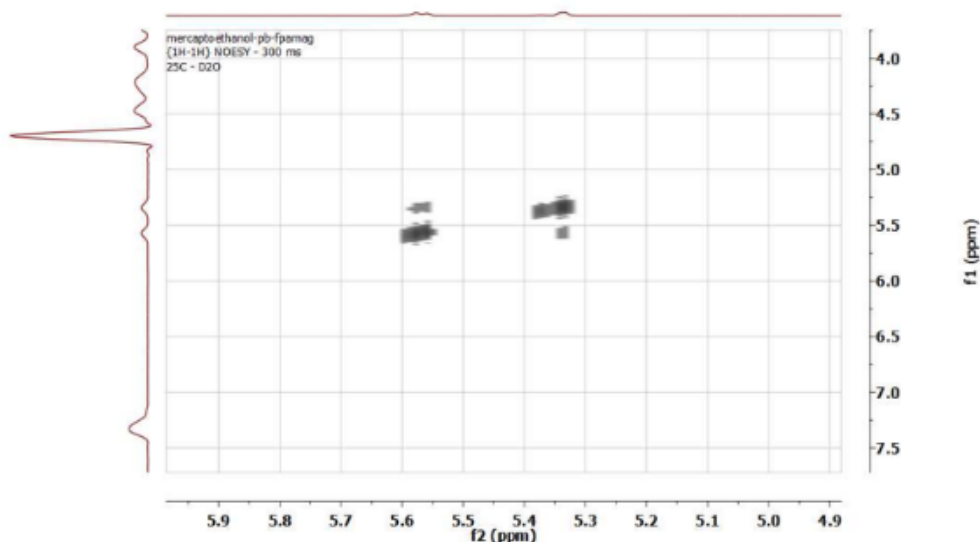
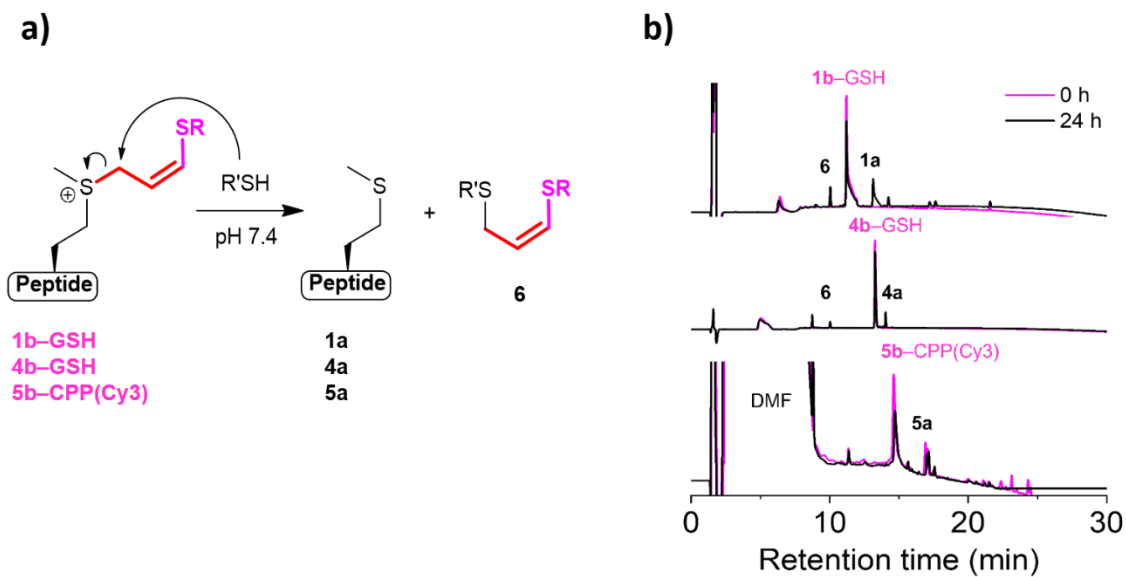


Figure S15.  $^1\text{H}$ - $^1\text{H}$  Nuclear Overhauser Effect spectrum spectra of 1b- $\beta$ ME showing correlation between protons  $H_j$  and  $H_k$  (Figure 2.3, main manuscript).



**Figure S16.** Stability of bioconjugates toward nucleophilic substitution. (a) The mechanism of the reaction presented in Figure 2.4a of the main manuscript. (b) Full chromatograms (absorbance at 214 nm) presented in Figure 2.4b of the main manuscript. Unidentified peaks relate to GSH, oxidized GSH, and trace solvents/impurities in the crude reaction mixtures.

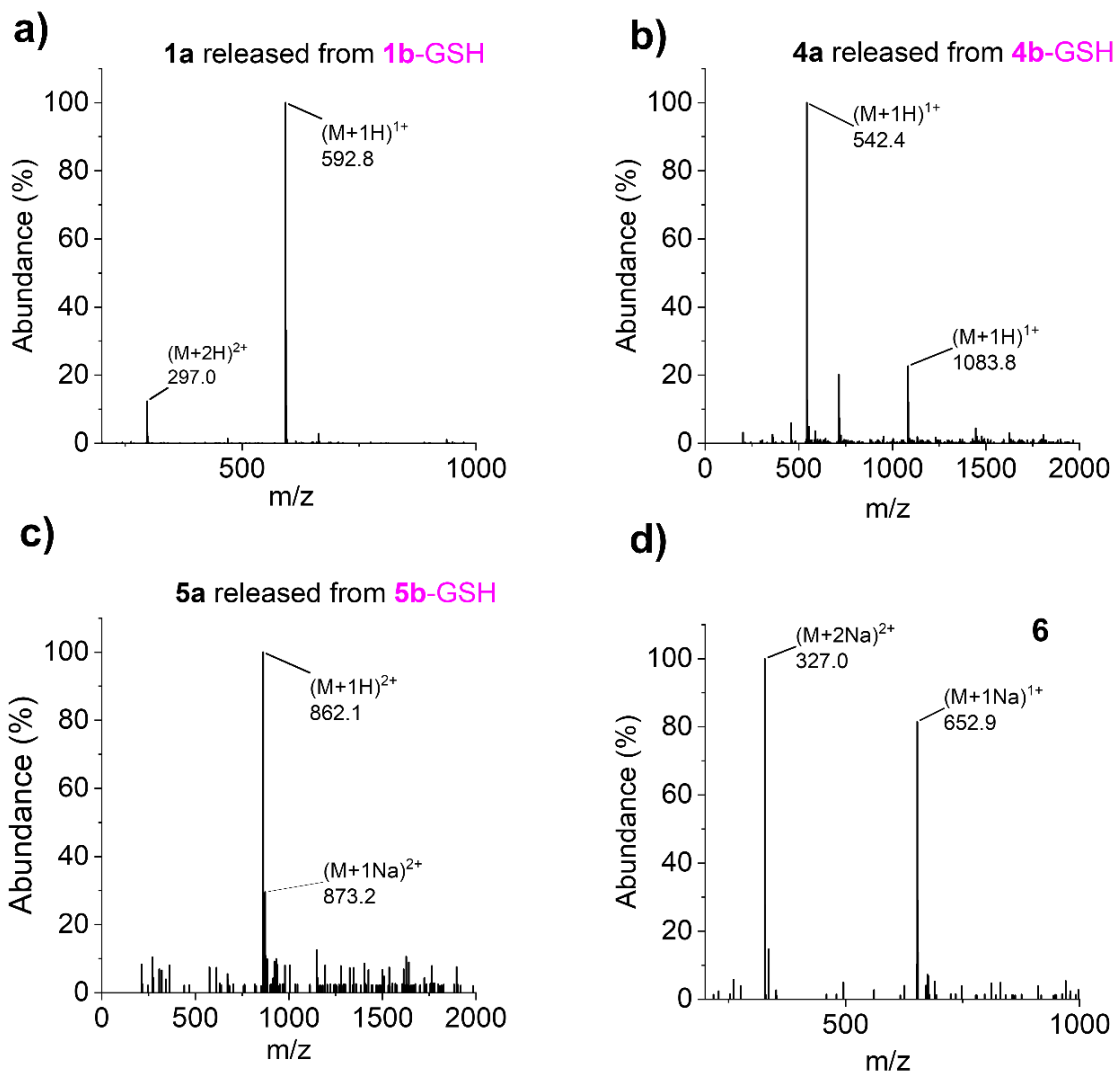
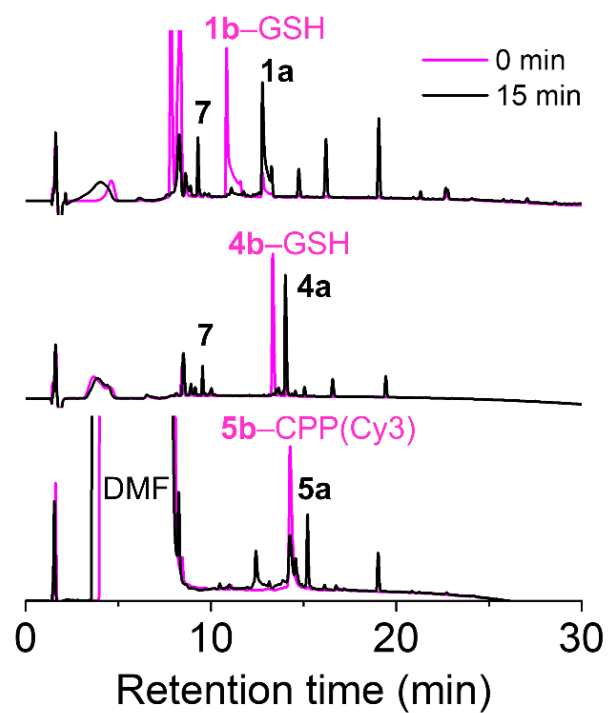


Figure S17. Mass spectra of conjugates presented in Figure S16.



**Figure S18.** Full chromatograms (absorbance at 214 nm) presented in Figure 2.4d of the main manuscript. Unidentified peaks relate to GSH, oxidized GSH, photoinitiators, compounds released by activation of the photoinitiator, and trace solvents/impurities in the crude reaction mixtures.

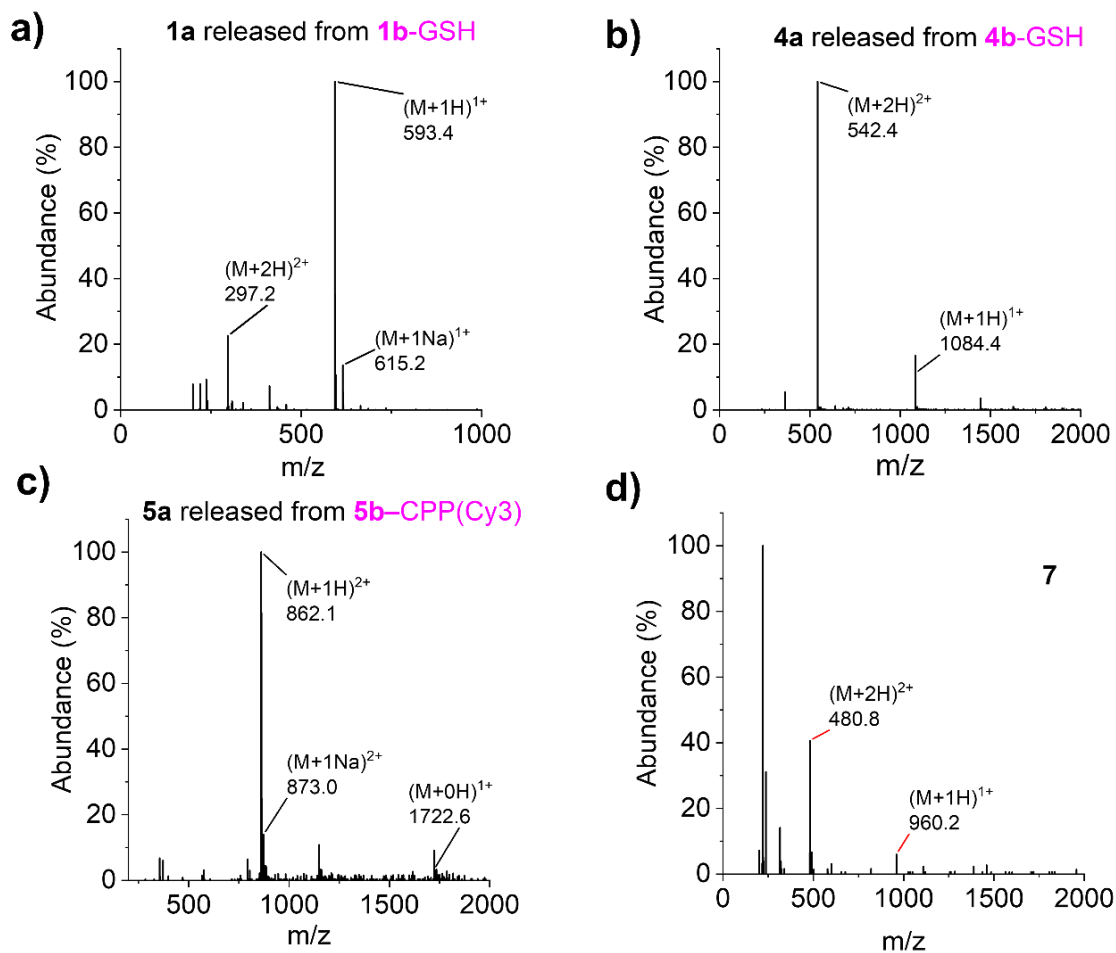


Figure S19. Mass spectra of conjugates presented in Figure S18.

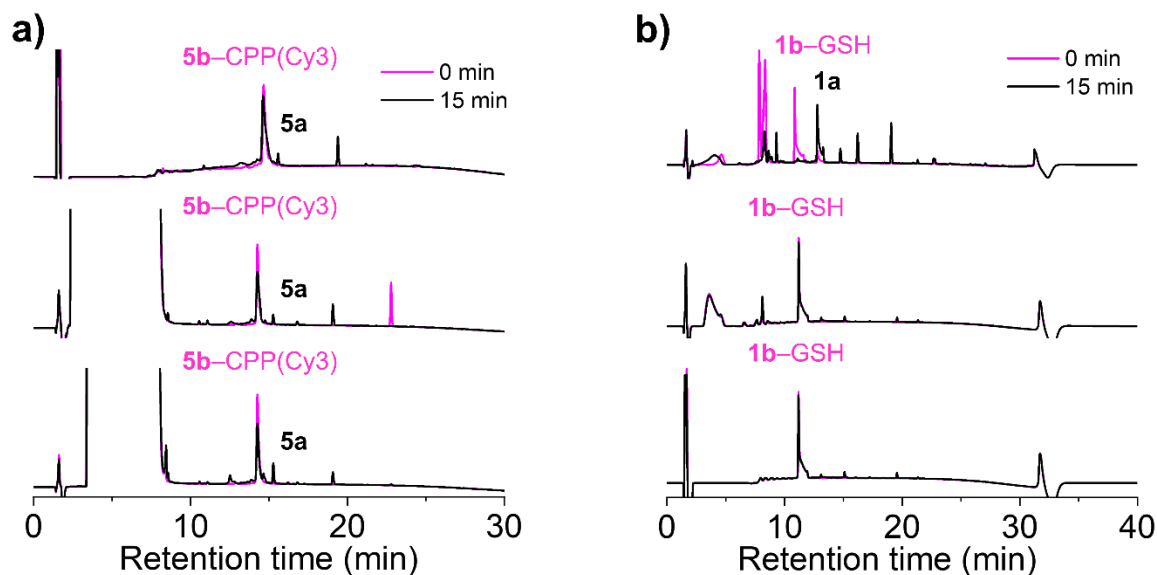


Figure S20. (a) HPLC chromatograms of Clip radical thiol-ene addition of GSH (10 eq.) to 5b-CPP(Cy3) in the presence of 1.5 eq. DMPA. From top to bottom, the concentration of 5b-CPP(Cy3): 0.1 mg·mL<sup>-1</sup>; 0.3 mg·mL<sup>-1</sup>; 0.8 mg·mL<sup>-1</sup>. (b) Clip of 1b-GSH by radical thiol-ene addition in the presence of different concentrations of GSH and DMPA. From top to bottom: 10 eq. GSH and 1.5 eq. DMPA; 10 eq. GSH and 0.1 eq. DMPA; 1.1 eq. GSH and 0.1 eq. DMPA.

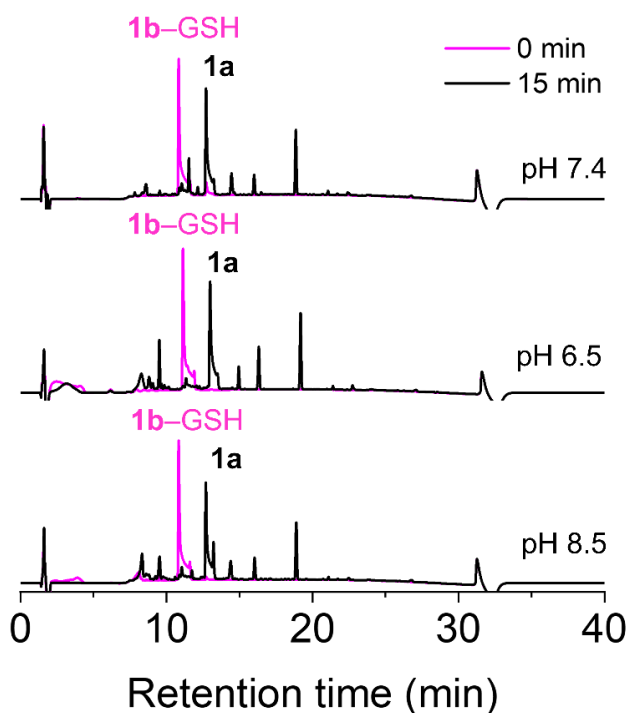
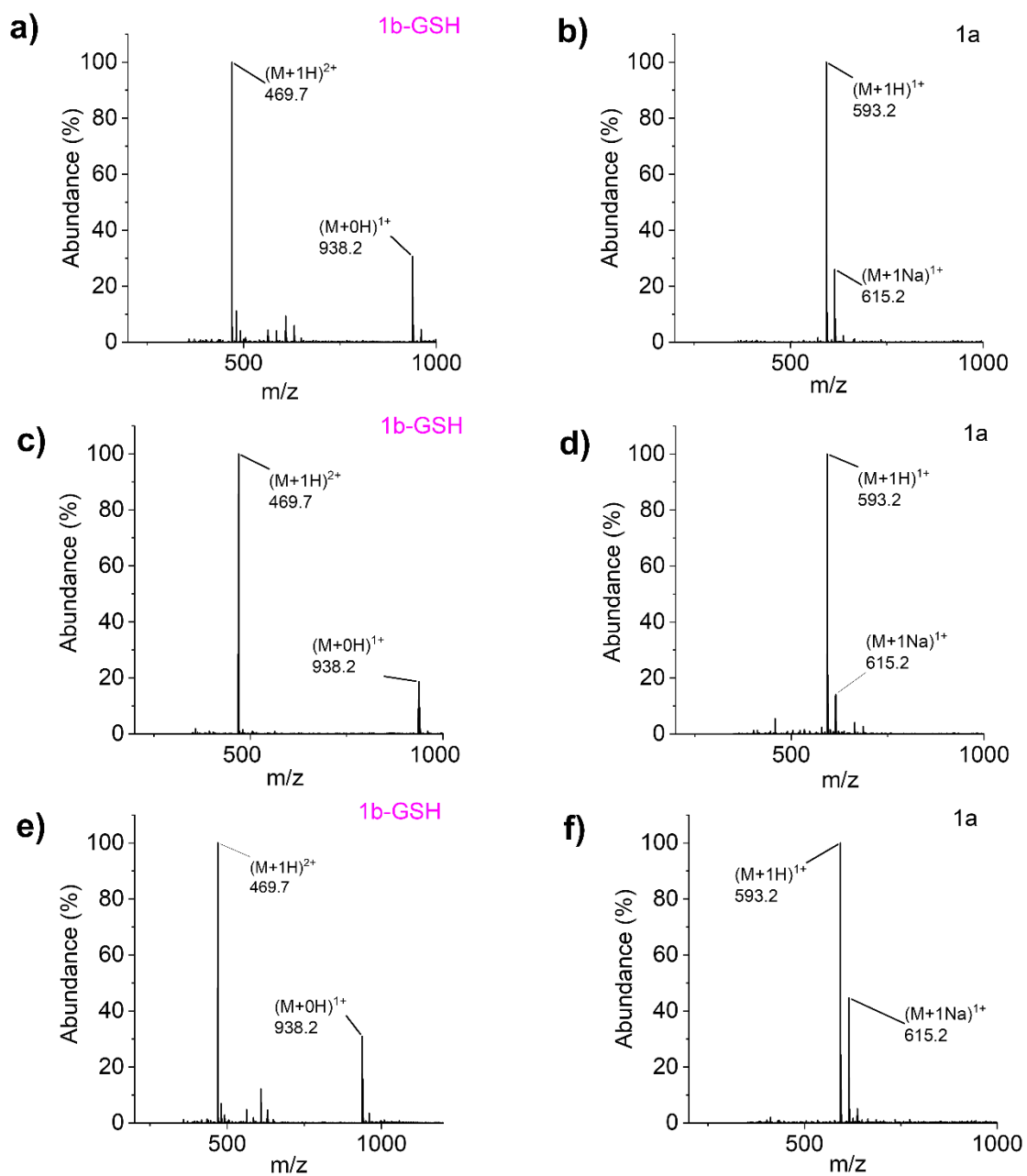
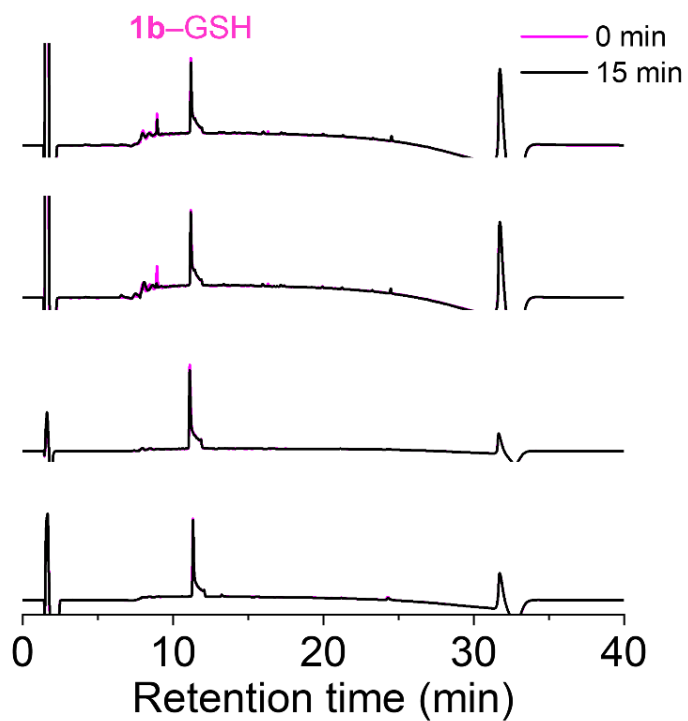


Figure S21. HPLC chromatograms of Clip radical thiol-ene addition of 10 molar eq. of thiols (cysteine or GSH) to 1b-GSH in the presence of 1.5 eq. DMPA at different pH. From top to bottom: Cysteine at pH 7.4; GSH at pH 6.5; GSH at pH 8.5.



**Figure S22.** Mass spectra of conjugates presented in Figure S21. (a,c,e) The mass spectra of 1b-GSH before UV irradiation and (b,d,e) The mass spectra of 1a after 15 min UV irradiation at pH 7.4, 6.5, and 8.5, respectively.



**Figure S23.** Clip radical thiol–ene addition of GSH to 1b–GSH and GSH, in the presence/absence of H<sub>2</sub>O<sub>2</sub> and presence/absence of UV light. Representative full chromatograms (absorbance at 214 nm) illustrating that very little reaction occurs under these conditions. From top to bottom: 10 eq. H<sub>2</sub>O<sub>2</sub>, 10 GSH, +UV; 10 eq. H<sub>2</sub>O<sub>2</sub>, 10 GSH, –UV; 10 eq. H<sub>2</sub>O<sub>2</sub>, –UV; 1.5 eq. H<sub>2</sub>O<sub>2</sub>, –UV.

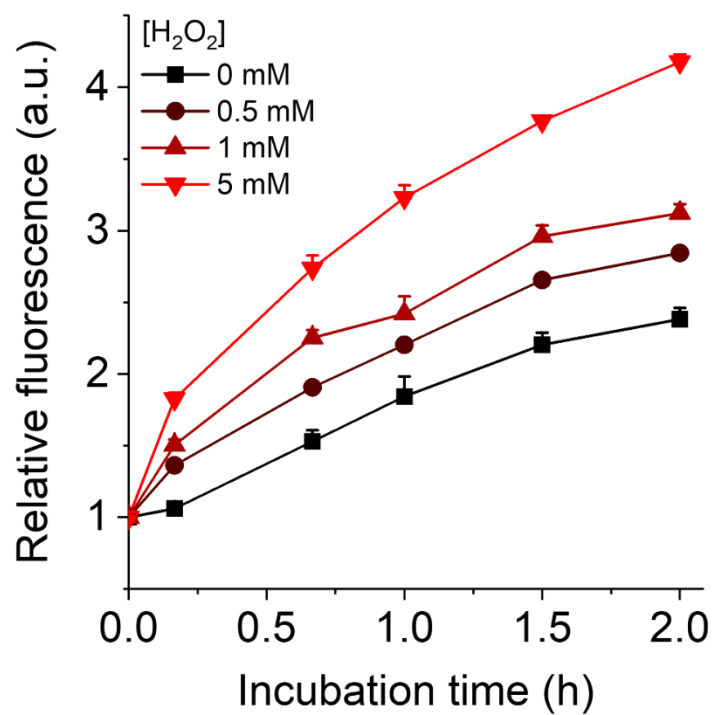


**Figure S24.** Analysis of reactive oxygen species in *E. coli* exposed to H<sub>2</sub>O<sub>2</sub> using H<sub>2</sub>DCFDA. The increase of fluorescence as a function of H<sub>2</sub>O<sub>2</sub> concentration indicates a greater level of oxidative stress. Data is presented as Mean + SD (n = 3).

**Table S1| Conjugates produced by the thiol–allene click reaction (n = 3)**

Sulfonium	Thiol	Ratio <sup>1</sup>	pH	Time (h)	Conversion (%)
<b>1b</b>	βME	1:1	7.4	1.5	94 ± 1
<b>1b</b>	GSH	1:1	7.4	1.5	84 ± 1
<b>1b</b>	GSH	1:1	6.5	2.5	50 ± 20
<b>1b</b>	GSH	1:1	8.5	1	97 ± 2
<b>1b</b>	mPEG–SH	1:2	7.4	1.5	84 ± 6
<b>1b</b>	SAMSA Fluorescein	1:1	7.4	2.5	90 ± 1
<b>1a</b> (butyrate)	GSH	1:10	7.4	3.5 <sup>2</sup>	0%
<b>3b</b> (Rho)	HSA	10:1	8.5	12	64 <sup>2</sup>
<b>4b</b>	βME	1:1	7.4	1	100 ± 1
<b>4b</b>	GSH	1:1	7.4	1.5	82 ± 7
<b>4b</b>	mPEG–SH	1:2	7.4	1.5	73 ± 3
<b>4b</b>	SAMSA Fluorescein	1:1	7.4	1.5	74 ± 11
<b>5b</b>	CPP(Cy3)	1:2	7.4	20	83 <sup>2</sup>

<sup>1</sup>: Sulfonium to thiol ratio; <sup>2</sup>: n = 1

**Table S2| Release of methionine-containing peptide by nucleophilic substitution or by Clip (thiol–ene addition) (n = 3).**

Conjugate	Thiol	DMPA (eq.)	H <sub>2</sub> O <sub>2</sub>	pH	Time	Conversion (%)
<b>1b</b> –GSH	10 mM GSH			7.4	24 h	21 ± 6
<b>1b</b> –GSH	10 mM Cys			7.4	22 h	66 <sup>1</sup>
<b>4b</b> –GSH	10 mM GSH			7.4	24 h	17 ± 7
<b>5b</b> –CPP(Cy3)	10 mM GSH			7.4	22 h	~63 <sup>1</sup>
<b>1b</b> –GSH	1.1 eq. GSH	0.1 eq.		7.4	15 min (+UV)	4 <sup>1</sup>
<b>1b</b> –GSH	10 eq. GSH	0.1 eq.		7.4	15 min (+UV)	7 <sup>1</sup>
<b>1b</b> –GSH	10 eq. GSH	1.5 eq.		7.4	15 min (+UV)	94 ± 2
<b>1b</b> –GSH	10 eq. GSH	1.5 eq.		6.5	15 min (+UV)	93 ± 1
<b>1b</b> –GSH	10 eq. GSH	1.5 eq.		8.5	15 min (+UV)	95 ± 1
<b>1b</b> –GSH	10 eq. Cys	1.5 eq.		7.4	15 min (+UV)	96 ± 1
<b>4b</b> –GSH	10 eq. GSH	1.5 eq.		7.4	15 min (+UV)	97 ± 2
<b>5b</b> –CPP(Cy3)	10 eq. GSH	1.5 eq.		7.4	15 min (+UV)	67 ± 1 <sup>2</sup>
<b>1b</b> –GSH	–		1.5 eq.	7.4	15 min (–UV)	2 ± 3
<b>1b</b> –GSH	–		10 eq.	7.4	15 min (–UV)	4 ± 5
<b>1b</b> –GSH	10 eq. GSH		10 eq.	7.4	15 min (–UV)	4 ± 2
<b>1b</b> –GSH	10 eq. GSH		10 eq.	7.4	15 min (+UV)	6 ± 3

<sup>1</sup>: n = 1; <sup>2</sup>: n = 2

**Table S3| Calculated and observed mass data.**

Compound	Composition	Exact mass	m/z
<b>1a</b>	C <sub>27</sub> H <sub>40</sub> N <sub>6</sub> O <sub>7</sub> S	592.3	Calc. (M + 1H) <sup>1+</sup> : 593.3 Obs.: 593.1
<b>1b</b>	C <sub>30</sub> H <sub>43</sub> N <sub>6</sub> O <sub>7</sub> S <sup>+</sup>	631.3	Calc. (M + 0H) <sup>1+</sup> : 631.3 Obs.: 631.0
<b>1b</b> + H <sub>2</sub> O	C <sub>30</sub> H <sub>45</sub> N <sub>6</sub> O <sub>8</sub> S <sup>+</sup>	649.2	Calc. (M + 0H) <sup>1+</sup> : 649.2 Obs.: 649.1
<b>1b</b> [2,3]σ	C <sub>30</sub> H <sub>42</sub> N <sub>6</sub> O <sub>7</sub> S	630.2	Calc. (M + 1H) <sup>1+</sup> : 631.2 Obs.: 631.0
<b>1b</b> -βME	C <sub>32</sub> H <sub>49</sub> N <sub>6</sub> O <sub>8</sub> S <sub>2</sub> <sup>+</sup>	709.3	Calc. (M + 0H) <sup>1+</sup> : 709.3 Obs.: 708.6
<b>1b</b> -GSH	C <sub>40</sub> H <sub>61</sub> N <sub>10</sub> O <sub>12</sub> S <sub>2</sub> <sup>+</sup>	937.4	Calc. (M + 0H) <sup>1+</sup> : 937.4 Obs.: 937.4
<b>1b</b> -SAMSA fluorescein	C <sub>54</sub> H <sub>60</sub> N <sub>7</sub> O <sub>15</sub> S <sub>2</sub> <sup>+</sup>	1110.4	Calc. (M + 0H) <sup>1+</sup> : 1110.4 Obs.: 1110.3
<b>1a</b> -butyne	C <sub>31</sub> H <sub>45</sub> N <sub>6</sub> O <sub>7</sub> S <sup>+</sup>	645.2	Calc. (M + 0H) <sup>1+</sup> : 645.2 Obs.: 645.2
<b>2a</b>	C <sub>27</sub> H <sub>40</sub> N <sub>6</sub> O <sub>8</sub> S	608.2	Calc. (M + 1H) <sup>1+</sup> : 609.2 Obs.: 609.1
<b>3b</b>	C <sub>63</sub> H <sub>71</sub> N <sub>8</sub> O <sub>11</sub> S <sup>+</sup>	1147.5	Calc. (M + 0H) <sup>1+</sup> : 1147.5 Obs.: 1147.6
<b>4a</b>	C <sub>46</sub> H <sub>77</sub> N <sub>13</sub> O <sub>15</sub> S	1083.5	Calc. (M + 1H) <sup>1+</sup> : 1084.5 Obs.: 1084.6
<b>4b</b>	C <sub>49</sub> H <sub>80</sub> N <sub>13</sub> O <sub>15</sub> S <sup>+</sup>	1122.6	Calc. (M + 0H) <sup>1+</sup> : 1122.6 Obs.: 1122.3
<b>4b</b> [2,3]σ	C <sub>49</sub> H <sub>79</sub> N <sub>13</sub> O <sub>15</sub> S	1121.6	Calc. (M + 1H) <sup>1+</sup> : 1122.6 Obs.: 1122.9
<b>4b</b> -βME	C <sub>51</sub> H <sub>86</sub> N <sub>13</sub> O <sub>16</sub> S <sub>2</sub> <sup>+</sup>	1200.6	Calc. (M + 0H) <sup>1+</sup> : 1200.6 Obs.: 1199.4
<b>4b</b> -GSH	C <sub>59</sub> H <sub>97</sub> N <sub>18</sub> O <sub>22</sub> S <sub>2</sub> <sup>+</sup>	1428.7	Calc. (M + 0H) <sup>1+</sup> : 1428.7 Obs.: 1429.5
<b>4b</b> -SAMSA fluorescein	C <sub>73</sub> H <sub>97</sub> N <sub>14</sub> O <sub>23</sub> S <sub>2</sub> <sup>+</sup>	1601.6	Calc. (M + 0H) <sup>1+</sup> : 1601.6 Obs.: 1601.1
<b>5a</b>	C <sub>79</sub> H <sub>116</sub> N <sub>15</sub> O <sub>22</sub> S <sub>3</sub> <sup>+</sup>	1721.8	Calc. (M + 0H) <sup>1+</sup> : 1721.8 Obs.: 1721.6
<b>5b</b>	C <sub>82</sub> H <sub>119</sub> N <sub>15</sub> O <sub>22</sub> S <sub>3</sub> <sup>2+</sup>	1760.8	Calc. (M + 0H) <sup>2+</sup> : 880.4 Obs.: 880.2
<b>5b</b> -CPP(Cy3)	C <sub>188</sub> H <sub>303</sub> N <sub>60</sub> O <sub>45</sub> S <sub>6</sub> <sup>3+</sup>	4313.2	Calc. (M + 1H) <sup>4+</sup> : 1078.5 Obs.: 1078.8
<b>6</b>	C <sub>23</sub> H <sub>38</sub> N <sub>8</sub> O <sub>10</sub> S <sub>2</sub>	650.2	Calc. (M + 1H) <sup>1+</sup> : 651.2 Obs.: 652.9
<b>7</b>	C <sub>33</sub> H <sub>56</sub> N <sub>12</sub> O <sub>15</sub> S <sub>3</sub>	956.3	Calc. (M + 1H) <sup>1+</sup> : 957.3 Obs.: 959.4

## 6.2 Appendix II: Supplementary Information of Article 2

### Biological fate of sulfonium vinyl sulfides – A competition between reactive nitrogen species, radical thiols, and thiol nucleophiles

Fatemeh Zare<sup>1</sup>, Patrick Laplante<sup>2</sup>, Jean-François Cailhier<sup>2</sup>, and Marc A Gauthier<sup>1\*</sup>

<sup>1</sup> Institut National de la Recherche Scientifique (INRS), EMT Research Center, Varennes, Canada

<sup>2</sup> Centre Hospitalier de l'Université de Montréal and Montreal Cancer Institute, Montreal, Canada

#### Corresponding author:

Marc A. Gauthier

Institut National de la Recherche Scientifique (INRS), EMT Research Center, 1650 boul. Lionel-Boulet, Varennes, J3X 1P7, Canada

E-mail: gauthier@emt.inrs.ca

Telephone: +1 514 228 69 32

Fax: +1 450 929 81 02

#### Author contributions:

FZ carried out the most experiments, responsible for the designing of the experiments, data collection, analysis, as well as manuscript composition and revision.

PL trained FZ for *in vitro* experiments and provided guidance, and prepared the cell cultures (RAW 264.7 and THP-1).

JFC provided supports and guidance for cells experiments.

MAG was the supervisory author, involved with the designing of the experiments, concept formation, manuscript composition and revision.

*Note: The work of this chapter is prepared for submission to a scientific journal.*

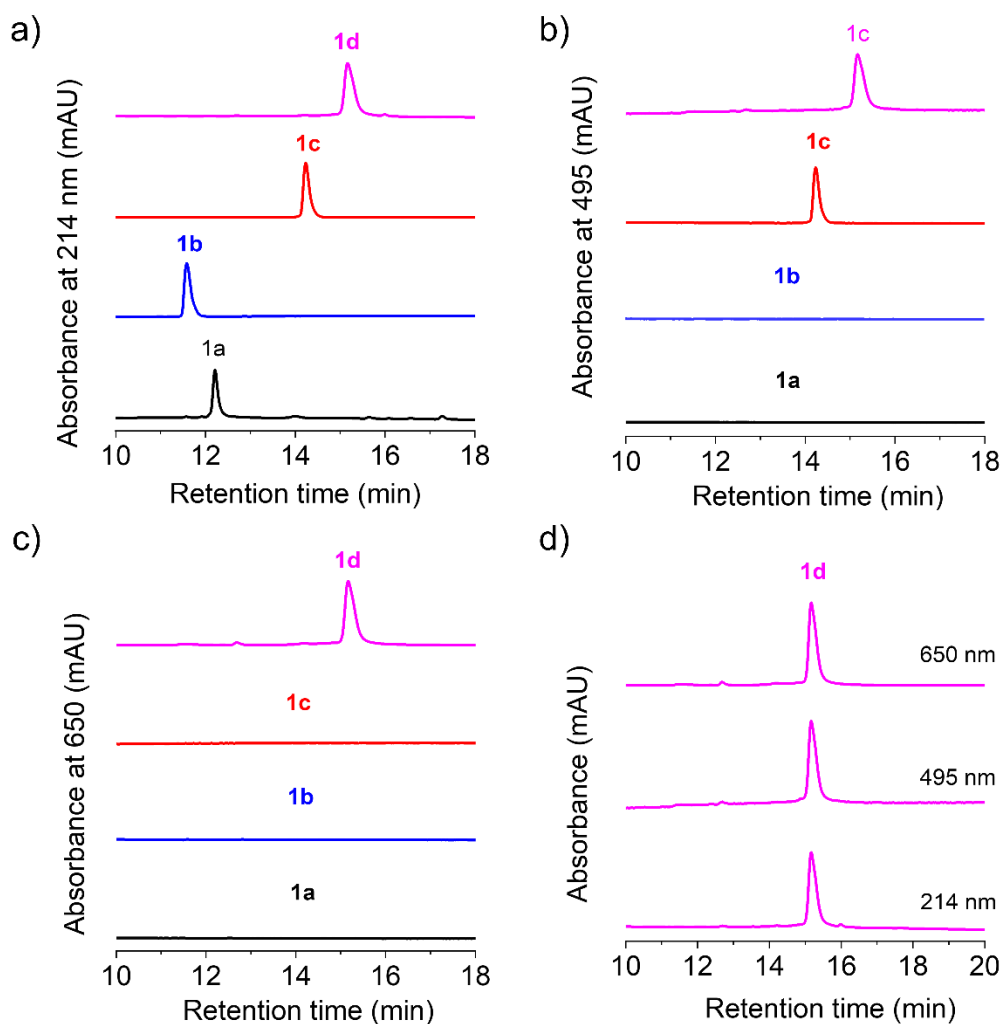


**Figure S1.** HPLC chromatograms related to synthesis of FRET-based sulfonium vinyl sulfide probe (1d). The absorbance of purified 1a (Tat-Met), 1b (Tat-Met-allene), 1c (Tat-Met-allene-SAMSA fluorescein), and 1d (FRET-based sulfonium vinyl sulfide probe) at (a) 214 nm, (b) 495 nm, (c) 650 nm, and (d) HPLC chromatograms of 1d at different wavelengths (214, 495, and 650 nm).

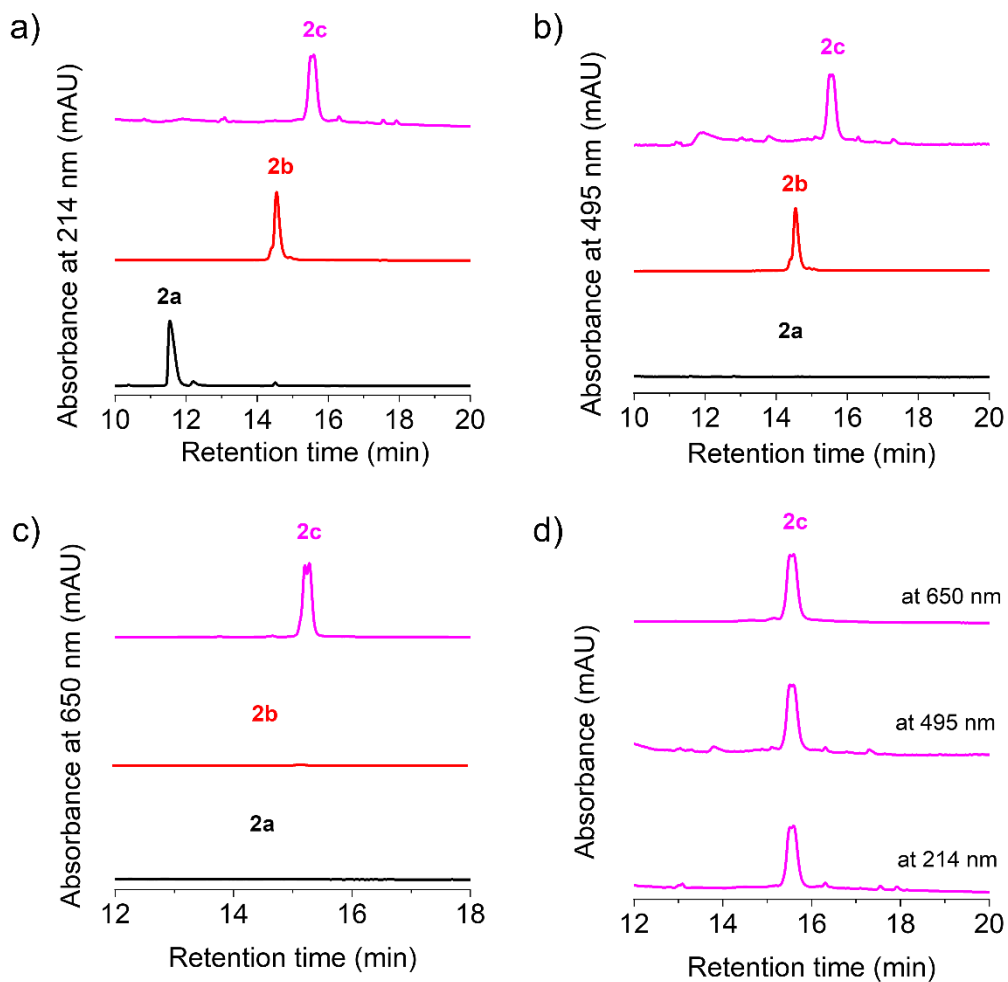


**Figure S2.** HPLC chromatograms related to synthesis of FRET-based thioether probe (2c). The absorbance of the purified 2a (Tat-Cys), 2b (Tat-Cys-flouresceine-5-maleimide), and 2c (FRET-based thioether probe) at (a) 214 nm, (b) 495 nm, (c) 650 nm, and (d) HPLC chromatograms of 2c at different wavelengths (214, 495, and 650 nm).

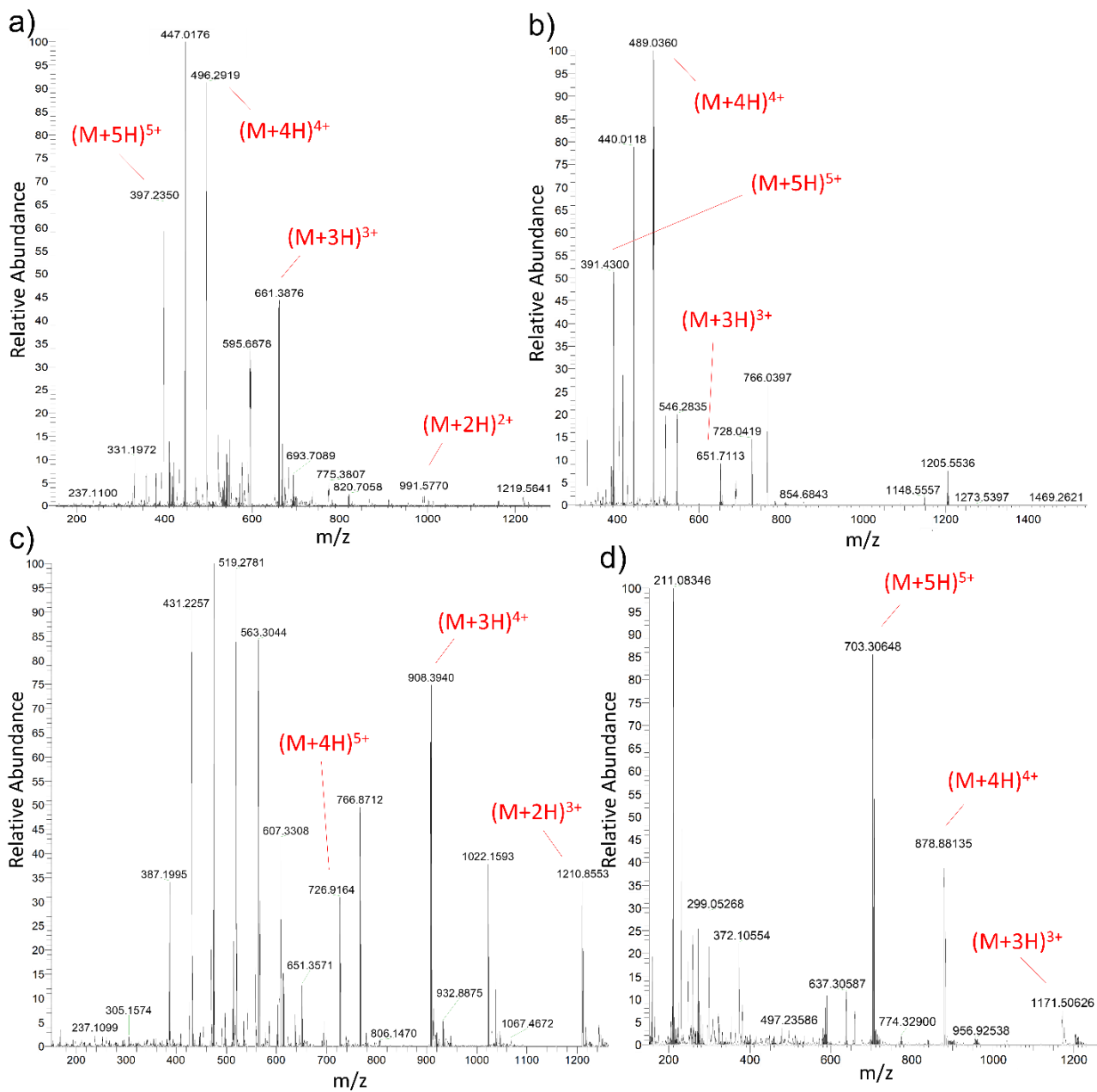
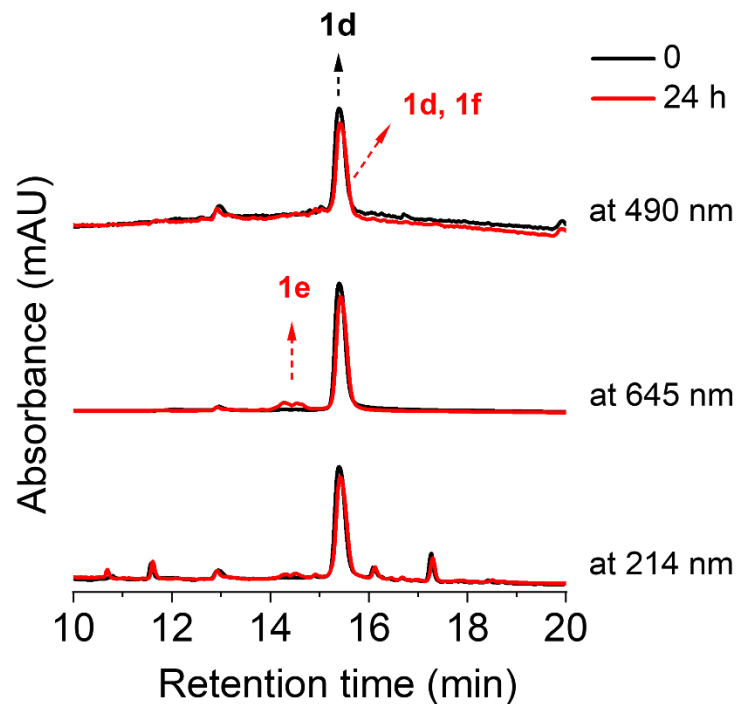
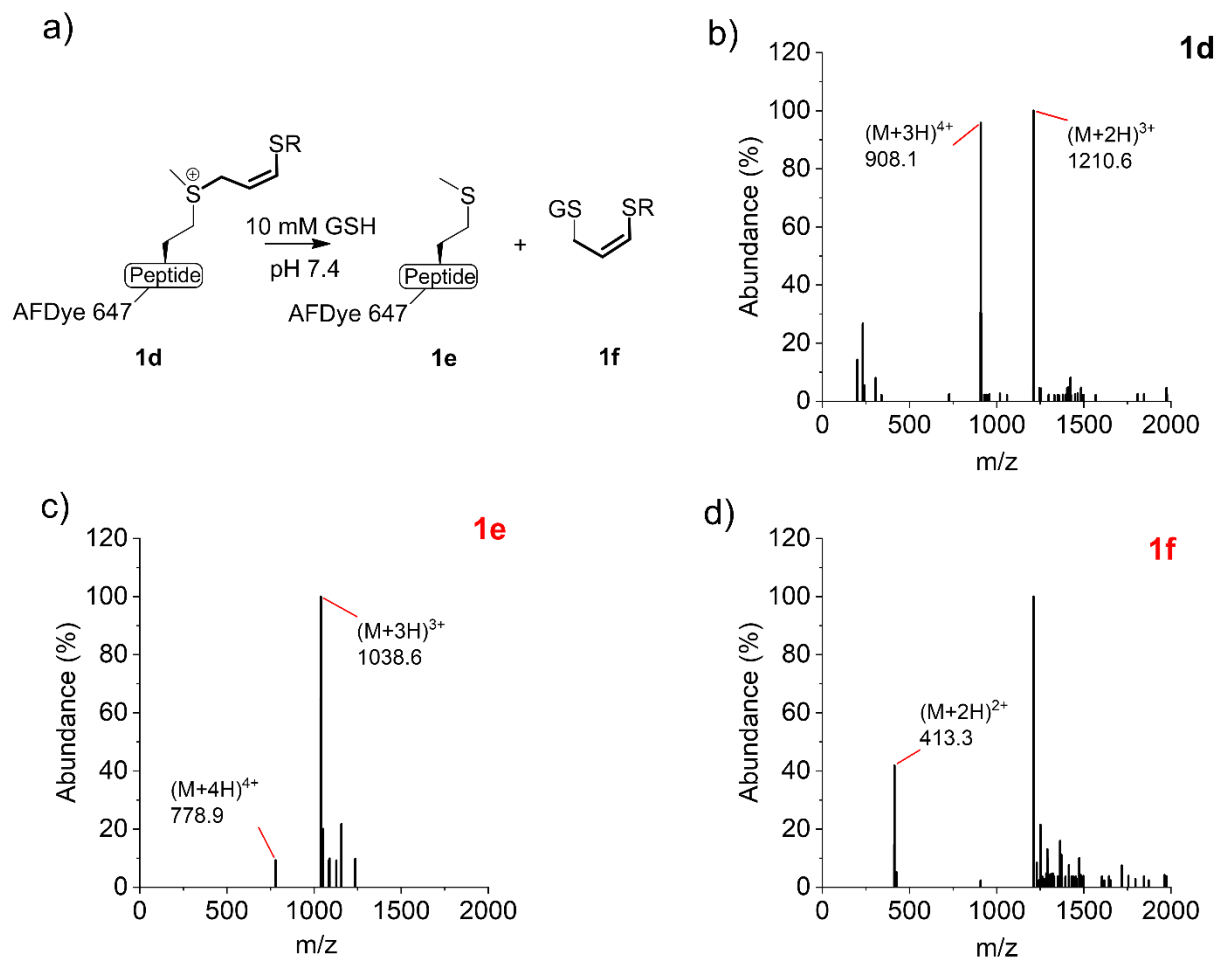


Figure S3. Full mass spectra of (a) 1a, (b) 2a, (c) 1d, and (d) 2c.



**Figure S4.** HPLC chromatograms at 214 nm, 645 nm, and 490 nm of Clip – Nucleophilic thiol–ene addition reaction in the presence of thiols. Upon prolonged incubation (over 24 h) of 1d in conditions mimicking the cytosol (i.e., 10 mM glutathione, pH 7.4), >92% of 1d remained intact. While, the slow nucleophilic addition of glutathione to the carbon adjacent to the sulfonium on 1d produced a peptide fragment with the recovery of the original methionine residue (1e) and a fluorescent adduct of glutathione (1f), without side reactions.



**Figure S5.** (a) Scheme illustrating the products formed by reaction of 1d with nucleophilic thiols presented in Figure 3.2a of the main manuscript. Thiol nucleophiles can react at the carbon adjacent the sulfonium, thereby the sulfonium vinyl sulfide fragmented to release the AFDye<sub>647</sub> modified peptide with the original methionine residue intact (1e,) and fluorescent adduct of GSH (1f). (b-d) Mass spectra of conjugates related to HPLC chromatograms presented in Figure 3.2a of the main manuscript.

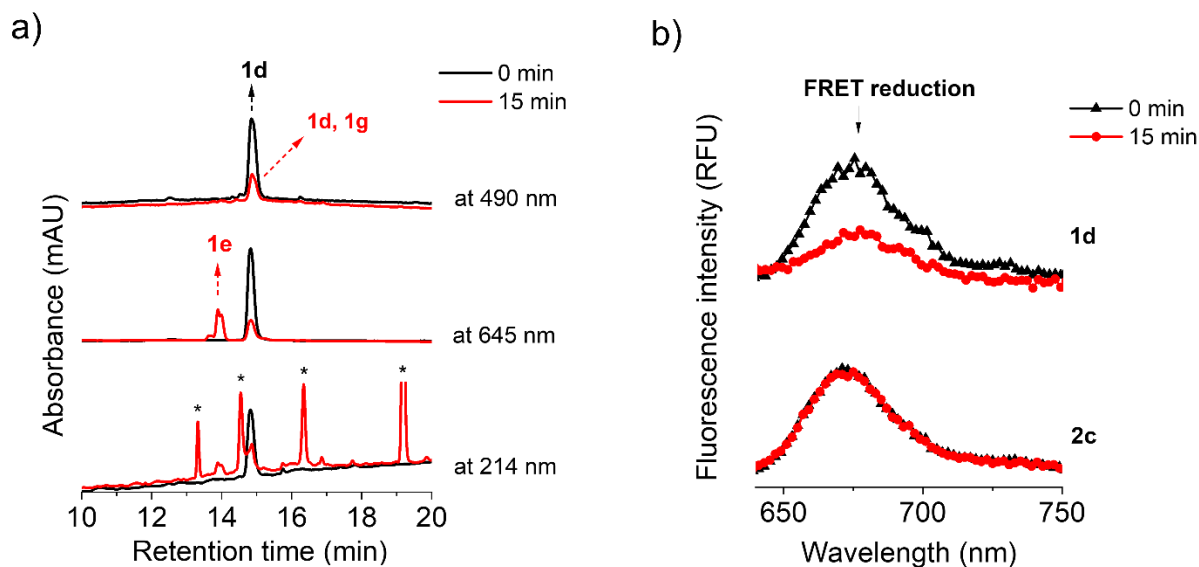


**Figure S6.** The reaction with radical thiols. (a) HPLC chromatograms at 214 nm, 645 nm, and 490 nm of Clip – radical thiol–ene addition reaction of 1d and radical thiols. Upon 15 min exposure to radical thiols, ~60% of the 1d fragmented to release the AFDye<sub>647</sub> modified peptide (1e, with the original methionine residue intact) and another fluorescent adduct of glutathione (1g). As shown above, 1d presented the absorbance at 214 nm, 645 nm, and 490 nm due to the presence of AFDye<sub>647</sub> and Fluorescein. While the peaks related to 1e and 1g exhibited the absorbance at 645 nm and 490 nm, respectively. (b) Clip reaction led to reduction in FRET signal ( $\lambda_{ex}/\lambda_{em}$  480/675 nm) of 1d due to linker breakage, leading to less possible energy transfer between SAMSA fluorescein and AFDye<sub>647</sub> and the release of 1e. However, the FRET signal of 2c remained constant.

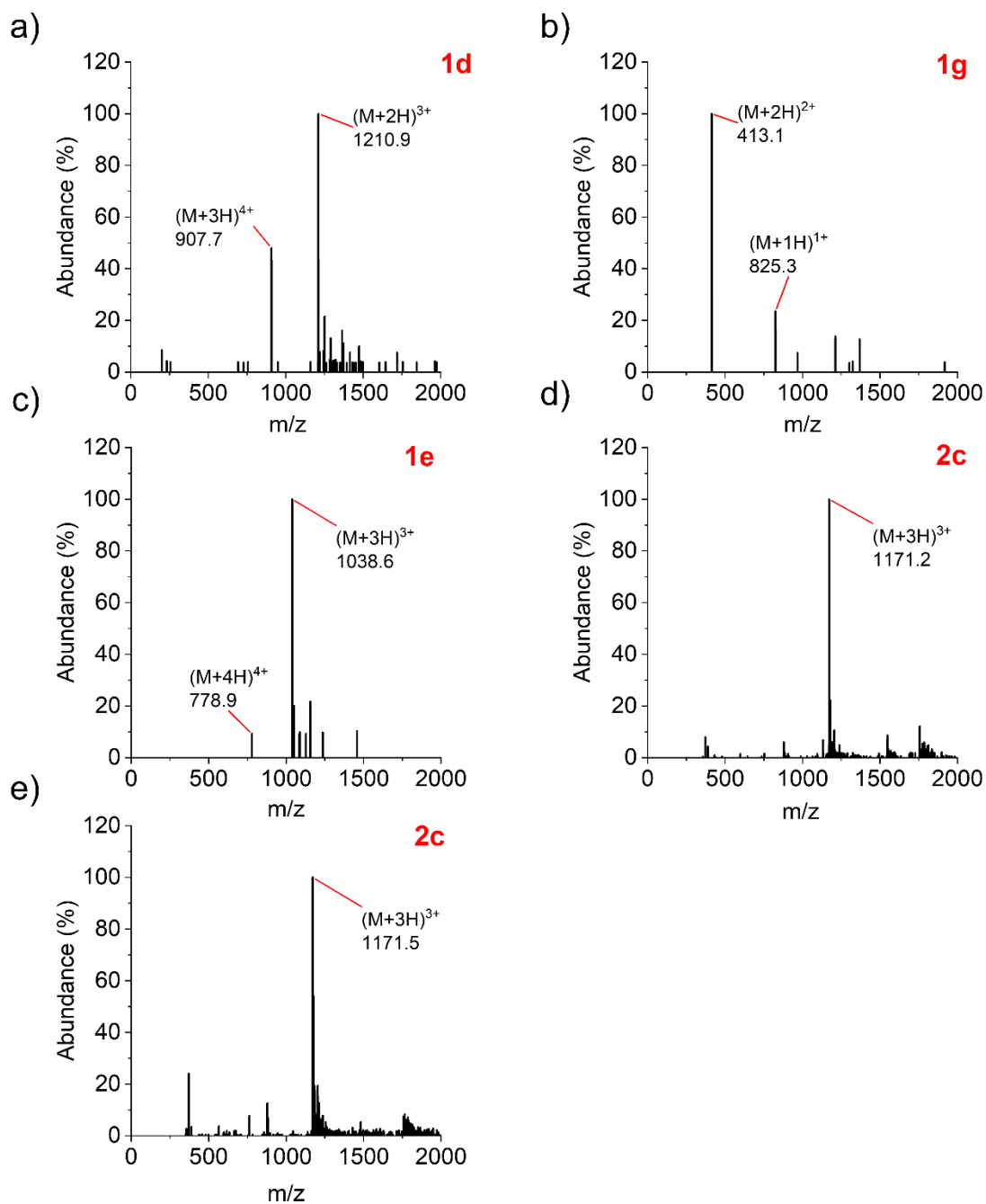


**Figure S7.** Mass spectra of conjugates related to HPLC chromatograms presented in Figure 3.2c of the main manuscript. (a) 1d before clip-radical thiol-ene reaction. (b,c) The generated 1g and released 1e upon exposure of 1d to radical thiols for 15 min. (d,e) Related to 2c before and after 15 min UV irradiation, respectively.

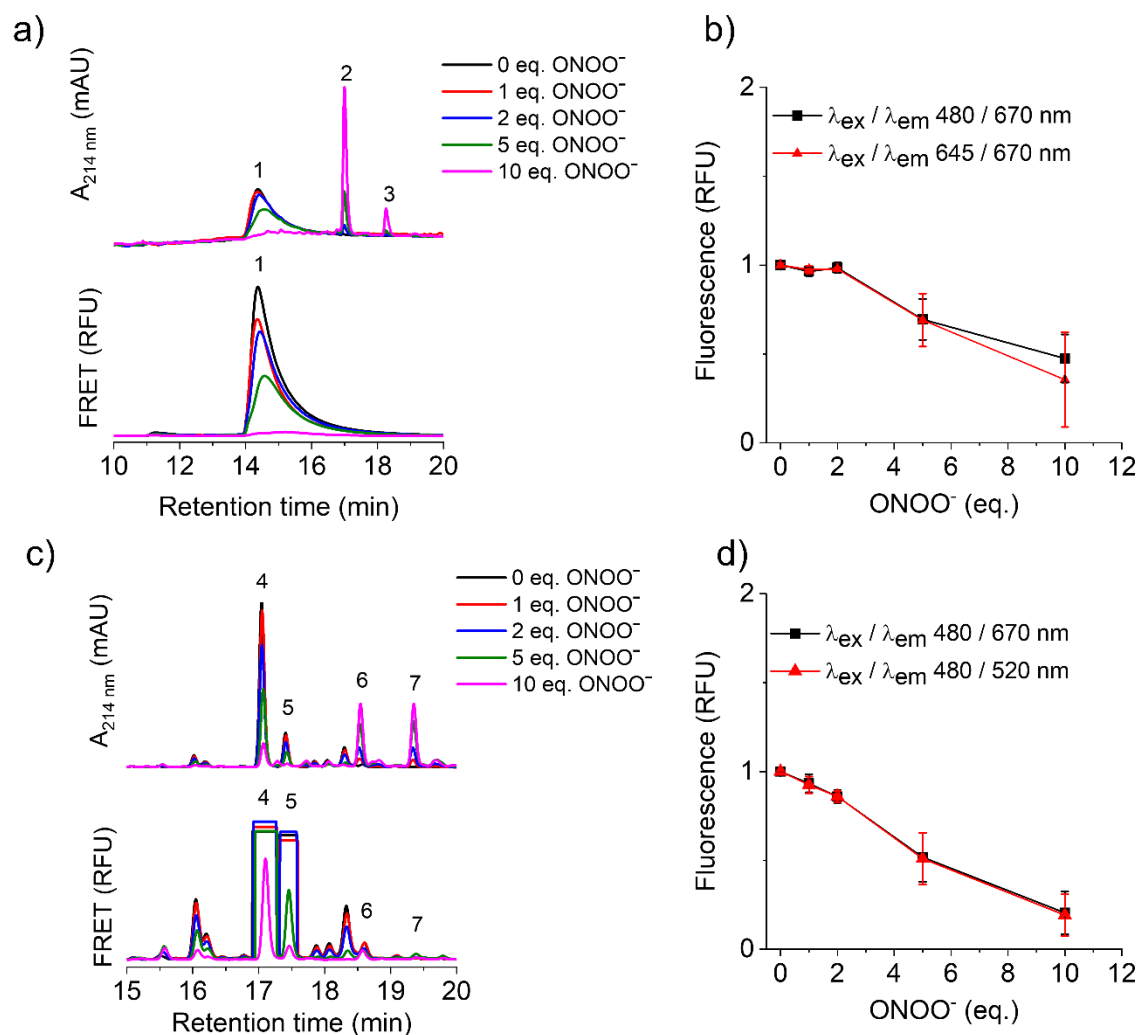


**Figure S8.** The effect of different molar eq. of peroxyntrite on AFDye<sub>647</sub> and Fluorescein. HPLC chromatograms (at 214 nm) of (a) AFDye<sub>647</sub> DBCO and (c) SAMSA fluorescein reacted with 0, 1, 2, 5, and 10 eq.  $\text{ONOO}^-$  at PBS buffer pH 7.4 within 2 min reaction. Fluorescence intensity of (b) AFDye<sub>647</sub> DBCO and (d) SAMSA fluorescein reacted with  $\text{ONOO}^-$  (0, 1, 2, 5, and 10 eq.) at PBS buffer pH 7.4 over 2 min. Both fluorophores were relatively stable in the presence of ~2 eq.  $\text{ONOO}^-$ . Upon exposure to higher eq. of  $\text{ONOO}^-$ , both fluorophores were degraded rapidly due to nitrosylation and/or oxidation reaction, leading to loss of their fluorescence intensity. The mass spectra of related compounds are presented in Figure S9,10. 1, AFDye<sub>647</sub> DBCO; 2, 3, products generated by the oxidation and degradation of AFDye<sub>647</sub> DBCO; 4, 5, SAMSA fluorescein; 6,7, nitrated Fluorescein.

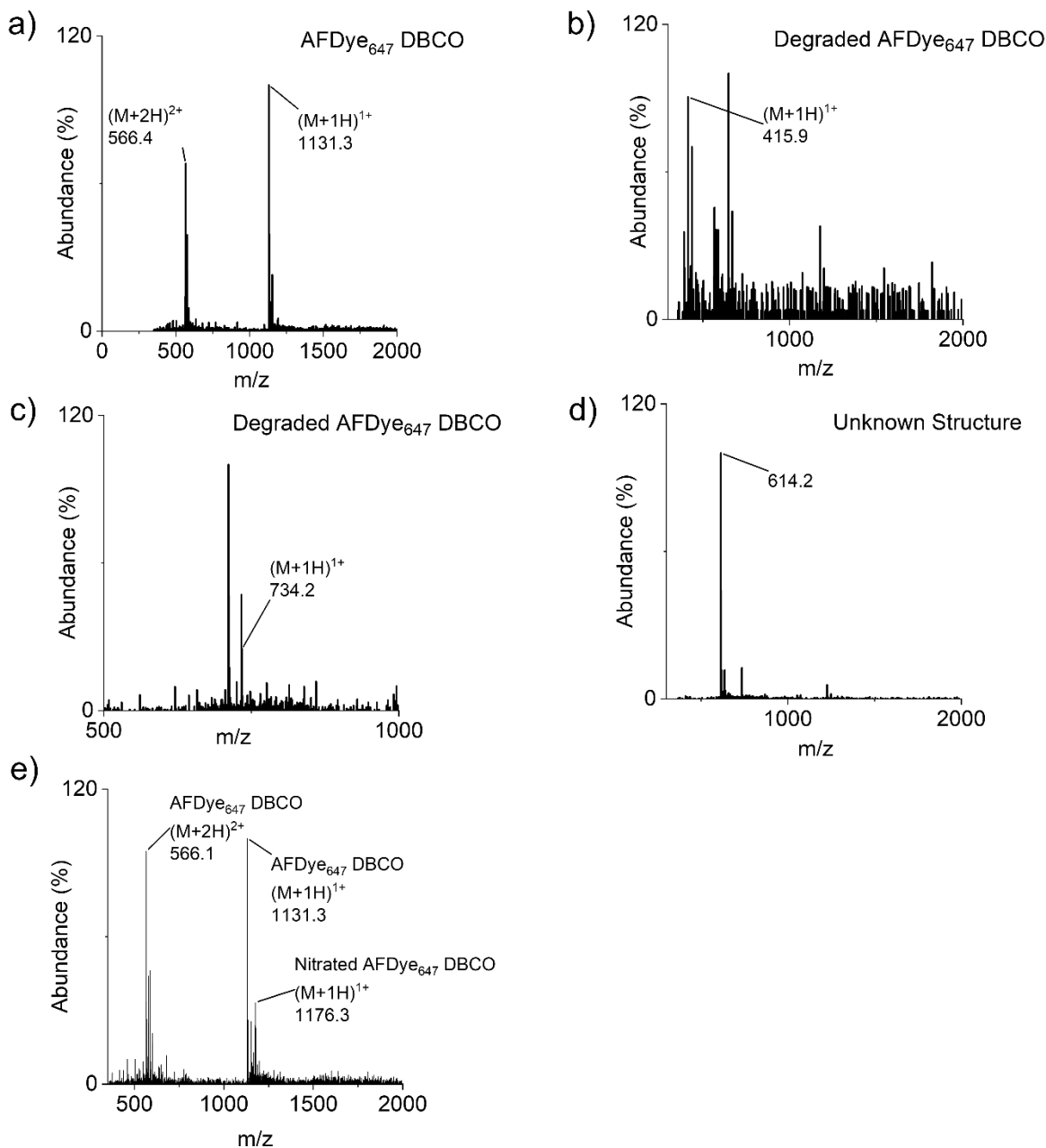


**Figure S9.** Mass spectra of compounds related to HPLC chromatograms presented in Figure S8a. (a) AFDye<sub>647</sub> DBCO located at peak No. 1. (b) Generated from the oxidation and degradation of AFDye<sub>647</sub> DBCO in the presence of ONOO<sup>-</sup> located at peak No. 1. (c) Generated from the oxidation and degradation of AFDye<sub>647</sub> DBCO in the presence of ONOO<sup>-</sup> located at peak No. 3. (d) Unknown structure and generated in the result of the reaction between AFDye<sub>647</sub> DBCO and ONOO<sup>-</sup> located at peak No. 2. (e) Nitrate AFDye<sub>647</sub> DBCO located at peak No. 1 and generated by the addition of a NO<sub>2</sub> to the molecule in the presence of 10 eq. ONOO<sup>-</sup>.

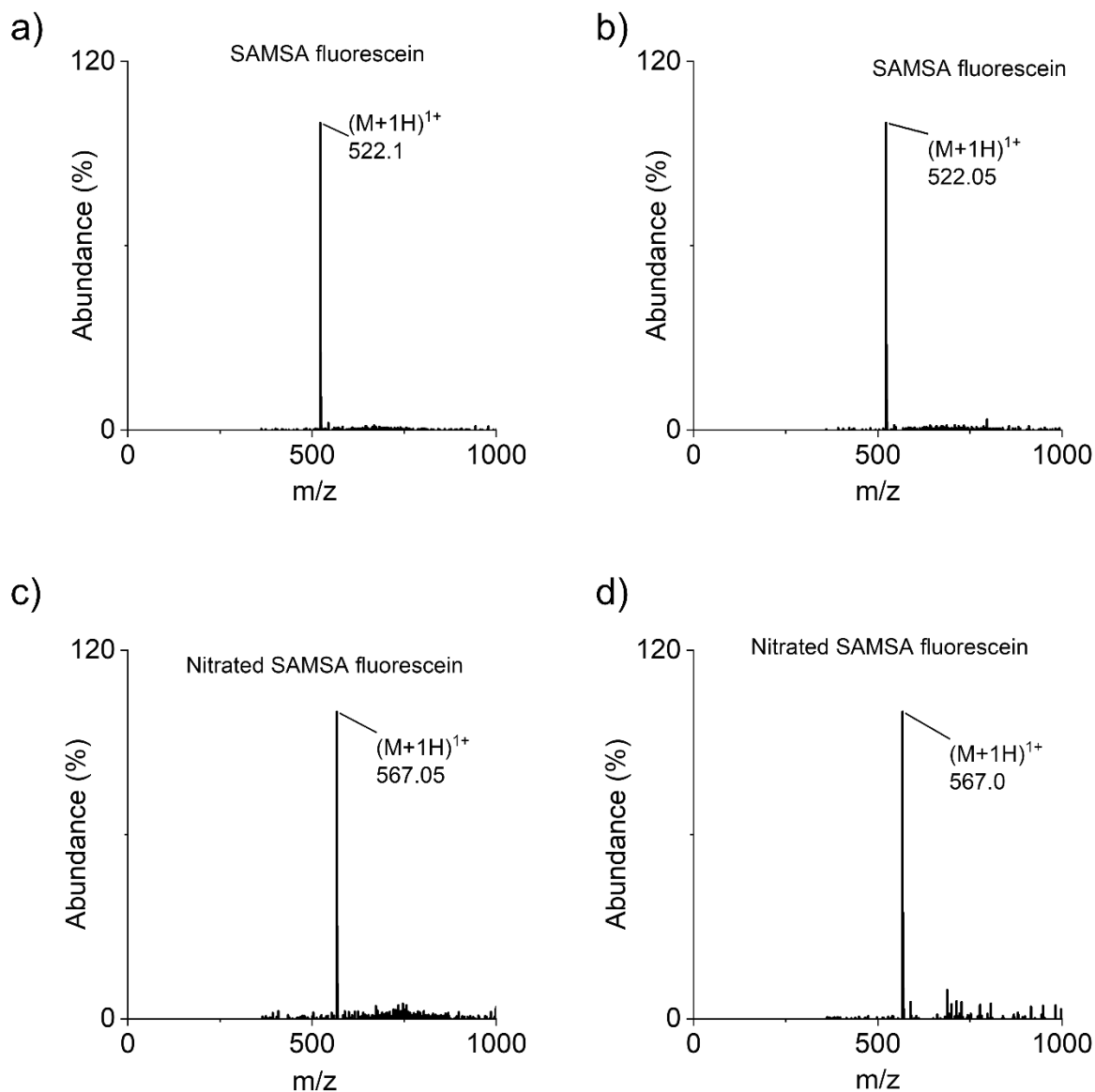


**Figure S10.** Mass spectra of compounds related to HPLC chromatograms presented in Figure S8c. (a,b) SAMSA fluorescein located at peak No. 4 and No. 5, respectively. (c,d) Nitrated SAMSA fluorescein located at peak No. 6 and No. 7, respectively.

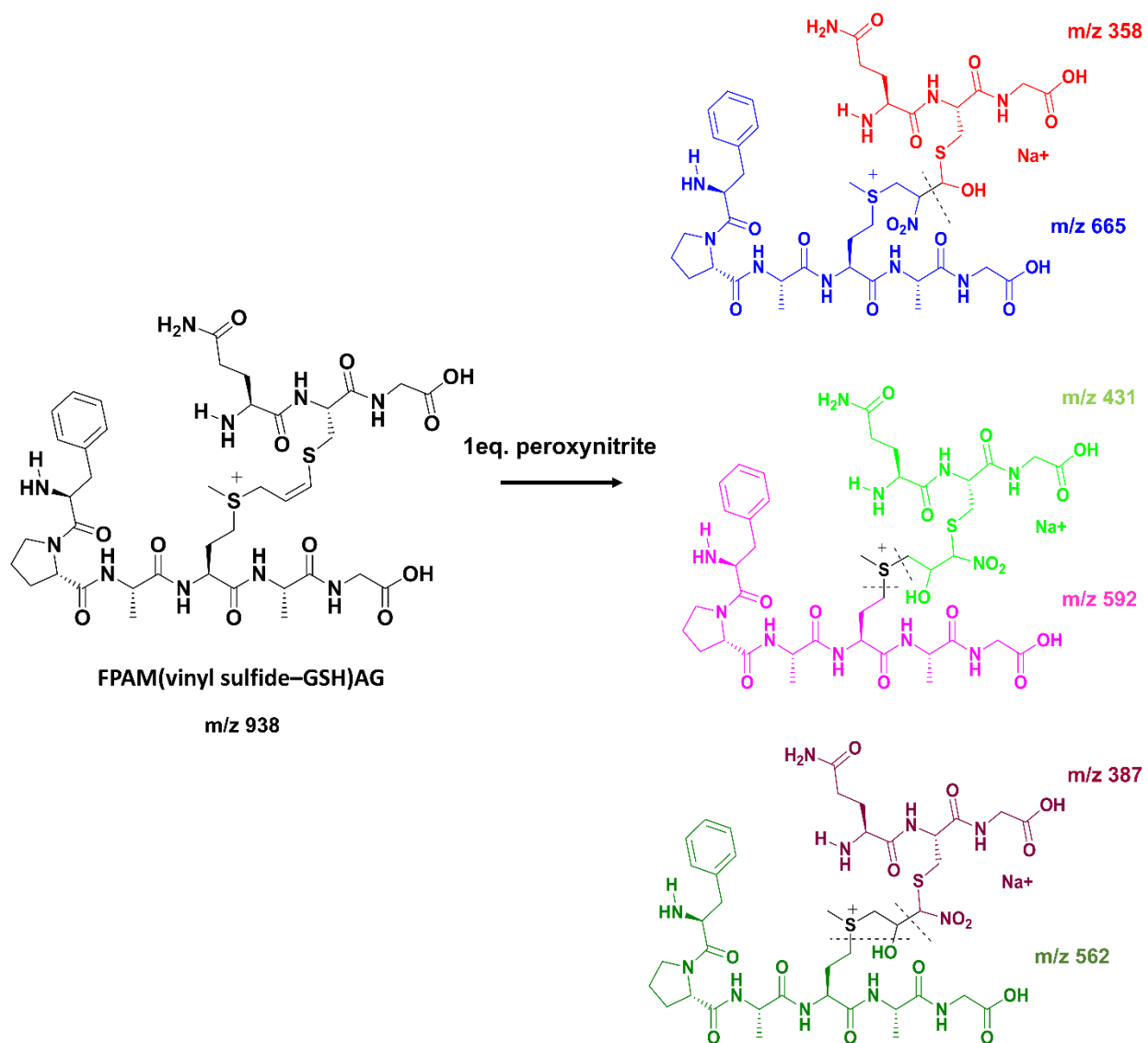
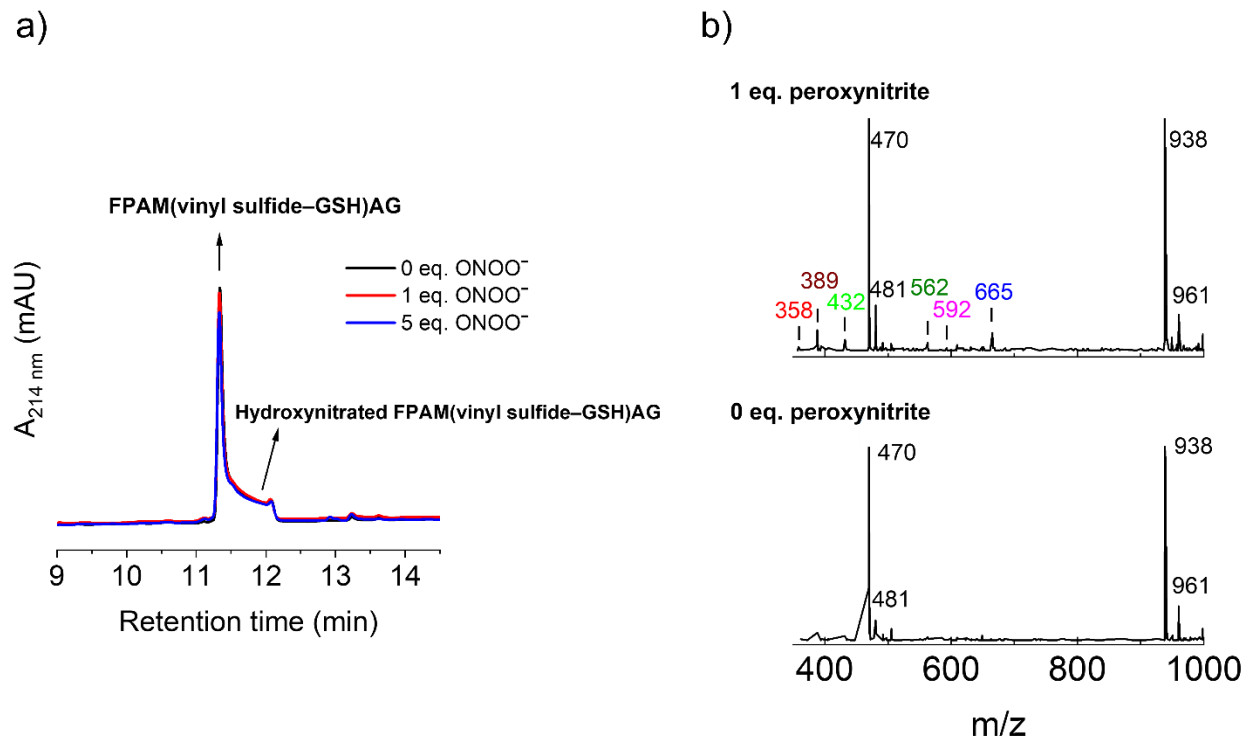
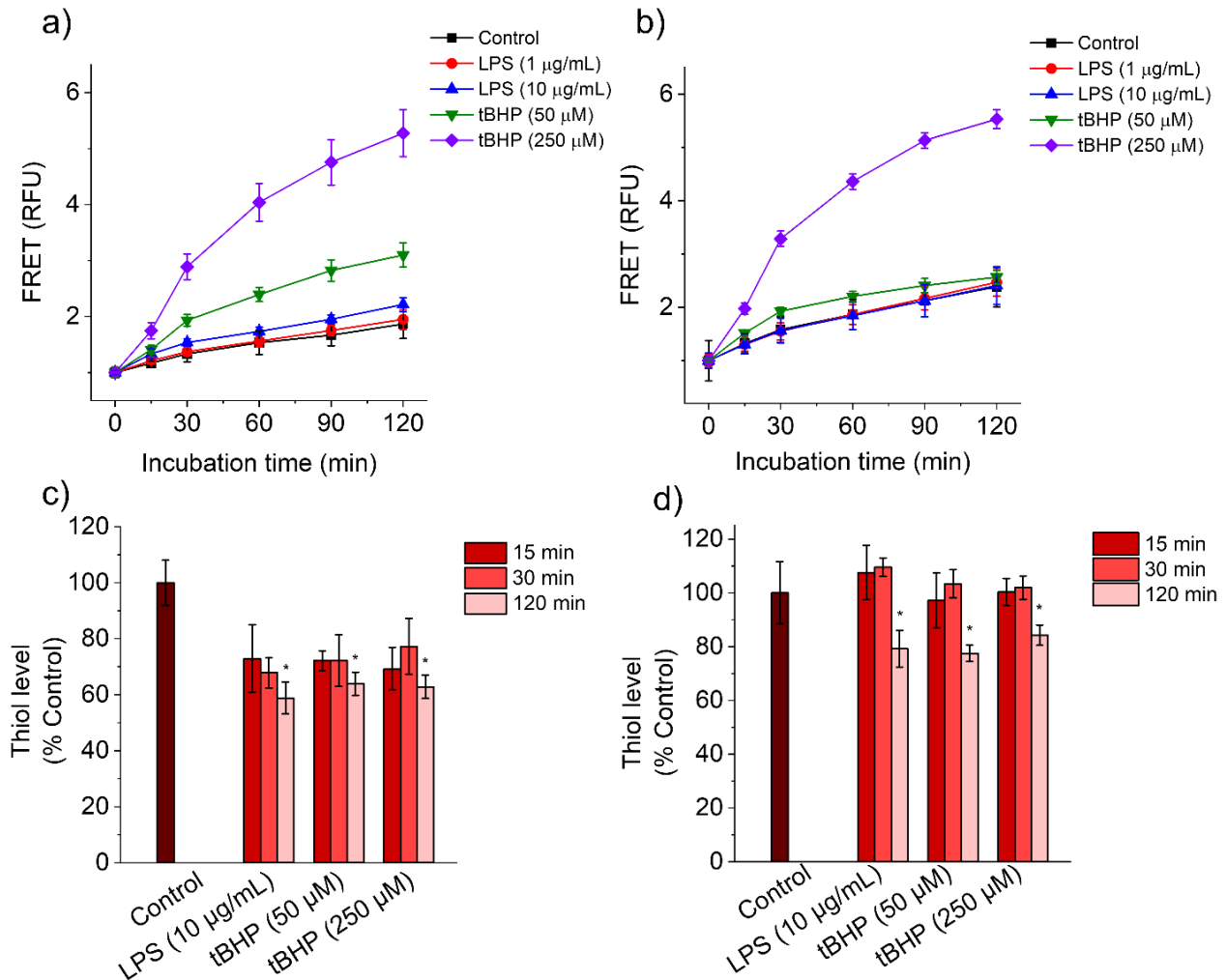


Figure S11. Scheme illustrating the hydroxynitrated sulfonium vinyl sulfide-containing model peptide (FPAM(vinyl sulfide-GSH)AG) upon exposure to ONOO<sup>-</sup>, and the possible mass fragmentation of hydroxynitrated FPAM(vinyl sulfide-GSH)AG.



**Figure S12.** The stability of sulfonium vinyl sulfide-containing model peptide (FPAM(vinyl sulfide-GSH)AG) upon exposure to  $\text{ONOO}^-$  (0, 1, 5, and 10 eq.) at PBS buffer pH 7.4. (a) HPLC chromatograms (at 214) presented the reduction in the absorbance of FPAM(vinyl sulfide-GSH)AG upon exposure to 1 and 5 molar eq.  $\text{ONOO}^-$  due to the hydroxynitration of sulfonium vinyl sulfide bond, leading to the addition of  $\text{NO}_2$  and  $\text{OH}$  to the sulfonium vinyl sulfide bond. (b) The mass spectrometry detected the mass fragmentation of FPAM(vinyl sulfide-GSH)AG and hydroxynitrated FPAM(vinyl sulfide-GSH)AG in solutions exposure to 0 and 1 eq.  $\text{ONOO}^-$ , respectively. Mass of 938  $m/z$  and 470  $m/z$  are related to FPAM(vinyl sulfide-GSH)AG at retention time of 11.3 min and presented its  $(M+\text{OH})^{1+}$  and  $(M+\text{OH})^{1+}$ , respectively. 358, 389, 432, 562, 592, and 665  $m/z$  presented the mass fragmentation of hydroxynitrated FPAM(vinyl sulfide-GSH)AG illustrated in Figure S11.



**Figure S13.** Analysis of reactive oxygen species (ROS) level and the concentration of intracellular thiols in cell lines (THP-1 and RAW 264.7) exposed to different stressors, including LPS (1 and 10  $\mu\text{g/mL}$ ) and tBHP (50 and 250  $\mu\text{M}$ ) by H<sub>2</sub>DCFDA and Thiol tracker violet assays, respectively. Upon exposure to the stressors, a greater level of oxidative stress and higher level of ROS were observed in (a) THP-1 and (b) RAW 264.7, which was confirmed by increasing the fluorescence intensity ( $\lambda_{Ex}/\lambda_{Em}$  485/528 nm) as functions of incubation time and concentration/type of the stressors. However, a reduction in the level of intracellular thiols (e.g., GSH) was detected upon 120 min exposure of (c) THP-1 and (d) RAW 264.7 to stressors due to consumption of intracellular thiols in order to control the cellular level of oxidative stress. Data is presented as Mean + SD (n = 3).

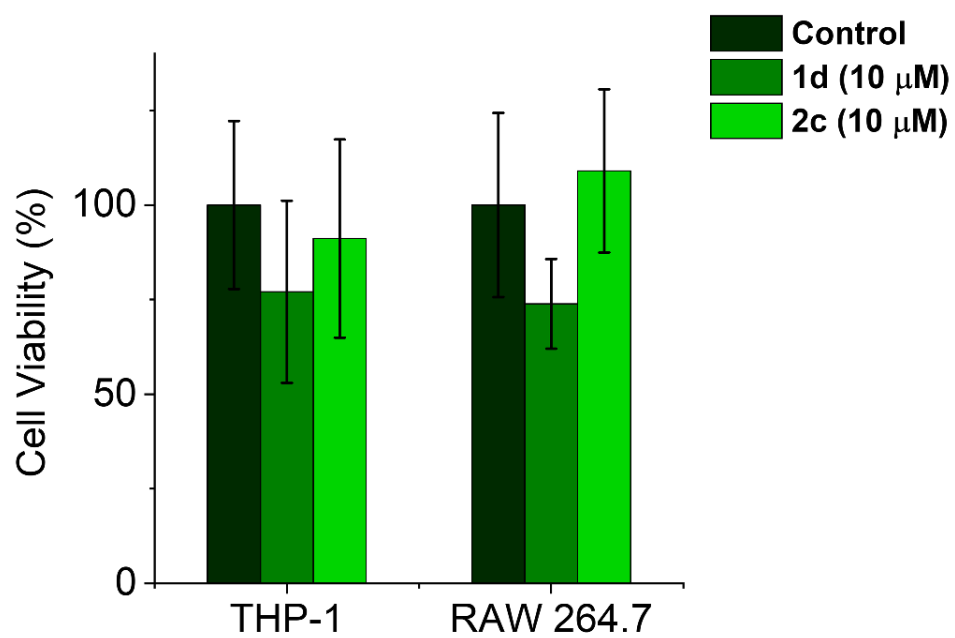
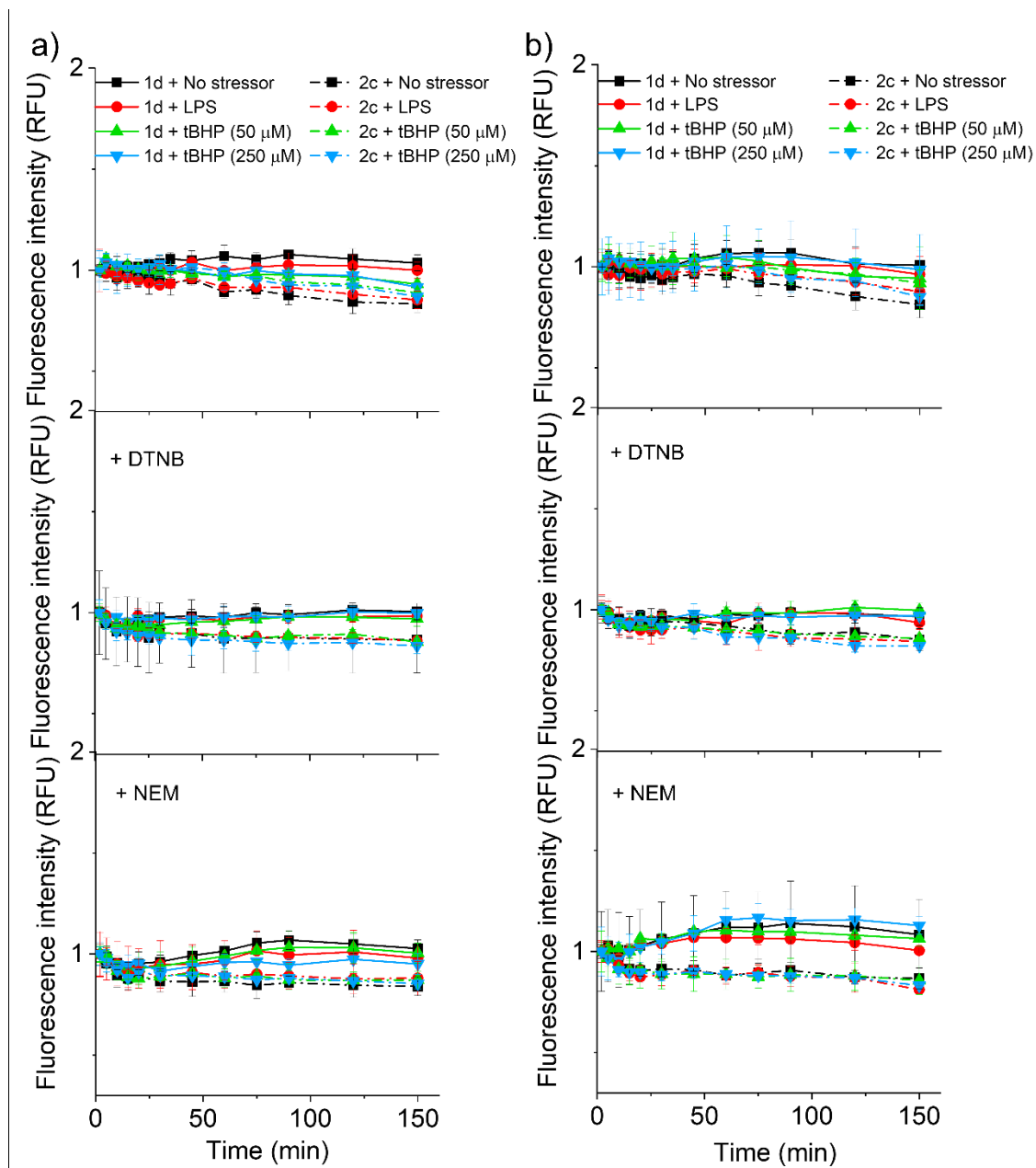


Figure S14. Cell viability of THP-1 and RAW 264.7 cells treated with 1d/2c (10 μM) after 3 h of investigation period. Data is presented as Mean + SD (n = 3).



**Figure S15.** Responsiveness of sulfonium vinyl sulfides in cell culture. Evolution of the AFDye<sub>647</sub> signal ( $\lambda_{ex}/\lambda_{em}$  643/673 nm) of 1d/2c in the presence of RAW 264.7 (a) and THP-1 (b) cells exposed to different stressors and thiol quenching agents. Data presented as Mean + SD (n = 3).

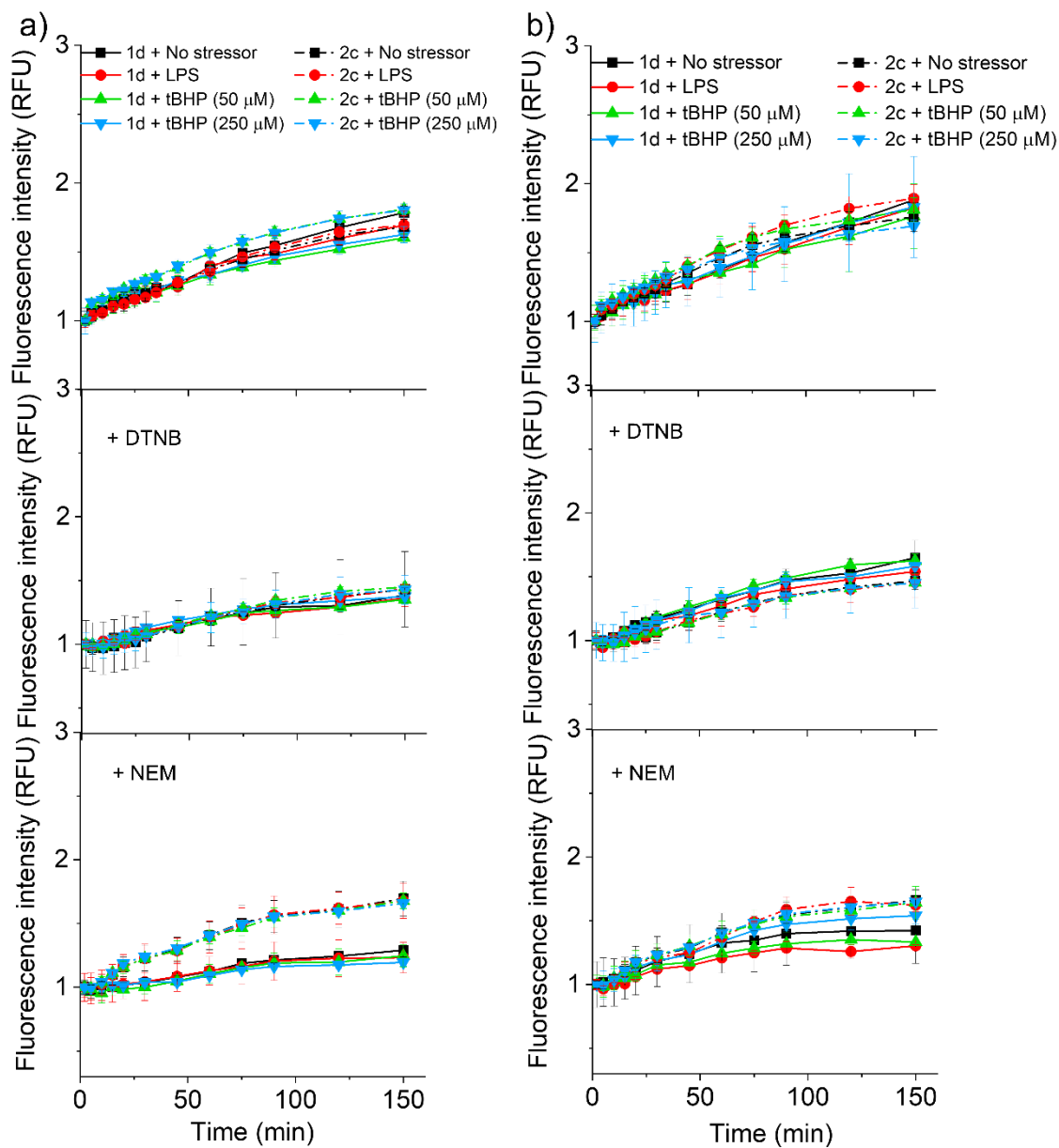


Figure S16s. Responsiveness of sulfonium vinyl sulfides in cell culture. Evolution of the fluorescein signal ( $\lambda_{\text{ex}}/\lambda_{\text{em}}$  480/520 nm) of 1d/2c in the presence of RAW 264.7 (a) and THP-1 (b) cells exposed to different stressors and thiol quenching agents. Data presented as Mean + SD (n = 3).

**Table S1. Calculated and observed mass data.**

Compound	Composition	Exact mass	m/z
<b>1a</b>	C <sub>77</sub> H <sub>145</sub> N <sub>41</sub> O <sub>19</sub> S	1980.1	Calc. (M + 2H) <sup>2+</sup> : 991.1 Obs.: 991.6
<b>2a</b>	C <sub>75</sub> H <sub>141</sub> N <sub>41</sub> O <sub>19</sub> S	1952.1	Calc. (M + 3H) <sup>3+</sup> : 651.7 Obs.: 651.7
<b>1d</b>	C <sub>159</sub> H <sub>227</sub> N <sub>46</sub> O <sub>41</sub> S <sub>6</sub> <sup>+</sup>	3628.5	Calc. (M + 2H) <sup>3+</sup> : 1210.2 Obs.: 1210.8
<b>2c</b>	C <sub>154</sub> H <sub>216</sub> N <sub>46</sub> O <sub>40</sub> S <sub>5</sub>	3509.5	Calc. (M + 3H) <sup>3+</sup> : 1170.8 Obs.: 1171.5
<b>1e</b>	C <sub>132</sub> H <sub>207</sub> N <sub>45</sub> O <sub>33</sub> S <sub>5</sub>	3110.4	Calc. (M + 3H) <sup>3+</sup> : 1037.8 Obs.: 1038.6
<b>1f</b>	C <sub>37</sub> H <sub>37</sub> N <sub>5</sub> O <sub>13</sub> S <sub>2</sub>	823.2	Calc. (M + 2H) <sup>2+</sup> : 412.6 Obs.: 413.3
<b>1g</b>	C <sub>37</sub> H <sub>37</sub> N <sub>5</sub> O <sub>13</sub> S <sub>2</sub>	823.2	Calc. (M + 2H) <sup>2+</sup> : 412.6 Obs.: 413.1
AFDye <sub>647</sub> DBCO	C <sub>55</sub> H <sub>62</sub> N <sub>4</sub> O <sub>14</sub> S <sub>4</sub>	1130.3	Calc. (M + 1H) <sup>1+</sup> : 1131.3 Obs.: 1131.3
AFDye <sub>647</sub> DBCO + NO <sub>2</sub>	C <sub>55</sub> H <sub>62</sub> N <sub>5</sub> O <sub>16</sub> S <sub>4</sub>	1176.3	Calc. (M + 1H) <sup>1+</sup> : 1177.3 Obs.: 1176.3
Degraded AFDye <sub>647</sub> DBCO	C <sub>17</sub> H <sub>21</sub> NO <sub>7</sub> S <sub>2</sub>	415.1	Calc. (M + 1H) <sup>1+</sup> : 416.1 Obs.: 415.9
Degraded AFDye <sub>647</sub> DBCO	C <sub>37</sub> H <sub>40</sub> N <sub>3</sub> O <sub>9</sub> S <sub>2</sub>	734.2	Calc. (M + 1H) <sup>1+</sup> : 735.2 Obs.: 734.2
SAMSA Fluorescein	C <sub>26</sub> H <sub>19</sub> NO <sub>9</sub> S	521.1	Calc. (M + 1H) <sup>1+</sup> : 522.1 Obs.: 522.1
SAMSA Fluorescein + NO <sub>2</sub>	C <sub>26</sub> H <sub>18</sub> N <sub>2</sub> O <sub>11</sub> S	566.1	Calc. (M + 1H) <sup>1+</sup> : 567.1 Obs.: 567.1

Note: the exact, calculated, and observed mass of hydroxynitrated FPAM(vinyl sulfide–GSH)AG are presented in Figures S11,12.

## 6.3 Appendix III: Letters of copyright permission

### Copyright for Figure 1.1

This Agreement between Institut National de la Recherche Scientifique -- Fatemeh Zare ("You") and Elsevier ("Elsevier") consists of your license details and the terms and conditions provided by Elsevier and Copyright Clearance Center.

License Number	5286530241571
License date	Apr 12, 2022
Licensed Content Publisher	Elsevier
Licensed Content Publication	Coordination Chemistry Reviews
Licensed Content Title	Metal-coordinated fluorescent and luminescent probes for reactive oxygen species (ROS) and reactive nitrogen species (RNS)
Licensed Content Author	Nahyun Kwon, Dayeh Kim, K.M.K. Swamy, Juyoung Yoon
Licensed Content Date	Jan 15, 2021
Licensed Content Volume	427
Licensed Content Issue	n/a
Licensed Content Pages	1
Start Page	213581
End Page	0
Type of Use	reuse in a thesis/dissertation
Portion	figures/tables/illustrations
Number of figures/tables/illustrations	1
Format	both print and electronic
Are you the author of this Elsevier article?	No
Will you be translating?	No
Title	Graduate student
Institution name	Institut National de la Recherche Scientifique
Expected presentation date	Jul 2022
Portions	Figure 1 on page 2

## Copyright for Figure 1.2

This is a License Agreement between Institut national de la recherche scientifique-Fatemeh Zare ("User") and Copyright Clearance Center, Inc. ("CCC") on behalf of the Rightsholder identified in the order details below. The license consists of the order details, the CCC Terms and Conditions below, and any Rightsholder Terms and Conditions which are included below.

All payments must be made in full to CCC in accordance with the CCC Terms and Conditions below.

Order Date	12-Apr-2022
Order License ID	1210314-1
ISSN	1744-1439
Type of Use	Republish in a thesis/dissertation
Publisher	PORTLAND PRESS
Portion	Image/photo/illustration

### LICENSED CONTENT

---

Publication Title	Biochemical Society symposia
Article Title	Thiyl radicals in biological systems: significant or trivial?
Author/Editor	Biochemical Society (Great Britain)
Date	01/01/1976
Language	English
Country	United Kingdom of Great Britain and Northern Ireland
Rightsholder	Portland Press, Ltd.
Publication Type	e-Journal
Start Page	55
End Page	63
Volume	61
URL	<a href="http://symposia.biochemistry.org">http://symposia.biochemistry.org</a>

### REQUEST DETAILS

---

Portion Type	Image/photo/illustration
Number of images / photos / illustrations	1
Format (select all that apply)	Print, Electronic

## Copyright for Figure 1.3



### Modular Design of Redox-Responsive Stabilizers for Nanocrystals

Author: Kathrin Fuhrmann, Anna Połomska, Carmen Aeberli, et al

Publication: ACS Nano

Publisher: American Chemical Society

Date: Sep 1, 2013

Copyright © 2013, American Chemical Society

---

#### PERMISSION/LICENSE IS GRANTED FOR YOUR ORDER AT NO CHARGE

This type of permission/license, instead of the standard Terms and Conditions, is sent to you because no fee is being charged for your order. Please note the following:

- Permission is granted for your request in both print and electronic formats, and translations.
- If figures and/or tables were requested, they may be adapted or used in part.
- Please print this page for your records and send a copy of it to your publisher/graduate school.
- Appropriate credit for the requested material should be given as follows: "Reprinted (adapted) with permission from {COMPLETE REFERENCE CITATION}. Copyright {YEAR} American Chemical Society." Insert appropriate information in place of the capitalized words.
- One-time permission is granted only for the use specified in your RightsLink request. No additional uses are granted (such as derivative works or other editions). For any uses, please submit a new request.

If credit is given to another source for the material you requested from RightsLink, permission must be obtained from that source.

## Copyright for Figure 1.4



### Photostable Ratiometric Pdot Probe for in Vitro and in Vivo Imaging of Hypochlorous Acid

Author: Li Wu, I-Che Wu, Christopher C. DuFort, et al

Publication: Journal of the American Chemical Society

Publisher: American Chemical Society

Date: May 1, 2017

Copyright © 2017, American Chemical Society

---

#### PERMISSION/LICENSE IS GRANTED FOR YOUR ORDER AT NO CHARGE

This type of permission/license, instead of the standard Terms and Conditions, is sent to you because no fee is being charged for your order. Please note the following:

- Permission is granted for your request in both print and electronic formats, and translations.
- If figures and/or tables were requested, they may be adapted or used in part.
- Please print this page for your records and send a copy of it to your publisher/graduate school.
- Appropriate credit for the requested material should be given as follows: "Reprinted (adapted) with permission from {COMPLETE REFERENCE CITATION}. Copyright {YEAR} American Chemical Society." Insert appropriate information in place of the capitalized words.
- One-time permission is granted only for the use specified in your RightsLink request. No additional uses are granted (such as derivative works or other editions). For any uses, please submit a new request.

## Copyright for Figure 1.6

### Stimuli-Responsive Layer-by-Layer Tellurium-Containing Polymer Films for the Combination of Chemotherapy and Photodynamic Therapy



Author: Fuqiang Fan, Lu Wang, Feng Li, et al

Publication: Applied Materials

Publisher: American Chemical Society

Date: Jul 1, 2016

*Copyright © 2016, American Chemical Society*

---

#### PERMISSION/LICENSE IS GRANTED FOR YOUR ORDER AT NO CHARGE

This type of permission/license, instead of the standard Terms and Conditions, is sent to you because no fee is being charged for your order. Please note the following:

- Permission is granted for your request in both print and electronic formats, and translations.
- If figures and/or tables were requested, they may be adapted or used in part.
- Please print this page for your records and send a copy of it to your publisher/graduate school.
- Appropriate credit for the requested material should be given as follows: "Reprinted (adapted) with permission from {COMPLETE REFERENCE CITATION}. Copyright {YEAR} American Chemical Society." Insert appropriate information in place of the capitalized words.
- One-time permission is granted only for the use specified in your RightsLink request. No additional uses are granted (such as derivative works or other editions). For any uses, please submit a new request.

## Copyright for Figure 1.7

This Agreement between Institut National de la Recherche Scientifique -- Fatemeh Zare ("You") and Elsevier ("Elsevier") consists of your license details and the terms and conditions provided by Elsevier and Copyright Clearance Center.

License Number	5286550572072
License date	Apr 12, 2022
Licensed Content Publisher	Elsevier
Licensed Content Publication	European Polymer Journal
Licensed Content Title	Sulfur-based oxidation-responsive polymers. Chemistry, (chemically selective) responsiveness and biomedical applications
Licensed Content Author	Mike Geven, Richard d'Arcy, Zulfiye Yesim Turhan, Farah El-Mohtadi, Aws Alshamsan, Nicola Tirelli
Licensed Content Date	Apr 15, 2021
Licensed Content Volume	149
Licensed Content Issue	n/a
Licensed Content Pages	1
Start Page	110387
End Page	0
Type of Use	reuse in a thesis/dissertation
Portion	figures/tables/illustrations
Number of figures/tables/illustrations	1
Format	both print and electronic
Are you the author of this Elsevier article?	No
Will you be translating?	No
Title	Graduate student
Institution name	Institut National de la Recherche Scientifique
Expected presentation date	May 2022
Portions	Figure 7a on page 13

## Copyright for Figure 1.8

### Disulfide Bond-Driven Oxidation- and Reduction-Responsive Prodrug Nanoassemblies for Cancer Therapy



Author: Bingjun Sun, Cong Luo, Han Yu, et al

Publication: Nano Letters

Publisher: American Chemical Society

Date: Jun 1, 2018

*Copyright © 2018, American Chemical Society*

---

#### PERMISSION/LICENSE IS GRANTED FOR YOUR ORDER AT NO CHARGE

This type of permission/license, instead of the standard Terms and Conditions, is sent to you because no fee is being charged for your order. Please note the following:

- Permission is granted for your request in both print and electronic formats, and translations.
- If figures and/or tables were requested, they may be adapted or used in part.
- Please print this page for your records and send a copy of it to your publisher/graduate school.
- Appropriate credit for the requested material should be given as follows: "Reprinted (adapted) with permission from {COMPLETE REFERENCE CITATION}. Copyright {YEAR} American Chemical Society." Insert appropriate information in place of the capitalized words.
- One-time permission is granted only for the use specified in your RightsLink request. No additional uses are granted (such as derivative works or other editions). For any uses, please submit a new request.

## Copyright for Figure 1.9

This Agreement between Institut National de la Recherche Scientifique -- Fatemeh Zare ("You") and Elsevier ("Elsevier") consists of your license details and the terms and conditions provided by Elsevier and Copyright Clearance Center.

License Number	5286551390909
License date	Apr 12, 2022
Licensed Content Publisher	Elsevier
Licensed Content Publication	Biomaterials
Licensed Content Title	Visible light-induced crosslinking and physiological stabilization of diselenide-rich nanoparticles for redox-responsive drug release and combination chemotherapy
Licensed Content Author	Shaodong Zhai,Xianglong Hu,Yongjun Hu,Baoyan Wu,Da Xing
Licensed Content Date	Mar 1, 2017
Licensed Content Volume	121
Licensed Content Issue	n/a
Licensed Content Pages	14
Start Page	41
End Page	54
Type of Use	reuse in a thesis/dissertation
Portion	figures/tables/illustrations
Number of figures/tables/illustrations	1
Format	both print and electronic
Are you the author of this Elsevier article?	No
Will you be translating?	No
Title	Graduate student
Institution name	Institut National de la Recherche Scientifique
Expected presentation date	May 2022
Portions	Figure 1 on page 7

## Copyright for Figure 1.10

Probing the impact of sulfur/selenium/carbon linkages on prodrug nanoassemblies for cancer therapy

Author:

Bingjun Sun et al

Publication:

Nature Communications

Publisher:

Springer Nature

Date:

Jul 19, 2019

Copyright © 2019, The Author(s)

Creative Commons

This is an open access article distributed under the terms of the [Creative Commons CC BY](#) license, which permits unrestricted use, distribution, and reproduction in any medium, provided the original work is properly cited.

You are not required to obtain permission to reuse this article.

To request permission for a type of use not listed, please contact [Springer Nature](#)

## Copyright for Figure 1.11

1,9-Dialkoxyanthracene as a 1O<sub>2</sub>-Sensitive Linker

Author: Dumitru Arian, Larisa Kovbasyuk, Andriy Mokhir

Publication: Journal of the American Chemical Society

Publisher: American Chemical Society

Date: Mar 1, 2011

Copyright © 2011, American Chemical Society



---

### PERMISSION/LICENSE IS GRANTED FOR YOUR ORDER AT NO CHARGE

This type of permission/license, instead of the standard Terms and Conditions, is sent to you because no fee is being charged for your order. Please note the following:

- Permission is granted for your request in both print and electronic formats, and translations.
- If figures and/or tables were requested, they may be adapted or used in part.
- Please print this page for your records and send a copy of it to your publisher/graduate school.
- Appropriate credit for the requested material should be given as follows: "Reprinted (adapted) with permission from {COMPLETE REFERENCE CITATION}. Copyright {YEAR} American Chemical Society." Insert appropriate information in place of the capitalized words.
- One-time permission is granted only for the use specified in your RightsLink request. No additional uses are granted (such as derivative works or other editions). For any uses, please submit a new request.

## Copyright for Figure 1.12

### Mechanistic Investigation on Oxidative Degradation of ROS-Responsive Thioacetal/Thioketal Moieties and Their Implications

Author: Bin Liu, S. Thayumanavan



Publication: Cell Reports Physical Science

Publisher: Elsevier

Date: 23 December 2020

© 2020

---

#### Creative Commons Attribution-NonCommercial-No Derivatives License (CC BY NC ND)

This article is published under the terms of the [Creative Commons Attribution-NonCommercial-No Derivatives License \(CC BY NC ND\)](#).

For non-commercial purposes you may copy and distribute the article, use portions or extracts from the article in other works, and text or data mine the article, provided you do not alter or modify the article without permission from Elsevier. You may also create adaptations of the article for your own personal use only, but not distribute these to others. You must give appropriate credit to the original work, together with a link to the formal publication through the relevant DOI, and a link to the Creative Commons user license above. If changes are permitted, you must indicate if any changes are made but not in any way that suggests the licensor endorses you or your use of the work.

### Copyright for Figure 1.13

This Agreement between Institut National de la Recherche Scientifique -- Fatemeh Zare ("You") and Elsevier ("Elsevier") consists of your license details and the terms and conditions provided by Elsevier and Copyright Clearance Center.

License Number	5286570111666
License date	Apr 12, 2022
Licensed Content Publisher	Elsevier
Licensed Content Publication	Journal of Pharmacological and Toxicological Methods
Licensed Content Title	A peroxyoxalate chemiluminescence-based assay for the evaluation of hydrogen peroxide scavenging activity employing 9,10-diphenylanthracene as the fluorophore
Licensed Content Author	Anis Arnous,Christos Petrakis,Dimitris P Makris,Panagiotis Kefalas
Licensed Content Date	November–December 2002
Licensed Content Volume	48
Licensed Content Issue	3
Licensed Content Pages	7
Start Page	171
End Page	177
Type of Use	reuse in a thesis/dissertation
Portion	figures/tables/illustrations
Number of figures/tables/illustrations	1
Format	both print and electronic
Are you the author of this Elsevier article?	No
Will you be translating?	No
Title	Graduate student
Institution name	Institut National de la Recherche Scientifique
Expected presentation date	May 2022
Portions	Adapted and modified Figure 1 on page 2

## Copyright for Figure 1.14

### The Chemistry of Boronic Acids in Nanomaterials for Drug Delivery



**Author:** Alexandra Stubelius, Sangeun Lee, Adah Almutairi

**Publication:** Accounts of Chemical Research

**Publisher:** American Chemical Society

**Date:** Nov 1, 2019

*Copyright © 2019, American Chemical Society*

---

#### PERMISSION/LICENSE IS GRANTED FOR YOUR ORDER AT NO CHARGE

This type of permission/license, instead of the standard Terms and Conditions, is sent to you because no fee is being charged for your order. Please note the following:

- Permission is granted for your request in both print and electronic formats, and translations.
- If figures and/or tables were requested, they may be adapted or used in part.
- Please print this page for your records and send a copy of it to your publisher/graduate school.
- Appropriate credit for the requested material should be given as follows: "Reprinted (adapted) with permission from {COMPLETE REFERENCE CITATION}. Copyright {YEAR} American Chemical Society." Insert appropriate information in place of the capitalized words.
- One-time permission is granted only for the use specified in your RightsLink request. No additional uses are granted (such as derivative works or other editions). For any uses, please submit a new request.

## Copyright for Figure 1.15

This Agreement between Institut National de la Recherche Scientifique -- Fatemeh Zare ("You") and Elsevier ("Elsevier") consists of your license details and the terms and conditions provided by Elsevier and Copyright Clearance Center.

License Number	5286570619233
License date	Apr 12, 2022
Licensed Content Publisher	Elsevier
Licensed Content Publication	Analytica Chimica Acta
Licensed Content Title	A near-infrared ratiometric/turn-on fluorescent probe for in vivo imaging of hydrogen peroxide in a murine model of acute inflammation
Licensed Content Author	Jingli Hou, Meng Qian, Huanhuan Zhao, Yingchun Li, Yongfang Liao, Guifang Han, Zhelong Xu, Feng Wang, Yuguang Song, Yangping Liu
Licensed Content Date	Sep 18, 2018
Licensed Content Volume	1024
Licensed Content Issue	n/a
Licensed Content Pages	8
Start Page	169
End Page	176
Type of Use	reuse in a thesis/dissertation
Portion	figures/tables/illustrations
Number of figures/tables/illustrations	1
Format	both print and electronic
Are you the author of this Elsevier article?	No
Will you be translating?	No
Title	Graduate student
Institution name	Institut National de la Recherche Scientifique
Expected presentation date	May 2022
Portions	Scheme 1 on page 2

## Copyright for Figure 1.16

---

04-12-2022 06:30:23 PM EDT - Raquel Picar-Simpson

Additional comments

Dear Fatemeh Zare,

RE: Copyright permission -- DOI: 10.1021/jm100020w -- Scheme 1

Your permission requested is granted and there is no fee for this reuse. In your planned reuse, you must cite the ACS article as the source, add this direct link <https://pubs.acs.org/doi/full/10.1021/jm100020w>, and include a notice to readers that further permissions related to the material excerpted should be directed to the ACS.

If you need further assistance, please let me know.

Best regards,  
Raquel

## Copyright for Figure 1.17

This is a License Agreement between Institut national de la recherche scientifique-Fatemeh Zare ("User") and Copyright Clearance Center, Inc. ("CCC") on behalf of the Rightsholder identified in the order details below. The license consists of the order details, the CCC Terms and Conditions below, and any Rightsholder Terms and Conditions which are included below.

All payments must be made in full to CCC in accordance with the CCC Terms and Conditions below.

Order Date	12-Apr-2022
Order License ID	1210308-1
ISSN	1759-9962
Type of Use	Republish in a thesis/dissertation
Publisher	Royal Society of Chemistry
Portion	Image/photo/illustration

### LICENSED CONTENT

---

Publication Title	Polymer chemistry
Article Title	Self-assembly and disassembly of a redox-responsive ferrocene-containing amphiphilic block copolymer for controlled release
Author/Editor	Royal Society of Chemistry (Great Britain)
Date	01/01/2010
Language	English
Country	United Kingdom of Great Britain and Northern Ireland
Rightsholder	Royal Society of Chemistry
Publication Type	e-Journal
Start Page	1817
End Page	1829
Issue	10
Volume	6
URL	<a href="http://www.rsc.org/Publishing/Journals/PY/Index.asp">http://www.rsc.org/Publishing/Journals/PY/Index.asp</a>

### REQUEST DETAILS

---

Portion Type	Image/photo/illustration
Number of images / photos / illustrations	1
Format (select all that apply)	Print, Electronic
Who will republish the content?	Academic institution

## Copyright for Figure 1.18

This Agreement between Institut National de la Recherche Scientifique -- Fatemeh Zare ("You") and Elsevier ("Elsevier") consists of your license details and the terms and conditions provided by Elsevier and Copyright Clearance Center.

License Number	5286600326599
License date	Apr 12, 2022
Licensed Content Publisher	Elsevier
Licensed Content Publication	Talanta
Licensed Content Title	A mitochondria-targeted ratiometric fluorescent nanoprobe for imaging of peroxynitrite in living cells
Licensed Content Author	Keqin Yang,Li Hou,Zhifang Li,Tianran Lin, Jianniao Tian,Shulin Zhao
Licensed Content Date	Aug 15, 2021
Licensed Content Volume	231
Licensed Content Issue	n/a
Licensed Content Pages	1
Start Page	122421
End Page	0
Type of Use	reuse in a thesis/dissertation
Portion	figures/tables/illustrations
Number of figures/tables/illustrations	1
Format	both print and electronic
Are you the author of this Elsevier article?	No
Will you be translating?	No
Title	Graduate student
Institution name	Institut National de la Recherche Scientifique
Expected presentation date	May 2022
Portions	Scheme 1B on page 3

## Copyright for Figure 1.19

This Agreement between Institut National de la Recherche Scientifique -- Fatemeh Zare ("You") and Elsevier ("Elsevier") consists of your license details and the terms and conditions provided by Elsevier and Copyright Clearance Center.

License Number	5286600727835
License date	Apr 12, 2022
Licensed Content Publisher	Elsevier
Licensed Content Publication	Elsevier Books
Licensed Content Title	Oxidative Stress and Biomaterials
Licensed Content Author	Kousik Kundu,Niren Murthy
Licensed Content Date	Jan 1, 2016
Licensed Content Pages	18
Start Page	207
End Page	224
Type of Use	reuse in a thesis/dissertation
Portion	figures/tables/illustrations
Number of figures/tables/illustrations	1
Format	both print and electronic
Are you the author of this Elsevier chapter?	No
Will you be translating?	No
Title	Graduate student
Institution name	Institut National de la Recherche Scientifique
Expected presentation date	May 2022
Portions	Figure 8.1 on page 2

## Copyright for Figure 1.20

### Multispectral optoacoustic imaging of dynamic redox correlation and pathophysiological progression utilizing upconversion nanoprobe

**SPRINGER NATURE**

**Author:** Xiangzhao Ai et al  
**Publication:** Nature Communications  
**Publisher:** Springer Nature  
**Date:** Mar 6, 2019

*Copyright © 2019, The Author(s)*

---

### Creative Commons

This is an open access article distributed under the terms of the [Creative Commons CC BY](#) license, which permits unrestricted use, distribution, and reproduction in any medium, provided the original work is properly cited.

You are not required to obtain permission to reuse this article.

To request permission for a type of use not listed, please contact [Springer Nature](#)

## Copyright for Figure 1.21

This Agreement between Institut National de la Recherche Scientifique -- Fatemeh Zare ("You") and John Wiley and Sons ("John Wiley and Sons") consists of your license details and the terms and conditions provided by John Wiley and Sons and Copyright Clearance Center.

License Number	5286601349885
License date	Apr 12, 2022
Licensed Content Publisher	John Wiley and Sons
Licensed Content Publication	Advanced Materials
Licensed Content Title	Injectable Bioresponsive Gel Depot for Enhanced Immune Checkpoint Blockade
Licensed Content Author	Zhen Gu, Xuesi Chen, Chaoliang He, et al
Licensed Content Date	May 22, 2018
Licensed Content Volume	30
Licensed Content Issue	28
Licensed Content Pages	8
Type of use	Dissertation/Thesis
Requestor type	University/Academic
Format	Print and electronic
Portion	Figure/table
Number of figures/tables	1
Will you be translating?	No
Title	Graduate student
Institution name	Institut National de la Recherche Scientifique
Expected presentation date	May 2022
Portions	Figure 1A on page 2

## Copyright for Figure 1.23

### Selective Photocatalysis Approach for Introducing ArS Units into BODIPYs through Thiyl Radicals



Author: Fangtao Ma, Li Zhou, Qingyun Liu, et al

Publication: Organic Letters

Publisher: American Chemical Society

Date: Feb 1, 2019

*Copyright © 2019, American Chemical Society*

---

#### PERMISSION/LICENSE IS GRANTED FOR YOUR ORDER AT NO CHARGE

This type of permission/license, instead of the standard Terms and Conditions, is sent to you because no fee is being charged for your order. Please note the following:

- Permission is granted for your request in both print and electronic formats, and translations.
- If figures and/or tables were requested, they may be adapted or used in part.
- Please print this page for your records and send a copy of it to your publisher/graduate school.
- Appropriate credit for the requested material should be given as follows: "Reprinted (adapted) with permission from {COMPLETE REFERENCE CITATION}. Copyright {YEAR} American Chemical Society." Insert appropriate information in place of the capitalized words.
- One-time permission is granted only for the use specified in your RightsLink request. No additional uses are granted (such as derivative works or other editions). For any uses, please submit a new request.

## Copyright for Figure 1.24

This Agreement between Institut National de la Recherche Scientifique -- Fatemeh Zare ("You") and John Wiley and Sons ("John Wiley and Sons") consists of your license details and the terms and conditions provided by John Wiley and Sons and Copyright Clearance Center.

License Number	5286610442917
License date	Apr 12, 2022
Licensed Content Publisher	John Wiley and Sons
Licensed Content Publication	Chinese Journal of Chemistry
Licensed Content Title	Fluorescence Sensing of Glutathione Thiyl Radical by BODIPY-Modified $\beta$ -Cyclodextrin
Licensed Content Author	Zhixue Liu, Xianyin Dai, Qiaoyan Xu, et al
Licensed Content Date	Dec 24, 2021
Licensed Content Volume	40
Licensed Content Issue	4
Licensed Content Pages	7
Type of use	Dissertation/Thesis
Requestor type	University/Academic
Format	Print and electronic
Portion	Figure/table
Number of figures/tables	2
Will you be translating?	No
Title	Graduate student
Institution name	Institut National de la Recherche Scientifique
Expected presentation date	May 2022
Portions	Scheme 1 and Figure 1

## Copyright for Figure 1.25

This Agreement between Institut National de la Recherche Scientifique -- Fatemeh Zare ("You") and John Wiley and Sons ("John Wiley and Sons") consists of your license details and the terms and conditions provided by John Wiley and Sons and Copyright Clearance Center.

License Number	5286610633000
License date	Apr 12, 2022
Licensed Content Publisher	John Wiley and Sons
Licensed Content Publication	Advanced Materials
Licensed Content Title	Photo-Click Living Strategy for Controlled, Reversible Exchange of Biochemical Ligands
Licensed Content Author	Kristi S. Anseth, Malar A. Azagarsamy, Navakanth R. Gandavarapu
Licensed Content Date	Feb 12, 2014
Licensed Content Volume	26
Licensed Content Issue	16
Licensed Content Pages	6
Type of use	Dissertation/Thesis
Requestor type	University/Academic
Format	Print and electronic
Portion	Figure/table
Number of figures/tables	1
Will you be translating?	No
Title	Graduate student
Institution name	Institut National de la Recherche Scientifique
Expected presentation date	May 2022
Portions	Scheme 1

## Copyright for Figure 1.26



### Radical-Mediated Thiol-Ene Strategy: Photoactivation of Thiol-Containing Drugs in Cancer Cells

**Author:** Gonçalo J. L. Bernardes, Gonzalo Jiménez-Osés, Bruno L. Oliveira, et al

**Publication:** Angewandte Chemie International Edition

**Publisher:** John Wiley and Sons

**Date:** Nov 2, 2018

© 2018 The Authors. Published by Wiley-VCH Verlag GmbH & Co. KGaA.

---

### Open Access Article

This is an open access article distributed under the terms of the [Creative Commons CC BY](#) license, which permits unrestricted use, distribution, and reproduction in any medium, provided the original work is properly cited.

You are not required to obtain permission to reuse this article.